Universidad de Alcalá

DEVELOPMENT OF BURNED AREA ALGORITHMS ON A GLOBAL SCALE

Tesis Doctoral presentada por

ITZIAR ALONSO CAÑAS

Bajo la dirección del

Dr. EMILIO CHUVIECO SALINERO

Catedrático de Análisis Geográfico Regional

Programa de doctorado en Tecnologías de la Información Geográfica.

DEPARTAMENTO DE GEOLOGÍA, GEOGRAFÍA Y MEDIO AMBIENTE

Alcalá de Henares, diciembre de 2015

Agradecimientos

En primer lugar estoy especialmente agradecida a mi tutor, Emilio Chuvieco, por la confianza que en mí ha depositado, por haberme sabido guiar a lo largo de esta tesis doctoral y por su aliento y apoyo en los momentos complicados que se dan a lo largo de un trabajo de investigación. También me gustaría mencionar al Departamento de Geología, Geografía y Medio Ambiente, por su valor profesional y humano. Gracias por crear ese clima agradable y colaborador, en el que resulta mucho más fácil trabajar. No me olvido del grupo del sótano, siempre preparado para hacer un chiste y sacarme una sonrisa, en especial gracias a Mariano, Stijn y Rubén.

Quisiera mostrar mi agradecimiento a Philip Lewis y José Gómez-Dans, por haberme acogido en su grupo para mi estancia en la UCL, por dedicar parte de su tiempo a enseñarme y facilitar mi trabajo allí.

A Bernard Pinty por su disponibilidad, enfoque y por haber estado pendiente de mis avances.

A la ESA, por la financiación recibida a través del proyecto Fire_CCI, que ha permitido el desarrollo de esta tesis, y a todo el equipo que ha formado parte del proyecto.

A mis amigos, los de Bilbao, los de Madrid, y los que están repartidos por el mundo. Por supuesto a mi cuadrilla, por darme eso que sólo las cuadrillas pueden dar y que es tan difícil de explicar. En especial, a Paula y a Edward por su amistad y apoyo incondicional en los momentos difíciles.

Por último, me gustaría agradecer a mis padres el amor y el apoyo recibido a lo largo de toda mi vida, el haberme enseñado, cuidado y querido tanto. Siempre he pensado que no podía haber tenido más suerte. Sin duda no sería como soy si no fuese por vosotros.

Muchas gracias a todos,

Itziar

TABLE OF CONTENTS

OVERVIEW

This manuscript contains the research work entitled “Development of Burned Area algorithms on a global scale”. This work was developed and funded in the framework of the fire_cci project within the European Space Agency’s Climate Change Initiative programme. The PhD aim was to obtain an algorithm to retrieve burned areas (BA) on a global scale from the MERIS sensor. The document is structured in the following chapters:

Chapter 1: Introduction: this chapter aims at putting in context the global relevance of fire and of accessing information on burned areas. The methods to characterize fire from space and the state of the art are reviewed here.

Chapter 2: Objectives: the aim of this chapter is to introduce the context of the PhD research as well as a more detailed description of the thesis objectives.

Chapter 3: BA algorithm development and testing: in this chapter an overview of general considerations required to build the algorithm is included. The methods developed and tested to obtain the algorithm to detect burned areas will be presented. Since results from these tests helped shaping the algorithm final configuration, the structure in this thesis is not separated in methods and results. Instead, results from the different phases of the algorithm are introduced in this chapter.

Chapter 4: BA product assessment: burned area global estimates for years 2006 to 2008 obtained with the MERIS algorithm developed are included here. Results analysis, validation and inter-comparison with other BA products are introduced in this chapter.

Chapter 5: Discussion: analysis and discussion on the steps taken to develop the algorithm, results obtained and limitations found are included in this section.

Chapter 6: Conclusions and perspectives: main outcomes and lessons learned from the development of this algorithm as well as the way forward are introduced in this chapter.

The first two scientific publications result of this work are included in Annex 2 and Annex 3. Annex 2 is a paper published in Remote Sensing of Environment containing the main algorithm developments. Annex 3 is a paper submitted and accepted with minor corrections to Geofocus – Revista Internacional de Ciencia y Tecnología de la Información Geográfica. It summarises the main improvements made on version 1 that lead to version 2 of the algorithm.

The main achievement of the work carried out within this thesis is the development of the first algorithm based on MERIS data to obtain BA on a global scale, at higher resolution than the current BA collections, and improving the quality of existing European BA collections. Although the algorithm presents some limitations and future work is still needed to improve current results, the interest stands now on obtaining a longer time series, and on ensuring the continuity of these measurements, to monitor BA and to use this information in the context of climate change. In fact, this algorithm will be the basis for computing the full MERIS BA time series for the second phase of the fire_cci project (2002 to 2012). It will also prepare for the upcoming generations of the European Space Agency BA products, particularly for those based on Sentinel-3 OLCI-SLSTR sensors. The algorithm will also be adapted to other sensors, such as MODIS bands 1 and 2, with higher spatial resolution and revisit time. The availability of alternative BA time series would complement existing BA products, providing more robust estimations and improvements in the uncertainty characterisation of BA inputs for climate models. Furthermore, different BA products can provide diverse regional accuracies and therefore, merging outputs from global synthesis may greatly improve the way BA trends are currently characterised.

RESUMEN

Este manuscrito contiene el trabajo de investigación titulado "Desarrollo de algoritmos de área quemada a escala global". Este trabajo ha sido desarrollado y financiando en el marco del proyecto fire_cci dentro del programa de cambio climático de la Agencia Espacial Europea. El objetivo del presente trabajo de tesis doctoral es obtener un algoritmo para la caracterización de áreas quemadas (AQ) a escala global a partir de información del sensor MERIS. El documento se estructura en los siguientes capítulos:

Capítulo 1: Introducción: este capítulo tiene como objetivo contextualizar la relevancia del fuego a escala global y el acceso a información sobre áreas quemadas. Los métodos para caracterizar los incendios desde el espacio, así como una revisión bibliográfica del estado del arte se detallan aquí.

Capítulo 2: Objetivos: en este capítulo se presenta el contexto en el que se centra este trabajo de investigación. Así mismo se detallan los objetivos de esta tesis.

Capítulo 3: Desarrollo y test del algoritmo de área quemada: en este capítulo se realiza una revisión de los requisitos necesarios para obtener un algoritmo de detección de áreas quemadas a escala global. Los métodos desarrollados y las diferentes pruebas realizadas para obtener el algoritmo se detallan. Los resultados de estas pruebas han ayudado a obtener la configuración final del algoritmo, por lo que los resultados de estos tests a lo largo de las distintas fases del algoritmo se incluyen también en este capítulo.

Capítulo 4. Análisis de resultados de AQ: las estimaciones de AQ para los años 2006 a 2008 obtenidos con el algoritmo MERIS desarrollado se introducen en este capítulo. Así mismo se presentan el análisis de resultados, la validación y la intercomparación con otros productos de AQ.

Capítulo 5: Discusión: en este capítulo se introducen el análisis y discusión de los pasos seguidos para desarrollar el algoritmo, así como de los resultados obtenidos y de las limitaciones encontradas.

Capítulo 6: Conclusiones y perspectivas: en este capítulo se detallan los hallazgos principales, las conclusiones obtenidas del desarrollo del algoritmo, y los posibles futuros pasos a seguir.

Los dos primeros artículos fruto del trabajo realizado se incluyen en los anexos 2 y 3. El anexo 2 es un artículo publicado en Remote Sensing of Environment, donde se recogen los principales pasos del algoritmo. El anexo 3 es un artículo enviado y aceptado con correciones menores en Geofocus – Revista Internacional de Ciencia y tecnología de la Información Geográfica. En el se recogen las principales mejoras realizadas en la versión 1 que dieron lugar a la versión 2 del algoritmo.

El principal logro del trabajo realizado dentro de esta tesis ha sido el desarrollo del primer algoritmo de áreas quemada a escala global a partir del sensor MERIS. Esto permite obtener productos de AQ a mayor resolución que la proporcionada por las colecciones de AQ existentes en la actualidad, y mejorando la calidad de las colecciones obtenidas a nivel europeo. Si bien el algoritmo presenta una serie de limitaciones y será necesario trabajo futuro para mejorar los resultados actuales, el interés reside actualmente en la obtención de largas series temporales de AQ, y en asegurar la continuidad de estas medidas, con el objetivo de monitorizar las áreas quemadas y de utilizar esta información en el contexto del cambio climático. Siguiendo esta línea, el algoritmo desarrollado en esta tesis será la base para obtener una serie temporal completa del producto de AQ, a partir de datos del sensor MERIS (2002 a 2012), en el contexto de la segunda fase del proyecto fire_cci. A su vez, esto servirá para preparar los futuros productos de AQ de la Agencia Espacial Europea, principalmente los basados en los sensores OLCI y SLSTR a bordo del Sentinel-3. Podrá también ser adaptado a otros sensores como MODIS, haciendo uso de sus bandas 1 y 2, que cuentan además con una mejor resolución espacial y temporal. La disponibilidad de series alternativas de AQ complementa los productos ya existentes, permitiendo obtener caracterizaciones más robustas y con mejoras en la incertidumbre de las medidas utilizadas en modelos climáticos. Además, la existencia de diferentes productos de área quemada puede proporcionar diferentes precisiones a nivel regional y por tanto, la fusión de los datos obtenidos puede mejorar de forma relevante la forma en la que las estimaciones de AQ están caracterizadas actualmente.

CHAPTER 1

INTRODUCTION

This chapter aims at introducing the global relevance of fire and of accessing information on burned area. A review of the methods to characterize fire from space and the state of the art is included in this chapter.

1.1. FIRE AND ITS RELEVANCE ON EARTH

Fire has been burning ecosystems for millions of years, helping to shape global biome distribution and to maintain the structure and function of fire-prone communities. Fossil charcoal indicates that wildfires began soon after the appearance of terrestrial plants in the Silurian (420 million years ago) (Scott and Glasspool 2006). Fire is an important element in human history. Its use made huge changes in human evolution. Humans have been using fire as a management tool (to facilitate hunting and food gathering) since Palaeolithic times (Stewart 1956).

Nowadays fire is still used to manage landscapes and natural resources, but it can also create dangerous situations, and affect lives and property, provoking huge losses. Fire is highly relevant in certain types of vegetation such as savannah, Mediterranean woodland, and boreal forest, but it is being introduced in other ecosystems, severely impacting them. Currently, the main areas that burn worldwide are tropical forests from Brazil and Indonesia, temperate in USA and Europe, boreal in Siberia, and Canada, China and in tropical savannah of Africa and agricultural regions of Northern USA and Europe.

The beginning of fire ignition is dual. It can be related to natural events such as lightning, but most authors recognize that the majority of fires worldwide have an anthropogenic origin. In the tropics and temperate regions, fire is often used as a tool for land management, being therefore predominantly human caused. On the opposite, boreal regions in Canada have an important share of lightning fires. These various kinds of fire activity generate a range of economic, ecological, atmospheric and climatic impacts, with magnitudes that are strongly dependent on the areal extent of the burns. Current estimations show that around 3.5 million km^2 burn every year (Alonso-Canas and Chuvieco 2015; Giglio et al. 2010).

Fire effects have influence in different domains such as atmosphere, global carbon budget and vegetation dynamics (Bowman et al. 2009; Krawchuk et al. 2009). All these effects have an impact on the radiation budget. From the thirteen radiative forcing terms identified in the IPCC 4th assessment, eight of them are influenced by fire emissions (Bowman et al. 2009): long-lived greenhouse gases, ozone, stratospheric water vapour from CH4, surface albedo, aerosols (direct and indirect), linear contrails and solar irradiance. In more detail, these effects are:

- Fire shapes vegetation structure and composition. This can therefore modify surface albedo and energy balance (López-Saldaña et al. 2015).
- Interactions between grassland fires and human land use may result in ecosystem degradation, hydrologic changes, soil disturbance and shrub encroachment (Archer 1994). Fire effects on soil are related to direct losses of nutrients during burning and post-fire changes due to low vegetation cover. When strategies are not put in place to recover the area affected by the fire, the habitat conditions will change. This implies loss of vegetation species, diminishing biodiversity and complicating animal survival.
- Deforestation fires, the most common in the Tropics, reduce tree cover and in consequence the ability of terrestrial ecosystems to sequester carbon (Yue et al. 2014).
- Biomass burning injects aerosols and trace gases into the atmosphere. The impact on the atmosphere varies heavily depending on the type of fire. In the case of CO_2, deforestation fires, fires in drained peatlands, and fires in areas with increasing levels of disturbance are a net source of carbon dioxide to the atmosphere (van der Werf et al. 2003). In the case of methane, peat fires, may emit almost ten times more CH_4 per unit biomass combusted than fires in savannah (Andreae and Merlet 2001; Christian et al. 2003; Yokelson et al. 1997). First global estimates of fire emissions were made by (Seiler and Crutzen 1980). In this study they estimated 2.6 Pg C year−1 (range of 1.7–3.5), being agricultural waste burning the largest source of fire carbon emissions (33%), followed by shifting agriculture (29%), savannah (21%), deforestation (12%), fires in temperate areas (4%) and fires in boreal areas (1%). Later, Crutzen and Andreae (1990) revised for the tropics the emissions for deforestation and savannah fires

upwards, with savannah burning becoming the main source of emissions. In the last decade burned area collections have been derived from satellite information at a global scale (Giglio et al. 2013; Gregoire et al. 2003; Plummer et al. 2007; Roy et al. 2008; Tansey et al. 2008). This BA information has been used with biogeochemical models to estimate emissions (Hoelzemann et al. 2004; Ito and Penner 2004; Jain et al. 2006; van der Werf et al. 2006) estimating fire carbon emissions to be around 2 Pg C year−1(Giglio et al. 2013; Randerson et al. 2005).

Fire has ultimately a direct link to climate. Even though the current understanding of climate-fire interactions is limited, there is also increasing evidence on their mutual influence (Kloster et al. 2012; Krawchuk et al. 2009; Mouillot and Field 2005; Pechony and Shindell 2010; Running 2006). Climate has a strong influence on all aspects of the fire regime. It is related to seasonal timing temperature and humidity, as well as wind (that helps spreading the fire). Climate also influences the nature and availability of fuel, through its influence on the productivity and type of vegetation. Expected increases in temperature and rainfall changes (dryer vegetation conditions) are likely to increase wildfire frequency in some regions, while others may experience decrease in fire activity as a result of decreased biomass production (Daniau A.L. et al 2012; Krawchuk et al. 2009). Increased fire in response to warming, especially in seasonally cold climates, is primarily explained by higher fuel loads resulting from increased vegetation productivity (Krawchuk et al. 2009) and a longer fire season (Westerling et al. 2006). This mechanism may be enhanced by the influence of temperature changes on fire-supporting weather. Warming is expected to enhance fire-supporting weather through increased storm intensity and lightning ignitions (Price 2009) and through increased duration of droughts leading to more rapid fuel drying. Warmer conditions during drought periods also accelerate fuel drying. The increment in fuel through higher productivity may be further enhanced by rise in tree mortality accompanying rapid warming (Adams et al. 2009). In dry environments, increasing precipitation leads to greater fuel loads and more fire; in wet environments, increasing precipitation leads to wetter fuels and therefore less fire (van der Werf et al. 2008a; van der Werf et al. 2008b). Therefore, biomass burning is likely to be greatest at intermediate moisture levels.

GHG emissions contribute to global warming whereas aerosol and albedo effects contribution to the overall radiation budget is still not clear. Hicke et al. (2012) and Randerson et al. (2006) showed that the impact of increasing boreal forest fires on climate warming may be limited or even result in regional cooling because of the negative forcing from increased surface albedo following a fire. In the tropics, aerosol emissions from fires have been shown to influence the radiation budget at regional scales (Duncan et al. 2003). Climate modelling studies suggest these aerosols may lengthen or intensify periods of drought in the Amazon (Zhang et al. 2008) and in Indonesia (Tosca et al. 2010).

In addition to climate effects, fire has an important impact on humans' health. Apart from life danger, and possible poisoning from gases directly emitted from the fire (especially from CO), some aerosol particles emitted as a result of fires can induce lung and heart diseases. The size of particles is directly linked to their potential for causing health problems. Particulate Matter (PM) of less than 10 μm in diameter poses the greatest problems. From these ones, $PM_{2.5}$ (2.5 μm or smaller) are found in smoke and haze, and can be directly emitted from sources such as forest fires (EPA 2008, 2009). Suspended particles can travel long distances, becoming the region affected by those particles much larger than the one affected by the fire. For instance, pollutants from the July 2002 forest fires in northern Quebec were linked to a major increase in the amount of fine particles in Baltimore or Montreal (Sapkota et al. 2005). This effect is also relevant in certain areas such as Indonesia, where Sumatran fires emit particles that are frequently transported into Malaysia and Singapore.

For all this, it is highly relevant to be able to monitor fire on a global scale. Remote sensing is one of the best means to do it, since it allows for constant monitoring and can provide information about areas that are difficult to access on ground. It is highly relevant to obtain detailed information on the location, extension and intensity at both local and global scale of fires and its consequences. This is necessary to evaluate economic losses as well as ecological effects, monitoring land use and land changes, modelling atmospheric and ecological impacts derived from biomass burnings and estimate post fire consequences at both short and long term. It is important to have BA as a way to estimate emissions. These are relevant since improvements in emissions estimates are also necessary to calibrate and validate prognostic fire modules in

dynamic global vegetation models and climate-carbon models, in order to make better predictions about future fire activity (Arora and Boer 2005; Kloster et al. 2010; Thonicke et al. 2001). These models can also take advantage of a better understanding of the drivers of fires based on new satellite information. Archibald et al. (2009) for example, showed that tree cover density, rainfall over the last 2 years, and rainfall seasonality explained more than half of the variability in burned area in southern Africa. In addition, inter-annual variability in precipitation rates controls part of the variability in fire-driven deforestation rates from year to year, with strongest relations in Equatorial Asia where annual variability in precipitation is highest (Le Page et al. 2007; van der Werf et al. 2008a).

The relevance of fire has been identified by several international initiatives. Among them is the Global Climate Observing System (GCOS), sponsored by the World Meteorological Organization (WMO), the Intergovernmental Oceanographic Commission (IOC) of the United Nations Educational, Scientific and Cultural Organization (UNESCO), the United Nations Environment Programme (UNEP) and the International Council of Scientific Unions (ICSU). This initiative has identified a series of Essential Climate Variables required to support the work of the UNFCCC (United Nations Framework Convention on Climate Change) and the IPCC (Intergovernmental Panel on Climate Change). These ECVs are intended to have a systematic and long-term record of observations. They are separated by themes: atmospheric, terrestrial and oceanic. Fire disturbance is one of the terrestrial ECVs. Other international initiatives such as the GOFC-GOLD also aim at joining efforts and promote collaboration and international cooperation in order to better characterize, understand and assess fire and its impacts. On the European side, the European Space Agency has a dedicated programme, the Climate Change Initiative (CCI) that aims at monitoring some of these variables. The European Commission has also projected a Copernicus Climate Change Service (C3S) where those variables will be monitored on an operational basis. The service will ensure long term monitoring and consistency of these variables. Fire disturbance is also one of the priorities identified in this service.

The work developed in this thesis has been funded by ESA's CCI, in the framework of the Fire Disturbance project (fire_cci from now on), which aims at developing and

improving tools for estimating burned areas on a global scale from medium resolution sensors (fire_cci, 2009).

1.2. SPECTRAL CHARACTERIZATION OF FIRE

Fire can be monitored from space as a result of the changes it introduces in the reflected or emitted radiance detected remotely. There are essentially four ways of detecting those changes:

1) Direct radiation from active fires: direct thermal radiation caused by high temperatures of fires was the first mean to detect them. Following the Planck's radiation law the most suitable spectral region to detect hot surfaces (such as active fires) is the MIR band, between 3 and 5 μm, since at this wavelength, radiation emitted by a fire is significantly higher than emission from the ground background (Kaufman and Justice 1998).

2) Changes in reflected radiation caused by aerosols and gases associated to the combustion process: smoke and aerosols can be better detected on the blue region, but little information about the burned areas can be inferred, since the quantities emitted will depend on the type of vegetation being burned and the intensity of the fire (particularly the type of combustion, whether it is flaming or smouldering) (Dubovik et al. 2002; Kaufman et al. 2002).

3) Changes in soil and leaf reflectance caused by vegetation combustion: changes in vegetation reflectance as a result of fire are more persistent than active fires and can be seen in different spectral bands. These changes are mainly noticed in the VIS, NIR, MIR and SWIR and microwave regions (Pereira et al. 1999b). Spectral signatures of charcoal, green vegetation and dry vegetation can be seen in Figure 1.

4) Long term changes in the vegetation structure: in this case there is a stronger and more permanent alteration of the vegetation structure. These changes will also be mainly noticed in the VIS, NIR, MIR and SWIR and microwave regions (Pereira et al. 1999b).

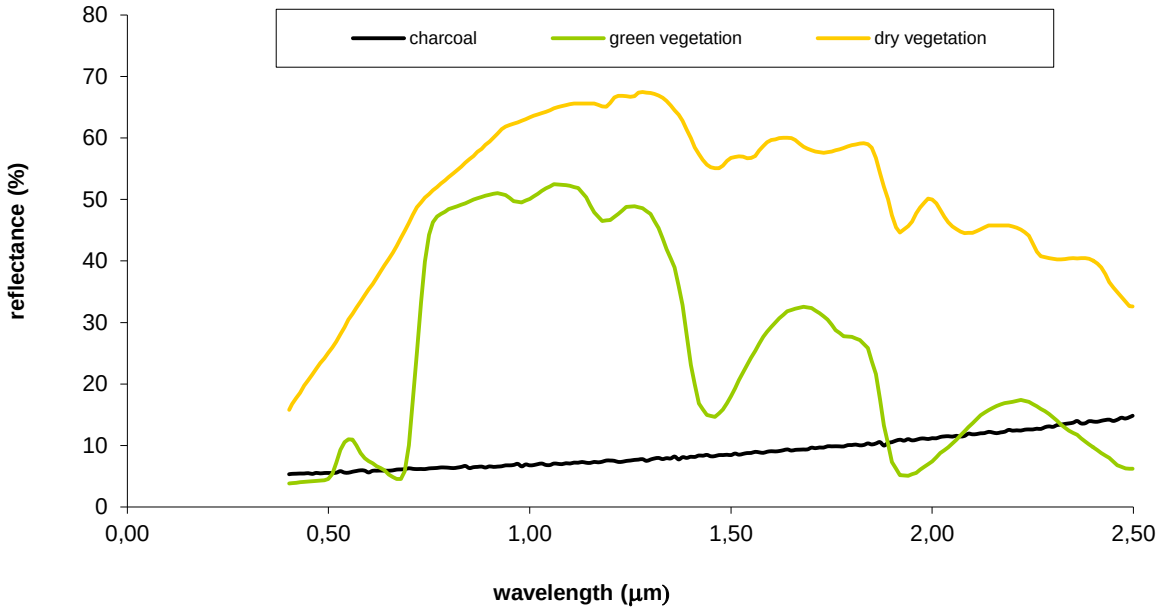

Figure 1. Typical spectral reflectance signatures of pure charcoal, green vegetation and dry vegetation (Pereira et al. 2014).

When focusing on the spectral changes fire induces in vegetation, some aspects need to be considered: time after fire, ash and char, and type and intensity of the fire.

1- Length of the post fire signal (Chuvieco and Congalton 1989). Two clear different types of post fire signals can be distinguished (Robinson 1991). The first one is based on the deposition of charcoal or surface charring. This is related to vegetation combustion and has a short duration, especially if attenuated by other factors such as wind or rainfall. This signal will not last longer than weeks or months after the fire. The second one is the alteration of vegetation structure and the abundance of remaining vegetation, and can be identified as a burned patch. This type of signal tends to be more stable compared to the first one in terms of persistence, lasting for 2 or 3 weeks in tropical regions up to years in boreal areas. The drawback is that other changes not related to a fire, and that imply removal of plant canopies (such as wind storms of forest cuts), will also have a similar behaviour.

2- Vegetation combustion produces a spectral response of ash and char with a clear change in colour. The ash and char products of combustion are quite different. Ash is the result of a complete combustion of high intensity that happens when there is no

restriction of oxygen supply. It has a light coloured appearance and is predominantly mineral residue (Cope and Chaloner 1985; Riggan et al. 1994). Char on the opposite is the result of incomplete combustion of biomass with restriction of oxygen supply. This is the product of less severe fires and presents darker colours (Ambrosia and Brass 1988; Chandler et al. 1983). These two products appear generally on the soil and are generally removed by wind and rainfall, exposing again the soil or being covered by vegetation.

3- Type and intensity of the fire: it will be also important to consider if the fire happens on the crown of the trees, on ground or underground, and also the intensity of the fire, since this will vary the quantity of charcoal on ground. Both intensity and height at which the fire occurs will vary the ability of the sensor to detect the fire from space. A fire happening under the crown will not be detectable from satellite except for the increase in temperature, but might not induce clear changes in vegetation reflectance, particularly at dense canopy covers.

Spectral properties of burned surfaces observed from space might be confused with other land cover types that have a similar spectral response but that are not affected by fire. Most common confusions are related to areas with low reflectivity such as water, dark soils, cloud shadows and topographic shadows (Chuvieco and Congalton 1988), pixels that mix water and land/vegetation, such as river borders or coastal zones (Martín and Chuvieco 2001) and pixels that mix burned and unburned areas or soil (Caetano et al. 1994).

It is important to note, especially when developing an algorithm for burned area detection on a global scale, that the spectral behaviour of burned areas might not be the same, or even not coherent in the variety of ecosystems that exist worldwide. This relates to the fact that vegetation type and condition, soil and fire intensity will vary depending on the ecosystem. In the NIR region, both green and dry vegetation have higher reflectance than recent burns, which normally translates into a darkening after the surface. In the SWIR region, the spectral reflectance of vegetation varies depending on its water content (green or dry, Figure 1). Therefore, fire induced changes in this band will be different depending on the climatic conditions of the ecosystem. The type of vegetation will also present different behaviours. For instance, in grasslands and

croplands, that are more predominant in temperate ecosystems, near-infrared (NIR) and short-wave infrared (SWIR) reflectance tend to decrease as a result of fire. In forests and woodlands, more typical of boreal and Northern European regions, SWIR and NIR can decrease simultaneously or it is also possible to observe an increase in SWIR and a decrease in NIR. The type of soil will also modify the spectral response, depending if it is dark or bright surface. Fire intensity will imply more or less exposition of the soil, and the presence/absence of green vegetation, as well as different quantities of ash or charcoal.

These different behaviours have been reported in literature, finding that the spectral bands that better discriminated burned areas in different ecosystems (boreal, template and tropical) were not the same (Silva et al. 2004). This information will need to be taken into account to perform the best possible discrimination of burned areas on a global scale. Many works have studied the adequacy of the different spectral regions to identify fire. A review of the behaviour of vegetation in the main spectral bands used for BA detection is introduced hereafter, as a way to better understand the impacts of fire on pre-fire reflectance, and in order to focus the BA discrimination strategy to follow.

1.2.1. VISIBLE REGION.

The spectral region covered by the visible goes from 0.4 to 0.7 μm. In this region vegetation has generally a low spectral response, depending on the chlorophyll content. It shows a peak in the 0.55 um. This general behaviour does not apply in certain regions such as savannah where vegetation shows a high reflectivity. It is one of the regions more extensively used for burned area mapping. Nevertheless, it is not one of the best regions for discriminating burns since confusion between recent burns, and other land cover types (water, wetlands, conifer forests) can happen in the VIS region. In addition, the dynamic range available in EO satellites to discriminate between these surfaces is quite narrow. Furthermore, the path radiance, which is an important component of the atmospheric effect, is predominant in this region over dark surfaces, causing a decrease in contrast between the different land cover types. Several authors indicate that the visible spectral range is not very effective for discriminating burns (Koutsias and Karteris 1998; López García and Caselles 1991; Pereira et al. 1999b; Pereira and Setzer

1993a; Ponzoni et al. 1986; Tanaka et al. 1983).

1.2.2. NEAR INFRARED REGION

This region covers the electromagnetic spectrum from 0.7 to 1.2 μm. It is one of the most used regions for BA mapping since the signal of recent burns is strongest. Green vegetation is highly reflective in the NIR and therefore burning will imply a significant decrease in this band. Therefore, the detection will be optimal when pre-fire fuel loadings are high, and combustion produces large amounts of charcoal deposited on the ground. For these reasons, the NIR is considered the best spectral region for BA mapping by several authors (Fredericksen et al. 1990; López García and Caselles 1991; Pereira and Setzer 1993b; Stroppiana et al. 2003; Tanaka et al. 1983). Phenological status of the vegetation is of relative relevance in this band since both green and dry vegetation have higher reflectance in the NIR than recent burns. Areas with less dense vegetation and lighter soils will have a smaller decrease in this band between pre and post fire conditions.

This region is often combined with the red region (0.45um) to create the Normalised Difference Vegetation Index (NDVI) extensively used to discriminate burned areas. This was especially used when only AVHRR was available to obtain BA products globally (Fernández et al. 1997; Kasischke et al. 1995; Martín and Chuvieco 1995; Domenikiotis et al. 2002; Fraser et al. 2000; Kucêra et al. 2005; Li et al. 2000; Roy et al. 1999). However, other studies have found that NDVI is not very sensitive to recent burns, as the signal tends to be mixed with dark soils or water. Actually, NDVI is more adequate to monitor chlorophyll content or vegetation turgor, but it does not provide good sensitivity for scorched vegetation or char. Even when only the NIR and red bands are available, other non-linear indices such as GEMI have been shown more robust to detect burned areas (Chuvieco et al. 2002).

1.2.3. SHORT WAVE INFRARED REGION.

This region covers the range between 1.2 and 2.5 μm. The SWIR region presents some advantages for BA detection. First, reflectance is higher than in the VIS, and therefore

the bi-spectral NIR/SWIR space is more appropriate than the NIR/VIS for burned area detection (Pereira et al. 1999b). Second, it is less affected by aerosols than the VIS and NIR ranges (Kaufman and Remer 1994), and third, it is sensible to water. There are some contradictions on this region depending on the type of ecosystem, fire severity, vegetation moisture and soil colour (Roy and Landmann 2005; Silva et al. 2004). Furthermore, temporal fire effects on this band might be less obvious than in the NIR region (Silva et al. 2004). Pleniou and Koutsias (2013) also found that this band is more sensible to the status of healthy vegetation than the NIR (showing lower mean + standard deviation values), being NIR more sensible to burned areas. After MODIS and AVHRR -15 launches, the SWIR was also combined with the NIR (Barbosa et al. 1999a; Fraser and Li 2002; López García and Caselles 1991; Pereira 1999; Pereira and Setzer 1993b; Roy et al. 2005; Silva et al. 2005; Silva et al. 2004; Stroppiana et al. 2003; Vafeidis and Drake 2005) providing in general better results than the NDVI.

1.2.4. MIDDLE INFRARED REGION

This region covers the spectral range between 2.5 and 8.0 μm. The regions previously introduced, VIS, NIR and SWIR, correspond to the reflective spectral range, because radiation in those regions is essentially solar radiation reflected from the Earth. From the MIR region onwards, the sensors measure mainly the radiation emitted by the Earth.

On the emission side, Planck function indicates that a black body emits spectral radiation according to its temperature, and for a given temperature, the emission varies as a function of the wavelength. Figure 2 illustrates this concept (Wooster and Xu 2012).

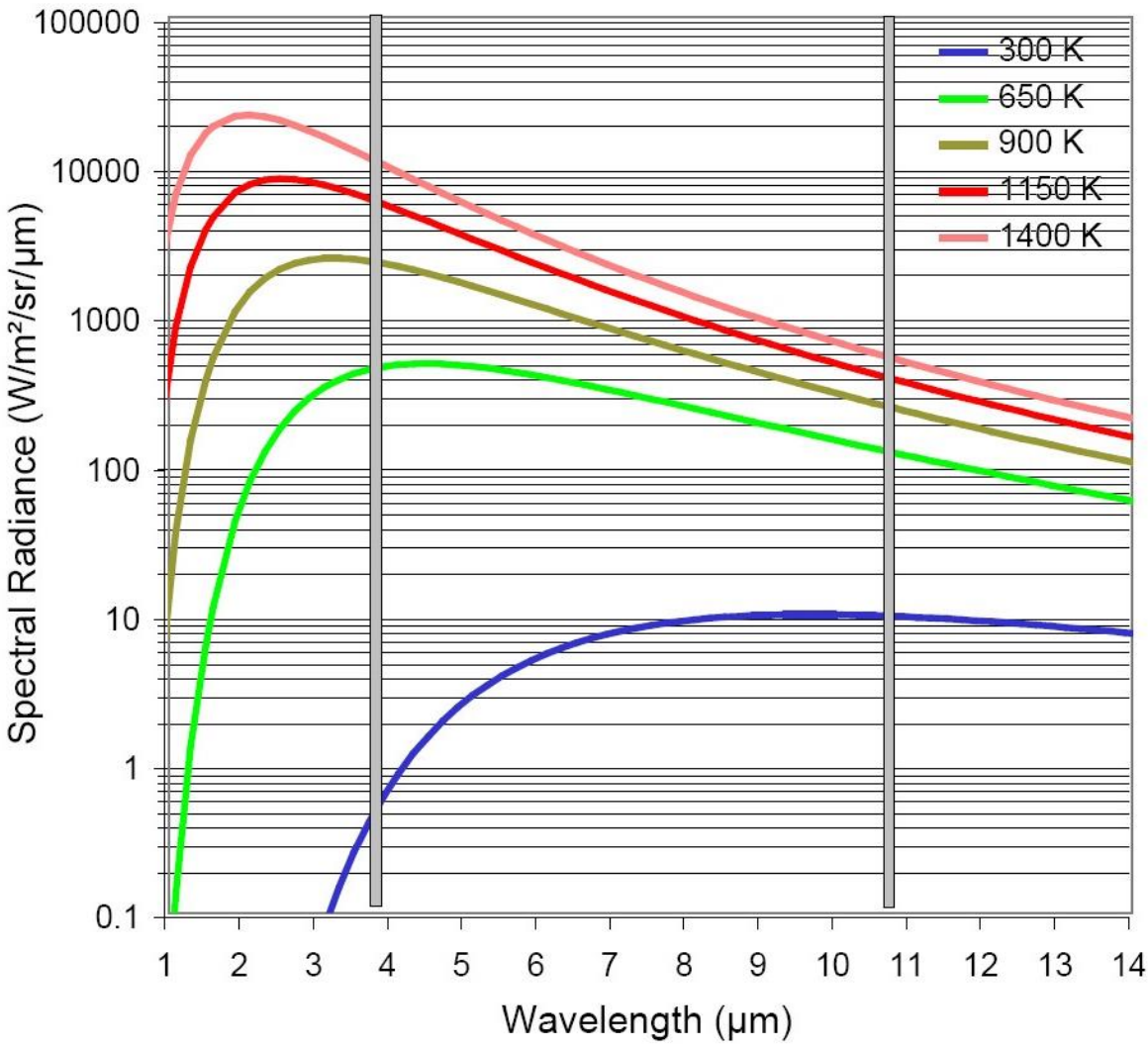

Figure 2. Spectral radiance emitted from blackbodies at different temperatures.

Temperatures of 1000°K and 600°K can be assumed as representative of typical flaming and smouldering combustion phases of vegetation fires, respectively (Lobert and Warnatz 1993). Earth's ambient temperature is 300 °K. According to Wien's Displacement Law, the peak emission of radiance for flames and smouldering surfaces would be located in the middle infrared (MIR), between 3µm and 5µm. This behaviour has been exploited for the identification of active fires, detected when there is an increase in the observed radiance in this region, compared to the surrounding areas (Arino and Piccolini 2000; Giglio et al. 2006b). For increasingly smaller and cooler fires, this contrast is progressively attenuated and becomes difficult to discriminate from natural spatial variability of the land surface temperature field. Additional perturbation sources for active fire detection may be the presence of atmospheric water vapour, a

strong reflection of solar radiation in the 3μm – 5μm region, or the presence of sub-pixel clouds (Kaufman and Justice 1998).

For what concerns the reflected energy, spectral behaviour in this region is similar to the one observed in the VIS, i.e. burned areas will reflect more than vegetation, and will appear darker than senesced vegetation. The mid-infrared spectral region has been identified by a few authors, mostly working on temperate ecosystems, as promising for detecting burns, since the fire-induced increase in brightness is larger than in the VIS range (Koutsias and Karteris 1998; López García and Caselles 1991). Pereira et al. (1999b) found that the reflective component of this band was more sensitive than the visible bands to recent burns and thus considered the NIR/MIR bi-spectral space more appropriate for burned area discrimination and mapping than the classical VIS/NIR space used in remote sensing of green vegetation. These studies aimed at exploiting the reflective part of the MIR range, present on Channel 3 of the AVHRR series. The inclusion of SWIR band from day-time acquisitions of AVHRR-15 onwards helped showing the better performance of SWIR band over MIR in detecting burned areas.

1.2.5. THERMAL INFRARED REGION

This spectral region covers the range between 8 and 14 μm. On the emission side, the peak of radiance emission at an ambient temperature of 290°K (17°C) is located in this region, at approximately 10μm. Active fire detection from remote sensing exploits this behaviour, and typically relies on some combination of brightness temperature measured in the 3μm - 5μm (MIR) and 10μm - 12μm (TIR) regions. The latter is used to obtain background temperature and to remove potential sources of confusions, such as warm soils.

1.2.6. MICROWAVE REGION.

The microwave region covers the region of spectrum for wavelengths > than 1mm. This band has not been extensively used in burned area mapping, but some studies have

been performed. Main advantage of this spectral region is that it is less influenced by clouds. Most studies in this region of the spectrum rely on C-band, and mainly HV and VV polarisation. Different authors have reported contradictory results. In certain studies a decrease in backscatter intensity was found (Kasischke et al. 1992; Kneppeck and Ahern 1989; Landry et al. 1995) whereas other studies (Bourgeau-Chavez et al. 1995; French et al. 1994; Kasischke et al. 1994; Malingreau and Duchossois 1995) observed increases in backscatter intensity induced after the fire. A possible explanation for these inconsistencies is related to the alterations induced by the fire in the vegetation, vegetation structure and moisture content. The increase in backscatter intensity over burn scars could for instance be explained by an increase in soil moisture caused by permafrost melting. More recently, Tanase et al (2010) used bands X, C, and L backscatter to evaluate the sensitivity of these bands to estimate burn severity in Mediterranean pine forests.

1.3. METHODS FOR BURNED AREA DETECTION

Monitoring areas affected by biomass burning has been performed over the last decades using a wide variety of sensors, from very high-spatial resolution such as IKONOS for fine scales (Kachmar and Sanchez-Azofeifa 2006), to medium resolution sensors such as Landsat-TM/ETM+ or SPOT-HRV for regional coverage (Bastarrika et al. 2011; Pu and Gong 2004) and to coarse spatial resolution sensors for continental to global studies (Chuvieco et al. 2008a; Giglio et al. 2009; Roy et al. 2002; Tansey et al. 2008).

First detections of fire from space started with the work of Dozier (1981) and Matson and Dozier (1981), in which the thermal response of the Advanced Very High Resolution Radiometer (AVHRR) sensor (on board the NOAA satellites) was analysed. The first attempts to globally map burned areas were also based on AVHRR data, mostly using multi-temporal changes of vegetation indices (Kasischke et al. 1993), although hybrid algorithms based on thermal and optical channels were also developed (Fraser et al. 2000; Roy et al. 1999). Since then, a huge variety of sensors has been used to detect burned areas on local and global scales. On the global scale, the most relevant

ones are ERS-ATSR, NOAA-AVHRR, SPOT-VGT and NASA-MODIS on board AQUA and TERRA.

There are many ways in which the methods for burned area detection can be classified. Here we will differentiate between methods based on active fires, methods based on post-fire reflectance detection and hybrid methods. The techniques considered here are mostly focused on the development of algorithms on global scale, which is the main purpose of this PhD research. Requirements and design of these differ in many aspects to the local ones. Main differences are related to the spatial and temporal resolution, and also to the spectral bands present in the different sensors.

1.3.1. BASED ON ACTIVE FIRES.

In this approach estimation of BA is based on the initial detection of active fires. Since fires have much higher temperatures than other natural surfaces observations in the MIR band have been primarily used for detecting them. Thermal radiance (and consequently the signal amplification) increases exponentially with temperature, and therefore the signal of active fires is easier to detect than that caused by changes in reflectance. Parameterisation of the Planck function with typical fire temperatures indicate that in the MIR spectral region the spectral emission from a fire can be up to four orders of magnitude greater than that from the ambient temperature background. Active fire detection methods exploit this behaviour, and use normally information from TIR and MIR bands to discriminate active fires. The intense MIR thermal signals emitted by the fire make its detection possible even for fires much smaller than the pixel size. False alarms due to other increases in the MIR pixel signal (for instance, due to hot bare rocks or soil or Sun glint) need to be avoided when implementing these strategies, by diminishing them with the use of other spectral criteria.

The approximation used by most authors to determine the BA from these active fires (Eva and Lambin 1998; Giglio et al. 2006b; van der Werf et al. 2003; van der Werf et al. 2004), assumes that the burned area is proportional to the proportion of the pixel being burned and fire temperature.

Main limitations of this approach are related to the fact that thermal signal lasts very shortly (while the fires are active), implying that fires can be missed by the satellite

overpass if they last short. Therefore, mapping burned areas from active fires will be dependent on spectral sensitivity and acquisition frequency of the sensor used to detect fires. Omission errors are more frequent, but false alarms can also occur, especially for hot soils, urban areas and gas flares. In summary, detection of active fires provides a sampling of the total BA, i.e. what is currently burning when the satellite observes the area and therefore other methods need to be used to infer the BA.

In spite of these problems, several sensors have been used to obtain BA. The most used sensors have been NOAA-AVHRR (Grégoire 1993; Malingreau and Belward 1989; Martín et al. 1999), ERS and ENVISAT ATSR (Arino and Melinotte 1998), TRMM-VIRS (Visible and Infrared Scanner) (Giglio et al. 2003b), and MODIS (Moderate Resolution Imaging Spectroradiometer) on the NASA Terra and Aqua EOS satellites (Giglio et al. 2003a). Geostationary platforms such as VAS/GOES (Prins and Menzel 1992), and METEOSAT (particularly the second generation, MSG) are also able to provide active fire information (Calle et al. 2006; Cisbani et al. 2002; Costantini et al. 2006; Prins et al. 1998; Roberts et al. 2005). The advantage of geostationary sensors is the high revisit time (data acquired every 15 to 30 min), but the detection in this case is limited by lower temporal resolution (3 km) and worse performance over mid latitudes and polar regions.

From these sensors, a series of standard active fire products have been derived and are currently available: MODIS 14 (Giglio 2010) and World Fire Atlas (WFA) derived from ATSR-2 data (Arino et al. 2001). More recently a new algorithm to derive active fires from VIIRS was published (Schroeder et al. 2014).

A recent paper by Hantson et al. (2013) studied the performance of the MODIS 14 product, characterizing the omission and commission errors for a series of study sites covering different biomes and ecosystems. A study by Mota et al. (2006) screened the potential of the ESA's Wolrd Fire Atlas active fires product derived from ATSR-2.

1.3.2. BASED ON POST-FIRE REFLECTANCE CHANGES.

This section reviews previous algorithms for BA detection based on reflectance changes. The first section gives an overview on the possible treatments given to the bands and images coming from the satellite sensors. The other sections describe different options to perform the burned area detection on those, based on pixel detection, object

detection and multi-phase algorithms. As in many other remote sensing applications dealing with imagery, detection of features can be applied to either pixels or objects and the combination of them in different phases. This review does not aim at covering all the possible techniques available for these types of detection, but more to focus on illustrating some of the techniques used up to date to retrieve BA, by giving special attention to the ones that aimed at generating global algorithms.

1.3.2.1. Indices.

Computation of indices has been used in remote sensing to retrieve certain types of information such as vegetation health and status, burned areas or fire severity. It is based on establishing certain relations between the different spectral bands from the satellite sensor. They are useful to estimate several biophysical parameters, enhance certain features within the image, and to help monitoring them. One of the reasons why indices are preferred to the direct use of reflectance is that normally the formula to obtain them includes a ratio. This helps diminishing noise and atmospheric effects. Main indices that have been used and developed to detect burned areas are introduced hereafter. Once the information is computed and converted into the index form, several techniques can be applied to discriminate the BA.

One of the most used vegetation indices is the NDVI (normalised difference vegetation index) (Rouse et al. 1974). It is computed as:

$$NDVI = \frac{\rho_{NIR} - \rho_{RED}}{\rho_{NIR} + \rho_{RED}}$$

This vegetation index has proven to be very useful for vegetation monitoring. Its values go from -1 to 1, being the values close to zero areas with low vegetation. It has also been widely used for mapping of burned areas in a variety of studies. One of the first studies, developed by Malingreau et al. (1985) used NDVI based on AVHRR time series to map Borneo fires during 1982 and 1983. The NDVI index has also been used to map burned areas on boreal regions (Kasischke et al. 1993; Kasischke and French 1995) and Mediterranean ecosystems (Domenikiotis et al. 2002; Martín and Chuvieco 1993). The NDVI index sharply decreases when a fire occurs, as chlorophyll and leaf area are reduced. Although it is not the most sensitive to burns, a big advantage of this index is that most sensors cover the spectral range needed to compute it (NIR and RED).

Nevertheless, it can present confusion with features with similar spectral behaviour to a burned area, such as dark soils, water or cloud shadows.

A variation to this index, called SAVI (Soil adjusted Vegetation Index), was formulated by Huete (1988). It was proposed to diminish the sensibility of NDVI to variations caused by the soil background. Its formula is as follows:

$$SAVI = \frac{(\rho_{NIR} - \rho_{RED}) * (1 + L)}{\rho_{NIR} + \rho_{RED} + L}$$

where L is a parameter that takes into account the relevance of the soil reflectance background. When L=0 the NDVI and SAVI are the same. A common value of 0.5 is used.

Pinty and Verstraete (1992) proposed a modified vegetation index called GEMI (Global Environment Monitoring Index), where the non-linear combination of bands allows to minimise atmospheric and soil effects. Its formula is:

$$GEMI = \eta * (1 - 0.25\eta) - \frac{\rho_{RED} - 0.125}{1 - \rho_{RED}}$$

Where:

$$\eta = \frac{2 * (\rho_{NIR}^2 - \rho_{RED}^2) + (1.5 * \rho_{NIR}) + (0.5 * \rho_{RED})}{\rho_{NIR} + \rho_{RED} + 0.5}$$

The GEMI index enhances discrimination between dark and light surfaces. A decrease in its value will appear when a fire occurs. The higher discrimination power of this index compared to the NDVI has been shown in several studies (Barbosa et al. 1999b; Pereira et al. 1999a; Stroppiana et al. 2003).

Other indices have been specifically formulated to detect burned areas and to avoid some of the limitations of the vegetation indices.

The BAI (burned area index) (Martín and Chuvieco 2001) was formulated to discriminate recently burned areas, by enhancing the char signal of the fire affected areas. The formula is as follows:

$$BAI = \frac{1}{(\rho c_{RED} - \rho_{RED})^2 + (\rho c_{NIR} - \rho_{NIR})^2}$$

Where pc_{RED} and pc_{NIR} are convergence values for RED and NIR, respectively.

This index will increase its value after the fire. A study performed by Chuvieco et al. (2002) compared the discrimination power of BAI, with NDVI, SAVI and GEMI, showing the higher ability of BAI to discriminate burned areas, followed by GEMI, but confusion with dark areas was also reported.

Another option used for BA discrimination based on indices has been to modify the vegetation indices already presented by using the SWIR band instead of the red. As discussed in the previous section, SWIR band is more sensible than the VIS and therefore its use on vegetation indices increases the ability of those to detect BA, obtaining better results in the SWIR/NIR space than in the NIR/VIS. For instance the VI3 index (Kaufman and Remer 1994) uses the reflective component of the MIR band 3 of AVHRR instead of the red band in the NDVI formula. In the last years the NBR (Normalized Burnt Ratio) (Key and Benson 1999) has been widely used for burn severity analysis. The NBR is computed similarly to NDVI but substituting the red band by the SWIR. It is the same formulation as the Normalized Difference Infrared (NDII) (Hunt and Rock 1989), Normalized Difference Water Index (NDWI) (Gao 1996), Short Wave Vegetation Index (SWVI) (Fraser and Li 2002). Other indices used for BA detection are the Normalized Difference SWIR (NDSWIR) (Gerard et al. 2003), VI7 (López García and Caselles 1991), VI3T (Barbosa et al. 1999b) or MIRBI (Trigg and Flasse 2001).

1.3.2.2. Thresholds in Pixel based techniques.

One of the most extended techniques for BA detection based on pixels is the use of thresholds, especially when applied to the multi-temporal comparison of pre and post burn imagery, and using spectral vegetation indices (Fernández et al. 1997; França and Setzer 2001; Kasischke et al. 1995; Kasischke et al. 1993; Martín and Chuvieco 1995). The technique focuses on establishing a threshold that will separate the pixels in two categories: burned and unburned. It is important to highlight that the selection and use of this threshold will have a huge impact on the performance of the algorithm to detect BA. There are several ways to identify and classify the criteria used to define the threshold, depending on the variables used (statistic, empirical, temporal, fixed). A

possible way to separate them is by focusing on the static or dynamic (spatial and temporal) nature of the threshold.

1.3.2.2.1. Static thresholds

This approach has been widely used in several BA detection algorithms. A clear advantage is the simple computation. Main drawback is that it is difficult to establish thresholds that apply properly to a set of images, and to different biomes, seasons and conditions. One of the first studies, based on AVHRR (Kasischke et al. 1993) used NDVI pre and post fire composites. The burned areas were identified following the thresholds computed as a result of the differences between the two composites. Two thresholds were identified, a first one more restrictive (that underestimated BA) and a second one less restrictive, that was able to map up to 89,5% of the fires bigger than 2.000 ha. A way to improve these results was shown by Kasischke and French (1995), by adding information from post –imagery collected from the year after and two years after. They added two extra pixel conditions. First, with the use of the new images, only the new detections within a three pixels distance of the already classified BA were labelled as burned. Second, all pixels within a 4 pixels distance from the already classified and with an NDVI lower than a certain value were also classified as burned. Martín et al. (1995) applied differences in NDVI to AVHRR to map fires in Spanish Mediterranean areas. A static threshold of 0.2 decrease in the NDVI was used to classify the pixels as burned. Overall accuracy with this method was found to be 97,4%. Other studies have mapped BA based on thresholds but using other measures different from the NDVI. For instance, Fuller and Fulk (2001) mapped BA in Kalimantan (Indonesia) for the fires of 1997 with temporal composites of AVHRR images based on minimum albedo and maximum temperature. The thresholds in this case were based on NDVI and temperature and were adjusted on an iterative process, obtaining an overall accuracy of 80%. Eva and Lambin (1998) developed the E1 algorithm based on ATSR-2 imagery used to obtain the GLOBSCAR product. The thresholds in this case were based on absolute values for several bands: red, NDVI, SWIR and TIR and a relation between NIR and SWIR. Ershov and Novik (2001) used a comparison between the NIR of a specific date and the median value of the 10 previous days. They established a threshold to classify pixels with a certain decrease as burned. Static thresholds have also been used in combination with logistic regression (Koutsias and Karteris 1998, 2000).

1.3.2.2.2. Contextual spatial thresholds.

In this approach the thresholds are established considering the values of the neighbouring pixels. The procedure is normally based on moving windows. This technique helps overcoming some of the limitations of static thresholds but is also more demanding computationally. On this line, Piccolini and Arino (2000) developed the K1 algorithm for the GLOBSCAR project based on ATSR-2 imagery. The algorithm is based on an adaptive method that decorrelated possible variations due to atmosphere, illumination or other effects that had influence on the reflectance. They computed the K1 parameter, proportional to the geometric distance, obtained with a scattergram formed by the NIR/TIR bands in the pixel analysed. The convergence point was defined as the mean between NIR and TIR and the TIR variance, in a fixed window of 50x30km. The K1 value was determined only for pixels that had a specific behaviour in the NIR/TIR space. The threshold used for the K1 parameter was 10.5, which was an adequate value for different ecosystems. García-Haro et al. (2001), used also contextual spatial thresholds in the Mediterranean coast to map BA in 1992. First, mean and standard deviation of areas with higher probability of being burned were computed, on a moving window of 9x9 pixels. The central pixel of the window was considered burn if the absolute difference was higher than the standard deviation.

1.3.2.2.3. Contextual temporal thresholds.

In this case, temporal information is also considered to compute the contextual algorithm. The advantage is that more specific information will be obtained for each case, but having again a higher computational cost. An example of this technique can be found in Barbosa et al. (1999a), who developed a method to map BA in Africa using AVHRR imagery and static temporal and contextual spatial thresholds. First, temporal thresholding was used to identify areas where there was a decrease in both GEMI and VI3T indices, and an increase in band 3. Five static thresholds were used for GEMI, band2 and 3 and VI3T. Contextual spatial thresholds were also applied to the VI3T. Nielsen et al. (2002) developed a statistical method based on 10 multi-temporal images from AVHRR to map BA in Senegal. The BA was identified when there was a fast change in NDVI, temperature and albedo. The threshold was based on the statistics from the first image of the temporal series, where little burns had occurred. Zhang et al. (2003) also used static, temporal and spatial contextual thresholds combined to map BA in

Russia in 2001. They established the use of 10 thresholds on two composites based on VGT imagery. The first were based on the temporal decrease on the NIR, SWIR, NDVI, SWVI and red, and on pre and post values of those bands. Riaño et al. (2007) used the long temporal series of AVHRR to map burns in Africa from years 1981 to 2000. In order to obtain BA, the Barbosa et al. (1999a) method was applied, using a series of fixed and temporal thresholds applied to the bands 2, 3, GEMI an VI3T by computing median and standard deviation values.

1.3.2.2.4. Time series changes.

Temporal changes observed in a pixel time series have also been used to map BA. On this line, Roy et al. (2005), developed an algorithm that studies temporal changes in bands 2 and 5 of the MODIS time series. They compared the difference from measurements to the estimated reflectance. The estimated reflectance was obtained by inversion of a bidirectional reflectance model (BRDF model) based on a 16-day temporal window, considering that certain changes in the temporal series are related to fire burns. A statistical measure is used to identify the change between predicted and observed reflectance, establishing restrictions to avoid confusions. This algorithm is used to obtain the MCD45 product and is further detailed in section 1.4.

Boschetti et al. (2002) developed a similar method using VGT imagery. Individual images were used to invert the equation that defines the bi-directional component of reflectivity to predict a reflectivity day value, based on the prior evolution of this reflectivity. Also in this case, expected and measured values were compared in the NIR and TIR spaces. A pixel was classified as burned if criteria related to changes in the reflectivity and signal persistence were fulfilled.

1.3.2.3. Object based techniques.

The basis of object and segmentation level spatial information relies on identification of spatial attributes instead of basing it only on the pixel values. This approach first segments the image into spatially continuous, disjoint and homogeneous regions. There is a wide range of image segmentation types. A simple division of the techniques can be to classify them between pixel, edge and region based segmentation methods. Pixel

based includes image thresholding and segmentation in feature space. Edge segmentation finds edges between regions and determines the segments as regions within these edges. Region based segmentation algorithms can be divided into region growing, merging and splitting techniques, and their combinations. In this case the image is divided into sub-regions and these regions are merged or split based on their properties. A few studies have used segmentation techniques to identify BA. The main drawback of this technique is that when used on an unsupervised manner the classification might create confusion between burned areas and other categories (dark vegetation, water bodies, and shadows).

Object based analysis to detect BA was applied by Mitri and Gitas (2002) to a set of 3 Landsat TM images in the Mediterranean island of Thasos and also to the Hoya de Buñol region in Spain, to check the consistency of the model. Segmentation was applied to the images, classified afterwards with fuzzy logic. Each class within the classification scheme contained a class description, based on a set of fuzzy expressions. A three level scale of segmentation was created in order to obtain different types of information from smaller and larger objects. Neighbouring objects with identical structures were merged. The study obtained an overall accuracy of 98.85%.

On the same line, Gitas et al. (2004), applied object based image classification to map BA on Creus Cape in Spain, based on AVHRR imagery. The model used spectral and contextual object information to obtain the BA, showing an overlap of 90% with the official burned area map, and demonstrating the potential use of object based methods to map BA with coarse resolution sensors.

In 2006, Quintano et al. (2006), used spectral mixture analysis (SMA) to map burned areas in the Mediterranean using NOAA AVHRR and Landsat TM imagery. A single-post fire image was required to perform the analysis. The method was based on the contextual classification of the fraction images obtained after applying the SMA. Results showed that the proposed method could accurately identify the burned surface area with a kappa coefficient of 0.8.

Later on, Polychronaki and Gitas (2010) developed an operational procedure to map BA based on ASTER imagery, by developing the method for an area in Portugal and then applying it to another ASTER image to map BA on the island of Rhodes, Greece. The

method applied segmentation on three scales and a classification based on intrinsic, topological and semantic features. Comparison with official maps showed a level of agreement of 92.5%. The same procedure was applied to the Rhodes Island, and compared to a perimeter derived from an IKONOS image, showing a level of agreement of 80.6%. The authors noted that modifications of thresholds would be necessary if applied to other areas.

In 2014, Dragozi et al. (2014) used the Fuzzy Complementary Criterion (FuzCoC) and Support Vector Machine (SVM) to map burns on VHR IKONOS imagery, in the areas of Parnitha and Rhodes in Greece. The classification accuracy obtained with the SVM object-based scheme was higher than with the pixel-based approach.

More recently, Shimabukuro et al. (2015), estimated BA in Mato Grosso, Brazil, with the help of an object based classification method applied to Landsat imagery. In this case, the semiautomatic method was adapted from the one used in the TREES-3 pan-tropical deforestation survey (Achard et al, 2014). Results were overlaid with MODIS HS, and visual interpretation was used to identify confusion cases. BA estimates were compared to a method developed by the Brazilian Institute for Space Research, applied to a wall-to-wall coverage of Landsat-5 TM imagery and to the MCD64, finding that the object based method obtained statistically valid estimates of burned areas for the Brazilian State of Mato Grosso in a more efficient manner. Furthermore, it enabled the inclusion of small burn scars typically missed by coarse resolution satellites.

1.3.2.4. Multi-phase algorithms

Multi-phase algorithms have been developed to overcome the limitations of the techniques previously reviewed. They are based on the combination of thresholds, multi-temporal and spatial analysis. Multiphase algorithms normally identify on the first phases the most clearly burned pixels, and then decrease the strict conditions applied in these early stages on the later phases of the algorithm, to improve the delimitation of burned areas. This approach has proven to give good results, and to offer a good way to balance omission and commission errors. This technique was first proposed by Martín and Chuvieco (1995) to map BA with AVHRR images. Benvenuti et al. (2001), applied this procedure to map BA in Italy using Landsat imagery. On the first

phase, pixels more likely to be burned (seeds) were identified, leaving the areas less affected by fire not detected in this phase. Afterwards, a region growing algorithm was applied. Following the same model, the ITALSCAR project (Paganini et al. 2003) mapped BA in Italy using Landsat data for years between 1997 and 2000. Seed pixels were identified in this case through time series change detection, applying a series of thresholds and a region growing algorithm in the second phase.

Vafeidis and Drake (2005) used a two-phase approach and combined thresholds on indices previously developed by Pereira et al. (1999a) and Barbosa et al. (1999a), and sub-pixel detection techniques. On the first phase, thresholds were computed for NDVI, VI3 and VI3T based on median and standard deviation values. On the second phase, the method developed by Razafimpanilo et al. (1995) and a sub-pixel detection technique were applied.

Chuvieco et al. (2008b) also developed a two-phase method to map BA bigger than 250ha in South America, using MODIS 32 day composites. The products were obtained for year 2004 in the framework of the Area Quemada (AQL) project. The indices used to identify BA were BAI and NBR, and combined static thresholds and a multi-temporal approach. Chuvieco et al. (2008a) also developed a multiphase approach to map BA on the boreal forests of Canada with AVHRR data, obtaining a time series for years 1984 to 2006. For this, they built 10 days composites, and detected on the first phase the seed pixels based on temporal thresholds from BAI and GEMI indices. Then, a contextual algorithm was used for the second phase, considering the changes in the GEMI index with more relaxed conditions. Bastarrika et al. (2011) used a multiphase technique to detect burned areas based on Landsat images. In this case, the BAI index and statistical thresholds were applied to identify the seeds. On the region growing, three options were tested, concluding that the one using fixed thresholds gave better results.

1.3.3. HYBRID ALGORITHMS

In this type of algorithms both active fire detection and post fire reflectance detection are combined. This implementation makes profit of the advantages of both techniques, i.e. the more sensitive thermal characterisation of active fires and the more permanent

reflectance changes of burned patches. In general, active fire detections are used to identify burned pixels or to select polygons if an object based classification has been used.

One of the first hybrid approaches was presented by Roy et al. (1999) using AVHRR and MODIS to obtain BA maps. Active fires from AVHRR were used to identify burned pixels and to obtain mean and standard deviation statistics, in order to later classify the rest of the pixels. Composites were created to compute the statistics. They were based on the difference between maximum and minimum pixel values of the VI3 index. The procedure was used to map burned areas in South Africa with a good level of agreement compared with visual interpretation of the AVHRR images.

Fraser et al. (2000) proposed the HANDS (Hotspot and NDVI differencing synergy) algorithm using AVHRR data. On a first step, HS were filtered by checking consistency with an NDVI difference image. The filtered HS were then used to derive a series of regional and local thresholds, based on median and standard deviation statistics, to classify the BA. The algorithm was used to map BA in Canada for 1995 and 1996. A similar version was used by Fraser and Li (2002), to map Canadian fires in 1998 and 1999 using SPOT-VGT data. In this case, the index was computed using the SWIR band instead of the red. Sukhinin et al. (2004) applied a similar technique to MODIS imagery to map BA in Russia. Here, the region growing algorithm was based on the Euclidean distance to the active fires and was applied to composites formed by bands 1, 2 and 5. Gong et al. (2006) mapped burned areas in California from AVHRR data with a modified version of the HANDS algorithm, and used 13 NDVI composites based on 10 days images. Pu et al. (2007) also used AVHRR images to map fires in California, for years 1989 and 2000, based on the HANDS algorithm.

Soja et al. (2004) combined AVHRR active fires and imagery to map BA in Siberia. Active fire detection was based on 5 different tests, and BAs were visually identified, using bands 1, 2 and 5. The final BA was computed by adding the BA already identified to the active fire detections outside of these BA. Kucêra et al. (2005) combined active fires with temporal changes in vegetation indices, and statistic thresholds, to AVHRR imagery to detect BA in China and Russia.

Several studies have combined the active fire product from MODIS (MOD14A1) with MODIS imagery. Loboda et al. (2007) used the 8 day composite (MOD09A1) with the active fire product to apply the technique developed by Roy et al. (1999). In this case

the thresholds were derived from the pixels where there was an active fire detection. George et al. (2006) used the 16-day BRDF corrected product (MCD43B4) to map forest changes in Siberia between 1992 and 2003. Based on an index computed from bands 2 and 6 from MODIS, they applied a contextual algorithm to identify the BA, using statistic thresholds obtained with the active fire information and individual images. Changes in NDVI composites were also used to improve the detection for years 2002 and 2003.

Giglio et al. (2009), presented an hybrid algorithm that combined active fires and MODIS reflectances to obtain a new global BA product. On a first step, seed pixels were identified, based on the VI index (obtained from bands 5 and 7) and active fires. Thresholds were established based on separability, temporal and probabilistic criteria to classify the BA. The technique is further detailed in section 1.4, since this algorithm is used to obtain the MCD64 fire product, which is the basis for the burned estimations of the global fire emissions database (GFED). According to validation results (Padilla et al. 2015) this product is the one with better accuracy from the global BA products evaluated in this study. It is currently widely used by climate modellers (Mouillot et al. 2014).

1.4. REVIEW OF EXISTING BURNED AREA PRODUCTS

In the last years several global burned area products based on satellite observations have been released. They are based on coarse resolution sensors, since these offer a better temporal resolution than sensors with higher spatial resolution. Global BA products are commonly used in the context of climate modelling and in global dynamic vegetation models.

The sensors that have been mainly used to detect burned areas on a global scale are: AVHRR, MODIS, SPOT VGT, ATSR2 and AATSR. Table 1 summarises the existing BA products and the sensors used in each case. A summary of the methods to obtain these products is available hereafter. Regional scale products are also reviewed as well as fire products obtained with the MERIS sensor.

Table 1. Global burned area collections.

	Sensor	Time series	Spatial res	Type of algorithm/detection	Reference
MCD 45	MODIS Aqua Terra	2001-present	500m	Bi-directional reflectance model- based change detection approach	(Roy et al. 2005)
MCD 64	MODIS Aqua Terra	2001-present	500m	HS and multi temporal spectral indices changes	(Giglio et al. 2009)
GBA 2000	SPOT VGT	11/1999-12/2000	1km	Multi temporal changes in daily reflectances or spectral indices (IFI and UTL algorithms)	(Ershov and Novik 2001) (Silva et al. 2003) (Grégoire et al. 2003)
GBS	NOAA AVHRR	1982-1999	8 km	Multi temporal change detection	(Carmona-Moreno et al. 2005)
GLOBSCAR	ERS2-ATSR2	2000	1km	K1: contextual algorithm based on geometrical characteristics of burned pixels in the near-infrared (NIR, 0.87 μm) / thermal infrared (TIR, 11 μm). E1: series of fixed thresholds applied to the data from four spectral channels.	(Piccolini and Arino 2000) (Eva and Lambin 1998)
GLOBCARBON	ERS2-ATSR2 SPOT VGT AATSR	1998-2007	1km	Based on two GBA2000 algorithms (IFI and UTL) and GLOBSCAR (K1 and E1).	(Plummer et al. 2007)
L3JRC	SPOT-VGT	2000-2007	1km	Temporal index, based on GBA2000 experience.	(Tansey et al. 2008)
GEOLAND 2	SPOT-VGT	1999-present	1km	Temporal index and thresholds	(http://www.geoland2.eu/)

1.4.1. GBS

Carmona-Moreno et al. (2005) used daily global observations from the Global Area Coverage (GAC) version of NOAA/AVHRR images, covering the period between 1982 and 1999 to create a weekly global burned area product at 8km spatial resolution. The algorithm used data from AVHRR channels 1–3, extending the approach of Barbosa et al. (1999b). Fire seasonality and fire distribution data sets were integrated as 0.5 degree resolution fire probability grid maps. Comparison with independently available fire data

indicate that although the time-series is inadequate to make quantitative and accurate estimates of global burned area, it is suitable to assess changes in location and season of burning at the global scale. It was concluded that the Pathfinder 8km dataset was affected by spurious temporal trends, limiting the temporal consistency of burned area products. Its low spatial resolution very likely lead to substantial underestimation of area burned in extensive areas of the planet.

1.4.2. GBA2000

The GBA2000 product was an initiative from the European Commission Joint Research Centre (JRC). It was based on SPOT VGT imagery and delivered a monthly product at 1km resolution for the year 2000 (Grégoire et al. 2003; Tansey et al. 2004). A series of algorithms were developed by an international network of partners, in order to take into account different ecosystems and the variety of climatic conditions worldwide. The various continental/regional maps were subsequently patched together to form a global product. A total of 11 regional algorithms were developed. The International Forest Institute (IFI) developed the IFI algorithm in Russian areas (Ershov and Novik 2001), Universidad Técnica de Lisboa (UTL) and Instituto de Investigación Tropical (TRI) developed the UTL algorithm for Africa Europe and Asia (Silva et al. 2003; Silva et al. 2002). The Canadian Centre for Remote Sensing (CCRS) developed the algorithm for Canadian regions (Fraser et al. 2003; Fraser et al. 2004). Universidad de Evora with UTL and TRI created the Brazilian algorithm (Silva et al. 2002). The JRC developed the algorithm for Australia (Stroppiana et al. 2003; Stroppiana et al. 2002). The Greenwich University established the algorithm for Eastern South Africa (Boschetti et al. 2002), Institute for Electromagnetic Sensing of the Environment (IREA) in Italy developed another algorithm for Africa (Brivio et al. 2002). JRC developed an algorithm for Central America at JRC (Tansey 2002). Data classification approaches used included change detection analysis, multiple logistic regression, Multi-Layer Perceptron (MLP) neural networks, expectation-based BRDF model inversion, classification and regression trees, and linear discriminant analysis. Overall, more than 3.5 million km^2 of burned areas were estimated, approximately 80% of which occurred in shrublands and woodlands. According to those estimates, about 17% of the burned area affected grasslands and croplands, and 3% occurred in forests (Tansey et al. 2004).

1.4.3. GLOBSCAR

The GLOBSCAR product was obtained in the framework of the GLOBSCAR project from the European Space Agency. It provided monthly burned area maps at 1km spatial resolution using information from the Along Track Scanning Radiometer (ATSR-2) instrument on board the ESA ERS-2 satellite. The product was obtained for year 2000. The image classification procedure combines two distinct algorithms, K1 and E1. K1 (Piccolini and Arino 2000) is a contextual algorithm based on the geometrical characteristics of the burned pixels in the near-infrared (NIR, 0.87μm) / thermal infrared (TIR, 11 μm) space. This algorithm presented systematic errors in some ecosystems and it was complemented with a second algorithm, the E1 algorithm (Eva and Lambin 1998) that applied a series of fixed thresholds to the data from four spectral channels and to the NDVI. A pixel would be classified as burned only if both algorithms were detecting it.

The products were validated against other field and remote sensing data (Simon et al. 2004). Commission errors were uncommon and affected mostly scattered pixels. The only large area of commission errors was due to older burned areas, in the mixed and evergreen needle leaf forests of Canada and, probably, also in similar ecosystems across Russia. Omission errors were common and very important in some regions, such as the United States (open shrubland and grassland areas), Australia (open shrubland), Zimbabwe (cropland), and Brazil (broadleaf evergreen forests).

1.4.4. GLOBCARBON

The European Space Agency GlobCarbon project, under the DUE programme, generated a global monthly 1-km burned-area product, using two regional GBA2000 (IFI and UTL) algorithms and the GLOBSCAR algorithms (K1 and E1) applied to 1-km SPOT VEGETATION and ERS2–ATSR2/ENVISAT AATSR data respectively, covering the period between 1998 and 2007. The project was developed in cooperation with the International Geosphere-Biosphere Program (IGBP), the International Human Dimensions Programme (IHDP) and the World Climate research Programme (WCP). The project aimed at obtaining vegetation temporal evolution information to be used in Dynamic Global Vegetation Models (DGVM) and Atmospheric Transfer Models (ATM). In addition to burned areas, other variables such as FAPAR, LAI and VGC were produced.

1.4.5. L3JRC

This product was developed by the University of Leicester, Catholic University of Louvain la Neuve, TRI and JRC. The sensor used to produce the BA was SPOT VGT with 1km resolution. The product was obtained for years 2000 to 2007. The algorithm was based on the one designed by Ershov and Novik (2001) for the GBA 2000, using a temporal index in the NIR for the detection (Tansey et al. 2008). Median and standard deviation of the index were computed for a moving window of 200 by 200 pixels. The pixel would be considered burned if the index was smaller than the median minus two times the standard deviation of the regional window. The total area burned each year (2000–2007) was estimated to range from 3.5×10^6 km^2 to 4.5×10^6 km^2.

1.4.6. MCD45

The MCD45 BA product is delivered by NASA as a level 3 standard product. It is obtained with the information from the MODIS sensor on board the EOS TERRA and AQUA satellites. MODIS bands 2 and 5 were identified to be the ones that better discriminate BA (Roy et al. 2002). The algorithm is based on temporal differences of observed versus predicted reflectance using the inversion of a bidirectional reflectance model (Roy et al. 2005). The model is applied on a sixteenth day temporal window where at least seven cloud free observations are needed in this temporal window to be able to invert the BRDF model. The algorithm deals with angular variations in multi-temporal data and uses a statistical measure to detect change from a previous state. Large discrepancies between predicted and observed values are attributed to change. A temporal consistency threshold is used to differentiate between sporadic changes, considered as noise, and persistent changes interpreted as burns. The product is delivered at 500 meters resolution, and apart from the BA date of detection, other fields are delivered: confidence layer, number of observations used for the BRDF inversion, land cover of the pixel and the number of consecutive days where information was not available.

1.4.7. MCD64

The second MODIS product, the MCD64, is part of the Collection 5.1 Direct Broadcast products. It is based on an hybrid algorithm combining active fire detections (1km) and

multi-temporal changes in spectral indices (500m bands) (Giglio et al. 2009). The algorithm is based on several steps. A time series extraction is performed to obtain valid pixels (cloud free and not coincident with an active fire detection on the same day). Afterwards, a spectral index (VI) based on bands 5 and 7 from MODIS is computed and used to create composites of potential pre-and post-burn dates, and obtaining a series of statistics (median and standard deviation). A measure of spectral separability is based on these values and a measure of temporal texture is also obtained. Burned and unburned training pixels are identified using spatial and temporal active fire information; to extract conditional probability densities for each land cover class. A measure of separability is then computed to ensure the discrimination ability between burned and unburned classes. A burned probability is then obtained and an initial classification is performed based on a series of rules. A final classification with a one pass filter is applied to the initial classification to obtain the final BA product estimation. The product is delivered at 500m resolution. This product is the basis for the BA estimation included in the GFED (Global Fire Emissions Database)(Giglio et al. 2013), widely used by climate and carbon modellers. GFED v4 is derived from the MCD64A1 product aggregated to 0.25° spatial resolution for the period 2000-present. Prior to 2000, GFED BA estimates are obtained by calibrating active fire data from the Tropical Rainfall Measuring Mission (TRMM), Visible and Infrared Scanner (VIRS) and Along-Track Scanning Radiometer (ATSR) with the MCD64A1.

1.4.8. GEOLAND-2.

The BA GEOLAND-2 product is derived from the SPOT-VEGETATION information. This product is an improvement of the GBA200 and the L3JRC products (Tansey et al. 2008). The V1 version of the GEOLAND2 BA product has been improved removing the need to use land cover maps, making possible processing the data with a near-real-time 10-day product. It uses the daily global atmospherically corrected SPOT/VGT synthesis (S1 products) and the algorithm detects burned areas using a temporal index in the near infrared band. The product provides the date of detection of burned areas at a spatial resolution of 1km.

1.4.9. THE EUROPEAN FOREST FIRE INFORMATION SYSTEM (EFFIS).

In 1999 JRC developed a research group with the aim to develop and implement methods to evaluate risk of forest fires and map burned areas on a European Scale. These activities led to the creation of the European Forest Fire Information System (EFFIS). Its objective is to provide information for European forest protection, by treating both pre and post fire conditions. There are two modules within the system: FDA and RDA. In the Fire Damage Assessment (FDA), burned area perimeters are obtained at the end of each season for fires bigger than 5-10 ha. Initially, the data used for this mapping was based on WiFS imagery at 180m. Currently, AWiFS is used, with spatial resolution of 56m. A second module, the Rapid Damage Assessment (RDA) was created after the extreme fire season of 2003 in Portugal, and aim to map burned areas bigger than 50ha on a daily basis. The imagery used for this purpose was coming from the MODIS sensor at 250m. The algorithm was based on the identification of active fires, with a region growing algorithm and reviewed with a final visual interpretation.

1.4.10. MERIS-BASED BURNED AREA STUDIES.

MERIS was primarily designed to provide quantitative ocean-colour measurements (Rast et al. 1999). However, its spectral characteristics make it appropriate to also serve applications like land surface and atmospheric characterisation. It is well known that one of the major drawbacks of MERIS images for BA identification is the lack of SWIR and MIR bands which as discussed in the previous sections, are useful to discriminate burned surfaces from water and non-combustible land cover and to detect active fires. On the other hand, its multi-spectral imaging capabilities in the VIS/NIR region of the spectrum and moderate spatial resolution, may in part circumvent this limitation. Moreover, the sensor was especially designed to detect chlorophyll concentration having bands in the red edge (located in the maximum of chlorophyll absorption). Such bands may be of use for BA detection, since an abrupt decrease in the chlorophyll content may be related to a fire.

Regarding fire applications, very few studies have been conducted using MERIS. Among the existing studies, there is one developed by Huang and Siegert (2004), where Level 1b MERIS RR product was used to identify smoke plumes. The BA detection was

achieved combining night time AATSR fire hot spots with BA detected with Advanced Synthetic Aperture Radar (ASAR). Another study concerning the estimation of fire severity using MERIS FR Level 2 imagery and MODIS daily reflectivity product (MOD09GHK) was conducted by Roldan-Zamarron et al. (2006). The BA mapping was performed applying the matched filtering method (Boardman et al. 1995) to Landsat TM data. Fire severity levels were then estimated through use of different techniques to MERIS and MODIS images. The authors concluded that, in general, the fire severity estimation performed by MERIS was more accurate than the one performed by the global product of MODIS. Gonzalez-Alonso et al. (2007) applied the same technique to MERIS FR Level 1b imagery to estimate fire severity levels and BA at a local scale. Validation performed comparing obtained results with the ones obtained using SPOT-5, showed a fairly high correlation between both sensors. Aiming to evaluate the ability of some sensors on the estimation of burn severity levels, Chuvieco et al. (2007) performed a comparative study using SPOT-5, Landsat TM, MERIS and MODIS. They concluded that Landsat TM was the one presenting the best performance. Nevertheless, MERIS proved to be capable of correctly identifying the spatial pattern distribution of the severity levels. It is worth noting that the above studies are not specifically oriented to burned area mapping, but rather to the analysis of some aspects related to level of damage caused by fires.

Only two works have been found in literature in relation to burned area mapping. The first one used Spectral Angle Images (SAI) technique at a regional scale (Oliva et al. 2011). The SAI methodology makes use of a reference spectrum (end members) obtained from the image (SAI-image) and from the field spectral measurements (SAI-field). The study used MERIS FR Level 2 images and compared BA discrimination using traditional vegetation indices (e.g., BAI, GEMI, η, NDVI) with SAI technique. Validation was carried out using AWiFS images. Results showed that index η (a component of the GEMI calculation) and the SAI-image were the ones that presented higher accuracy. According to the author, NIR bands in the red edge (bands 9 to 12) region present a higher power of burned area discrimination than NIR bands (bands 13 to 15), in the spectral region traditionally used by the sensors designed for earth observation (Oliva et al. 2011). From these ones, when using only one post-fire image, band 10 (in the spectral range 750 nm – 757.5 nm) was the one with the highest discrimination power, even though all NIR bands (from band 10 to band 14) presented similar discrimination

power. On the other hand, when using spectral indices for purposes of burned pixels detection, band 10 in the red edge and band 8 in the red region, were the ones with highest discrimination power.

The second study was conducted by González-Alonso et al. (2009). They used MERIS FR Level 1b data for burned land discrimination at a regional scale. The method used in a synergetic way fire hotspots from MODIS with NIR reflectance values from MODIS and MERIS imagery. The algorithm computed a threshold that maximized the agreement between the burned areas discriminated using the NIR band of a post-fire image and the existence of an active fire as detected by MODIS. Validation was performed using an image from AWiFS and obtained results were very similar when using MODIS and MERIS reflectance values, although slightly better in the case of MERIS. These studies were applied to the Northern Western part of the Iberian Peninsula in summer 2006 and to the Province of Heilongiang in the North of China, in the framework of the ESA DRAGON-2 project (González-Alonso et al. 2009).

Studies performed at regional scale show the potential of this sensor to detect burned areas, especially when using hybrid algorithms. This thesis is the first attempt to use MERIS data to obtain a global burned area product.

CHAPTER 2

OBJECTIVES

Nowadays climate change has become an acknowledged environmental fact. In words of the IPCC "scientific evidence for warming of the climate system is unequivocal" (IPCC 4th Assessment Report, Synthesis Report, Observed Changes in Climate and their Effects, page 1). Its relevance has been recognised in a variety of papers and studies, which are summarized in the IPCC reports. In fact, the IPCC first assessment report from 1990, gathered some of these facts and favoured the creation of the UNFCCC in 1992. One of the main tasks of the UNFCCC was to establish a systematic observation and development of data archives to monitor the climate system. In order to do so, the GCOS, also created in 1992, was identified as the mechanism to pursue these tasks. In 2003, on its second report, the GCOS established a list of Essential Climate Variables, which are physical, chemical or biological variables, or groups of linked variables, that critically contribute to the characterization of Earth's climate (Bojinski et al. 2014). Therefore ECVs are key parameters of the Earth system, needed to monitor climate and identify relevant changes. GCOS identified 50 ECVs that could be monitored, comprising atmospheric, oceanic and terrestrial domains. The complete list of these ECVs is detailed in Table 2.

Table 2. GCOS ECVs.

Domain	GCOS Essential Climate Variables
Atmospheric (over land, sea and ice)	Surface: Air temperature, Wind speed and direction, Water vapour, Pressure, Precipitation, Surface radiation budget. Upper-air: Temperature, Wind speed and direction, Water vapour, Cloud properties, Earth radiation budget (including solar irradiance). Composition: Carbon dioxide, Methane, and other long-lived greenhouse gases, Ozone and Aerosol, supported by their precursors.
Oceanic	Surface: Sea-surface temperature, Sea-surface salinity, Sea level, Sea state, Sea ice, Surface current, Ocean colour, Carbon dioxide partial pressure, Ocean acidity, Phytoplankton. Sub-surface: Temperature, Salinity, Current, Nutrients, Carbon dioxide partial pressure, Ocean acidity, Oxygen, Tracers.
Terrestrial	River discharge, Water use, Groundwater, Lakes, Snow cover, Glaciers and ice caps, Ice sheets, Permafrost, Albedo, Land cover

	(including vegetation type), Fraction of absorbed photosynthetically active radiation (FAPAR), Leaf area index (LAI), Above-ground biomass, Soil carbon, Fire disturbance, Soil moisture.

In 2006, GCOS established the systematic observation requirements for satellite based products for climate (GCOS, 2006). The specifications aim at characterizing the state of the global climate system and enabling long term climate monitoring. This document enhances the need to use satellite measurements to monitor the Earth. In fact observations from space provide a unique way to monitor and gather information about the climate system, since they allow obtaining global coverage and continuous measurements.

In this context, the European Space Agency set up the Climate Change Initiative (CCI) (cci.esa.int last access November 2015) programme to respond to this need for climate quality satellite data. The aim of the CCI is to monitor and provide stable and long term ECVs data, derived from multiple satellite datasets, and to make this information available to the scientific community. The programme has a budget of 75Meuros, with two phases identified, running from 2009 to 2017. Thirteen projects have been selected as the ECV's to be monitored within the programme. These projects make use of the wide range of satellite data available, as can be seen in Table 3.

Table 3. Satellite data used by the 13 ECV projects of ESA's CCI

(circle: primary contribution, square: indirect contribution or validation activities)

(Source http://cci.esa.int/content/cci-projects)

	SST	Sea level	Ocean colour	Sea-ice	Clouds	GHG	Aerosol	Ozone	Fire	Land cover	Glaciers	Soil moisture	Ice sheets
AATSR/ATSR-2/ATSR-1	●				●		●		●				
MERIS			●		●	■	●		●	●			
SPOT 4,5											■		
SPOT VGT									●	●			
Landsat TM/ETM+				■							●		●
SAR (ENVISAT/ERS/ALOS/TSX/PALSAR)				■						●	●		●
SEVIRI	●				■								
MODIS			●	■	●		●						
Sciamachy						●	●	●					
GOSAT						●							
GOME-1/2							●	●					
AVHRRs	●				●		●						
GOMOS							●	●					
IASI						●							
AIRS						●	■						
AMSU						●							
ACE						●		●					
SeaWIFS			●										
MIPAS						●		●					
OMI							●	●					
Radar Altimeters (TOPEX-POSEIDON)		●											
Radar Altimeters (JASON-1/2)		●											
Radar Altimeters (GEOSAT-Follow-on)		■											
Radar Altimeters (ENVISAT, ERS)		●		●							●		●
Scatterometers				●								●	
SMMR				●								●	
TMI	●											●	
SMOS												●	
AMSR-E	●			●								●	
WINDSAT												●	
SSM/I & SSMIS				●								●	
PARASOL							●						
ASTER											●		■
ICESAT				■							●		
ODIN/OSIRIS							■	●					
ODIN/SMR							■	●					
POLDER							●						
CRYOSAT				■									
CALIPSO/Caliop					■								
CLOUDSAT/CPR					■								
TOMS							■						
RadarSAT											■		■
TerraSAR-X											■		■
Cosmo-Skymed											■		■
ALOS Palsar											■		■
IRS1C/1D											■		

One of these projects, the fire_cci project, responds to the need to monitor the identified ECV "fire disturbance". The first phase of the fire_cci project aimed at developing algorithms (for the MERIS, VGT and ATSR data) to obtain long-term and consistent time series of burned area (BA) information, with proper error and uncertainty characterization, and to improve the use of this information by climate modellers.

The work presented in this thesis has been developed within the framework of the fire_cci project and has therefore implicitly the aim of contributing to the international initiatives and programmes mentioned, by monitoring burned areas on a global scale, in

order to study its relation to climate change. More in particular, the main objective of this thesis was to develop an algorithm to detect burned areas on a global scale from the MERIS sensor. In order to achieve it, several factors were considered, related to the study and implementation of the different techniques and approaches required to obtain the algorithm. Within this main objective three major aims were identified:

1- First, study the spectral behaviour of burned areas, which will be very diverse on a global scale, together with the use of specific MERIS bands and indices optimal for the retrieval of burned areas.

2- Second, develop and test different procedures to incorporate the MERIS input data into the algorithm (composites, individual images), as well as required auxiliary data (MODIS).

3- Third, develop and implement different techniques to obtain a two-phase algorithm. Seed and growing phases of the algorithm were tested with different approaches in order to identify the optimal configuration for the algorithm.

These objectives were related to the election of MERIS as the main input sensor for detecting global BA. This choice was based on the requirements of ESA for the fire_cci project, as there was a strong interest in the of use European datasets. In addition to this interest, the scientific challenge was also relevant, as the use of MERIS imagery in its full resolution mode would allow obtaining a BA collection with higher spatial resolution than the existing ones (300m versus the 500m resolution offered by current BA collections). It was also foreseen within this thesis to test the impact this resolution improvement might have in the detection of fires (especially small fires, which according to Randerson et al. (2012) contribute to 35% of the fire emissions), and on the fire perimeter characterization. In order to study the BA estimation results and the resolution impact, the product was validated and compared with other BA estimations. On the validation side, a complete strategy was put in place within the fire_cci project, using Landsat derived fire perimeters (Padilla et al. 2014). An added assessment exercise was developed in the framework of this thesis, based on fire perimeters obtained from national agencies, and that cover large areas. This exercise would help

understanding the size of fires detected. A comparison with the main BA collections that currently exist was also foreseen. The objective of this comparison study was to check the consistency with other products as well as to highlight and identify areas where the products had better and worse performances, in order to diminish the uncertainty relative to each one of them.

MERIS (MEdium Resolution Imaging Spectrometer) was an instrument on board ENVISAT, launched in 2002 and active until 2012. The use of this sensor has a specific interest to make use of European capabilities and to ensure continuity, since its successor the OLCI on-board Sentinel 3 (launch date December 2015), will have similar characteristics. Therefore an additional interest of this thesis was to test the viability of obtaining a semi-operational BA product based on MERIS. Similar sensors could benefit from similar approaches to the one used in the MERIS BA algorithm to obtain BA products. This way continuous monitoring of fire disturbance from space would be ensured.

CHAPTER 3

BA ALGORITHM DEVELOPMENT AND TESTING

3.1. CHAPTER OVERVIEW.

In this chapter the methods developed and tested to obtain the algorithm to detect BA will be presented. At the beginning of the algorithm development a series of tests were designed. The results obtained with these tests were used to modify the initial version of the algorithm, and to develop other ideas. Although the main aim of this chapter is to introduce the methods for the algorithm development, some test results will also be introduced, as they are needed to illustrate certain choices and further steps taken.

The first part of the chapter gives an overview of general considerations and aspects required and needed to build the algorithm. This includes the product to be obtained, as well as the study sites used to perform the algorithm tests, the validation sites, the pre-processing, the main characteristics of the sensor used, and the auxiliary input data. On the second part of the chapter, the main aspects to be taken into account for the algorithm design are presented, introducing the bands to be used, the compositing criteria and the seed and growing phases of the algorithm. At the end of the chapter, a wrap-up of the final algorithm configuration is introduced.

3.2. BA PRODUCT REQUIREMENTS.

The product obtained with the MERIS algorithm has the purpose to contribute to the monitoring of the ECV fire disturbance as well as providing the users (climate, atmospheric and vegetation modellers) with a product that would satisfy their needs. GCOS three target requirements expressed in 2006 (GCOS 2006) are as follows:

- Accuracy: 5% (maximum error of omission and commission)
- Spatial resolution: 250m horizontal resolution
- Temporal resolution: daily observing cycle.
- Stability: 5%.

User consultations were performed at the beginning of the project to determine product requirements (Mouillot et al. 2014). Main specifications are (Schultz et al. 2011):

- Accuracy: ideal = 5% error, reasonable = 15%, minimum = 25% error, with demonstrated systematic and adequate validation using internationally agreed validation protocol.

- Unbiased product.
- Temporal resolution:
  - daily data with original spatial resolution of the sensor.
  - weekly, 10-day or monthly basis on grid scale.
- Spatial resolution: originally 250 m (or minimum 500 m), horizontal resolution 1km acceptable, 0.5 degree or higher resolution on grid scale.
- Error traceability and uncertainty characterisation: in a manner that can be easily understood and utilised by users in various applications.
- Temporal stability and consistency: highest standard 5% (temporal stability in annual continental-scale averages), 15% acceptable.
- Long-term series data:
  - understanding the long-term fire, climate and vegetation interaction.
  - can be made from various sensors but temporal consistency is essential.
- Easy access to data: standard formats (Netcdf preferably).
- Auxiliary information and metadata: vegetation cover; burn severity...

It is important to note that these GCOS and user requirements are difficult to reach. Some of these requirements can be considered unrealistic with current technologies. For instance, a recent accuracy assessment of several global BA products found that none meet the commission and omission error limits (Padilla et al, 2015). Nevertheless, they can be seen as guidelines, and reachable purposes in some cases.

The internal climate users of the fire_cci project helped to define the variables that should be included in the BA product. These recommendations were the basis for the Product Specifications (Chuvieco et al, 2014). Following these specifications, two products were generated from the output of the BA algorithm: pixel and grid. The former includes the date of burn detection, the confidence level and the burned cover. It is delivered in geotiff monthly files, at 300m resolution. From the pixel product, the grid product variables were generated every 15 days, in netcdf format with a resolution of 0.5x0.5 degrees and 22 layers. They include total burned area, standard error, observed area, burned patches and burned land cover in 18 categories as defined by the Globcover product (Arino et al. 2007).

In order to obtain these output layers, the MERIS BA algorithm had to compute extra layers apart from the BA detection date. These layers were: date of the year of burn

(from 1 to 366), confidence level, number of valid images per month, total observations per month, number of observations with clouds, and last valid observation before the date of burn.

3.3. STUDY SITES.

The algorithm was developed and tested in ten study sites. These sites were selected taking into account the different biome types and fire regime conditions. The different algorithm configurations were tested on those study sites. Several years were processed on those areas, in order to study the temporal stability and adequacy of the algorithm to the conditions varying through the years.

The biomes used to define the study sites were a simplification of the ones defined in Olson et al. (2001). Seven categories of biomes were used: temperate grasslands, savannah and shrublands, mediterranean forest, temperate forest, tropical and subtropical forest, tropical savannah, boreal and others. Figure 3 shows this biomes distribution as well as the location of the study sites.

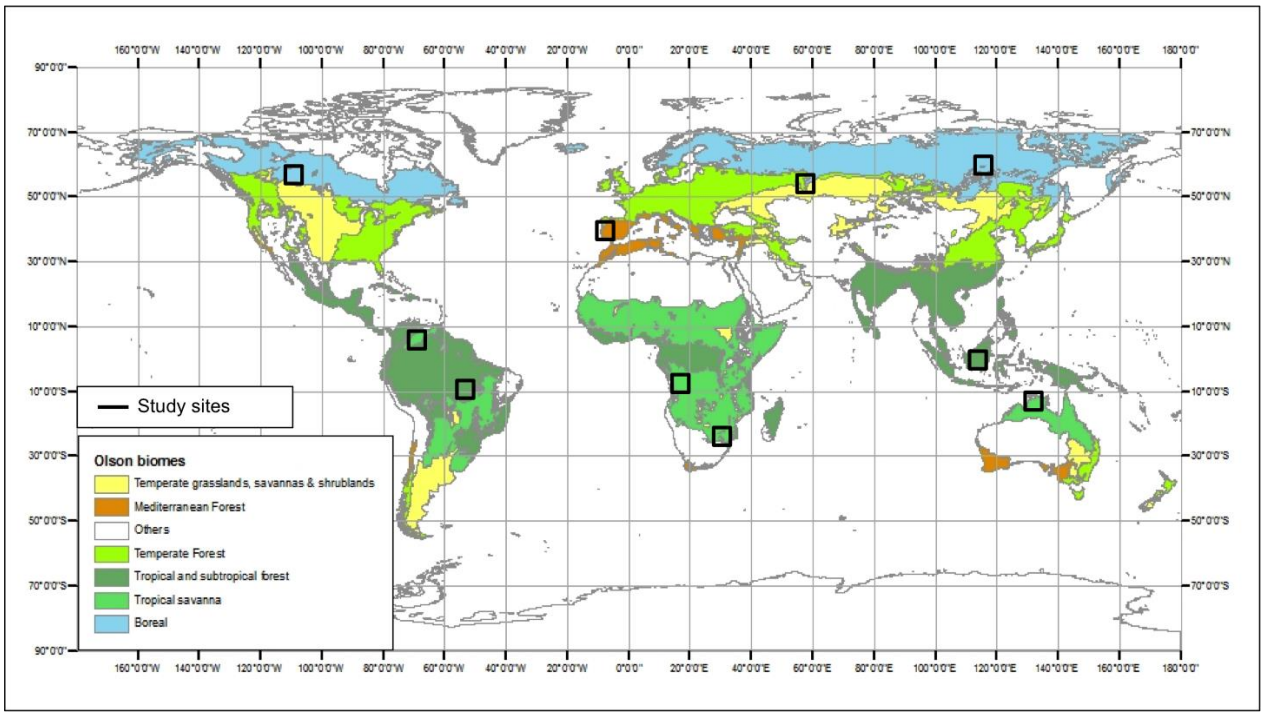

Figure 3. Olson biomes simplification and study sites location.

Fire activity was also taken into account for the study sites selection. In order to do so a map derived from GFED version 3 (Giglio et al. 2013) emissions was used. Figure 4 shows this emission activity and the study sites location.

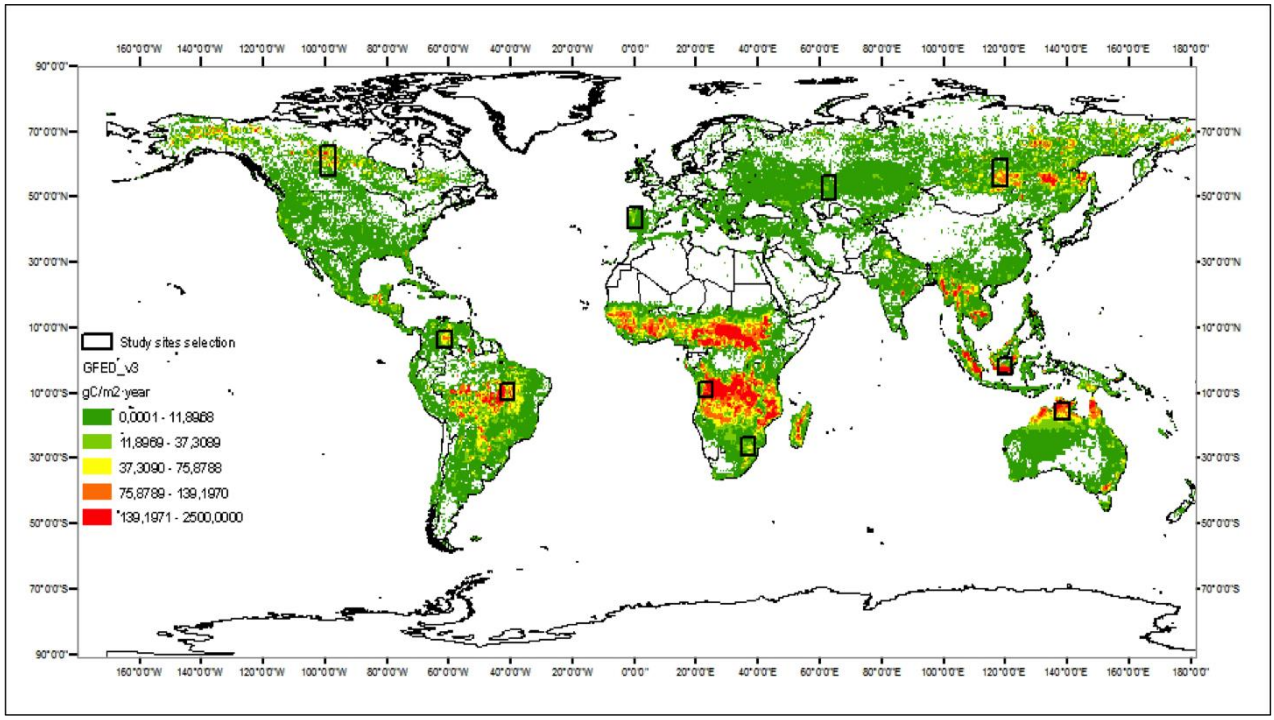

Figure 4. GFED v3 emissions and study sites location.

Therefore, the ten study sites covering the criteria of different biomes and fire activity were selected. They were located in: Canada, Colombia, Brazil, Portugal, Angola, South Africa, Russia, Kazakhstan, Borneo and Australia. All have an approximate size of 500x500 km.

3.4. VALIDATION AND ASSESSMENT SITES.

Two strategies were developed to assess the BA product. The first one, named properly validation, was developed within the fire_cci project, and aimed to verify the BA product obtained with the MERIS BA algorithm as well as other BA collections. The second strategy, named fire perimeter assessment, was used to assess the products while the algorithm was under development. The sites selected for the validation and the fire perimeter assessment are illustrated in Figure 5, together with the study sites.

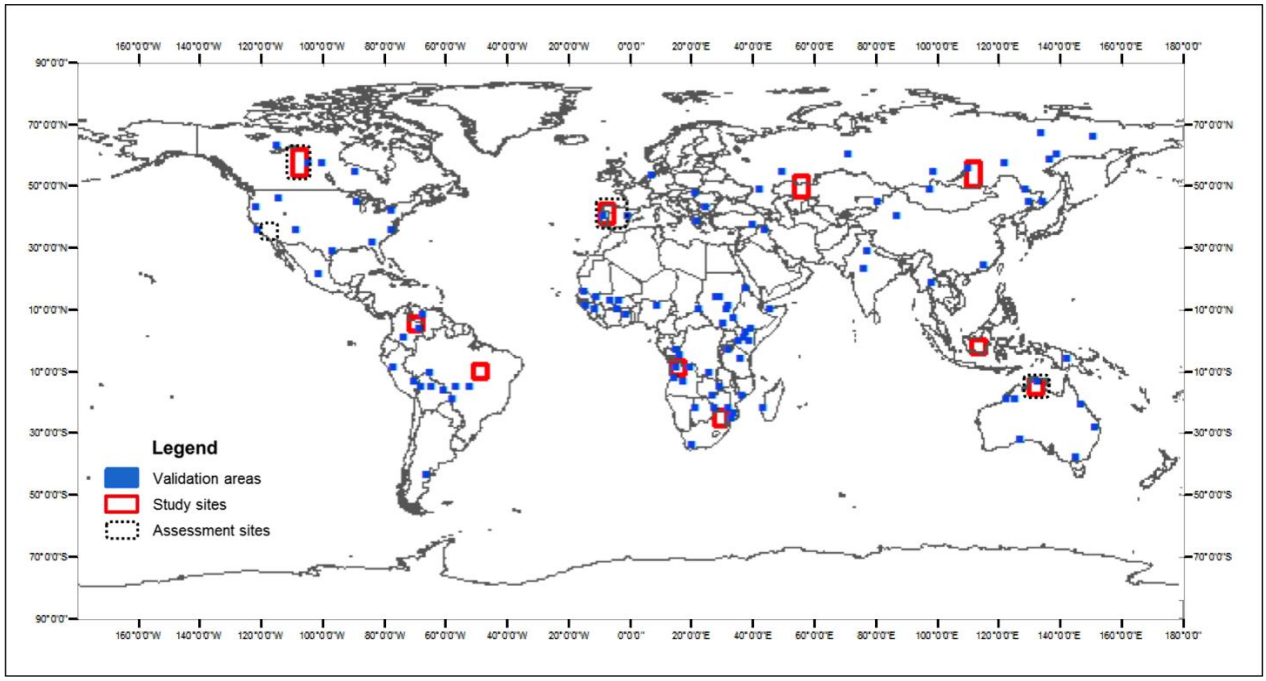

Figure 5. Validation, fire perimeter assessment and study sites location.

3.4.1. VALIDATION SITES.

The validation of the different BA products was performed using a statistically selected global sample of reference BA sites. The year 2008 was selected as the reference for validation following a CCI programmatic decision. Stratified random sampling was used to select 105 non-overlapping Thiessen scene areas (TSA), considering both ecosystem variation and historical fire occurrence (Padilla et al. 2014). Reference fire perimeters were generated by a semi-automatic BA algorithm developed by Bastarrika et al. (2011) applied to two multi-temporal Landsat TM/ETM+ images for each sampled TSA. The reference files followed the standard protocol defined by the CEOS Cal-Val (http://lpvs.gsfc.nasa.gov/fire_home.html). Whenever the input images were ETM+, only the central strip of the images was processed, to avoid the impacts of the SLC-off gaps.

The validation metrics were derived from fuzzy error matrices to account for the different pixel size of TM/ETM and MERIS sensors. Six accuracy measures were computed (overall accuracy, omission error, commission error, Dice coefficient, bias and relative bias) to satisfy criteria specified by end-users of burned area products. More details on the validation strategy can be found in Padilla et al. (2014) and Padilla et al. (2015).

3.4.2. EXTERNAL FIRE PERIMETERS.

Since the validation sites were extracted from short periods of time (in between two Landsat acquisitions) and small areas, the assessment of the final BA product was complemented by comparing the MERIS BA results with fire perimeters produced by external sources. This comparison complements the strict validation by considering within each site a much larger territory (>150.000 km^2 versus < 34.000 km^2), which would help the analysis of large burn patches. Additionally, these selected sites included fires occurring during a complete year, thus reducing the impact of temporal reporting errors in the actual assessment of BA accuracy. Since the Landsat-based validation protocol restricts the analysis of BA pixels to those occurring between the two satellite acquisitions, pixels properly classified as burned, but labelled a few days later, might be considered as commission errors (if they truly occur a few days before the first Landsat acquisition), or as omission errors (if they are labelled a few days after the second Landsat acquisition). Temporal reporting errors are more relevant in the case of MERIS than in other global sensors, since the temporal coverage and the number of available observations with this sensor are quite limited in some regions. This comparison was performed for the 3 years when global MERIS BA products were obtained (2006 to 2008) and was based on four selected areas where reference burned area perimeters were available. These sites (Figure 5) cover different ecosystems (Boreal, Temperate and Tropical).

The sources of reference data were:

- Canada: burned area perimeters were downloaded from the Canadian Wildland Fire information System (cwfis.cfs.nrcan.gc.ca/ha/nfdb/ last access November 2015), which includes the Canadian National Fire Database (CNFDB). The CNFDB is a collection of forest fire data provided by different Canadian fire management agencies (provinces, territories, and Parks Canada). From this database the region selected covered 1.150.000 km^2 including the Boreal Forest of Alberta and Saskatchewan.
- Australia: perimeters for the Australian site (located in the Northern Territories) were downloaded from the North Australian Fire Information database (NAFI) (http://www.firenorth.org.au /nafi3/, last access November 2015). The area covered a region of 750.000 km^2 mainly including savannah and Tropical forest.

NAFI burned patches were processed by the Darwin Centre for bushfires research at Charles Darwin University (for Northern and Western fire patches) and Cape York Peninsula sustainable futures (for Queensland). They were obtained from multi-temporal comparison of 250 m MODIS imagery, using segmentation and visual interpretation.

- California: Californian perimeters were downloaded from the Fire and Resource Assessment programme (FRAP) webpage (frap.fire.ca.gov last access November 2015). The validation site covers an area of 150.000 km^2 including California and neighbour states.
- Portugal: perimeters were obtained from the European Forest Fire Information System (EFFIS) (http://forest.jrc.ec.europa.eu/effis/applications/data-and-services/ last access November 2015). The area was selected to include part of the Iberian Peninsula and France, covering an area of 500.000 km^2.

Errors and overall accuracy were obtained following the same scheme for both the validation and the fire perimeter assessment exercises. This scheme was based on the concept of confusion matrix (Congalton and Green 1999) where columns represent the reference data (either the Landsat or fire perimeters in our case) and rows represent the BA classification. In this confusion matrix Pij represents the proportion of area of agreement (diagonal cells) or disagreement (off diagonal cells) between the BA product (map) class and the reference class, where $\sum Pij=1$ and the row and column margins are the sum of the cell entries in that row or column. The confusion matrix is defined in Table 4.

Table 4. Confusion matrix.

	Reference data		
Algorithm estimate	Burned	Unburned	Row total
Burned	P11	P12	P1+
Unburned	P21	P22	P2+
Column total	P+1	P+2	1

In this context commission error, omission error and overall accuracy of the BA category are defined as follows:

- Commission error: CE= P12/P1+
- Omission error: OE= P21/P+1
- Overall accuracy of the BA category: OA = P11+P22

It is important to note that in the case of burned areas only two classes exist in the error matrix: burned and unburned. Normally the number of unburned pixels is higher than the number of burned pixels. This implies that the overall accuracy is strongly influenced by the number of correctly classified pixels from the unburned class, leading to high values in the overall accuracy. In order to put in context the relevance of this measure, the Burned area proportion is also computed for each case.

3.5. MERIS CHARACTERISTICS

MERIS (MEdium Resolution Imaging Spectrometer) is a 15 band programmable spectrometer that was launched on board ENVISAT (Environmental Satellite) in 2002 (Rast et al. 1999). The satellite describes a sun synchronous polar orbit at 800km. It orbits the Earth in about 101 minutes with a repeat cycle of 35 days. MERIS was mainly designed for ocean colour applications, and provides high spectral resolution (Table 5) in the range of the blue to the near infrared regions (Gower and Borstad 2004). The total field of view of MERIS is 68.5 degrees around nadir, covering a swath width of 1150 km, and yielding to a 3 day revisit time for equatorial regions. The spatial resolution is 300 m in the full resolution mode (FR) and 1200m in the Reduced Resolution (RR) mode. The use of MERIS data to fire applications is scarce: identification of smoke plumes (Huang and Siegert 2004) and discrimination of burn severity (Chuvieco et al. 2007; Roldan-Zamarron et al. 2006). Mapping BA with MERIS was performed only at regional level by Oliva et al. (2011) using different vegetation indices, while González-Alonso (2009) combined fire hotspots from MODIS and near infrared (NIR) reflectance values from MODIS and MERIS imagery.

Table 5. MERIS spectral bands and bandwidths (ESA 2006).

Band	Band centre (nm)	Bandwidth (nm)	Region	Application
1	412.5	10	Blue	Yellow substance and detrital pigments
2	442.5	10	Blue	Chlorophyll absorption maximum
3	490	10	Blue	Chlorophyll and other pigments
4	510	10	Green	Suspended sediment, red tides
5	560	10	Green	Chlorophyll absorption minimum
6	620	10	Red	Suspended sediment
7	665	10	Red	Chlorophyll absorption and fluorescence reference
8	681.25	7.5	Red	Chlorophyll fluorescence peak
9	705	10	Red edge	Fluorescence reference, atmospheric corrections
10	753.75	7.5	Red edge	Vegetation, cloud, O2-absorptionband reference
11	760	2.5	Red edge	O2-R branch absorption band
12	775	15	Red edge	Atmospheric correction
13	865	20	NIR	Atmospheric corrections
14	890	10	NIR	Vegetation, water vapour reference
15	900	10	NIR	Water vapour

MERIS presents some challenges for mapping burned areas. Spectral and temporal resolutions are not ideal for BA discrimination. In fact, MERIS spectral range covers the 400 to 905 nm spectral region where as other sensors previously used for BA discrimination have wider ranges (MODIS 620nm-14.4µm, VGT 430nm-1.75µm), covering the SWIR and MIR spectral ranges (in the case of MODIS) which are useful bands for BA retrieval as previously discussed. Nevertheless, MERIS presents multiple spectral narrow bands in the RED-NIR space, which make it also interesting for BA mapping purposes. It includes four bands in the red edge, which might be particularly useful for burned surface retrieval. The red-edge region is defined as the position of main inflexion point of the RED-NIR slope. It is located between 670 and 780nm, where there is a sharp rise in reflectance of green vegetation. As pointed out by Clevers et al. (2001) imaging spectrometers (such as MERIS) might provide additional information in the red-edge region, not covered by the information derived from a combination of NIR and VIS broad spectral bands.

On the temporal side, MERIS global coverage of the Earth is obtained every three days. The number of images available is a factor to consider when building a strategy for

detecting burned areas. In the case of MERIS, implementations based on temporal series detection changes will be limited, since there will be few images to perform the detection. Figure 6 shows the number of valid observations in 2008 for four areas: Canada, Australia, California and Portugal. The number of images is highly variable depending on the region. Canada, for instance, has a very low number of images, up to 40, whereas Portugal or Australia can have 100 valid images per year in certain areas. This is due to the number of satellite passes, sun coverage, gaps in data reception but also to cloud coverage. Cloud obscuration effect is quite clear in the case of the Portuguese study site, where Northern region of Spain and Western of France have a lower number of valid images compared to other regions of Spain or Portugal, due to the cloud persistence in those areas. When considering maximum number of images available per area results are also quite different depending on the region and period of the year. This is illustrated in Figure 7. Canada can have up to 17 images between June and October, and none in December or January, whereas Portugal will not have more than 10 valid images per month during the whole year. The number is also highly variable for California, whereas it remains more stable in Australia.

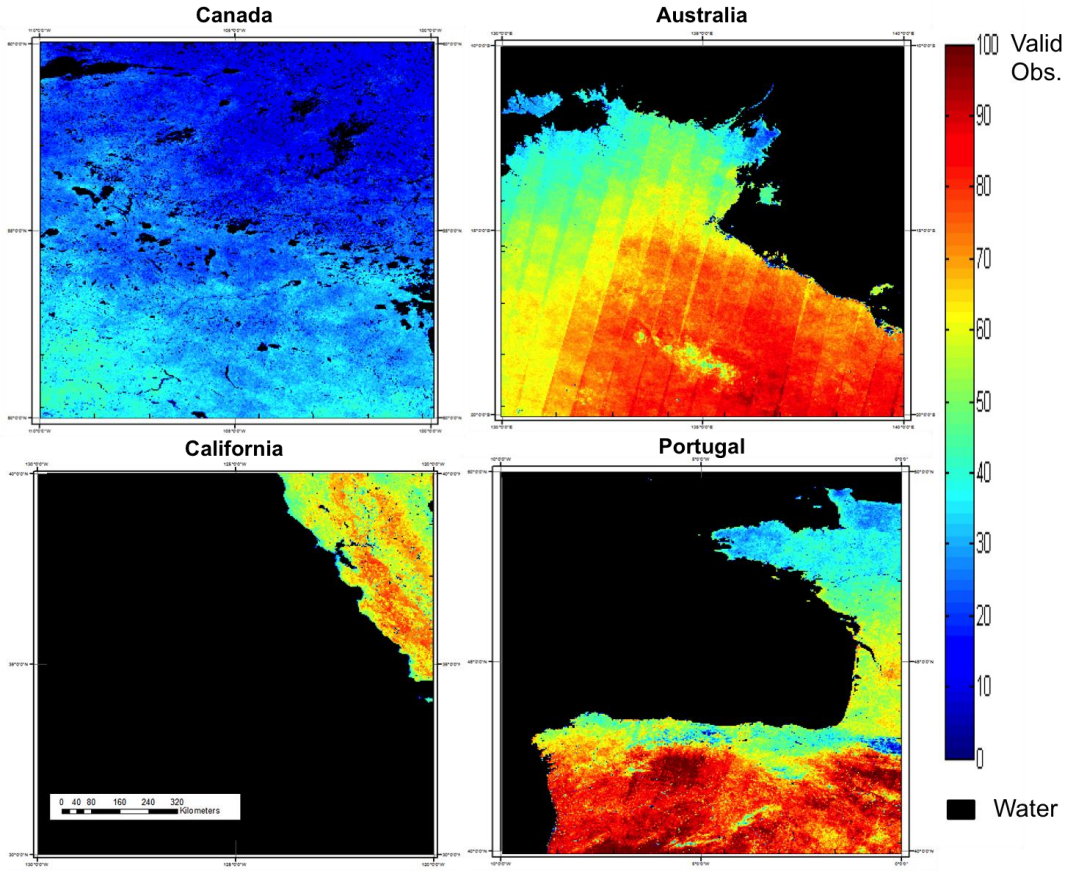

Figure 6. MERIS valid observations for 2008 in Canada, Australia, California and Portugal.

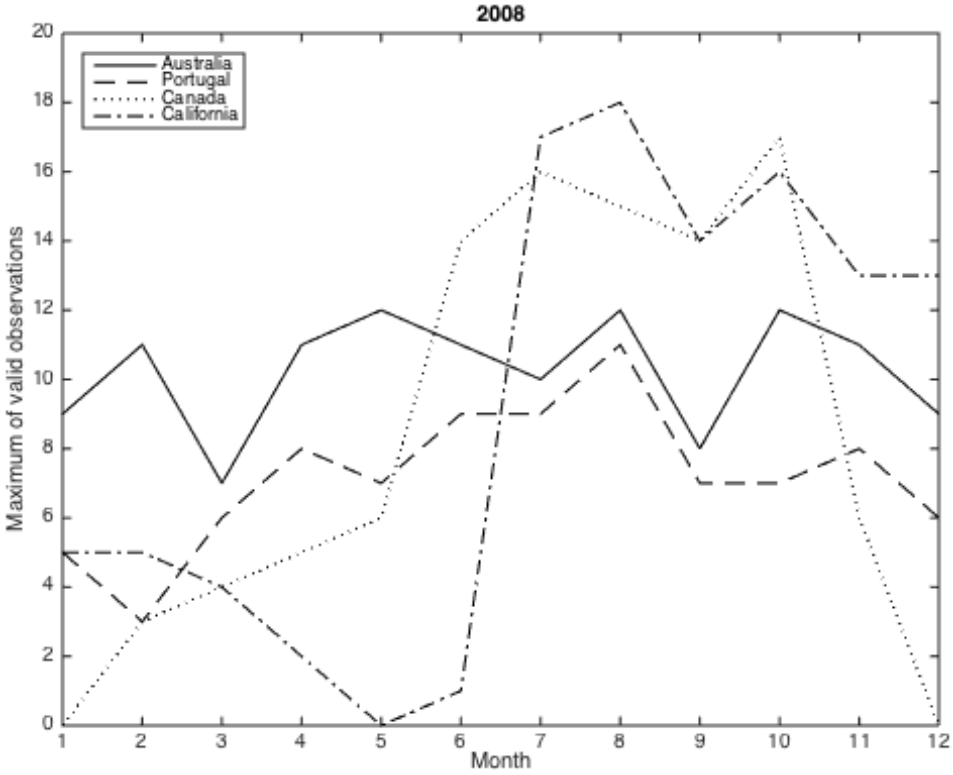

Figure 7. MERIS maximum valid observations in Canada, Australia, California and Portugal.

In terms of algorithm development this already suggests that the strategy designed will need to be flexible enough to cope with these differences, since the algorithm will be designed to obtain results globally.

Even though there are some challenges in terms of spectral and temporal resolution, the potential of MERIS for improving current information of BA relies on its greater spatial resolution in the FR mode, thus potentially providing better detection of small burn patches than coarser resolution sensors, and its multiple bands in the RED-NIR space. Furthermore, this sensor has a follow up version on the OLCI (Ocean and Land Colour Instrument) sensor, and will be complemented with the SLSTR (Sea and Land Surface Temperature Radiometer), both payloads on board Sentinel 3, scheduled for launch in 2015 within the EC Copernicus programme (www.sentinel.esa.int last access November 2015). The OLCI will include 6 more bands than MERIS (covering the range between 385nm and 1040nm). Revisit time will also be higher (less than 2 days when both satellites are launched), allowing for possible improvements in the algorithm implementation, and leading to longer and semi-operational monitoring of BA.

3.6. PRE-PROCESSING.

Several studies have acknowledged the relevance of pre-processing on the accurate and reliable detections performed in land change estimations (Jensen 2005; Lu et al. 2004; Scheidt et al. 2008). This is also applicable to fire detection, since a fire also implies a change in the land cover. Pre-processing includes activities such as data selection, co-registration, radiometric calibration, normalization, atmospheric correction and BRDF correction. As noted by Justice et al. (2006) time series changes in NIR reflectance due to BRDF effects can have important effects in wide field of view sensors, and can imply a drop in NIR reflectance as relevant as the one caused by a fire effect.

For this reason there was a special interest in treating the data properly according to the needs of the BA algorithm development. Two pre-processing chains were evaluated and tested. The first one developed by DLR (Bachmann et al. 2014) had a special focus on the atmospheric correction. The second one, developed by BC (Kirches et al. 2013), had a simpler approach but faster processing times. In both cases output files were gridded into tiles of 10x10° (3600x3600 pixels at MERIS FR).

The DLR pre-processing scheme main steps were:

- Geometric correction based on the AMORGOS software (Accurate MERIS Ortho Rectified Geo-location Operational Software, (Bourg 2011).
- Land water masking: based on the use of a static mask, and further identification of pixels using the Dynamically Self-Learning Evaluation Method (DySLEM)
- Snow/Ice, cloud and haze classification: based on brightness, NDSI indices followed by soft or fuzzy classification as introduced by Ackerman et al. (1998).
- Cloud and topographic shadow identification: based on spectral relationships and geometric approach. The use of the GETASSE DEM model was introduced for the topographic shadow identification.
- Atmospheric correction: based on the ATCOR code (Richter 1997).

The surface directional reflectances were delivered as floats between 0 and 1. The images included Sun and satellite zenith and azimuth angles. Layers with cloud, snow, static and dynamic water masks, and haze were provided. A quality status layer was also included.

The BC pre-processing scheme main steps were:

- Geometric correction: based on the AMORGOS SW and improving MERIS FR geolocation (RMS < 70 m).
- Radiometric and smile correction. The smile effect is related to the way measurements are performed in the MERIS sensor. MERIS is composed of 5 cameras. Each camera is equipped with a spectrometer and a two-dimensional CCD array installed at the optics focal plane. Ideally, a row on the detector array should correspond to a constant wavelength across the field-of-view, but optics characteristics and slight misalignments of the sub-systems generally induce small variations. These small variations are often referred to as the "smile effect" (Bourg et al. 2008). The correction applied is based on two steps. First, the irradiance correction is performed using per pixel in-band equivalent irradiance in the conversion of radiance into top-of-atmosphere (TOA) reflectance. Second, the reflectance correction is performed, correcting TOA reflectance from pixel wavelength to the nominal one, using a first order Taylor expansion.
- Cloud, water and snow identification: based on the Multi Sensor Pixel Identification approach which classifies each pixel to be processed according to a series of pixel categories: cloud, clear land, clear water and clear snow. The classification is based on probabilistic combination of a series of features (pressure, NDVI, brightness, glint risk, radiometric land value, radiometric water value, a priori land value, a priori water value).
- Atmospheric correction based on inverse modelling of radiative transfer simulations using artificial neural network (ANN) techniques and on Globalbedo (Muller et al., 2011) processing chain .

The BC pre-processing scheme was based on the chain developed for the Landcover CCI project (lc_cci). The fire_cci and lc_cci pre-processing chains differ on the type of aggregation obtained at the end of the chain. The fire-cci one obtained daily reflectances instead of weekly composites (required by the lc_cci). The surface directional reflectances were delivered as floats between 0 and 1. In addition to corrected reflectances, the images included a standard error associated to each band, as well as the Sun and satellite zenith and azimuth angles. A status layer was provided as well, with values 1 (clear land), 3 (snow/ice), or 0 (i.e. water, cloud, no observation).

In order to evaluate the performance of both pre-processing chains, temporal stability analysis was performed in a series of extracted pixels for different fire seasons and areas. Temporal series over different areas were also plotted, to evaluate the temporal series stability. Figure 8 shows the temporal evolution for a pixel in Australia relative to a case with no fires. BAI and GEMI indices are plotted. BC time series shows a higher stability in comparison to the DLR one. The number of valid observations is lower in the case of BC's (39) compared to DLR's case (46).

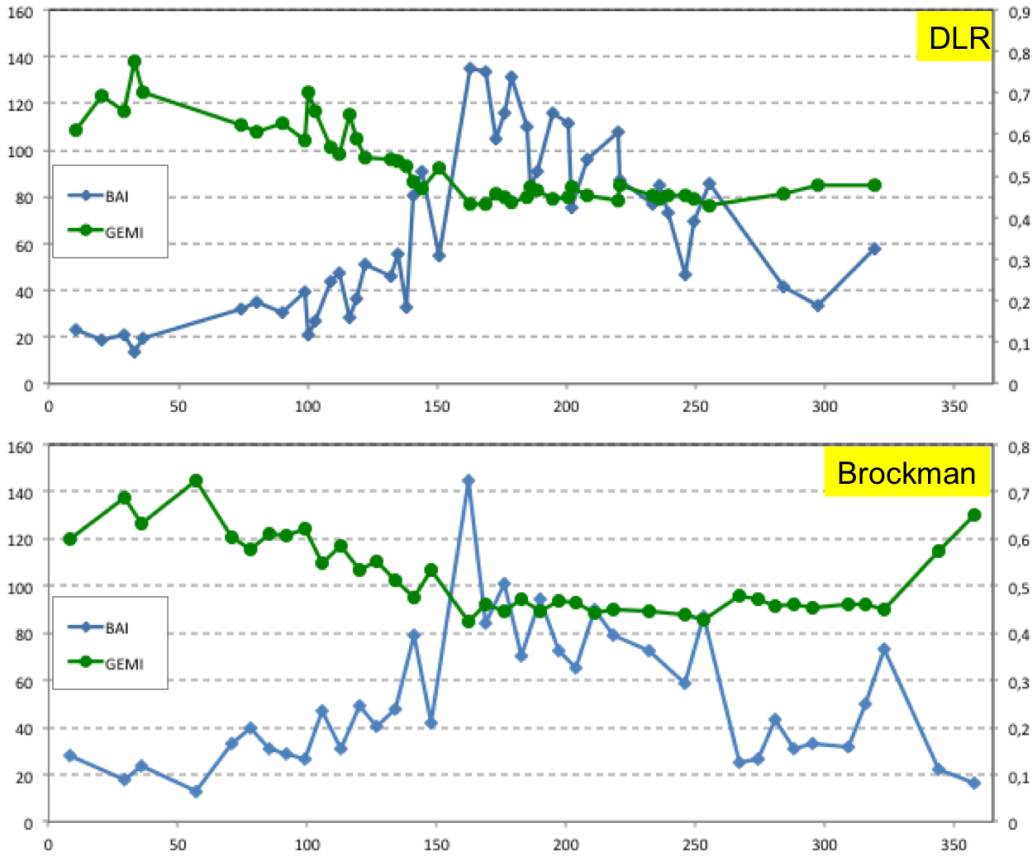

Figure 8. Temporal evolution for a pixel in the Australian study site with the DLR and BC pre-processing chains.

Temporal stability was based on the standard deviation computed for BAI and GEMI indices, in four different fire scenarios: early season, middle season, late season and no fires. Results are shown in Table 6.

Table 6. Standard deviation for BAI and GEMI indices in different fire scenarios for the DLR and BC processing chains.

	DLR		BC	
	BAI	GEMI	BAI	GEMI
Late season	22.792	0.040	20.257	0.032
Early season	27.112	0.047	26.889	0.058
Middle season	36.543	0.061	24.669	0.049
No fires	35.579	0.092	29.156	0.081

From these two data sets, the DLR pre-processing showed higher temporal stability on the BAI and GEMI indices (except for early season fires with the GEMI index). On the other side, DLR's showed more sensitivity, particularly for the day of burning. Results were similar with both pre-processing chains, having BC's shorter processing times. In fact, the processing time required to obtain data of DLR's quality was too high for the purpose of obtaining a global pre-processing with MERIS for a long-term time series. Furthermore, the BC chain was also used by the lc_cci project, and using this data pre-processing chain would help ensuring consistency between these products. Therefore it was decided to use the BC pre-processing scheme as the basis for the input data into the MERIS BA algorithm.

3.7. ALGORITHM MAIN SCHEME.

After literature review and initial study of the pre-processed MERIS data a general scheme on the initial algorithm configuration was defined. Three main lines were drawn:

- Auxiliary data: as already mentioned, MERIS does not provide information in some bands that are useful for burned area detection, and therefore the use of auxiliary information was already foreseen. MODIS HS product was chosen for this purpose. The use of a fuel mask, to map out non-burnable areas was also included.

- Type of algorithm: it was also decided that the algorithm would be based on a two-phase approach (seed and growing phases). It was concluded from the literature review that this configuration would give better results than other implementations, as it would be more flexible to address the spatial heterogeneity of BA conditions in different regions.
- Type of BA identification: the basis to perform BA detections would be the creation of a series of composites and identification of indices that would better identify the burns. Pixel and object based strategies would be tested on these composites.

The general scheme of the algorithm is shown in Figure 9.

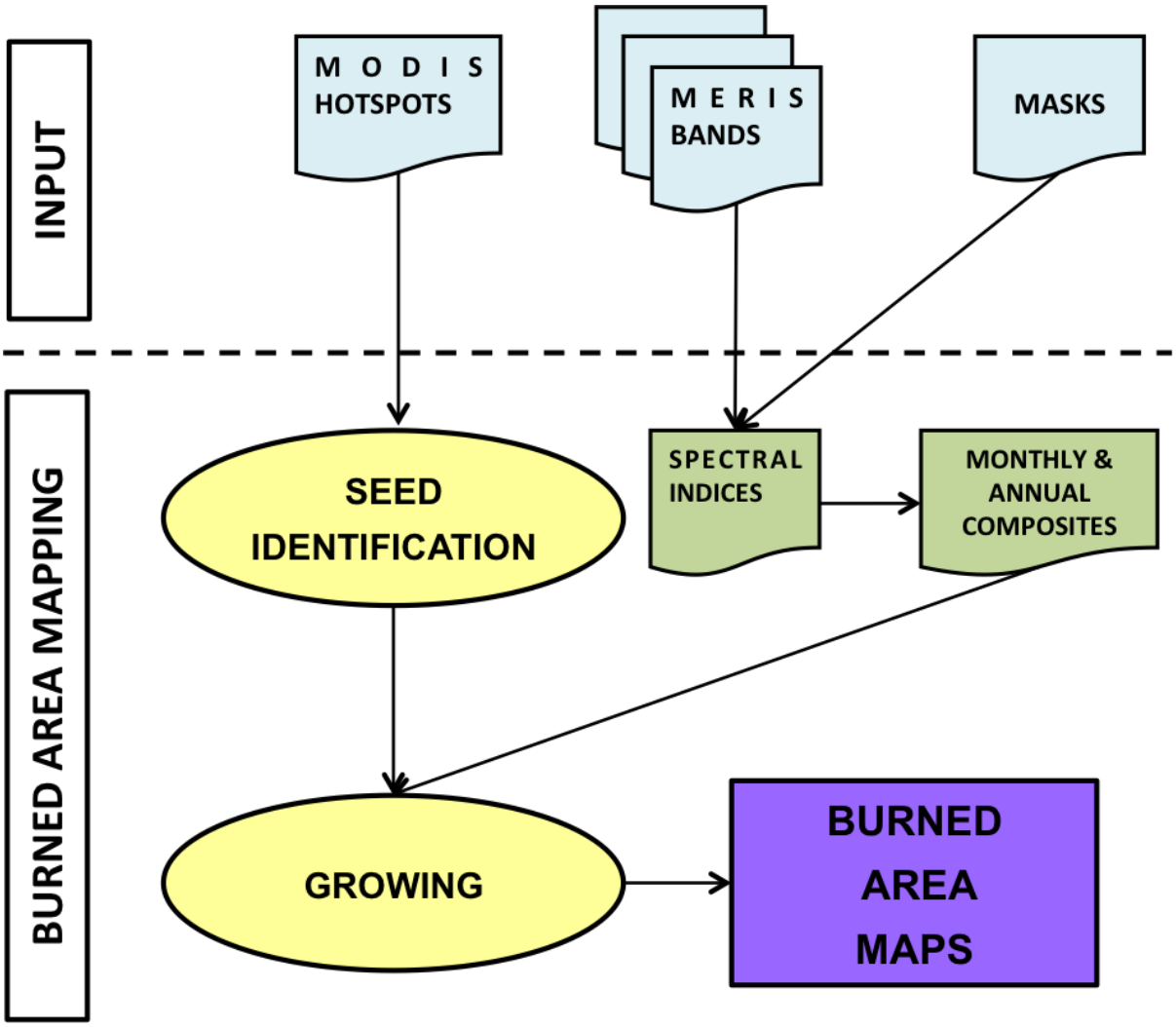

Figure 9. Algorithm main scheme definition.

3.8. AUXILIARY DATA.

In order to obtain the BA maps the MERIS BA algorithm makes use of two auxiliary data products: active fires and a fuel mask.

3.8.1. ACTIVE FIRES.

The active fires or hotspots (HS) product used is generated by combining the information from the MIR and TIR bands of the MODIS sensor using a contextual algorithm. On a first step fixed thresholds are applied to the MIR and TIR channels and then false detections are excluded by analysing the brightness temperature in neighbouring pixels (Giglio et al. 2003a). Information available from MODIS in both TERRA and AQUA satellites (10.30 and 13.30 Equatorial cross time respectively) was used. The product was downloaded from the Fire Information for Resource Management System (FIRMS) (Davies et al. 2009). The product reports fires that are burning at the time of the satellite overpass at 1km resolution. The product has been used in other global BA algorithms (Giglio et al. 2009). A recent study by Hantson et al. (2013) showed that the product has a tendency towards omission, having low commission error rates. The behaviour of the product in different regions was also identified. The low commission reported in this study made its use interesting in the MERIS algorithm for the seed phase, since the aim is to avoid commission errors at this stage of the retrieval. Other products such as the World Fire Atlas, VIIRS active fires or SLSTR fire product (in the upcoming Sentinel 3) could be used in a similar way to feed the BA algorithm.

3.8.2. FUEL MASK.

A fuel mask is introduced as auxiliary data into the algorithm for two reasons. Firstly, it will improve processing time of the algorithm since pixels that are already masked as not burnable will not be processed. Secondly, it will avoid commission errors in areas that are not burnable but that for different reasons could be mapped as burned by the algorithm.

The fuel mask is a binary mask with two classes: burnable/not burnable. It was derived from the Globcover 2005 map (Arino et al. 2007), by converting into the burnable class

all vegetation classes, whereas urban areas, deserts and water were considered non-burnable class.

3.9. SELECTION OF MERIS INPUT BANDS FOR BURNED AREA DISCRIMINATION.

MERIS has 15 bands covering the VIS to NIR electromagnetic region of the spectrum. Eight of these bands are in the visible region, four in the red-edge and three in the NIR. As mentioned, the NIR region has been identified in several studies as being the most suitable region of the spectrum to detect BA. Furthermore, the red-edge bands have the potential to increase this BA discrimination. Therefore there is a need to identify the most adequate bands in the MERIS sensor for BA discrimination. A separability study was designed to perform this analysis. In addition, there are different possibilities to use these bands in indices and composites. An analysis on these different options was also performed. These two studies are shown in the following sections.

3.9.1. SEPARABILITY ANALYSIS.

An analysis is performed to evaluate the adequacy of the different bands to discriminate burned areas, by obtaining the separability between the burned and unburned classes. The sensitivity of a band will be higher if there is a high variance between the classes, i.e. a high external contrast, and low variance within the classes (high internal homogeneity). This strategy has been used in several studies (Chuvieco et al. 2002; Lasaponara 2005; Roy et al. 2002) to discriminate the most adequate bands to retrieve BA. First, a variety of scenarios needs to be created to evaluate how the different variables perform in different cases (simulation framework section). Second, a measure of this performance needs to be obtained in order to identify the most suitable variables for the two classes discrimination (statistical analysis section).

3.9.1.1. Simulation framework.

In this simulation framework, the aim is to test the separability between the burned and unburned classes for the different MERIS bands. More specifically, what needs to be

evaluated is how much the reflectance in those bands changes when there is a fire, in comparison to the pre-fire situation. Therefore, a set of pre and post fire scenarios should be defined.

These pre and post fire scenarios were simulated with the GEOSAIL and PROSPECT canopy reflectance models. In GEOSAIL, the SAIL (Scattering from Arbitrarily Inclined Leaves) model was combined with the Jasinski geometric model to simulate canopy spectral reflectance and absorption of photosynthetically active radiation for discontinuous canopies. The SAIL model was developed by Verhoef (1984). The code is a modified version of the code written by Alexander (1983). The geometric part of the model is based on Jasinski's geometric model (Jasinski and Eagleson 1990). A complete description of GEOSAIL is in Huemmrich (2001). GEOSAIL uses the SAIL model to calculate canopy spectral reflectance and transmittance. Shadowed background reflectance is the product of the background reflectance and the transmission from SAIL. The component reflectances: illuminated canopy, illuminated background, shadowed canopy, and shadowed background are then used as inputs into a geometric model. The geometric model determines the fraction of each of the components in a scene, given a crown shape, the canopy coverage, and the sun angle. In this model tree crowns are assumed to be identical and do not overshadow each other. For the leaf properties of the simulation analysis, the well-known PROSPECT model (Jacquemoud 1990; Jacquemoud et al. 2009) was used, assuming two situations: green leaves for pre-fire conditions, and scorched leaves for surface fires. The parameters related to foliage simulation are based on data from Chuvieco et al. (2006) using the cases of dry (scorched)/ green leaves (pre-fire) (0 and 100).

The pre-fire and post-fire scenarios parameters and values were defined as shown in Table 7.

Table 7. Pre and post fire scenarios parameter values used in the GEOSAIL model.

	PRE-FIRE SCENARIO	POST-FIRE SCENARIO
SHAPE OF THE LEAVES	Cone or cylinder	Cone or cylinder
TYPE OF SOIL	Alfisol, aridisol or entisol	Dark charcoal
CANOPY TYPE	Erectophile or plagiophile	Erectophile or plagiophile
TYPE OF FIRE		Surface or crown
LAI	0.5 TO 12	Surface: up to 4 Crown: 0.1 & 0.3
HEIGHT TO WIDTH RATIO OF CROWN	0.5 to 8	0.5 to 8 (simplifying the cases of 2, 4 and 6)
SOLAR ZENITH ANGLE	10-70	10-70
CROWN COVERAGE	0.2 to 0.8	Surface: 0.2 to 0.8 Crown: 0.2
N (structural parameter)	1.4	Surface: 1.4 Crown: 3
WATER CONTENT (g/cm^2)	0.0075	Surface: 0.0075 Crown: 0.0006
CHLOROPHYL CONTENT ($\mu g/ cm^2$)	42	Surface: 42 Crown: 28
DRY MATTER CONTENT (g/cm^2)	0.0006	0.0006

A total of 60000 scenarios were defined, simulated and evaluated. For each scenario reflectance values were obtained every 5 nm in the spectral range between 405 and 905 nm. These values were filtered with the correspondent MERIS spectral response function (SRF) (ESA Cal/Val Portal calvalportal.ceos.org), in order to obtain the response that the sensor will actually provide. An example of all MERIS SRFs with a simulated pre and post fire (surface and crown) spectra is shown in Figure 10.

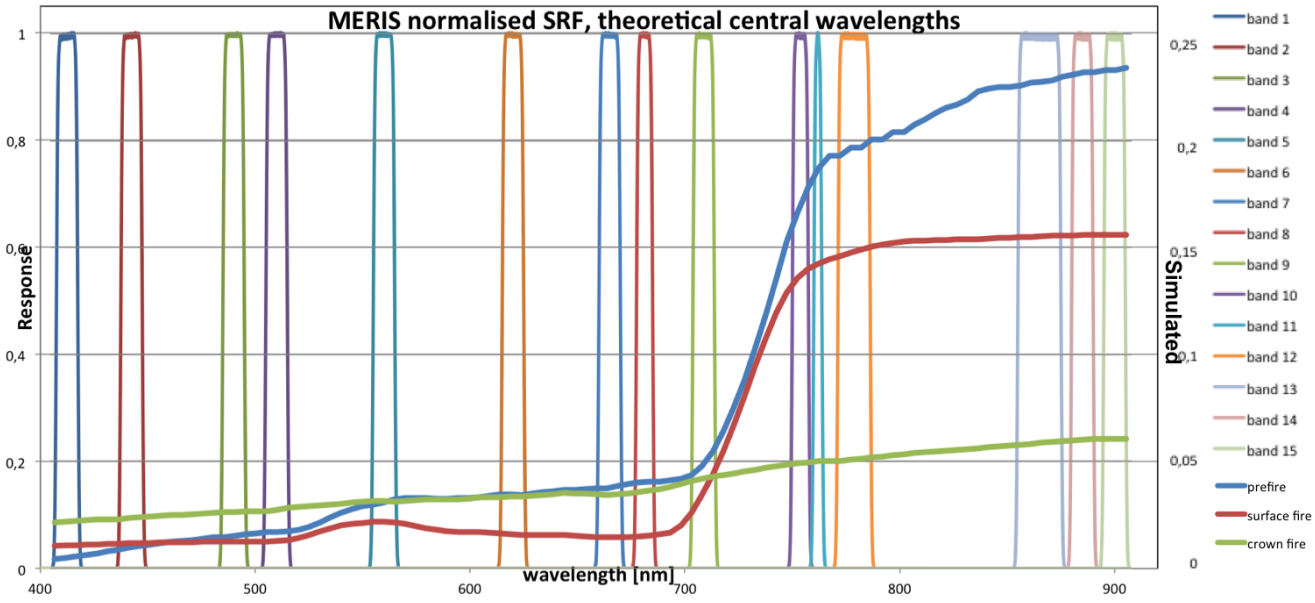

Figure 10. SRFs from MERIS 15 bands and simulated spectra for pre and post fire surface and crown scenarios.

3.9.1.2. Statistical analysis.

The statistical measure used to estimate the separability of each band was the Bhattachariyya distance, which measures the similarity of two distributions. It is defined as (Kailath 1967):

$$D_B = -\ln(BC(p,q))$$

where the Bhattacharyya coefficient (BC) is:

$$BC(p,q) = \sum_{x \epsilon X} \sqrt{p(x)q(x)}$$

In the case of multivariate normal distributions, where $\rho_i = N(u_i, v_i)$ being u_i and v_i the means and covariances of the distributions, the Bhattachariyya distance is defined as:

$$D_B = \frac{1}{8}(u_1 - u_2)^T V^{-1}(u_1 - u_2) + \frac{1}{2}\ln\left(\frac{detV}{\sqrt{detV_1 detV_2}}\right)$$

Being $V = \frac{V_1 + V_2}{2}$

Higher values of D_B imply better separation between classes. This measure has been used in a variety of remote sensing studies to measure the separability between classes (Roy et al. 2002, Bastarrika et al., 2011).

3.9.2. SPECTRAL INDICES AND BANDS ANALYSIS.

Spectral indices are a useful way to retrieve certain characteristics of the surface. In the case of burned areas some of them have proven to be a good way to detect the changes associated to a fire. They present certain advantages respect to the direct use of the bands such as the ability to have less influence from atmospheric, soil or BRDF effects.

3.9.2.1. Indices and bands identification.

The indices and bands chosen to test in the algorithm are the BAI, GEMI and NIR. The BAI index was specifically designed for BA discrimination and has shown to be effective in several studies (Martín and Chuvieco 2001, Chuvieco et al. 2002). From the vegetation indices, GEMI is the one that has been identified more often in the literature as performing better to detect BA (Pereira et al, 1999b). Furthermore, this index was specifically designed to diminish the influence of atmospheric and soil effects (Pinty and Verstraete 1992). The NIR band has been identified in several studies to be the one (together with the SWIR) that performs better when detecting burned areas. All of them present advantages and drawbacks, and therefore the three will be compared in different scenarios, to determine how these indices and bands should be used in the algorithm.

A study based on the generation of monthly composites and annual reference trends was performed. Two types of composites were built: monthly and annual. The monthly composites are post fire composites. The composite concept is already introduced here since they were used as means to group the information to identify the selection of bands and indices. The detailed analysis and strategy followed to build the monthly composites is detailed in section 3.10. The annual composites were based on the difference between the monthly composites, and the annual pixel values that would be close to the period when vegetation had a maximum productivity. Therefore, the expected change between that maximum (for GEMI and NIR) or minimum (for the BAI) value and the post-fire value would be highest, thus emphasising post-fire spectral changes. Three alternatives were used to build the reference composites:

- Min BAI: this composite was obtained by selecting the minimum BAI value per pixel and year. As the BAI index is related to the proximity to char signal, minimum BAI values should select the brightest soil conditions (either snow-vegetation or bare soil).

- Max GEMI: this composite was obtained by selecting the maximum GEMI value per pixel and year. The maximum GEMI value should be the period of the maximum vegetation cover.
- Max NIR: this composite is obtained by selecting the maximum NIR value per pixel and year. The maximum NIR value should be the period of the maximum vegetation cover.

Subtraction of these 3 reference composites to the post-fire composites was performed. For the GEMI and NIR, the difference was computed from the reference and the post-fire value (DifGEMI = MaxGEMI-GEMIHS, and DifNIR= MaxNIR-NIRHS), while for BAI, the difference was from the post-fire values and the reference (difBAI = BAIHS-BAIMin) to always use positive numbers. An example of these composites for the GEMI index is shown in Figure 11.

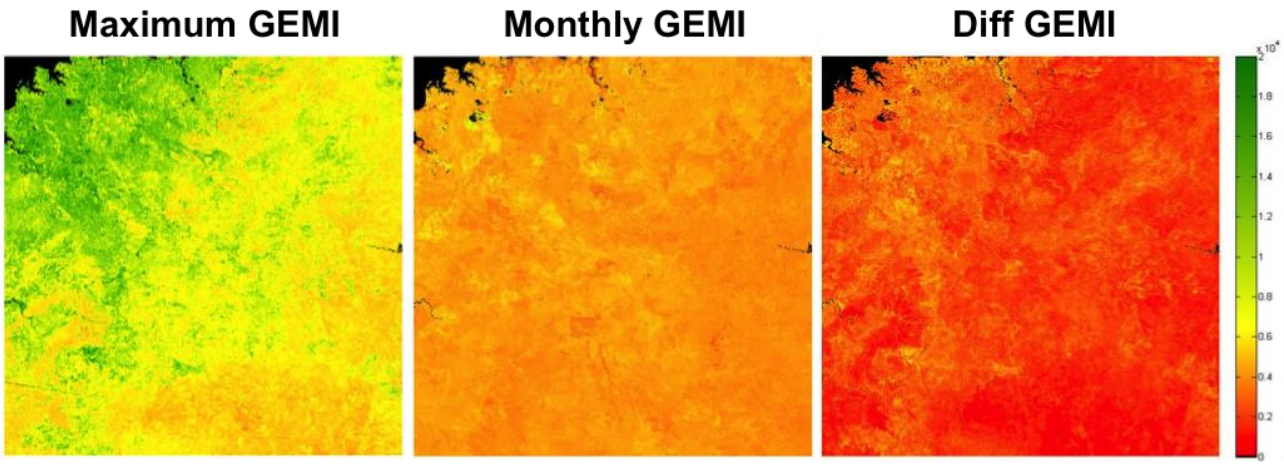

Figure 11. Maximum GEMI for 2005, GEMI in October 2005 and DifferenceGEMI composites in the Australian study site.

3.9.2.2. Statistical analysis

In order to determine which bands and indices were more adequate for retrieving burned areas a separability test using Bhattachariyya distance was performed. A sample of burned and unburned pixels was extracted from four study sites: Canada, Kazakhstan, Australia and Portugal. These four study sites were chosen because they were representative of the different biomes and fire regimes. The burned pixels were identified with the HS, while for unburned areas a random sample of 10 % of all pixels within the limiting area of 10 km to any HS was extracted. The extraction was done by

previously removing all pixels that were considered burned in the MODIS MCD45 BA product. Sample sizes were between 4500 and 23000 for burned pixels (depending on the fire occurrence in the four study sites), while for unburned pixels the sample size was between 45000 and 92000 pixels. Bhattachariyya distance was computed for 6 composites: post-fire composites (GEMI, NIR and BAI) and three temporal differences (DifGEMI, DifBAI, DifNIR).

3.9.3. RESULTS.

Results from the separability analysis and from the spectral indices and bands analysis are shown in these sections.

3.9.3.1. Separability analysis.

From all the different scenarios, the type of fire (surface or crown) was used to separate and interpret the results. The reason for this is that from space the sensitivity to these fires will be different. Crown fires will be more evident and easier to detect from space. In the surface fires, only the cases where LAI was going up to 4 were considered, since for higher LAI values the difference from space will be negligible. Results are shown in Table 8 for crown fires, surface fires, and considering both types of fire combined.

Table 8. Bhattaacharyya distance values for the 15 MERIS bands in the crown and surface fire scenarios.

Band	Crown fire	Surface fire	Total
1	0.0361	0.3305	0.0350
2	0.1130	0.0066	0.1103
3	0.1926	0.0310	0.1894
4	0.2201	0.0509	0.2168
5	0.3442	0.1392	0.3408
6	0.4110	0.2734	0.4076
7	0.4334	0.3452	0.4302
8	0.3945	0.3245	0.3922
9	0.3805	0.2412	0.3780
10	0.6085	0.1201	0.5907
11	0.5546	0.1050	0.5382

12	0.6559	0.1391	0.6358
13	0.6975	0.2192	0.6783
14	0.6002	0.1896	0.5845
15	0.6008	0.1902	0.5853
GEMI	0.4220	0.0738	0.4063

Band 13 located in the NIR region, is the one that gives better total separability, being the Bhattacharyya distance the biggest for this band. It also presents the higher separability for crown fires. The second and third bands that perform better are 10 and 12, located in the red edge. Bands that present smaller Bhattacharyya distances are the ones in the blue region. The use of the GEMI index, computed here with bands 8 and 10, provides a better separation than the use of single band 8. Band 7 is the one that gives better separation in the red region.

The results from this study are still preliminary. A more comprehensive version of these results is in preparation, and will be combined with the same methodology applied to the OLCI sensor bands.

3.9.3.2. Spectral indices

Selection of the most sensitive bands to use in the seed and growing phases of the algorithm was based on the Bhattachariyya distance. The single band composite (NIR, GEMI or BAI) and the annual differences were selected as having the bigger distance. Table 9 includes the results for the bands evaluated.

Table 9. Bhattaacharyya distance values in 4 study sites for the 6 composites analysed, between burned and unburned pixels.

	Australia	Canada	Portugal	Kazakhstan
GEMI	1.1645	0.2853	0.4490	0.7809
BAI	0.7488	0.2457	0.6031	0.5636
NIR	1.5739	0.3394	0.5420	0.8363
DifGEMI	0.8631	0.1343	0.3697	0.3223
DifBAI	0.8774	0.0062	0.6317	0.2999
DifNIR	1.0314	0.0113	0.2557	0.5711

The post fire composite chosen is the NIR one as it is the most sensitive in three of the four cases analysed, except for Portugal, where the BAI index performs better (Table 9). In the case of the temporal differences DifNIR performs better in Australia and Kazakhstan, DifGEMI in Canada and DifBAI in Portugal.

Correlation matrices between the composites were also computed, in order to identify which composites should be combined, in case more than one of them was used for the detections. These matrices are shown in Table 10.

Table 10. Correlation matrices between the composites for burned and unburned scenarios in 4 study sites.

BURNED PIXELS

AUSTRALIA

	GEMI	BAI	NIR	Dif GEMI	Dif BAI	Dif NIR
GEMI	1.000					
BAI	-0.124	1.000				
NIR	0.915	-0.287	1.000			
DifGEMI	-0.048	0.481	-0.255	1.000		
DifBAI	-0.158	0.980	-0.317	0.506	1.000	
DifNIR	-0.067	0.485	-0.342	0.949	0.512	1.000

UNBURNED PIXELS

AUSTRALIA

	GEMI	BAI	NIR	Dif GEMI	Dif BAI	Dif NIR
GEMI	1.000					
BAI	-0.671	1.000				
NIR	0.809	-0.734	1.000			
DifGEMI	-0.549	0.436	-0.518	1.000		
DifBAI	-0.638	0.980	-0.710	0.529	1.000	
DifNIR	-0.417	0.461	-0.631	0.869	0.551	1.000

CANADA

	GEMI	BAI	NIR	Dif GEMI	Dif BAI	Dif NIR
GEMI	1.000					
BAI	-0.598	1.000				
NIR	0.952	-0.565	1.000			
DifGEMI	-0.546	0.402	-0.370	1.000		
DifBAI	-0.549	0.973	-0.482	0.548	1.000	
DifNIR	-0.468	0.367	-0.315	0.968	0.522	1.000

CANADA

	GEMI	BAI	NIR	Dif GEMI	Dif BAI	Dif NIR
GEMI	1.000					
BAI	-0.616	1.000				
NIR	0.934	-0.599	1.000			
DifGEMI	-0.511	0.364	-0.301	1.000		
DifBAI	-0.546	0.957	-0.485	0.553	1.000	
DifNIR	-0.455	0.352	-0.271	0.969	0.547	1.000

PORTUGAL

	GEMI	BAI	NIR	Dif GEMI	Dif BAI	Dif NIR
GEMI	1.000					
BAI	-0.412	1.000				
NIR	0.946	-0.494	1.000			
DifGEMI	-0.762	0.321	-0.746	1.000		
DifBAI	-0.403	0.980	-0.485	0.335	1.000	
DifNIR	-0.608	0.303	-0.664	0.911	0.326	1.000

PORTUGAL

	GEMI	BAI	NIR	Dif GEMI	Dif BAI	Dif NIR
GEMI	1.000					
BAI	-0.687	1.000				
NIR	0.850	-0.759	1.000			
DifGEMI	-0.414	0.334	-0.462	1.000		
DifBAI	-0.634	0.980	-0.729	0.429	1.000	
DifNIR	-0.175	0.288	-0.423	0.813	0.408	1.000

KAZAKHSTAN						
	GEMI	BAI	NIR	Dif GEMI	Dif BAI	Dif NIR
GEMI	1.000					
BAI	-0.380	1.000				
NIR	0.977	-0.405	1.000			
DifGEMI	-0.602	0.132	-0.629	1.000		
DifBAI	-0.373	0.980	-0.401	0.175	1.000	
DifNIR	-0.618	0.166	-0.667	0.931	0.209	1.000

KAZAKHSTAN						
	GEMI	BAI	NIR	Dif GEMI	Dif BAI	Dif NIR
GEMI	1.000					
BAI	-0.584	1.000				
NIR	0.947	-0.634	1.000			
DifGEMI	-0.482	0.323	-0.554	1.000		
DifBAI	-0.559	0.980	-0.617	0.388	1.000	
DifNIR	-0.435	0.342	-0.564	0.911	0.406	1.000

After analysing these results, and taking into account the noise in the time series (see section 3.10.3.1) the following bands were selected:

- Seed phase: it was decided to use only one band. The reason for it was that this phase was mainly based on statistics and extraction of pixels and therefore the interest was in using only the band that gave better separation between classes, therefore the post fire composite based on the NIR was chosen.
- Growing phase: it was decided to use two bands, the one that gave better separability results (NIR), and one band that would take into account inter-annual variations (DiffGEMI, DiffNIR and DiffBAI). The correlation between the NIR and the DiffGEMI, DiffNIR and DiffBAI was analysed. In Australia, the lowest correlation for the NIR band was with the DiffGEMI for both burned and unburned pixels. In Canada, the highest correlation was with DiffBAI, for unburned and burned, being lower for DiffNIR and DiffGEMI. In Portugal, the lowest correlation was found with DiffBAI for the burned pixels. On the opposite, for unburned pixels the highest correlation with NIR was found with DiffBAI. The same behaviour was observed for Kazakhstan. Taking into account these results it was decided to use the DiffGEMI band. The correlation analysis showed that correlation between diffGEMI and NIR is lower than between the diffBAI and NIR in most cases. Correlation between NIR and DiffNIR and DiffGEMI showed similar behaviours, but DiffNIR was finally excluded since it was decided that there would be more benefit in adding information from another index. Furthermore, GEMI was specifically designed to reduce soil and atmospheric effects, being also less affected by the noise in the time series. An example of this noise is shown in Figure 12. A temporal series extraction is represented for the NIR, GEMI and BAI for a random pixel in Portugal. In comparison, BAI is less

robust to the noise in the time series giving lower stability than the GEMI time series.

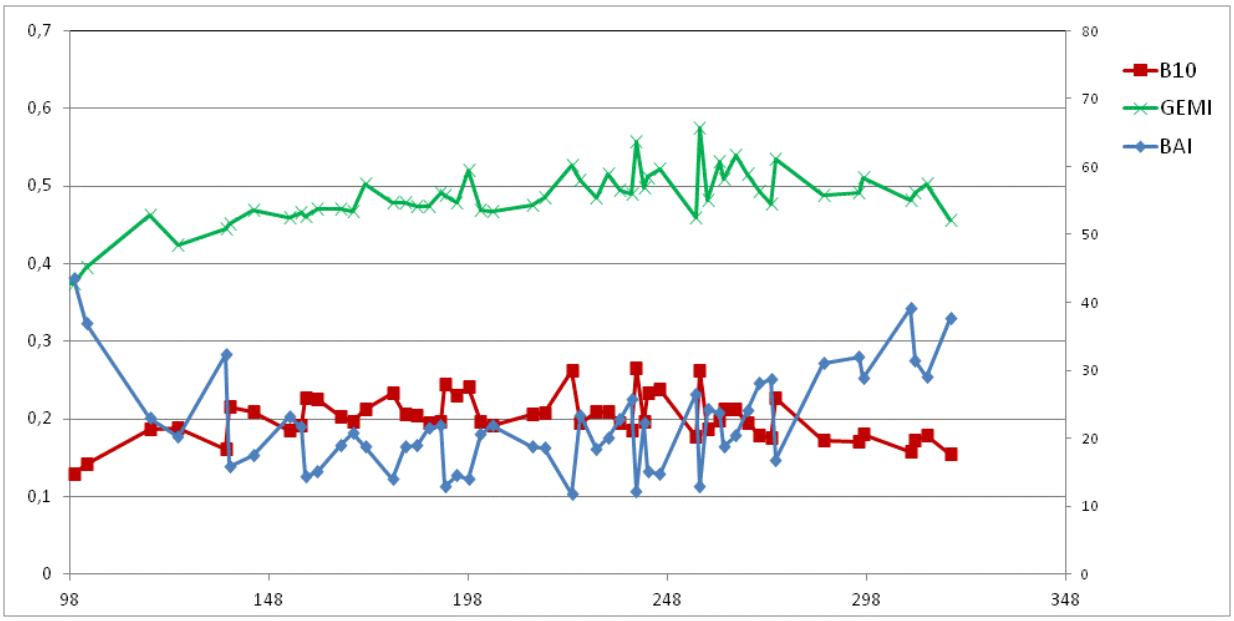

Figure 12. Temporal evolution of NIR BAI and GEMI for a pixel in Portugal.

3.10. COMPOSITING CRITERIA.

Composites are generally built to reduce noise in the time series and to fill the temporal gaps when observations are not available. Two aspects need to be defined when creating composites. First, which bands will be used for compositing. Second, which criterion will be used to select the pixel that will be kept in the compositing. Compositing techniques have been widely used as means to group the information acquired and to overcome temporal discontinuities in the context of burned area detection. Kasiscke et al. (1995; 1993) created NDVI 15 day composites based on AVHRR series to detect burned areas in the boreal forests of Alaska during 1990 and 1991. In a similar way, Fernández et al. (1997) mapped large fires in Spain during years 1993 and 1994 using AVHRR 10 day composites looking for maximum NDVI in the time series. Later on, efforts were made to select criteria that would enhance the BA detection, since the NDVI ones enhanced the vegetation response. Fraser and Li (2002) used SPOT-VGT data in Canada, to create 10 days composites of NDVI to perform the BA detection. On this line, Chuvieco et al. (2005) compared different compositing techniques and found that maximum brightness temperature was enhancing the BA.

More recently, Giglio et al. (2009) used ten days composites of VI index (relation between MODIS bands 5 and 7) as the basis for the MCD64 BA algorithm.

As mentioned previously MERIS temporal resolution does not provide daily coverage. Furthermore, taking into account cloudy regions a composite strategy was envisaged to be able to retrieve consistent information on burned areas. The aim is to obtain a spatial and temporal consistent picture of the area to analyse. Different compositing techniques were considered. They can be divided in two main categories: annual and monthly composites. Two main criteria need to be considered when building a composite: temporal and spatial consistency.

3.10.1. TEMPORAL CRITERIA

Considering the number of valid observations in MERIS for the different areas and months (Figure 6 and 7), the initial approach was to build an annual composite. The minimum NIR value per pixel and year was selected to create this annual composite. The day when this minimum occurred was also kept for further analysis. Low NIR values are expected in areas where char or scorched leaves are present, although they can also be caused by water or dark soils. Therefore, in case of a fire event, the NIR value should decrease, presenting significantly lower values on the days after the fire event. Following this logic, the day of the minimum NIR value per year should be the date of the fire event.

A second test that could help minimising potential errors was to use the 2nd NIR minima instead of the first one. This strategy would avoid potential problems not detected in the pre-processing such as cloud shadows. The 2nd NIR minima should still be representative of the fire event.

In order to test the consistency of this method, and analyse its performance, a series of extractions were performed. The date from MERIS detection was compared with the date of MODIS HS detection. Three scenarios were considered: HS and MERIS, HS only, MERIS only. The purpose of these extractions was to evaluate how the algorithm was performing at its earlier stages in terms of spatial and temporal consistency in comparison with the HS product. As already mentioned, since this product has low commission errors it could therefore be used to evaluate the adequacy of the MERIS detections for the pixels where a HS was also present.

3.10.2. SPATIAL CRITERIA.

The temporal criteria tests aimed at obtaining the possible burn date for the different pixels over the temporal period selected. It is also important to obtain a good spatial consistency in the composite, in order to be able to retrieve the total extent of the burned area. The use of HS to create this spatial consistency was envisaged. Different strategies were tested. In all of them the basic spatial criteria was based on the use of Thiessen polygons (Brassel and Reif 1979) to extend the HS. A first composite, named the Thiessen matrix assigned to each pixel the value of the closest HS. Afterwards, the aim was to build a NIR post-fire composite guided from this Thiessen matrix, relying therefore on the accuracy of HS to describe sampling points within fire perimeters. It is well known that HS do not provide a full description of fire-affected areas, as satellite sensors only detect those fires that are active when the satellite overpasses the fires. However, the high thermal contrast between burning and background pixels and the sensitivity of MODIS thermal channels, ensures a high confidence in detecting actual fires, avoiding commission errors. Hantson et al. (2013) performed an exploratory analysis of HS performance to detect burned perimeters by comparing HS with fire reference data extracted from Landsat TM/ETM+. Commission errors found were very low (<3 %) for all study sites, but omission errors (burned patches undetected) were relatively high (>25%) particularly for small BA patches. However, considering the limitations of MERIS data for detecting a strong BA signal, HS were used to establish the most appropriate date for the post-fire temporal compositing. The technique of using HS for labelling fire dates has been proposed by other authors (Boschetti et al. 2010).

Different tests to build the Thiessen matrix and the post fire NIR composite were implemented. The options tested are detailed in the following sections.

3.10.2.1. Thiessen (50%, 100%, 11.4 km and extended) + value after

In this case the first valid image after the date indicated in the HS matrix would be used to keep the NIR value in order to build the composite. If no data existed for that day or the data was considered not valid (it was filtered by the mask thresholds) the next day available was used to compute the spectral index. A maximum range of 45 days between the data used to compute the index and the date of the HS was established, to avoid

selecting a date when the BA signal was already blurred. This value was selected as a compromise between post-fire vegetation recovery in some ecosystems, where fire signal lasts shortly, and the number of valid images available. In case no data was available in 45 days the value assigned to the pixel was -4, and that pixel was considered unobserved.

Different strategies were also tested to build the HS Thiessen matrix.

- Input HS: two sub-options were tested, the first one using all HS detected, and the second one using only those HS with a confidence higher than 50 and 70 percent.
- Distance pixel – HS: two sub-options were tested, in one the date of the closer HS would be assigned to the pixel independently of the distance between this pixel and the HS. On the second case this distance was limited to a radius of 38 pixels (11.4 km) to any HS. This value was computed from an exploratory analysis performed in different study sites with grassland fires, by comparing fire perimeters extracted from Landsat TM/ETM data and HS distribution (Hantson, personal communication). The maximum distance between a HS and a Landsat perimeter was obtained, and this distance was never bigger than 10 km. A similar value was suggested by Giglio et al. (2009) to limit the growing of burned areas. In case pixels did not have a HS at shorter distance than 11.4 km, the value assigned to the resulting composite image was 0, as it was assumed the likelihood of being burned should be very low.

3.10.2.2. Thiessen with 3 NIR minima (over 2 months).

This strategy aimed at obtaining a higher spatial and temporal consistency, combining the benefits from the minima approach (3.10.1) with the HS Thiessen matrix one (3.10.2.1.). For this test, 3 NIR minima after the HS were obtained over two months, and the one closer to the HS was selected. If no values were available after the HS then the 2nd minima before the HS date was selected.

3.10.3. RESULTS.

Results from the different tests performed for the temporal and spatial compositing criteria are shown in the following sections.

3.10.3.1. Temporal criteria.

A graphical visualisation of the NIR and Julian date annual composites in the Australian study site is shown in Figure 13.

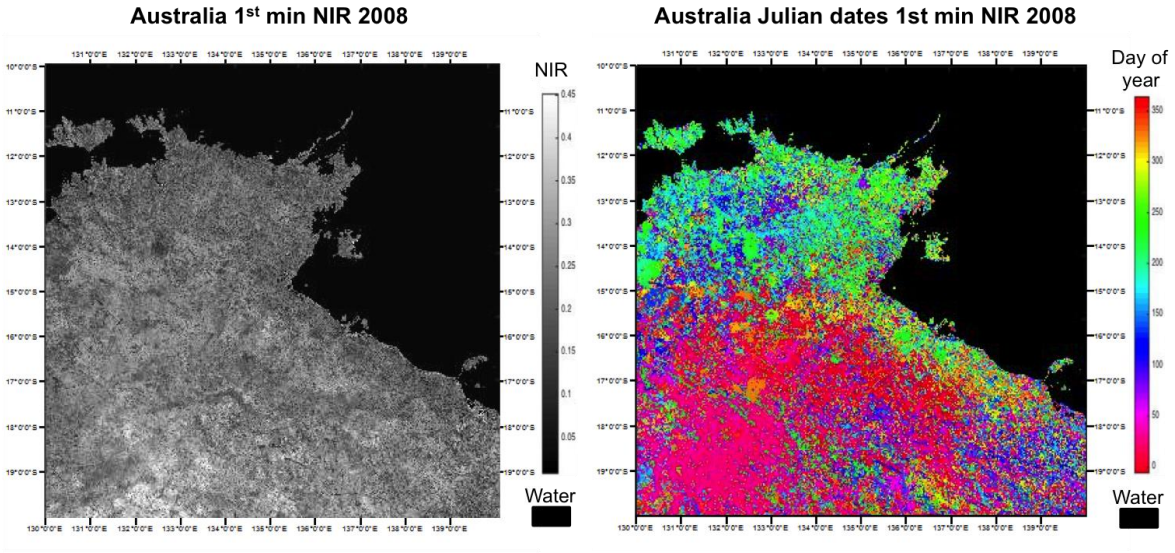

Figure 13. First minimum NIR composite and Julian dates associated for the annual test in Austalia 2008.

Dark regions can be identified from the NIR composite, as well as a certain level of aggregation in the Julian dates associated to these NIR values. In order to further evaluate the results obtained a series of extractions were performed for the 10 study sites. Three cases were defined in the study: agreement between the MODIS HS product and MERIS, only MERIS detection, and only HS detection. This analysis was proven to be useful to understand the commission and omission errors in the MERIS images using the HS product as reference. When analysing the extractions many inconsistencies were found. An example of this is shown in Figure 14. In this case MERIS and HS product agreed on detecting a burned pixel. Nevertheless, the fire according to the HS product occurred on day 260 (grey arrow), whereas MERIS was mapping a burn on day 228, more than 30 days prior to this date. On day 228 (blue arrow) the minimum NIR and GEMI values of the time series were found, classifying the pixel as burned. These values could correspond to a cloud shadow not properly masked, since the values of NIR and GEMI become higher again for the following days. In fact, the second minima in the NIR

and GEMI values is found on the same date indicated by the HS (grey arrow), finding also low NIR and GEMI values on the following days.

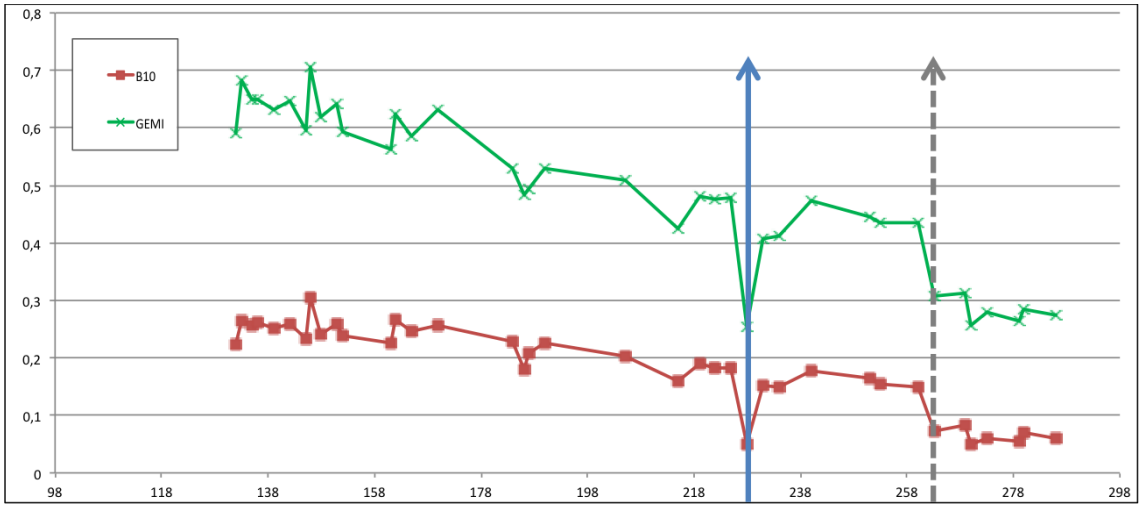

Figure 14. Bands 8 and 10 for a pixel in Kazakhstan in 2005, the date of fire is 260.

The main conclusion from these extractions was that the MERIS time series presented noise instability and that this lead to most of the errors (commission and omission but also date errors). The noise in the time series affects the composite in two ways:

- The date of the fire (as extracted from HS) was, in several cases, different from the date of the minimum NIR value, up to more than 100 days earlier or later in the worse cases, as exemplified by Figure 14. Similar cases were reported in other sites, such as Portugal (Figure 12), where the minimum NIR values were observed at the beginning of Spring, which is a very unlikely season for burnings in this region. In this case, the criterion of the minimum NIR value labelled a fire at the beginning of the Spring season (day 100), which is more than 150 days earlier than when the fire occurs (date of burn is 261). Similar issues were found in other sites. Although seasonality patterns could be used to discard some of the false positives, noise in the data still remains, making difficult the correct fire date identification.
- Spatial inconsistency: if a fire occurs and pixels in the same region are burned, the date related to the minimum NIR should be equal or at least similar. When applying this method to the MERIS data, minimum NIR values in neighbour pixels did not correspond to similar dates. Therefore when a growing algorithm was applied, the dates related to the same fire event were not consistent. A detail of this dates for the region highlighted in the red box in Australia (Figure 15) is shown in Table 11.

Figure 15. Region for dates extraction related to the minimum NIR composite. Red box indicates pixels shown in Table 11.

Table 11. Detail of Julian dates from red window (pixels from 11 rows and 11 columns) in Figure 15.

326	326	329	113	113	348	348	113	113	113	329
91	326	300	224	224	113	113	113	329	240	329
81	74	74	224	224	227	329	221	326	329	326
81	329	240	240	43	43	329	326	326	326	240
116	81	240	240	43	224	300	326	52	326	348
52	224	240	240	167	167	224	167	326	227	329
224	224	224	240	224	167	167	167	326	326	81
224	224	326	218	224	211	43	43	227	326	167
224	326	326	224	208	2	211	43	329	81	52
218	326	326	221	221	227	211	43	329	81	52
300	148	300	329	148	148	148	91	329	329	81

Analysing these results it can be seen that some neighbouring pixels are more than 150 days apart. Therefore in many cases no temporal relation exists between pixels. This effect was particularly noticeable at the borders of the fire areas. This behaviour is also related to the noise in the time series.

In light of these results some modifications to the initial configuration were made:

- It was decided to test the use of monthly composites, since this would minimise the noise effects found in the annual test. Applying the same method on a monthly basis increased spatial consistency but the temporal consistency was not ensured due to the noise in the time series. Therefore, other options for building the composite were needed.
- It was decided to use the HS dates to guide MERIS detections. A Thiessen matrix based on the HS dates would be computed. The date of the closest HS would be assigned to each pixel within the matrix. The NIR values of the MERIS images that correspond to the dates obtained in the Thiessen matrix (or the first image available posterior to those dates) would be used to build the NIR composite.
- It was decided to use the second NIR minima since the first one would not get rid of potential cloud shadows and the second one would minimise this effect, while keeping a good retrieval of the burned area. A comparison between the 1st and the 2nd minimum NIR is shown in Figure 16. As it can be seen darker areas (burned patches) remain while cloud shadow presence is reduced. This effect is particularly noticeable on the coastal areas, where speckle effects are clearly reduced. This way also higher spatial consistency is obtained.

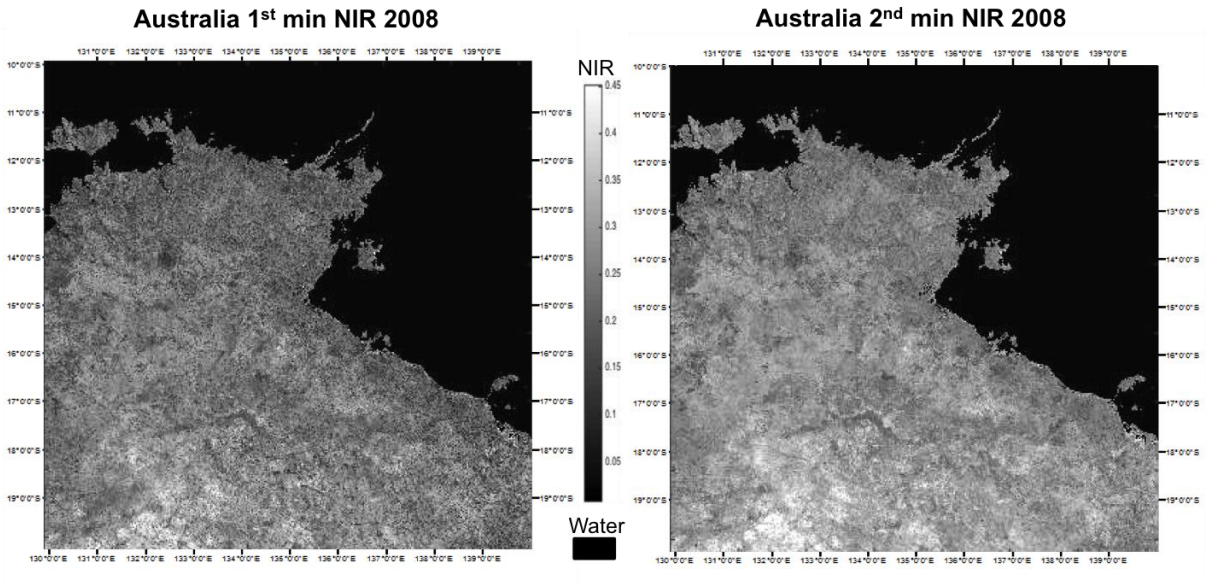

Figure 16. First and second annual NIR minima for 2008 in Australia.

3.10.3.2. Spatial criteria.

Spatial and temporal consistencies were obtained by computing a Thiessen matrix based on the HS dates. For each pixel the date of the closest HS was assigned. It was decided to use all HS independently of their confidence level since the commission errors from this product are low (Hantson et al. 2013) and further tests and filtering were applied in the next steps of the algorithm to help avoiding these errors.

3.10.3.2.1. Thiessen (50%, 100%, 11.4 km and extended) + value after

Results for the test that used the MERIS first valid observation after the HS date are available hereafter. It was decided to keep the distance to its maximum and not to the 11.4 km limit since results did not vary significantly and completing the Thiessen matrix guarantees a higher spatial consistency.

Figure 17 shows on the left side the Thiessen polygons matrix associated to the HS dates for October 2008. On the right, the dates of the first MERIS image available after the date indicated by the HS are plotted. It is important to highlight the date difference between the HS detection and the first MERIS valid observation, which can go up to 20 or 30 days (light blue polygons on the right side figure). This gives also an idea on the reporting accuracy of the MERIS observations.

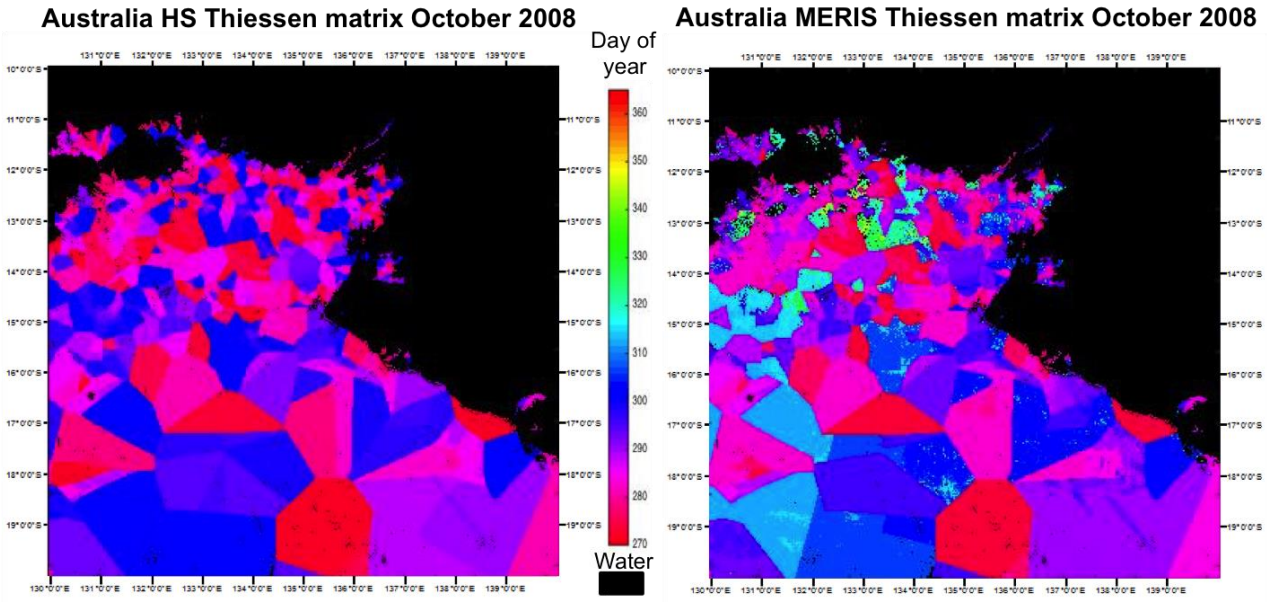

Figure 17. Australian HS and MERIS Thiessen matrices in October 2008.

This method guarantees a higher spatial consistency, and reduces the temporal errors. Temporal consistency was found higher with this method. Nevertheless, some artificial structures that follow the Thiessen polygons and that do not correspond to natural fire patterns were still present in the composites. These artificial structures associated to the use of the Thiessen matrix are illustrated in Figure 18, where the NIR of the MERIS images associated to the MERIS Julian dates Thiessen matrix is shown for October 2008 in the Australian study site.

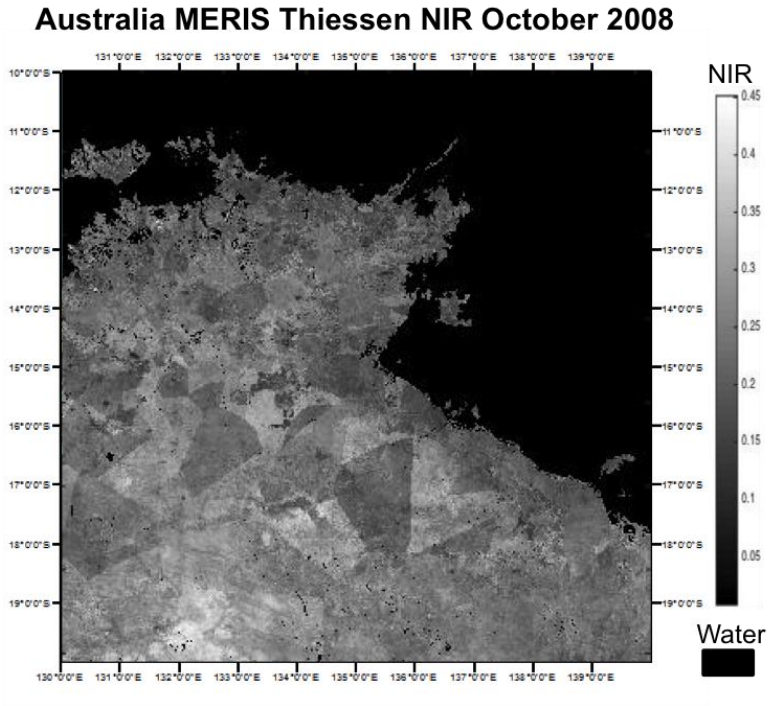

Figure 18. NIR composite using the Thiessen criterion of the HS dates.

3.10.3.2.2. Thiessen +3 NIR minima.

The strategy to diminish these artificial structures was based on combining the benefits of both the 2nd minimum NIR (spatial consistency) and Thiessen + value after (temporal consistency) approaches. Thiessen + 3minNIR is the approach that combines these two. Results from this implementation are shown in Figure 19. As it can be seen the NIR composite from the Thiessen + 3minNIR approach (top right corner) does not present the strong features that were observed on the Thiessen + value after, while keeping the temporal consistency, as shown in the Julian dates matrix of this method (bottom right corner).

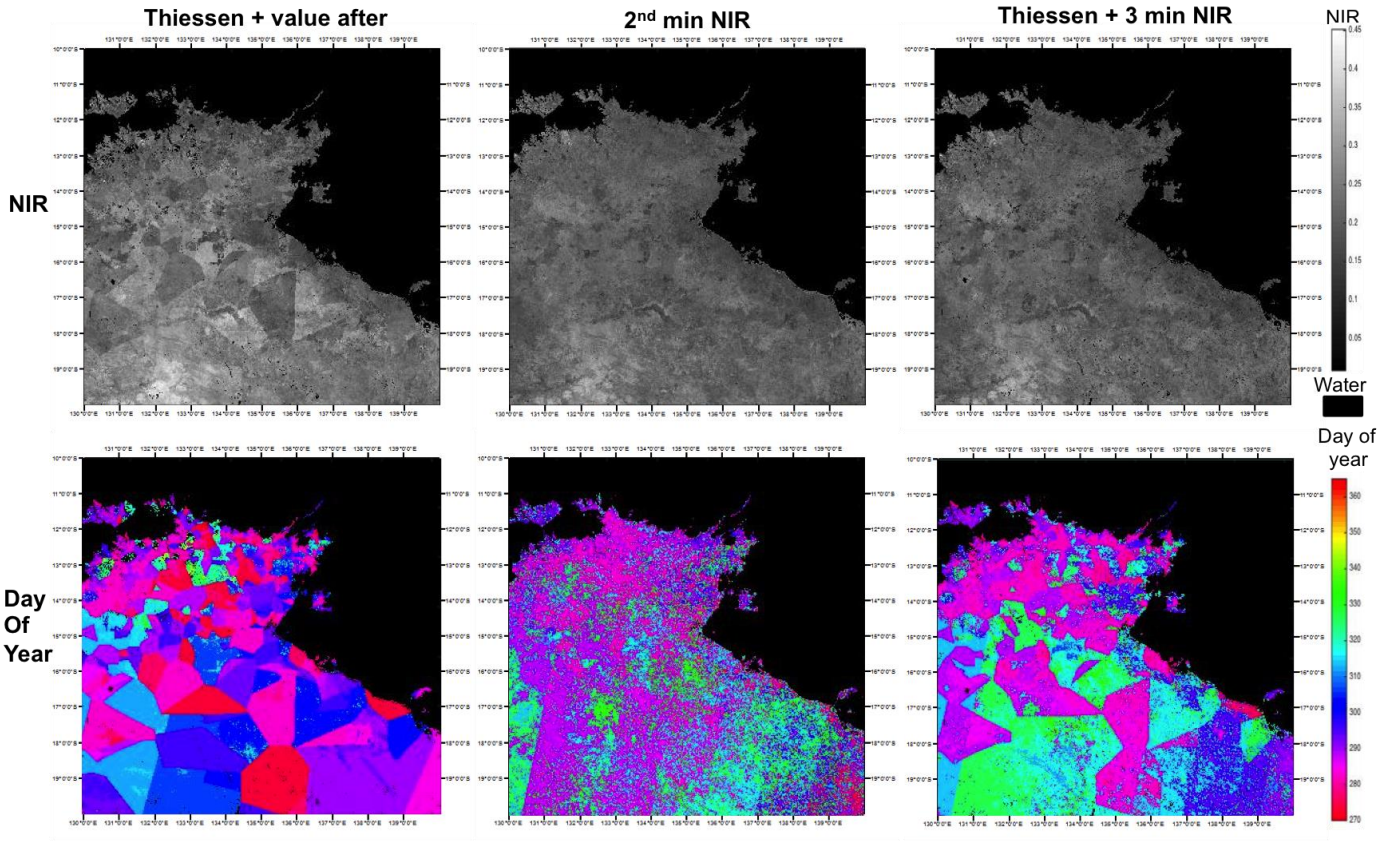

Figure 19. Thiessen+value after and 2nd minNIR approaches, combined in the Thiessen+3minNIR final approach.

In order to increase the spatial consistency it was decided to extend the compositing time. Composites were built for each month by selecting images from a bi-monthly time series (Figure 20) to mitigate the impact of low MERIS temporal resolution. This strategy decreases the effects of low number of valid observations for cloudy regions and helps detecting fire burned areas that occurred at the end of the monthly period.

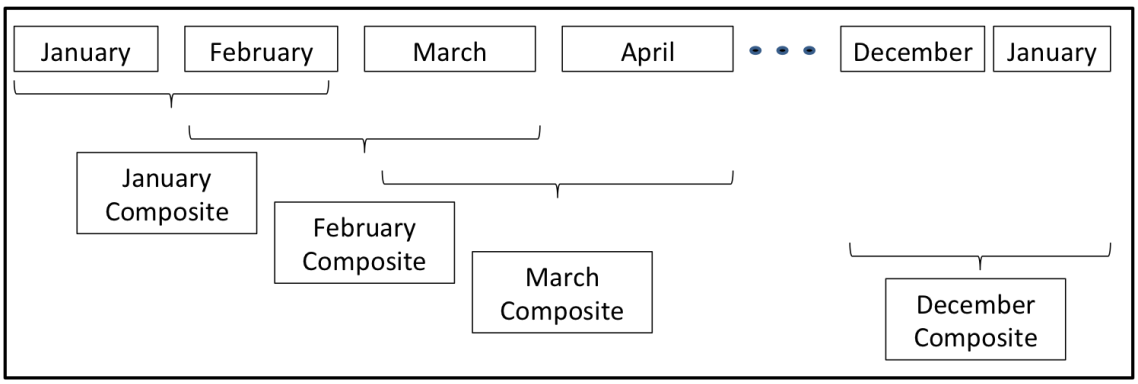

Figure 20. Monthly composites generation based on MERIS information from two consecutive months.

3.10.4. COMPOSITE FINAL CONFIGURATION.

NIR and Julian date composites were obtained with the method detailed in this section. As mentioned previously (3.9.2), in addition to the monthly post-fire composites, an annual reference composite was created for the contextual phase of the algorithm. This annual reference composite was obtained as the difference between the annual maximum GEMI value and the monthly GEMI composite. The annual composite maximised the GEMI value to account for the maximum seasonal greenness of each pixel. The difference with the monthly GEMI indices was obtained as it was assumed that the change between the annual maximum and the post-fire value (included in the GEMI monthly composite) should be the highest for burned pixels, thus emphasising post-fire spectral changes. The GEMI monthly composite is obtained by computing the GEMI index for the dates from the Julian composite, derived from the method described in the previous section.

The steps to build the monthly composites are illustrated in Figure 21. Final composites (NIR, Julian dates and DiffGEMI) are highlighted in green. The first two will be used in the seed and growing phases of the algorithm, while diffGEMI will be used only in the growing phase of the algorithm.

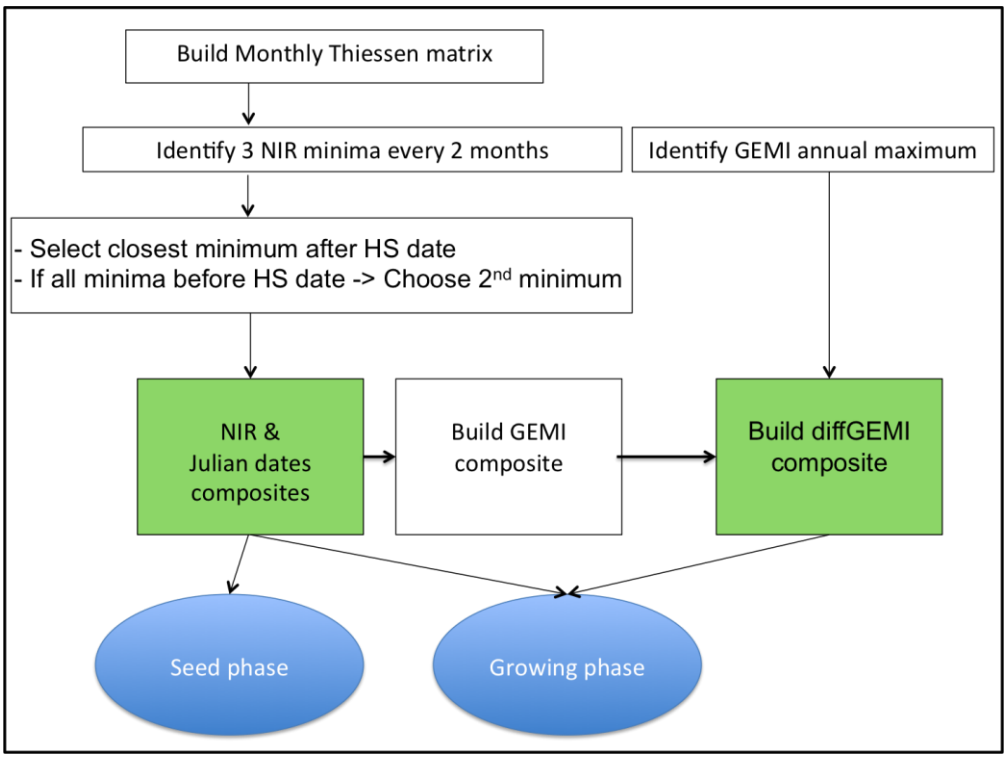

Figure 21. Steps to build the final composites.

3.11. SEED PHASE

3.11.1. GENERAL CONSIDERATIONS.

The seed concept is based on the identification of some pixels where there is a high confidence on those pixels having burned. There is a variety of techniques used to implement this phase. They can go from user identification and training algorithms, to the use of automatic methods. The bottom line is to have little omission in this phase (detection of maximum number of perimeters), while keeping a low commission rate. In the MERIS BA algorithm, the starting point is based on the definition of two different classes (burned and unburned). The purpose is to maximise the distance between these two classes to identify a threshold that could reasonably separate them. In addition, these thresholds should be dynamically (spatially and temporally) adapted to the fire characteristics of each region and season, as fire characteristics change both spatially and temporally.

For doing so, a series of rules were needed to identify the set of pixels that would help defining the burned and unburned classes. The approach was based on the use of HS to identify potential burned pixels, and by contrast the unburned ones. Those pixels that fulfilled a set of requirements were used to build the cumulative distribution functions (CDFS), used to represent the burned and unburned classes. From these functions, a threshold was established to identify seed pixels. Those threshold values were chosen to minimise the confusion between the two classes and were computed for each tile of the input MERIS reflectances (10°x10° or 3600x3600 pixels at MERIS FR). Figure 22 aims at illustrating the distributions and CDFs concept. On the left side two normal distributions are plotted. The top left one shows the case where the two distributions are closer, and therefore more confusion between the classes existed, since more values were shared between them. This translated also into closer CDFs (top right). On the bottom, the opposite case is represented, with a much clearer separation between classes, i.e. the distributions shared less values and therefore the confusion was lower.

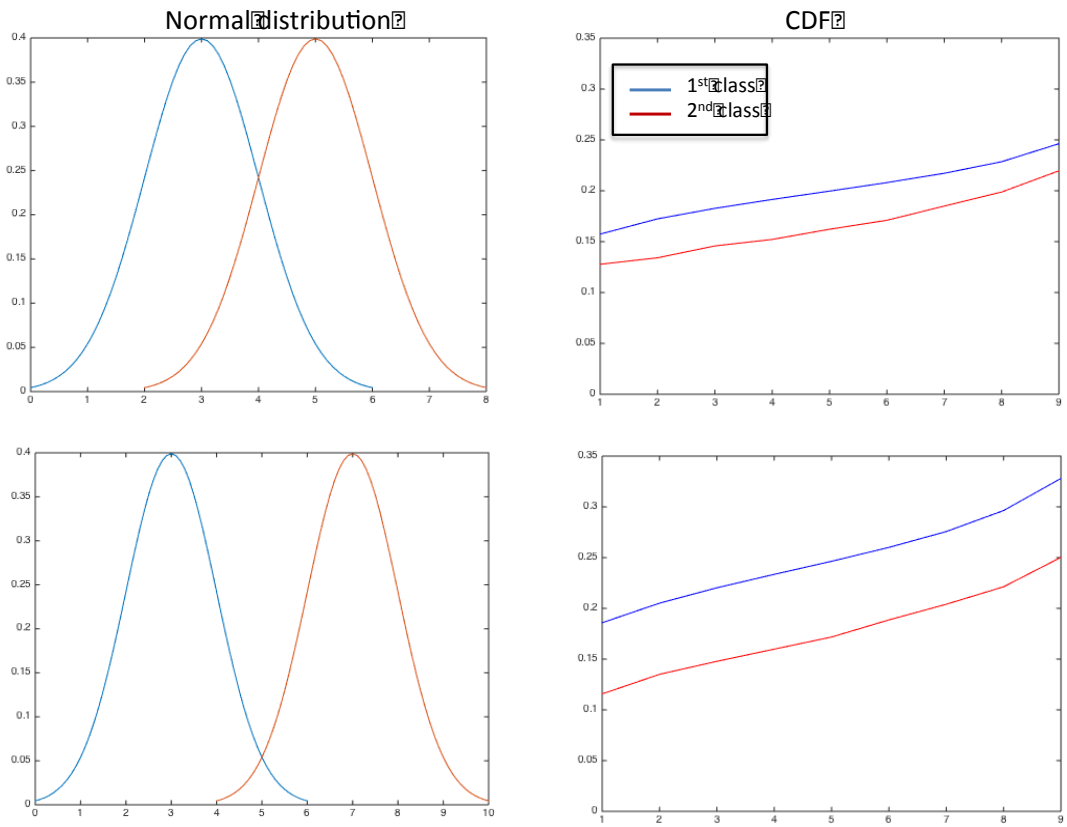

Figure 22. Normal distributions and CDFs showing the poor and better separation between classes.

The 10°x10° tiles that were the output of the BC pre-processing chain were used to obtain the statistics and CDF values. It was decided to keep them as input to the algorithm and to obtain the CDFs as this division offered a good balance between regional diversity and processing time. A series of tests were envisaged to obtain the best configuration to build the CDFs and to identify the final seed pixels. Other configurations were developed to optimise the results obtained.

It is important to note that the seed phase has a big impact on the final BA results, and it was very relevant to avoid commission errors in this phase since applying a growing algorithm to a commission seed pixel could lead to large commission errors (for instance in areas with dark soils). At the same time, omission errors should be kept to a minimum, since perimeters not detected in this phase would not be detected in the growing phase, and therefore would become omission errors in the final product. When developing the algorithm it was acknowledged that in order to optimise this phase, results from the growing phase would need to be taken into account to obtain the final

configuration. Furthermore, the statistics obtained in the seed phase were used to obtain some of the conditions for the growing phase.

3.11.2. THRESHOLDING APPROACHES.

3.11.2.1. Fixed thresholds.

Once the burned and unburned CDFs were built there were different ways to identify the threshold to be applied in each tile. A simple option was to determine a fixed relative threshold (for instance, using percentile 80 of the burned CDF) and use this value for all regions to be covered by the algorithm. Clearly this was a simple method and had also a big advantage in terms of processing time, which is an important point to consider when building a global algorithm. On the other hand, this way of determining the threshold was less flexible, and may not well adapt to the different conditions that exist worldwide and to the seasonality in the different regions, leading to large omission and commission errors. Nevertheless, due to its simplicity a test was performed with this approach to evaluate its performance.

3.11.2.2. Regional thresholds.

In this approach regionally-oriented NIR thresholds were obtained. They were adapted to different post-fire reflectance conditions. The CDFs and thresholds selected were computed for each tile and period. It was expected that this approach would better tackle the spatial and temporal variations of BA, obtaining a more tailored approach to the great diversity of fire conditions worldwide. The drawback was the required time to calculate regionally the thresholds, longer than when using fixed ones. These regional thresholds were determined using both the burned and unburned CDF value. Since the purpose was to minimise commission errors, the unburned distribution values determined which values were valid from the burned curve. When the curves were closer, more risk of confusion existed. Therefore, the NIR threshold value of the burned category (TB) was computed by selecting the immediately lower decile of the burned pixels' CDF that intersected the first decile of the unburned pixels' CDF. This criterion implies having as much as 10% commission error. Figure 23 illustrates this concept. In fact decile 1 of the unburned curve implies that all values below that decile could be

considered burned, when values of the unburned distribution will fall in the range between 0 and decile 1. The omission error in the seed phase would be estimated by the selected decile of the burned CDF, being higher when the curves are closer.

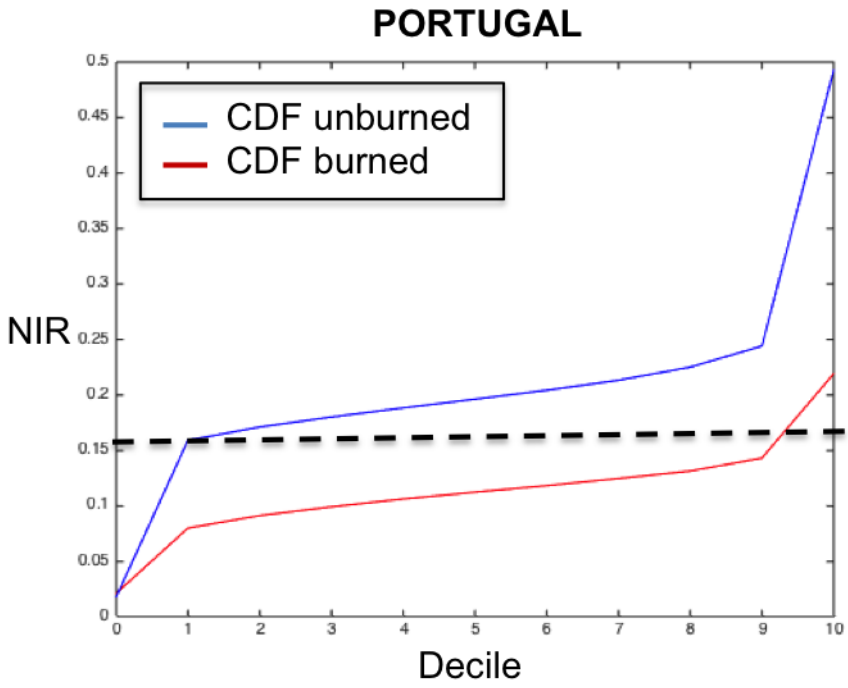

Figure 23. CDFs of burned and unburned classes. Decile 1 of the unburned class is identified with the black line.

3.11.3. DETERMINATION OF POTENTIAL ACTIVE FIRES. TESTS FOR THRESHOLD SELECTION.

The tests performed were designed with the objective of selecting the conditions to build the CDFs on a way that would maximise the separation between the burned and unburned classes. The pixels that were considered to build the burned CDFs were called Potential Active Fires (PAF). The different tests performed to identify the method to build the burned and unburned CDFs were:

a) Use of all HS.

In this approach all HS as obtained from the MOD14 active fires product were considered PAFs and were used to obtain the burned CDF. This approach does not take into account the potential commission errors associated to the product. However, since Hantson et al. (2013) did not find significant commission errors, even for low

confidence levels, it was decided to keep all HS and to filter the possible errors in further steps during the different phases of the algorithm. Furthermore, the Thiessen matrix built to obtain the monthly composites was also based on all HS, so it was decided to maintain all HS at this stage to ensure consistency between the different steps of the algorithm.

b) HS with decrease in NIR reflectance.

A simple way to filter out HS was to keep only the ones that had a decrease in NIR reflectance compared to the previous month observed. Those pixels were used to extract the burned CDF.

c) Unburned CDF.

Unburned pixels were extracted from areas without a single HS in the vicinity. This neighbour criterion was defined by different matrix sizes: 9x9, 16x16 and 64x64 MERIS pixels. Values below 9x9 would not be considered since they would be too close to the MODIS HS pixel size. Values bigger than 64x64 could give problems in areas with very high fire activity, or in areas where the proportion of land in the tile is low (water or non-burnable pixels).

d) Minimum NIR with decrease in NIR reflectance.

The spatial resolution is different between a HS (1km) and a MERIS pixel (300m). Therefore, 9 MERIS pixels will fall within a single HS. Up to now the MERIS centroid of these 9 pixels was used to identify the HS NIR value. In this test it was decided to study from the 9 MERIS pixels within the HS pixel which one had the lowest NIR value, identifying this one as more representative of the burning. In this test the pixels with minimum NIR showing a decrease in NIR reflectance compared to the previous month were identified as PAFs and used to build the burned CDF. Figure 24 illustrates this concept. The 9 MERIS pixels that fall within a HS are represented, with the centre of the HS being the red dot. The minimum NIR pixel is highlighted in blue. This pixel would be selected as PAF, if it also fulfilled the requirement of decrease in NIR.

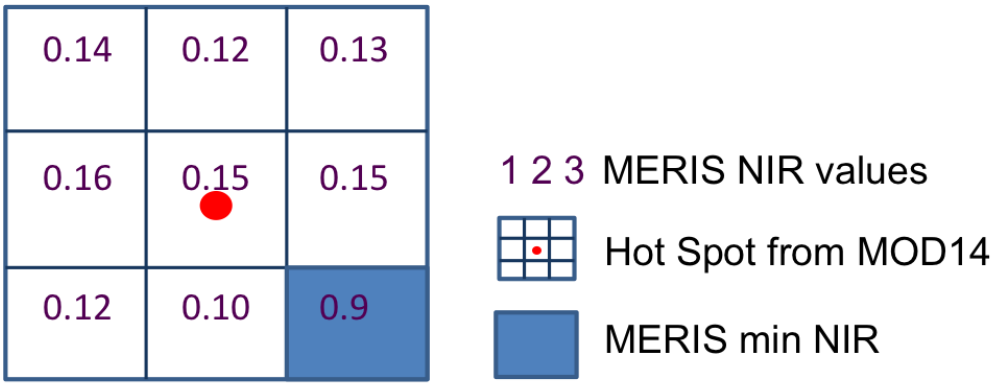

Figure 24. Selection of PAF within a MERIS 3x3 window with a HS.

3.11.4. DETERMINATION OF SEED BURNED PIXELS. TESTS FOR SEED EXTENSION.

Once the threshold was identified, PAF and the surrounding pixels were analysed to obtain the final burned pixel seeds. Four conditions were established to accept a pixel as a burned seed:

- Maximum distance to a PAF should be below a certain value. The options tested were PAF in a 3x3, 9x9 and 16x16 matrices around the pixel analysed. In the results section the results from this test are called 1PAF 3x3, 1PAF 9x9, 1PAF 16x16.
- Number of PAFs: the number of PAFs (within a distance around the pixel analysed) required to classify the pixel as seed will be studied. 1PAF or 2PAFs within the distance matrix were tested. The requirement of 2 PAFs is more restrictive but can be more robust against commission errors from the HS, as more than one HS is needed. The drawback is that this restriction diminishes the detection of smaller fires (since they will not have more than one HS associated). In the results section the results from this test are called 1PAF 9x9 and 2PAF 9x9.
- NIR decrease: Three options were tested:
    - The pixel should show a decrease in NIR value compared to the previous temporal composite. This option was implemented in the tests 1PAF 3x3, 1PAF 9x9, 1PAF 16x16 and 2PAF 9x9.
    - Median: instead of using a single pre and post-fire NIR reflectance, in this case the median of the NIR reflectance for 5 daily values before and after the HS date was computed. This criterion tried to mitigate the potential

impact of noise in the time series. This test is called median in the results section.

  - Median with restriction: the number of pixels resultant from the filtering of HS with the median technique provides an idea on the number of commission errors that exist in that area for the MOD14 product. Therefore, this information could also be used to define more or less restrictive conditions to classify the pixels as seed. The ratio between HS and PAFs (filtered after applying the median technique) was computed. If this relation was bigger than 2, the number of PAFs per matrix required to classify a pixel as burned increased. This test is called median_restriction in the results section.

- NIR value lower than the threshold identified from the CDF.

Main previous steps (from section 3.11.3) together with the new conditions to test (highlighted in yellow) are illustrated in the diagram in Figure 25.

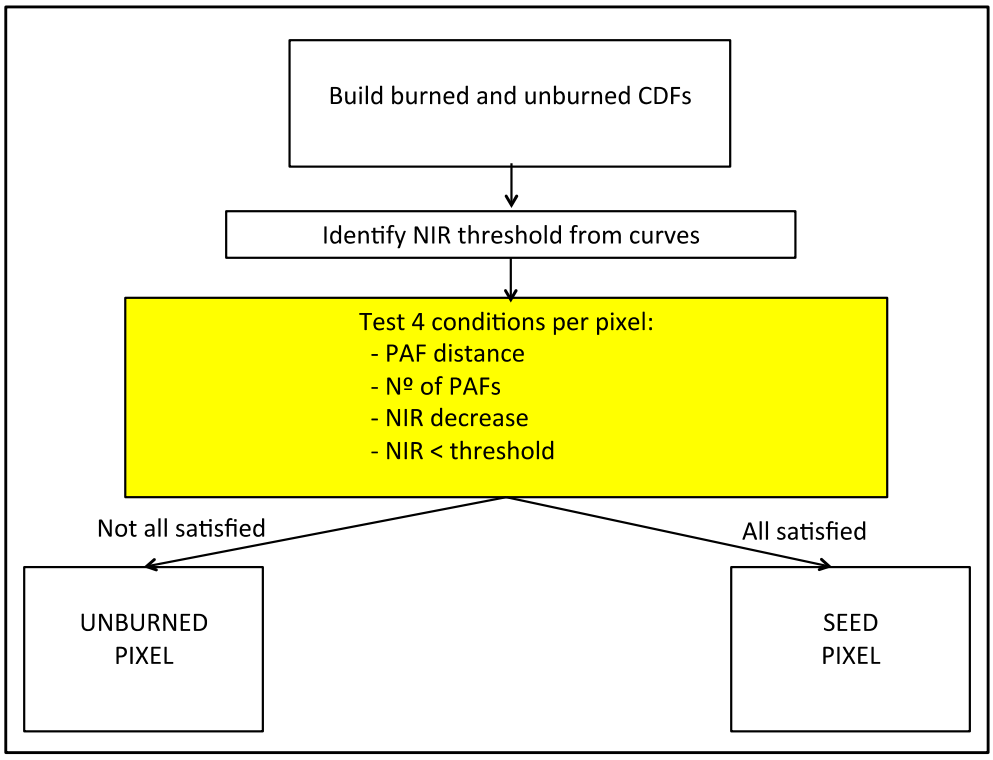

Figure 25. Conditions to verity to classify a pixel as seed.

3.11.5. RESULTS.

Two types of criteria were used to determine which tests were giving the best results. For the threshold selection methods (section 3.11.3.) the selection was based in maximising the distance between the burned and unburned CDFs. For the seed extension (3.11.4.) the number of reference perimeters detected in 4 study areas (Australia, Canada, Portugal and California) and selected global results were the criteria used to determine the method. Reference perimeters are the ones detailed in section 3.4.2

3.11.5.1. Results from tests for threshold selection.

Fixed threshold:

Figure 26 represents the CDFs obtained for Portugal in January 2008 (left) and Australia in January 2008 (right). The black line represents the threshold relative to the fixed decile 7th of the burned CDF.

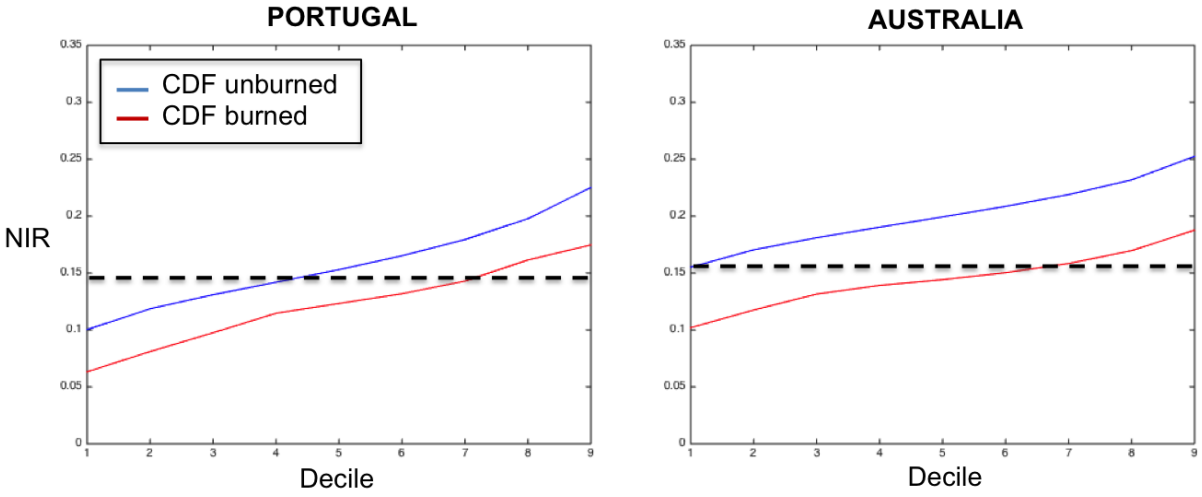

Figure 26. CDFs of burned and unburned using a fixed threshold, based on decile 7th of the burned CDF.

As it can be seen from the figure interpretation, in the case of Australia, the decile 7th gives a good separation between the burned and unburned curves, since few values from the unburned distribution will fall within the threshold limits. This is not the case for Portugal, where the same decile sets up a threshold that implies higher confusion between the burned and unburned classes, since more values from the unburned curve

are included. Therefore the fixed threshold does not give an optimal separation between classes for the seed phase.

Regional thresholds:

a) HS: in this case all HS as delivered by the MOD14 product are used to build the burned CDF. The results of this test can be seen in Figure 27. As in the previous example (fixed thresholds) the study sites are Portugal and Australia, in January 2008. In this case, the first decile of the unburned class will be chosen to define the threshold. This will establish the threshold correspondent on the burned curve of decile 3 in Portugal and decile 6 in Australia, represented by green arrows in the figure. This approach gives for both cases lower confusion and therefore lower commission errors.

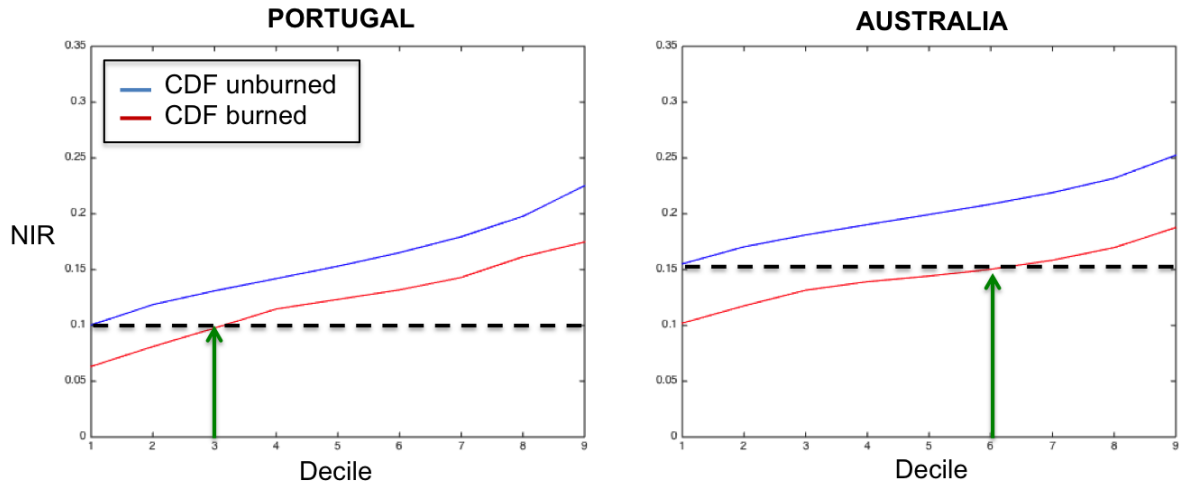

Figure 27. CDFs and associated deciles and thresholds when using the regional approach.

b) HS with decrease in NIR reflectance: results of this test are shown in Figure 28, where January and December 2008 CDFs are computed for Australia. The CDF built with all HS is plotted in red, whereas the CDF in green represents the one built with only the HS that have a decrease in NIR reflectance with respect to the previous month. The change is not obvious in January but shows a clear decrease in December. This tendency was verified in all study sites and showed that a filtering of HS with the decrease in NIR reflectance criteria would help improving the definition of the burned CDF and therefore of the threshold.

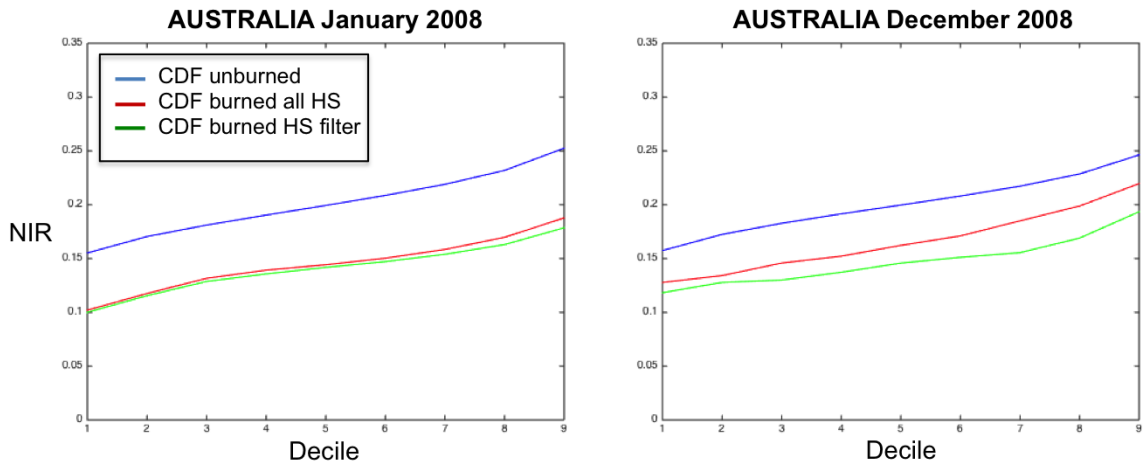

Figure 28. CDFs of all HS and HS filtered (decrease in NIR from the previous month) for January and December 2008 in the Australian study site.

c) Unburned CDF: results from this test are shown in Figure 29 for Australia in December 2008. The unburned CDFs are computed for matrices not having any HS. The matrix size considered was 9x9 (green), 16x16 (red) and 64x64 (blue). As can be concluded from the figure, the CDF obtained with the matrix not having any HS in 64x64 pixels gives the best result since it will lead to a clearer separation from the burned CDF than the other two unburned curves. Therefore less confusion between classes should be obtained in this case.

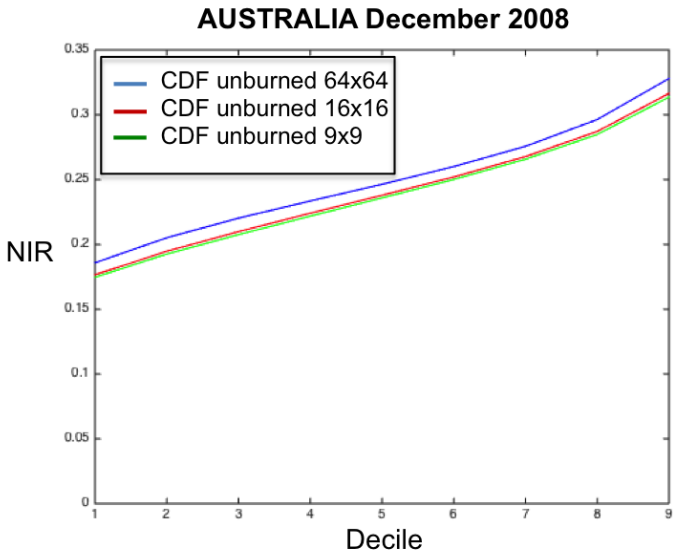

Figure 29. Example of unburned CDFs with matrices not having any HS in 9x9, 16x16 and 64x64 pixels, for Australia in December 2008.

d) Minimum NIR with decrease in NIR reflectance: results for this test are shown in Figure 30 for Australia in January and February 2008.

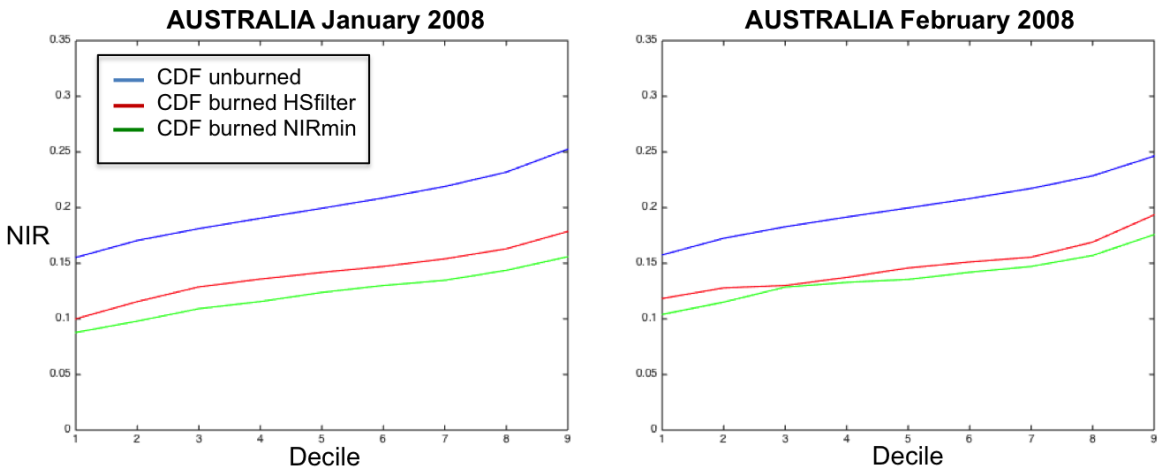

Figure 30. CDFs of unburned, burned with HS filter and minimum NIR, in January and February 2008 for Australia.

The unburned CDF computed with the 64x64 matrix is plotted in blue. The red curve represents the burned CDF computed with the HS filtered (decrease in NIR, case b). The green curve is the CDF computed with the pixels selected with the minimum NIR method, and that had a decrease in NIR reflectance compared to the previous month. This last test shows a higher separation between the burned and unburned CDFs. This effect is more obvious in January but is also present in February. The minimum NIR with decrease in NIR reflectance was therefore chosen as the final configuration to compute the CDFs, and to select the threshold to separate between burned and unburned classes. The threshold will be selected from the immediate lower decile of the burned curve that corresponds to the first decile of the unburned curve.

An example to illustrate this final procedure to select the threshold is shown in Figure 31. The plots represent the CDFs for Canada (a) and South Africa (b) for May and June 2008 respectively. Here the deciles are represented as steps. The purpose is to illustrate the fact that the threshold (black arrow) will be chosen as the immediate inferior value that intersects the first decile of the unburned curve, corresponding to the step right under the intersection.

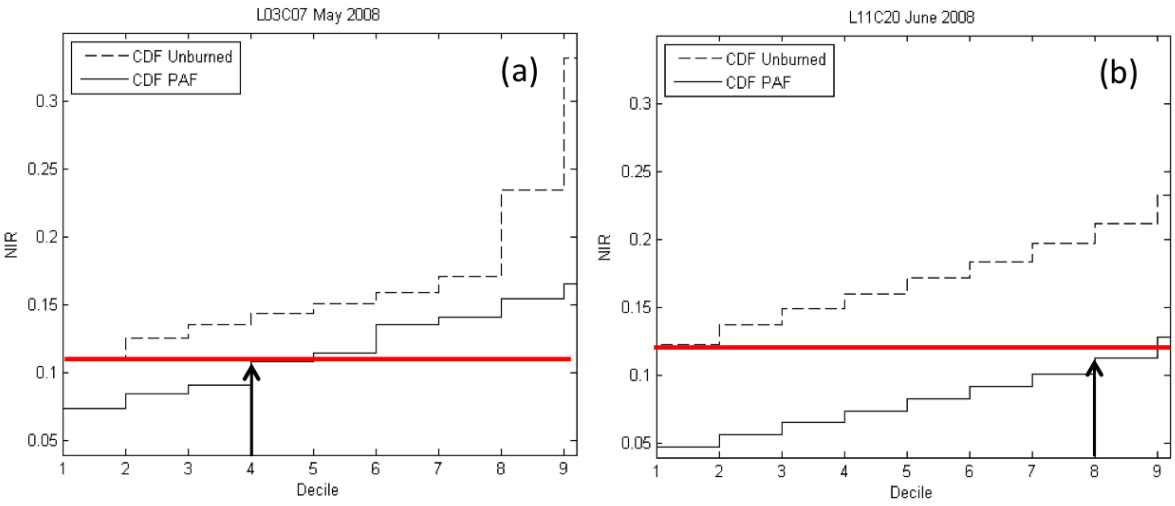

Figure 31. Threshold based on decile 1 of the unburned CDF for cases with worse (a) and better (b) discrimination between classes, correspondent to May 2008 in tile L03C07 (Canada) and June 2008 in L11C20 (South Africa) respectively.

3.11.5.2. Results from tests for seed extension.

Fire perimeters derived from national agencies have been used to compare with the burned areas obtained in four study sites when developing the algorithm, and to extract conclusions from the different options tested. The study sites and fire perimeter information are detailed in section 3.4. Table 12 summarizes the results for the different tests. Results are separated by study site, fire size, and represent the percentage of fire perimeters detected according to the fire size. Omission and commission errors are also shown in the table. It is important to note that these errors are presented as a way to estimate how each test is performing, but they do not give a proper estimation on the omission and commission errors on burned area in these sites, since only seed pixels are being evaluated. It should be noted as well that the commission error shown has a higher relevance than the omission error for two reasons. First, because commission errors introduced in this phase will propagate into the growing phase. Second, the fact that the omission error is smaller in one case or another, if the same number of perimeters is detected, is of low relevance. It is not necessary to detect all burned pixels at this stage of the algorithm, since those pixels can be detected in the growing phase.

Table 12. Fire perimeters detected and omission and commission errors, for the different seed extension tests in four study sites: Australia, Canada, Portugal and California.

Study site		Fire size (ha)			O.E.	C.E.
AUSTRALIA	<100	<1000	<10000	>10000		
Total nº of per.	12174	4652	1373	209		
% of per. detected						
1PAF 3x3	14%	56%	94%	100%	0.8386	0.1520
1PAF 9x9	35%	72%	95%	100%	0.5409	0.1752
1PAF 16x16	47%	81%	97%	100%	0.4341	0.2119
2PAF 9X9	21%	52%	91%	100%	0.6745	0.14
Median	37%	74%	96%	100%	0.5245	0.1752
Median_restriction	36%	72%	94%	100%	0.5500	0.1670
CANADA	<100	<1000	<10000	>10000		
Total nº of per.	30	20	28	34		
% of per. detected						
1PAF 3x3	0%	30%	57%	88%	0.8886	0.1120
1PAF 9x9	0%	35%	57%	88%	0.7191	0.1257
1PAF 16x16	0%	35%	57%	88%	0.6605	0.1523
2PAF 9X9	0%	25%	54%	88%	0.7809	0.1022
Median	3%	45%	75%	94%	0.6028	0.1007
Median_restriction	3%	45%	75%	94%	0.6028	0.1075
PORTUGAL	<100	<1000	<10000	>10000		
Total nº of per.	24	19	4	0		
% of per. detected						
1PAF 3x3	46%	68%	50%	-	0.8541	0.8949
1PAF 9x9	50%	79%	50%	-	0.6509	0.9254
1PAF 16x16	50%	79%	50%	-	0.5829	0.9561
2PAF 9X9	33%	68%	50%	-	0.7482	0.8475
Median	54%	79%	50%	-	0.6416	0.9446
Median_restriction	33%	58%	50%	-	0.7675	0.8106
CALIFORNIA	<100	<1000	<10000	>10000		
Total nº of per.	98	48	25	5		
% of per. detected						
1PAF 3x3	4%	8%	68%	80%	0.5913	0.1111
1PAF 9x9	4%	13%	68%	80%	0.4247	0.2254

1PAF 16x16	4%	13%	68%	80%	0.4037	0.3466
2PAF 9X9	4%	8%	60%	80%	0.4479	0.0996
Median	6%	29%	80%	100%	0.3793	0.2090
Median_restriction	4%	21%	80%	100%	0.3829	0.1117

From the first set of options: 3x3, 9x9 and 16x16, the third one detects more perimeters in Australia, where as the number of perimeters detected for the other 3 areas is the same. The omissions in this case are probably due to an omission error from the HS product or by an omission error created during the seed selection (because the pixels that had a HS associated did not satisfy the other conditions and were therefore not classified as PAFs). Since the purpose was to increase the number of seeds with this extension, the first option 3x3 did not provide the best results. The 16x16 option increased the number of perimeters detected in Australia, which is something desirable, but at the same time did not increase the number of perimeters detected in the other 3 areas, while it largely increased the commission errors. Therefore from the 3 matrix tests performed, the 9x9 option was selected. Nevertheless, tests performed globally in areas that could be problematic showed in effect large errors due to commission related to the HS. An example of these errors is shown in Figure 32. These results let to the implementation of a new test, which required having more than 1HS per matrix. This test was called 2PAF 9x9. This strategy managed to avoid commission errors in the problematic regions. On the other hand, increasing the number of PAFs required per matrix, implied a decrease in the number of perimeters detected. Figure 32 shows the different BA detected when implementing the option of 9x9 1 PAF (left) and 9x9 2PAFs (right) for two tiles L04C29, located in China, and L03C21 located in Russia. On the upper left part of the figure a big burned area patch in orange is noticeable. This corresponds to a commission error, largely increased after applying the growing phase. There is also a properly detected fire on the top left corner (blue). In comparison, the right side of the figure, which corresponds to the 9x9 2PAF implementation, shows the detection of the top left corner fire (blue), whereas the big commission error has disappeared using this method. Similarly on the area L03C21, on the left side blue and red perimeters correspond to large commission errors. These ones are avoided using the 2PAF9x9 method shown on the right side.

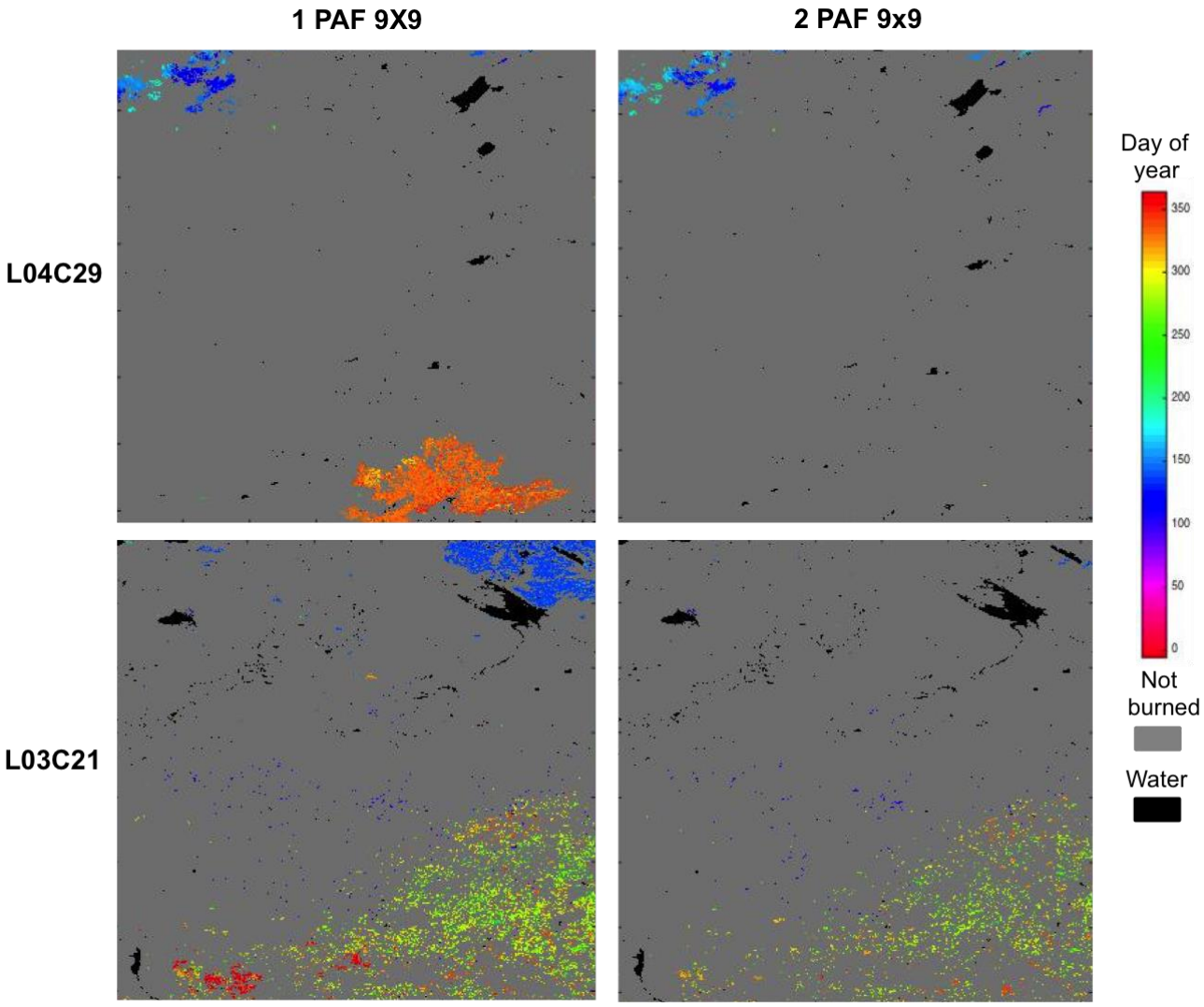

Figure 32. Test results for two different tiles (L04C29 and L03C21) located in China and Russia respectively, for year 2008, with the 1PAF 9x9 and 2PAF 9x9 implementations.

In order to avoid these large commission errors it was decided that the 9x9 2 PAFs implementation would be the best compromise between detecting number of perimeters versus diminishing commission errors.

Results shown in Chapter 4 of this thesis were obtained with this implementation. These results were analysed for the 3 years that were obtained with the global processing. The validation exercises showed that the algorithm had a tendency towards omission. Therefore it was decided that an approach based on the previous developments but that would increase the detection of perimeters needed to be developed. This led to the definition of the other two tests: median and median with

restriction. Taking into account the results shown in Table 12 the median with restriction method was selected as a compromise between the more restrictive 2PAF 9x9 and the less restrictive 1PAF 9x9. The median with restriction approach combines the benefits of lower commission and omission errors in most cases, maintaining the number of perimeters detected. In the study sites analysed the median with restriction method detects more perimeters than the previous options selected (1 PAF 9x9 and 2PAF 9x9), while keeping a similar commission error, in three of the four areas: Australia, Canada and California. In the case of Portugal a decrease in the commission error was observed but also in the number of perimeters detected. As already mentioned, the balance between omission and commission errors will always be a compromise when building a global burned area algorithm. It was considered that the commission error in this area was too high, and therefore the focus was on diminishing it, even if this implied increasing the omission error. Another important thing to note is that the Burned Area proportion (BAp) in Portugal was very low (<0.001) compared to the BAp in the other three regions (Australia = 0.181, Canada = 0.026 and California 0.013) and therefore its influence is minor. Furthermore, from the Hantson et al. (2013) study, Portugal was one of the areas identified where commission errors in the HS were higher and therefore an effort to restrict errors in this region was needed.

3.11.6. SEED FINAL CONFIGURATION OVERVIEW.

The tests designed and implemented produced a series of results that helped obtaining the final configuration of the algorithm. The selection of the different steps was first based on maximising the separation between the burned and unburned classes, and second on minimizing commission errors while keeping the number of perimeters detected to the maximum possible. The seed implementation designed and used to obtain the global BA product for years 2006 to 2008 (version 1) is summarised in Figure 33. Results obtained with this version are the ones presented in Chapter 4.

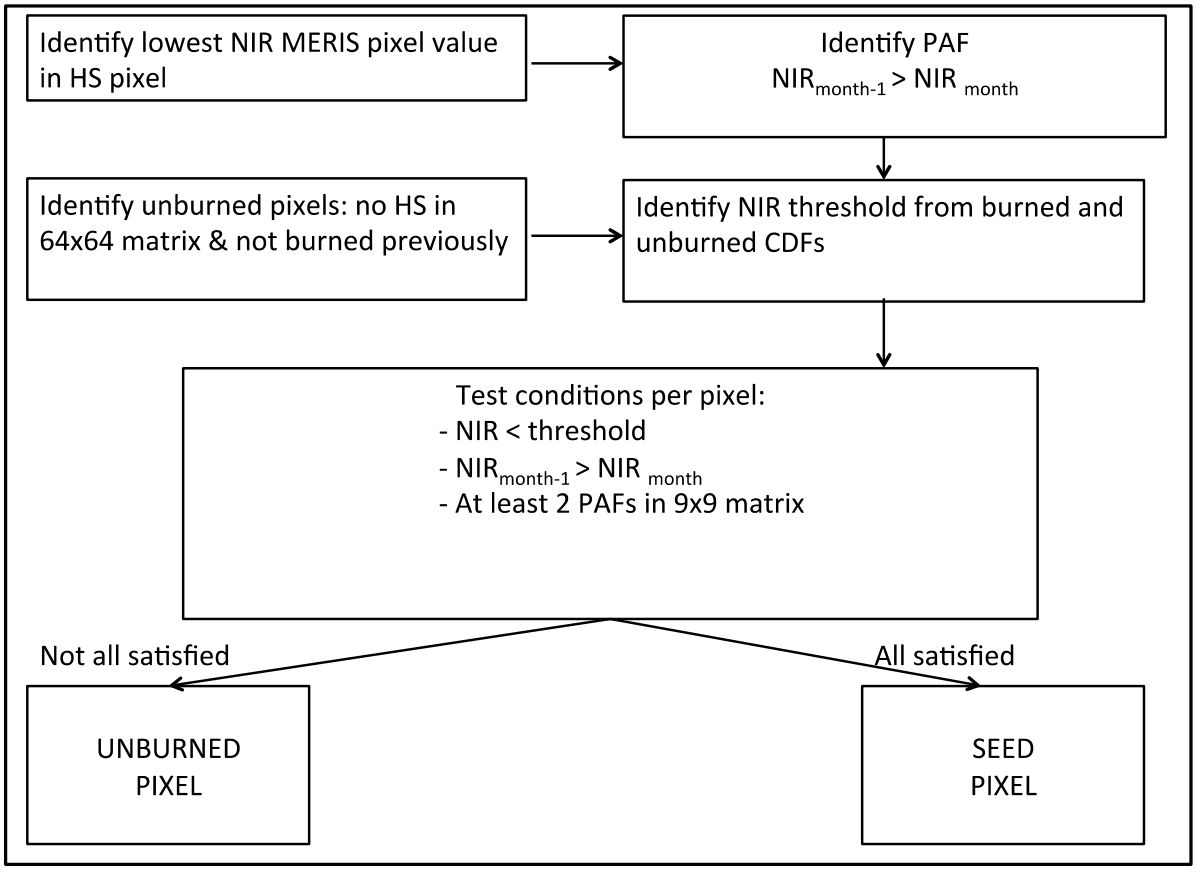

Figure 33. Seed pixel algorithm version 1 configuration.

The final configuration (version 2), which will be used to process the MERIS full time series, is shown in Figure 34. More details on this configuration are available in Annex 3. There are two main differences between the seed implementation of the final version of the algorithm and the previous one. The first difference is that in version 1 PAFs (used to build the CDFs) were identified as the HS that had a decrease in NIR compared to the previous month. In version 2 PAFs are identified as the HS where the median NIR of the 5 previous observations is bigger than the median of the 5 posterior observations. This way a more robust strategy is built against the noise in the time series. The second difference is that in version 2 the ratio between HS and PAFs filtered (after the 5 median pre and post values) is computed. If the ratio is lower than 2 only one PAF will need to be found in the 9x9 matrix around the pixel analysed. If the ratio is higher than 2, at least 3 PAFs will need to be found in the 9x9 matrix around the pixel. In contrast, in version 1 PAFs needed to be found in the 9x9 matrix for all cases, independently on the ratio between HS and PAFs. This new condition helps identifying areas where there is a

higher rate of commission errors in the HS product, becoming more restrictive in the conditions applied to classify a pixel as seed, and therefore creating a more robust strategy against those errors. On the other hand, when commission errors in the HS are not high, the number of PAFs needed in the 9x9 matrix around the pixel is lower (1PAF vs 2PAFs) in version 2 than in version 1. This allows detecting smaller fires, where only one HS is present.

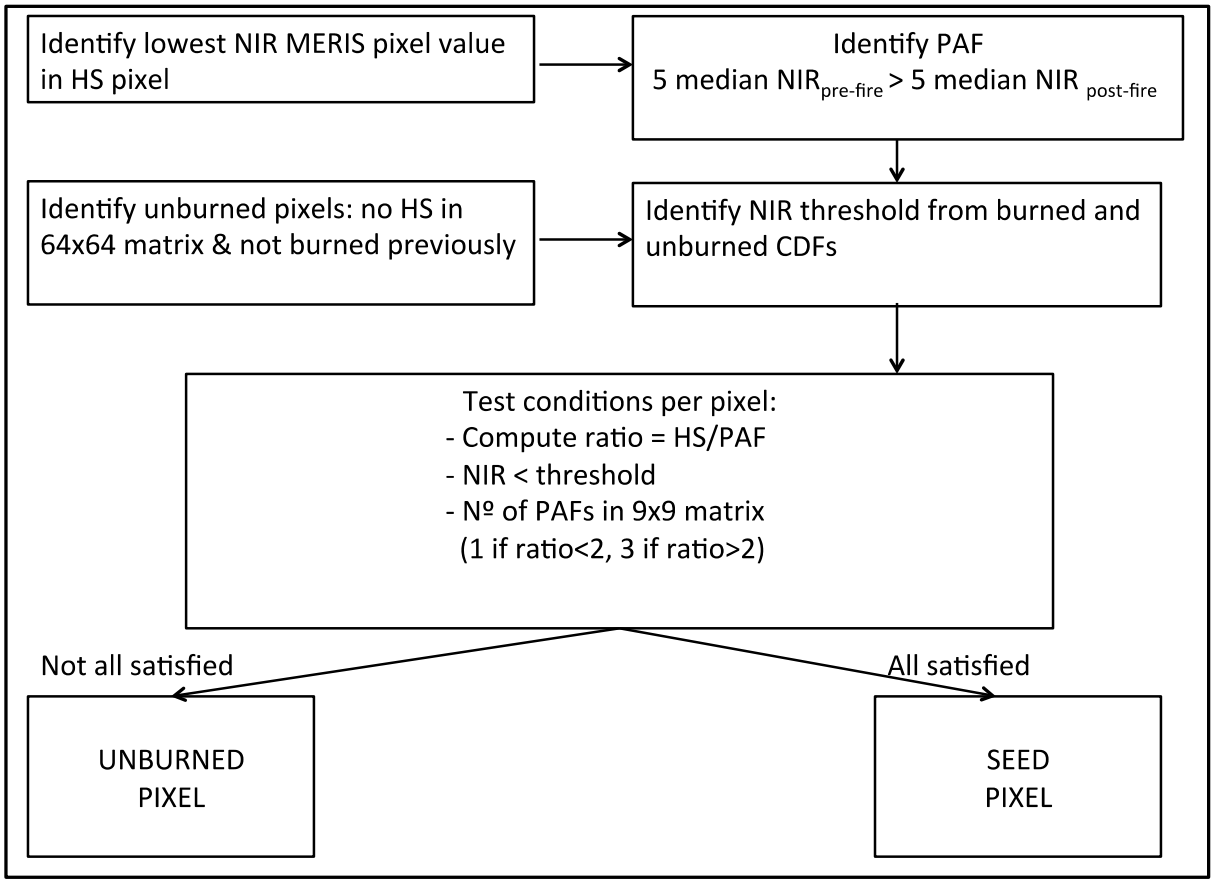

Figure 34. Seed pixel algorithm version 2 configuration.

3.12. GROWING PHASE.

3.12.1. ALTERNATIVES FOR GROWING.

Once the seed pixels were identified, this phase aimed to improve the spatial characterization of the burned patches, by analysing pixels around those detected as seeds. Many contextual methods are available for this purpose. They can be grouped into two large categories: pixel or object identification techniques. In the first case, the region grows around the pixel based on a series of conditions. The second approach defines a number of objects delimited by different spectral and spatial characteristics and these objects are classified as burned or not based on the seed location that will help selecting them. In pixel based techniques certain criteria need to be fulfilled by each pixel to be classified as burned. Generally, these criteria are based on thresholds that can be obtained statically or dynamically. In the case of object-based approaches also several implementations exist, but the basis for all of them is to first segment pixels into objects based on spectral and spatial similarity.

3.12.2. TESTED ALGORITHMS.

From the variety of options to carry out region growing approaches, the following were selected to implement the second phase of the BA algorithm. The selection was based on different criteria, such as characteristics of the input data, performance in other BA collections, and processing time. Five approaches were selected. Three of them were pixel-based (neighbour value, neighbour median and edge detection) and two of them were object based (OTSU and watershed). In the object based algorithms the seeds will be used to select the objects. Description of each algorithm is detailed hereafter.

3.12.2.1. Neighbour value.

In this region growing approach the pixels around the seeds are analysed. For each one of them a series of criteria are checked and if they are fulfilled the pixel will become a new seed. In this case, also the pixels around it will also be analysed. Normally the criteria to classify are based on thresholds. Different criteria were tested, all based on the composite and seeds obtained in the previous phases of the algorithm. A wide

variety of tests was performed but only the configuration that gave better results is introduced here for simplicity. This configuration was based on three criteria:

- NIR threshold: the threshold value used in the seed phase was selected from the CDF, as in the seed phase, but reviewing the decile chosen. In case there was a high separation between classes the conditions on the growing phase would be less restrictive. Assuming a normal distribution, if the burned decile used to define the seed threshold was 7 or higher, the burned/unburned curves intersect after at least one standard deviation of the mean burned values. In those cases the ability to distinguish between burned and unburned classes was considered high. Therefore, the new threshold condition for the growing phase was raised up to the decile 9 of the burned pixels curve, obtaining a higher NIR value (and a less restrictive condition). If the burned decile used to define the seed threshold was lower than 7 then the ability to discriminate burned and unburned classes was considered low. In this case, in order to ensure less commission errors in the growing phase, the threshold was kept with the value defined in the seed phase.

- The diffGEMI annual composite had to verify a decreasing threshold between seed and neighbour pixels. Pixels were classified as burned if the neighbours to a seed pixel had higher values than the threshold. The threshold was defined from the diffGEMI value found in the seed pixel multiplied by 0.9.

- The third condition relied on a minimum drop that had to be verified for each pixel. The decrease in the NIR values (DNIR) between t and t-1 for each candidate BA pixel had to be higher than the decrease observed for unburned areas. The aim when introducing this criterion was to avoid neighbour areas to the seeds that might have fire-unrelated changes.

The main advantage of this technique is that it is based on the values of the pixels themselves, having the possibility to tailor the thresholds more specifically in each case. Main drawbacks are that computationally it is less efficient than other methods, and that in case there is a commission error in the seeds located in a dark surface it can lead to large commission errors.

3.12.2.2. Neighbour median.

In this region growing approach only the NIR value needed to be lower than the median + the standard deviation of the burned pixels (already classified as burned). This technique was based on the findings by Libonati et al. (2014), who applied a similar procedure to MODIS images. Two cases were tested. In the first one, a matrix of 5x5 pixels around the pixel analysed was studied. If at least 3 pixels were burned in the matrix, mean and standard deviation from these 3 pixels was computed. If the addition of mean and standard deviation was bigger than the NIR value of the pixel analysed then it would be classified as burned.
In the second test the matrix analysed was of 3x3 pixels and the number of burned pixels was reduced to two. In order to avoid large processing times (and excessive growing) a maximum number of ten iterations per pixel were allowed. Therefore after 10 iterations, the next seed pixel would be analysed.

3.12.2.3. Edge detection.

This technique was used to detect the boundaries of objects in the images, based on discontinuities in brightness. The idea when implementing this test was to limit the growing on the neighbour value approach, by establishing those limits with already defined simple edge detection functions. In this case a threshold was needed to establish the boundaries between regions. The threshold identified in the seed phase was used for this purpose. Several edge detection techniques exist, the most popular ones include Sobel, Canny, Prewitt, Roberts, and fuzzy logic methods. The Canny method was chosen since it has a good performance balancing noise (it improves the signal to noise ratio) and preserving edges (with the use of the threshold) (Shrivakshan 2012).

3.12.2.4. Otsu method.

In this case the objective is to set a threshold that separates the two classes by minimizing the combined spread between classes, i.e. the within-class variance, therefore maximizing the between class variance. This option was chosen as it had a similar theoretical approach to the one chosen to obtain the seed pixels. This

segmentation strategy was preferred to others such as the K-means clustering. The K-means aims at minimizing the error between the burned and unburned classes but this method gives good results when the spreads of the distributions are approximately equal, i.e when the distributions have similar variances, which is not the case for burned and unburned classes (unburned has higher variance).

3.12.2.5. Watershed.

This method is based on the concept of finding peaks (local maxima) and valleys (local minima) in the image. The definition of regions was based on the gradient of an image. In the NIR space, the burned areas will correspond to minimum or at least the lower values in the monthly composite, while the unburned areas will represent the maximum values. The advantage of this method is that it in terms of processing time it can be faster than a pixel based analysis. The difficulties are related to the way the regions are defined, and the size of these regions, which might not be the same worldwide and might not adapt in the same way to the different types of fire and fire sizes. The first step in this method is to use the gradient magnitude as the segmentation function. Then, some pre-processing steps will need to be considered to separate the minima and maxima. Since the composite may be noisy, it can have too many local minima and maxima, this is why the histogram is normally smoothed (to create flat maxima inside each object) before finding the minima and maxima, in order to avoid over-segmentation. Foreground and background markers will also be computed and the gradient magnitude image will be modified, so that regional minima and maxima exist only on certain locations. This way also the object size is defined. On the last step the watershed function itself is applied to the treated data, obtaining the regions of the image with unique identifiers. Once these regions are defined they will be intersected with the seed pixels in order to obtain the final burned areas.

3.12.3. RESULTS

Results are presented in the following sections, giving attention to the ones that showed better performance in detecting the burned areas. First, results from each case are shown, illustrating with figures the BA obtained in each case and study site. In the

method selection section (3.12.3.6.) omission and commission errors obtained for each test are compared.

3.12.3.1. Neighbour value.

This technique gave good results for the four study sites. Results are shown for Australia in Figure 35. Fire perimeters for the same region derived from NAFI are shown in Figure 36. There is a good level of agreement between the two figures. Temporal and spatial consistency between fires is achieved. Some omission errors can be noticed with this method especially at the end of the year.

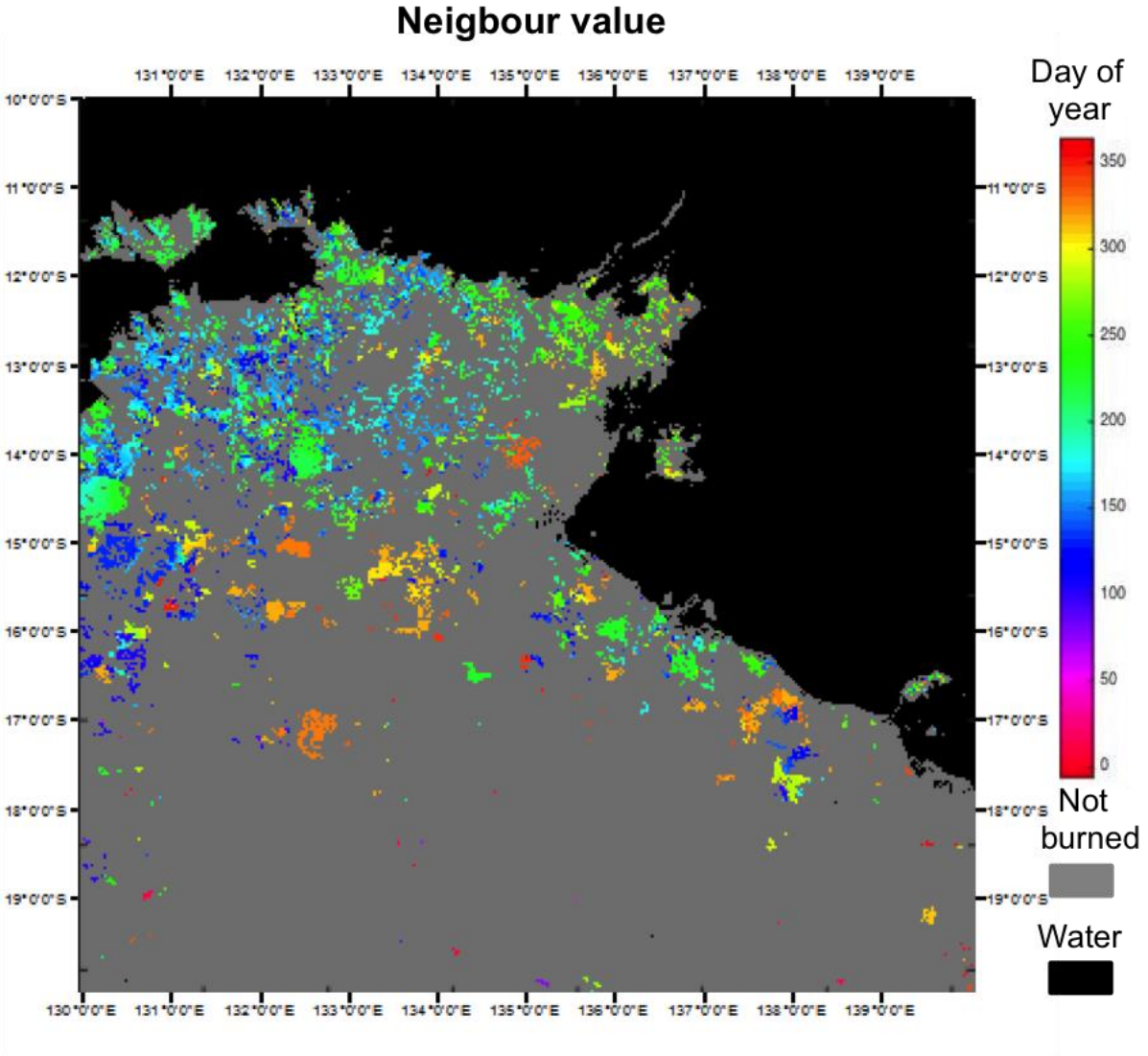

Figure 35. Neighbour value BA detection for Australia in 2008.

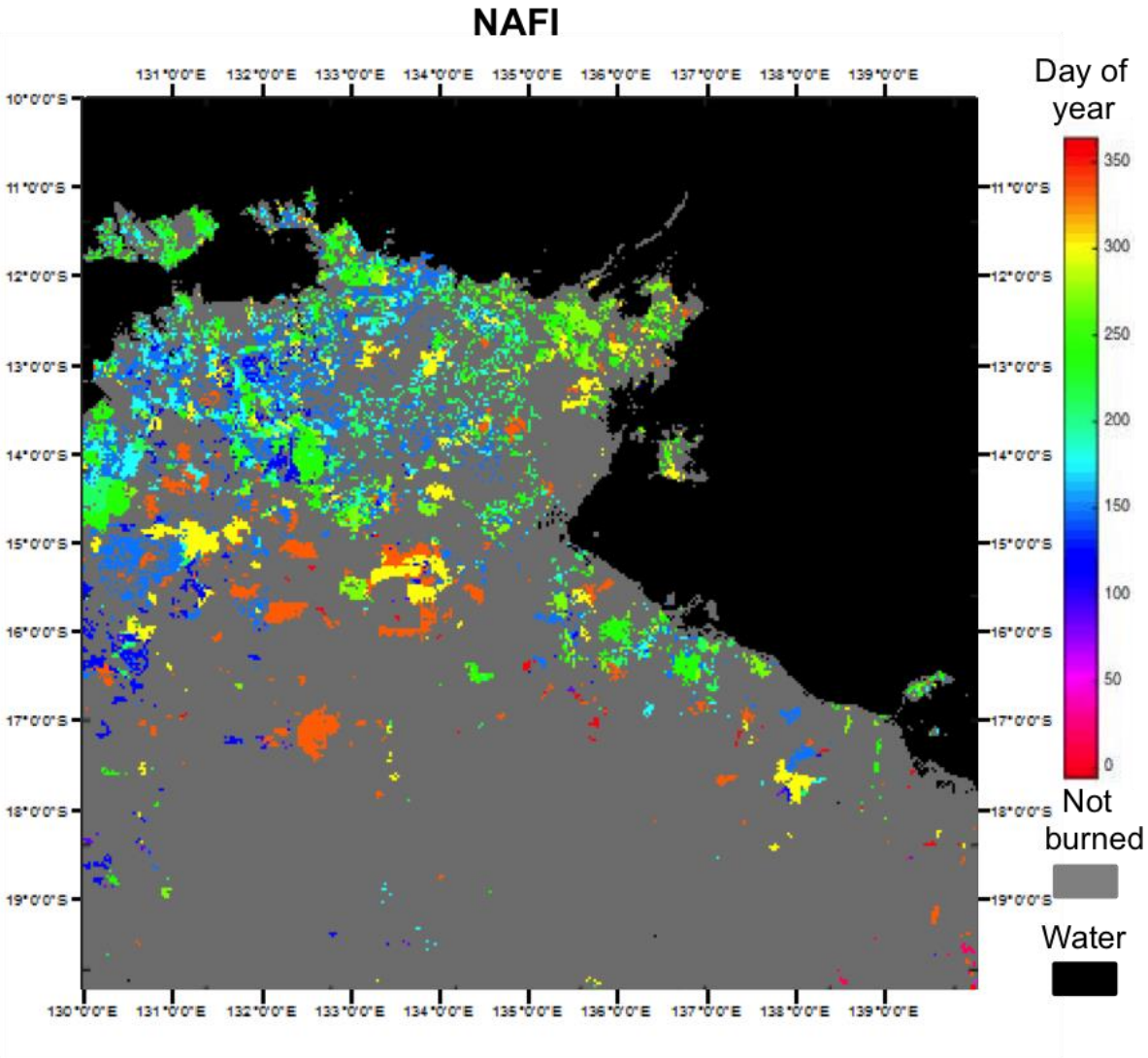

Figure 36. NAFI fire perimeters for the Australian study site in 2008.

Temporal and spatial consistency for the other 3 study sites was also observed. In the Canadian and Californian study sites omission was predominant whereas commission was more relevant on the Portugal study site. Results from these 3 study sites can be seen in Figure 39, 40 and 41.

3.12.3.2. Neighbour median.

The first test, named 5x5 3HS, implemented with this technique gave too large commission errors. The second option, 3x3 2HS, provided better results observing the same tendency as in the neighbour value test, where Australia, Canada and California showed a tendency towards omission in contrast with Portugal that had larger

commission errors. This method was the fastest between the ones tested. Results can be seen in Figure 39, 40 and 41 for Canada, Portugal and California respectively.

3.12.3.3. Edge detection.

The test that combined the edge detection method with the neighbour value showed very little variation with the results obtained with the neighbour value method tested individually. Omission errors increased in 5%, 0.1%, 0.1% and 0.2%, respectively for the Australian, Canadian, Portuguese and Californian study sites and commission errors decreased in 0.1%, 0.1%, 0.05% and 0.1%. Therefore no advantages were found by applying this method.

3.12.3.4. OTSU method.

This method did not give acceptable results, the areas identified were too big in most of the cases, and did not correspond to any of the burned areas delimited. No intersection with seeds was performed since too large perimeters were identified and the intersection with the seeds would have led to very large commission errors.

3.12.3.5. Watershed.

In this case seeds were the pixels that had at least 3 PAFS in a 9x9 pixels matrix around and the minimum NIR verified a decrease compared to the previous month. In the watershed segmentation case there is no need to extend the seeds (as it is done for the pixel strategies), since the purpose of using them is to select the segments, not to be the basis to a growing around a seed. Using all the seeds obtained in the seed phase of the algorithm would have resulted in an increase of the commission errors. This method is faster than the neighbour value method. Results are shown for Australia in Figure 37. Direct comparison with NAFI perimeters shows similar trends in time and space but omission is noticeable for the fires from the middle until the end of the year. Some commission errors in certain regions (top right) are also noticeable.

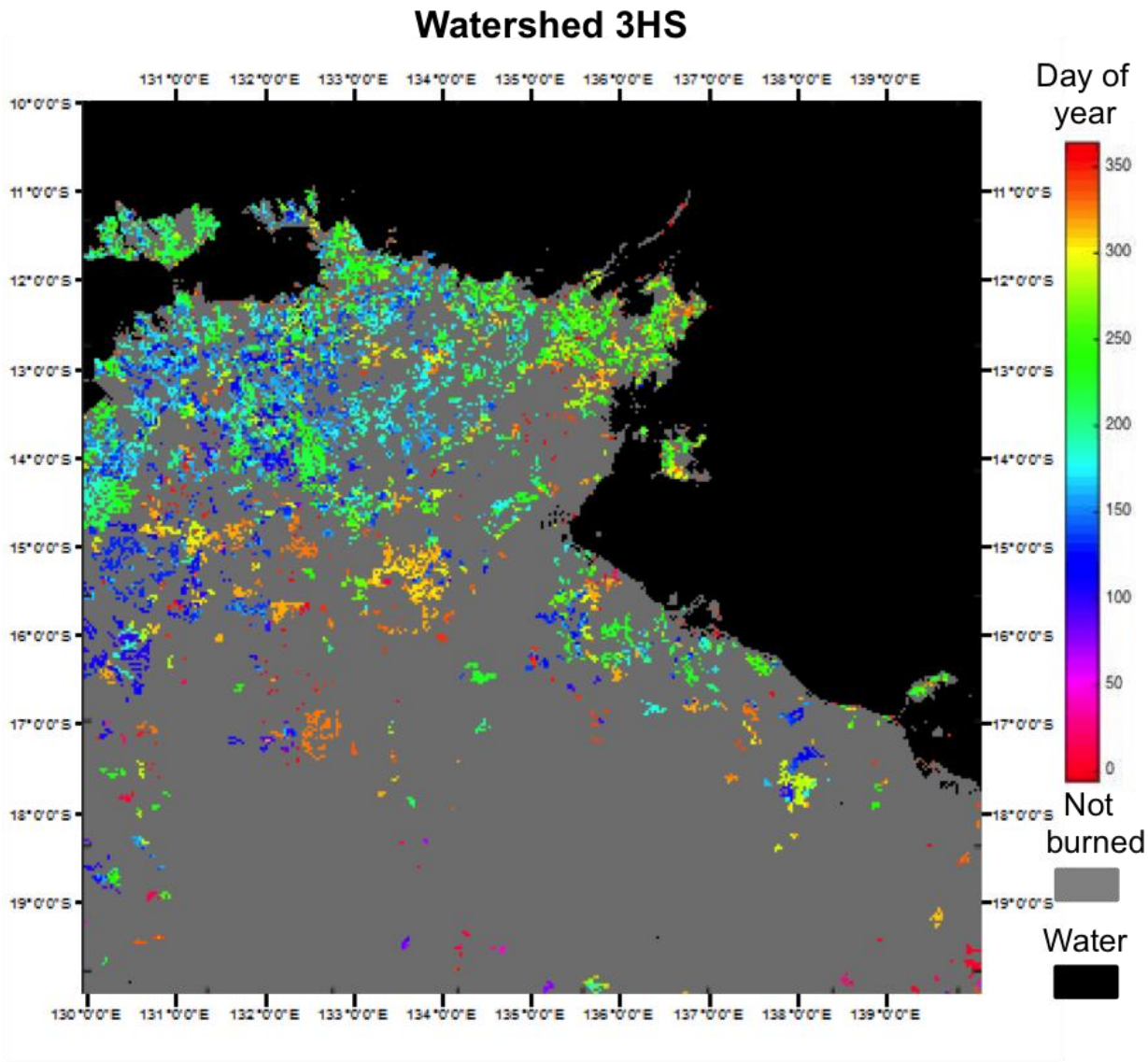

Figure 37. Watershed BA detection for Australia in 2008.

In the Canadian study site the use of this method gave better fire perimeter characterization than the other methods, as reported in Figure 39. Some commission errors were found in California at the end of the season (Figure 41). The performance of this method in the Portuguese study site was particularly low (Figure 40). Commission errors in this site were higher with this method, obtaining proper fire perimeter detections but with an overestimation on the areas burned on those fires. This is related to the object size used for the tests, which does not allow to obtain fire sizes as small as they are in this area.

A study based on the use of NIR composite combined with two other bands (bands 8 and 5) was developed. The purpose was to add some additional information from these

bands. Figure 38 illustrates this test. Commission errors can be noticed if compared to the NAFI perimeters (Figure 36) especially on the upper left corner, where there is a big patch at the end of the year (red colours) that does not appear in the fire perimeters case. OE and CE obtained with this method were 0.4287 and 0.3935 respectively. When compared to the results obtained when using one band (Table 13) it can be seen that the inclusion of bands 5 and 8 does not ameliorate the burned area detection, compared to the individual use of the NIR composite, since both omission and commission errors increase in this case.

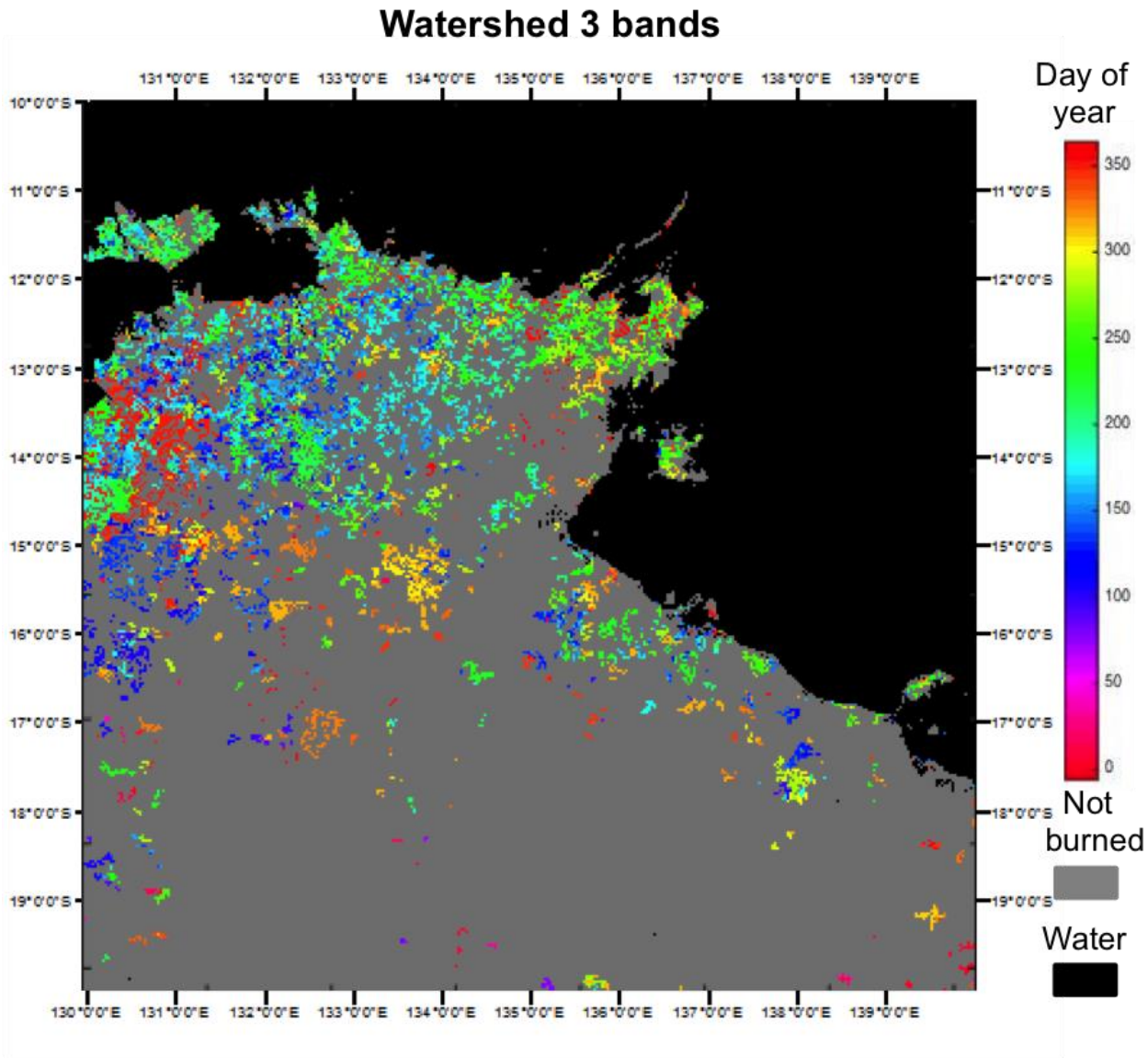

Figure 38. Watershed method applied to 3 bands in Australia for 2008.

The next figures show the results obtained for the Canadian, Portuguese and Californian sites with the 3 methods that performed better, i.e the neighbour value, neighbour

median 3x3 2HS, and the watershed. Fire perimeters are included in order to compare the results.

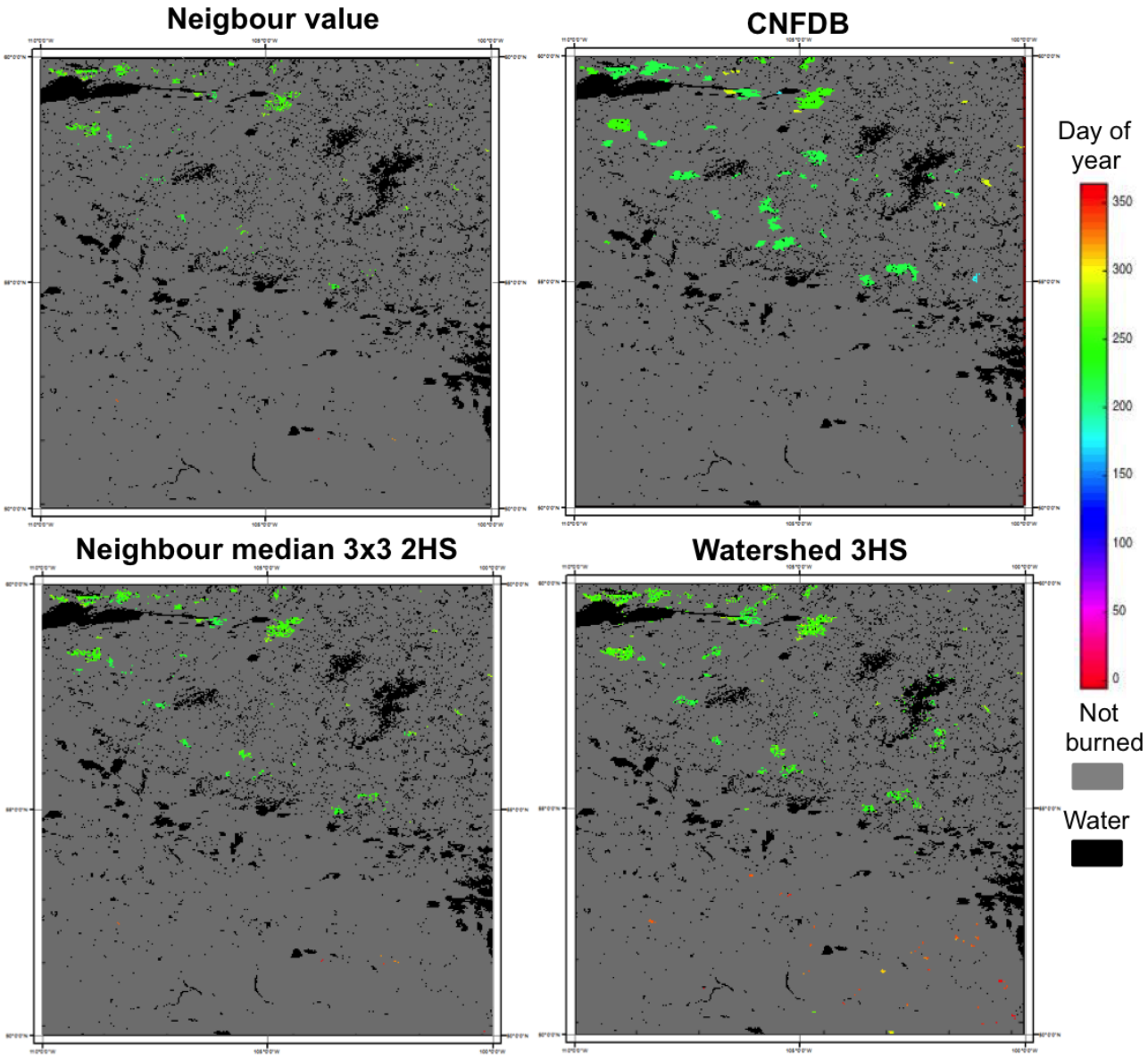

Figure 39. Results for neighbour value, neighbour median, watershed and fire perimeters for the Canadian study site in 2008.

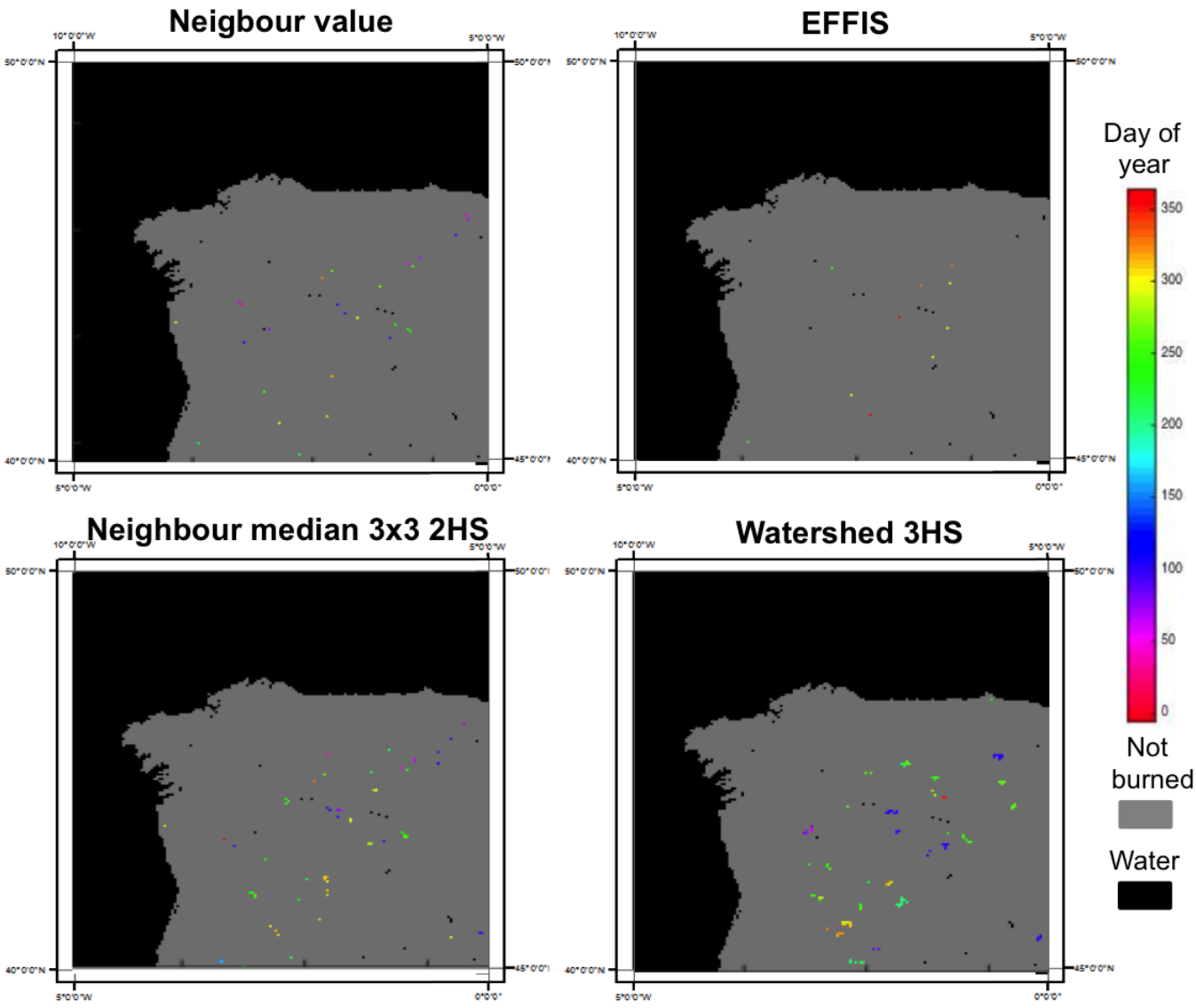

Figure 40. Results for neighbour value, neighbour median, watershed and fire perimeters for the Portuguese study site in 2008.

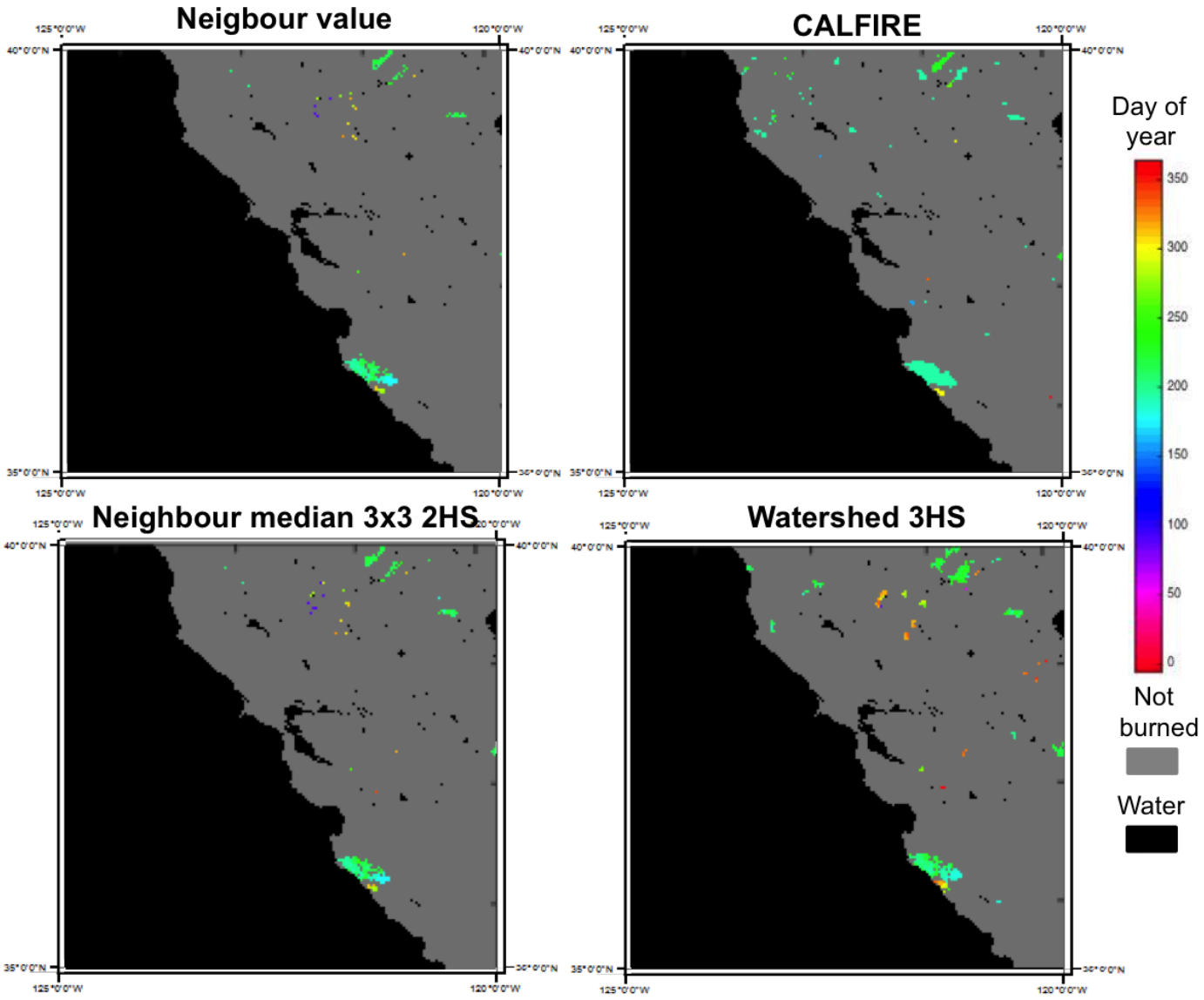

Figure 41. Results for neighbour value, neighbour median, watershed and fire perimeters for the Californian study site in 2008.

3.12.3.6. Method selection

A comparison with the fire perimeters was performed for the different methods tested. Omission and commission errors were obtained for each study site. Table 13 summarizes these results.

Table 13. Omission and commission errors for the growing methods tested in the four study sites.

TESTED ALGORITHM	ERROR	STUDY SITE			
		Australia	Canada	Portugal	California
Neigbour pixel	C.E.	0.1756	0.1022	0.8512	0.1437
	O.E.	0.4441	0.7530	0.6429	0.4379
Median + std 5x5 3HS	C.E.	0.4180	0.1795	0.9798	0.5010
	O.E.	0.1804	0.5178	0.5476	0.2759
Median + std 3x3 2HS	C.E.	0.2023	0.1028	0.9296	0.1754
	O.E.	0.4770	0.6269	0.6203	0.3970
Watershed 3HS	C.E.	0.3204	0.3571	0.9697	0.4654
	O.E.	0.4265	0.5124	0.7162	0.3554

The two techniques that performed better were neighbour value and watershed since OE and CE were lower than for the median cases. OE was significantly lower in 1 of the four cases in the watershed, whereas commission error was significantly lower in the 4 study sites for the neighbour value pixel strategy. Overall OE were smaller in watershed technique than in the neighbour median, but at the cost of increasing too much the CE. This, in combination with the knowledge acquired while developing these techniques lead to the decision of choosing the neighbour pixel strategy. It is more time consuming than watershed but does guarantee a higher control of the burned areas. When different regimes are present, and with very different fire sizes, it is more difficult to control how an algorithm of these characteristics will perform with the watershed technique. Region growing offers several advantages over conventional segmentation techniques. Unlike gradient and Laplacian methods, the borders of regions found by region growing are perfectly thin (since we only add pixels to the exterior of our region) and connected. The pixel based region growing algorithms are also very stable with respect to noise (Kamdi and Krishna 2012).

In the final neighbour value pixel implementation, an extra condition was applied once the burned area was retrieved. The purpose was to avoid large commission errors in a few areas with dark covers, where the region growing process might not perform properly (specific regions of Australia, China and India, for instance). Large polygons were filtered out when the number of burned pixels exceeded largely the number of hotspots. An empirical value of 30 times (MERIS BA pixels/HS) was established, based on previous findings from Hantson et al. (2013), who compared the distribution of HS

and Landsat derived burned patches in the same study sites used to develop this algorithm.

The general scheme of the algorithm version 1 is shown in Figure 42.

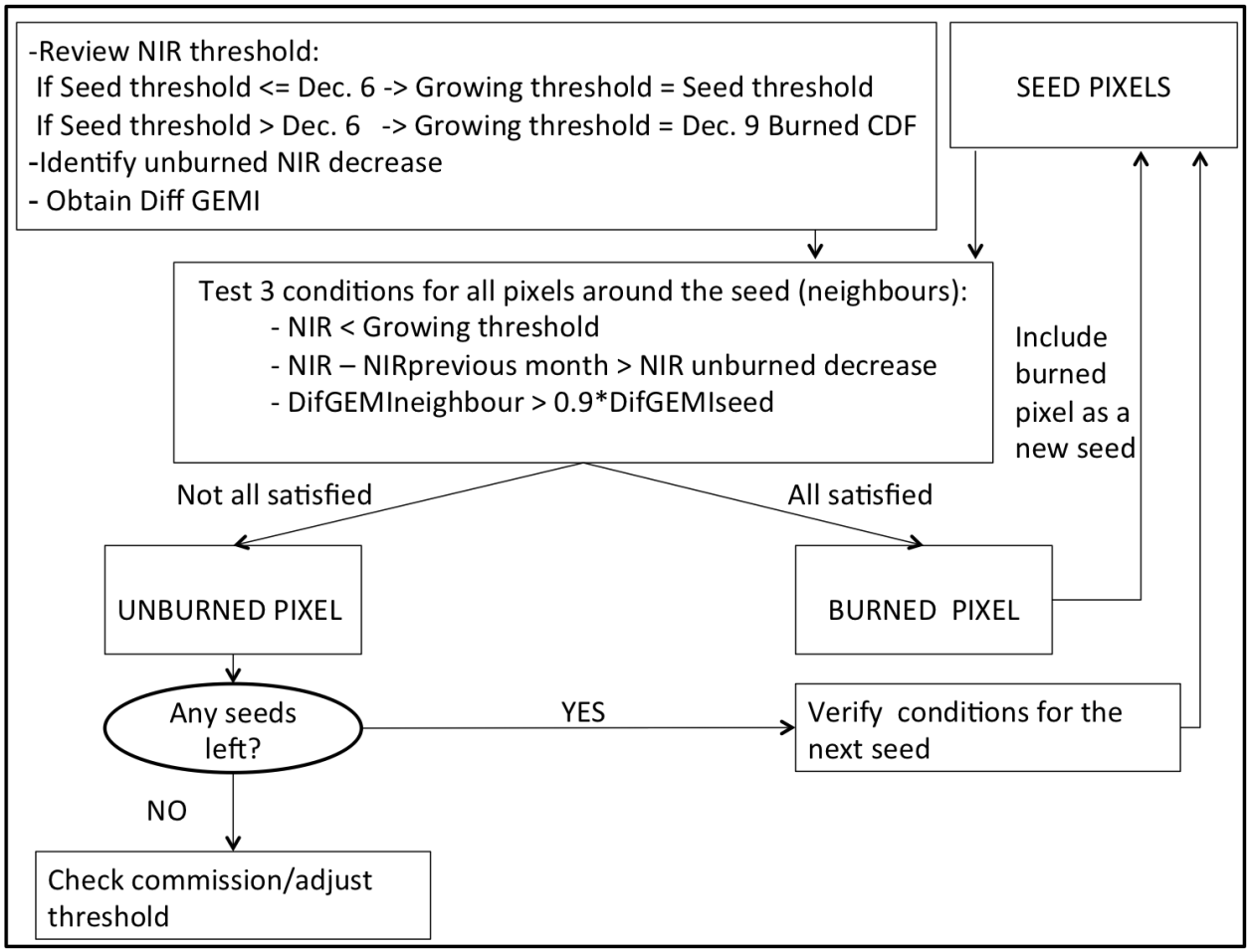

Figure 42. Region growing final configuration scheme.

The configuration introduced is version 1 of the algorithm, since results for the 3 years processed and introduced in Chapter 4 are obtained with this configuration. A paper summarising the main steps of the algorithm was recently published (Alonso-Canas and Chuvieco 2015). The complete paper is available in Annex 2. Nevertheless, some changes were applied afterwards to this configuration, once global results were available. The changes in the growing phase were based on the use of individual images instead of composites, using similar conditions to the ones presented here. Commission and omission errors of versions 1 and 2 for the four assessment sites will be shown in section 4.2.2. of the product assessment (Chapter 4). Version 2 of the algorithm is the

one that will be used to process the full MERIS time series (2002-2012). Some of the modifications to obtain this version are summarised in a paper accepted (with minor corrections) to Geofocus. The preliminary version of this paper is available in Annex 3.

3.13. BA MERIS OUTPUT PRODUCT.

The MERIS BA product delivered to the users included other layers apart from the Julian date of burn. Some of them required to generate auxiliary information from the MERIS algorithm, such as the confidence level, which was obtained based on the Bayes theorem:

$$P(B/NIR) = \frac{100 * P(NIR/B) * PB}{P(NIR/B) * PB + P(NIR/U) * PU}$$

Where :

- P(B/NIR) = probability of having burned given the fact that it has a particular NIR value
- P(NIR/B) = probability of observing a certain value of NIR knowing that it has burned
- P(NIR/U) = probability of observing a certain NIR value knowing that it has not burned
- PB = 0.5 = a priori probability of burning
- PU = 0.5 = a priori probability of not burning

The other 4 layers are the last valid observation before the date of burn, number of valid images, number of images with clouds and total number of images. All these layers are computed after obtaining the BA Julian date and the confidence level, directly from the MERIS images used to obtain the composite.

3.14. VERSION 1 ALGORITHM CONFIGURATION OVERVIEW.

A flowchart diagram showing the main steps of the algorithm version 1 is shown in Figure 43 to summarise the main findings of this chapter. The two phases of the algorithm, seed and growing, are presented with the main steps present in each one of them.

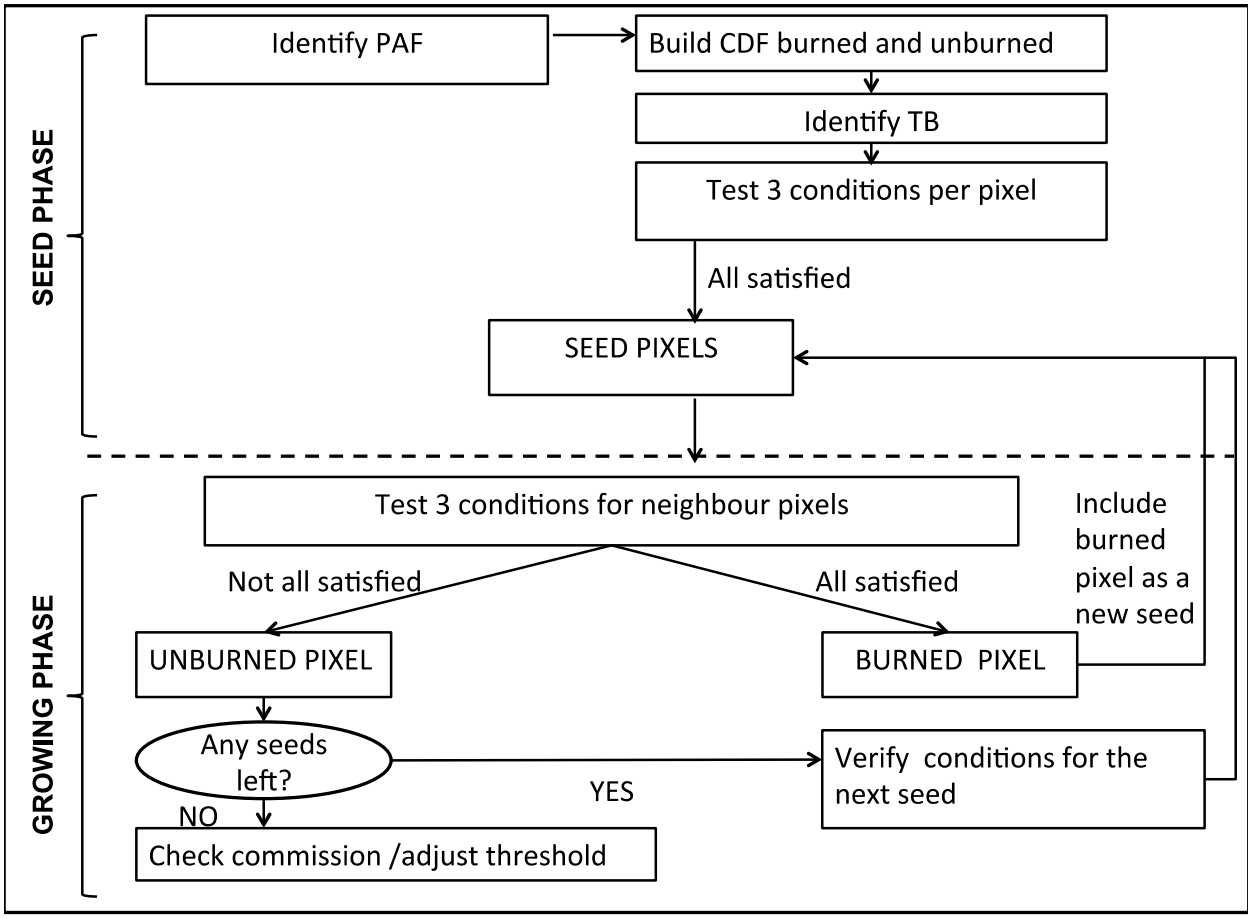

Figure 43. MERIS BA algorithm final configuration.

CHAPTER 4

BA

PRODUCT

ASSESSMENT

In this chapter the results from the processing of three years of MERIS data will be presented. A global validation on the 2008 results will be introduced as well as the fire perimeter assessment for four study sites. Inter-comparison with other products will also be presented, identifying spatial and temporal behaviours.

4.1. SPATIAL AND TEMPORAL VARIATIONS OF BA.

Three years of data were processed with the MERIS BA algorithm: 2006 to 2008 at GMV facilities (GMV was the system engineering partner for the first phase of the fire_cci project). The total BA obtained for the three years was 3.6, 3.8 and 3.6 km^2 respectively. Gridded BA for these three years is shown in Figures 44 to 46.

In terms of spatial distribution, the three years present little variation between them. The most extensive burnings occurred in the Tropical regions, particularly in the African continent, followed by the Northern regions of Australia, Central Brazil, Venezuelan and Colombian Llanos, and SE Asia. A second belt of burned regions is noticeable in the temperate grasslands and croplands of central Asia, and SE USA. The boreal forests of Russia and Canada have also a substantial role in global biomass burnings. 2006 presents more BA in Eastern Europe and Australia, where as for 2007 more BA is identified in Brazil. 2008 presents less BA in North America, especially in the Eastern region, compared to the other years. Northern and Southern parts of Africa have very similar BA for the three years.

In terms of temporal distribution, the date of detection (used also to compute the BA) showed seasonal trends of fire activity, with predominant January-March fires in the Northern Tropical belt, July-September in the Southern Tropical fringe, Northern Boreal and Temperate Regions of America and Eurasia. Figure 47 illustrates these tendencies for 2008. The seasonality shows the same trends for the three years and is in good agreement with results estimated from other authors (Csiszar et al. 2005; Giglio et al. 2006a; van der Werf et al. 2006).

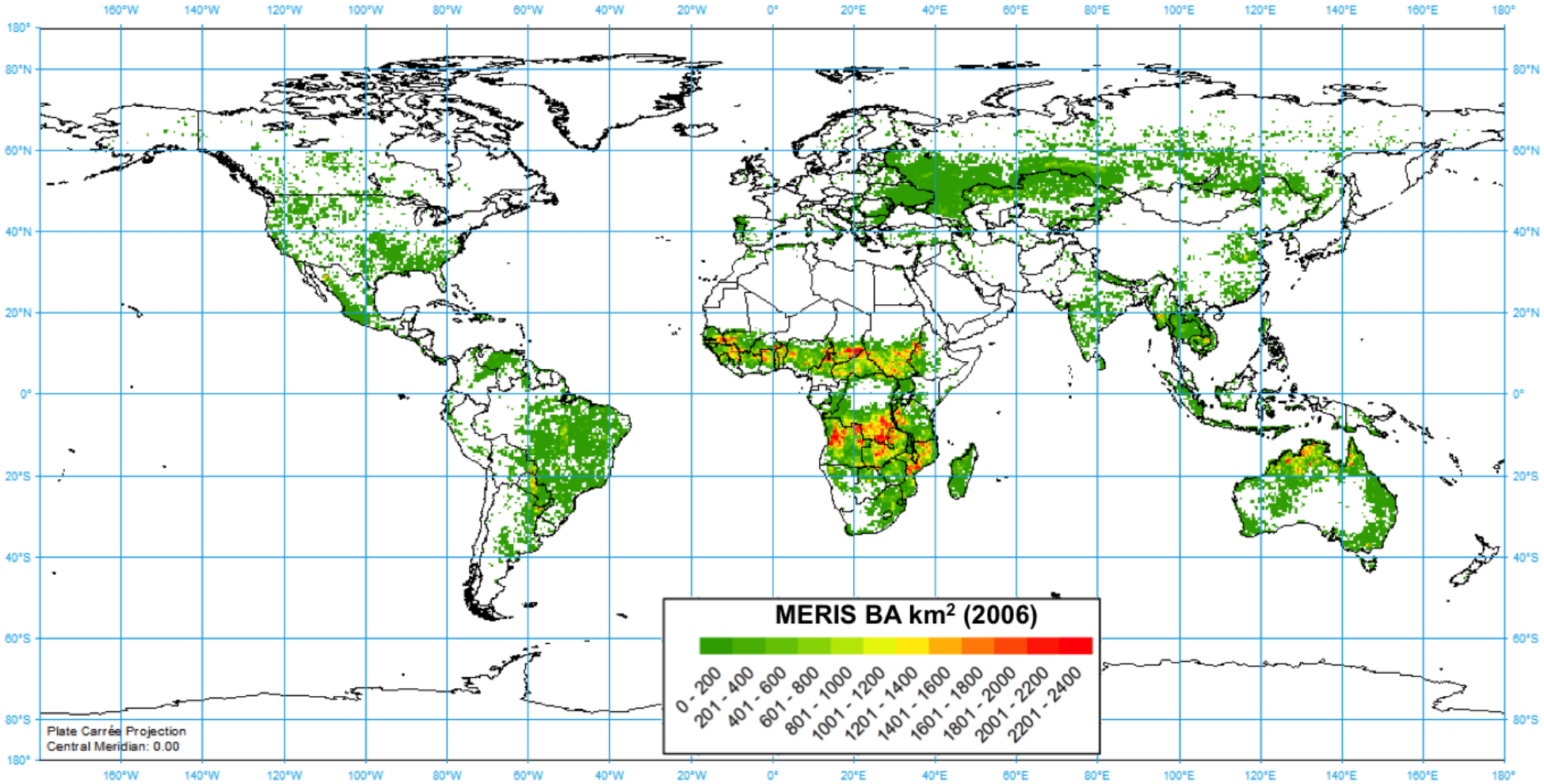

Figure 44. Global BA obtained with the MERIS algorithm for 2006

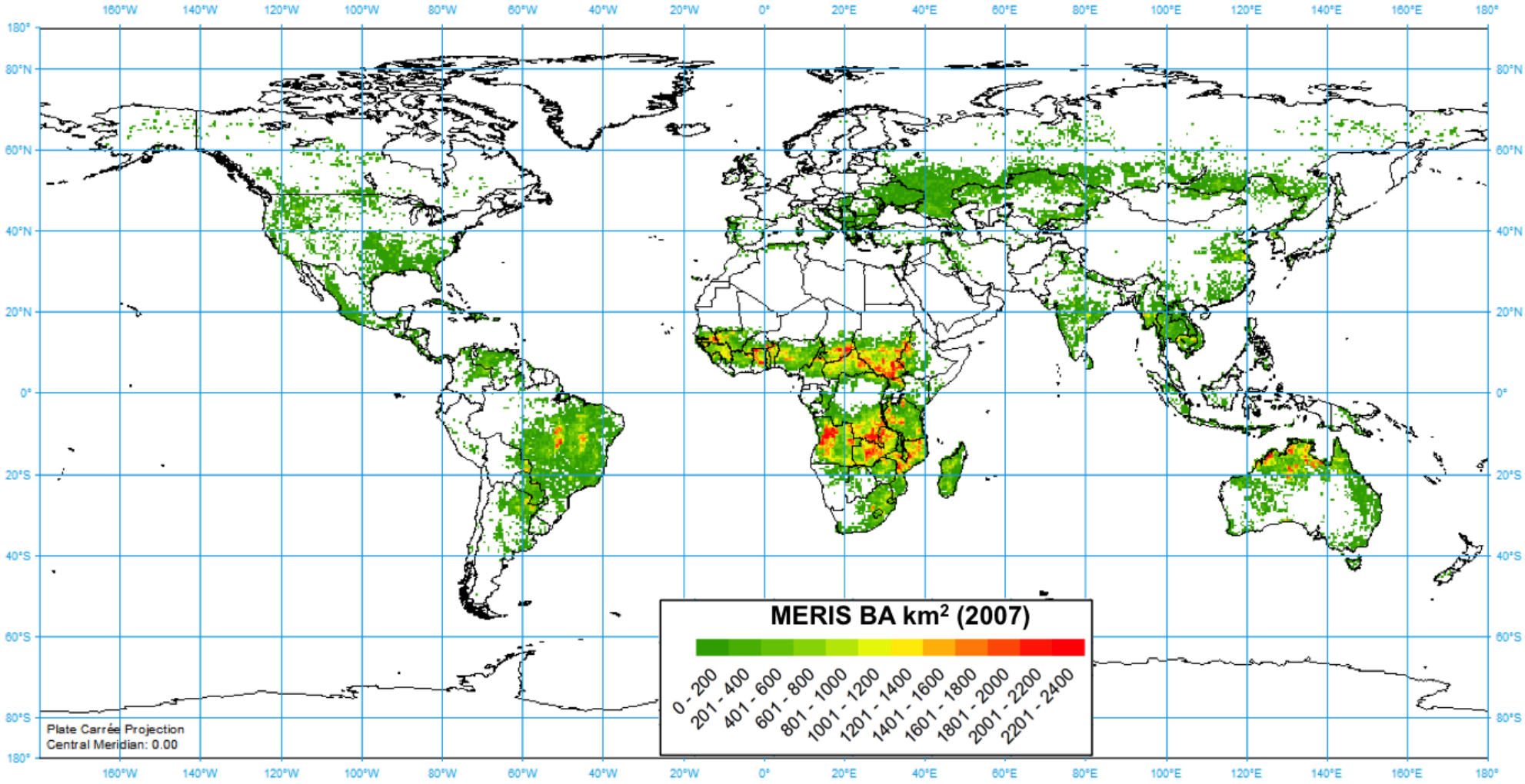

Figure 45. Global BA obtained with the MERIS algorithm for 2007.

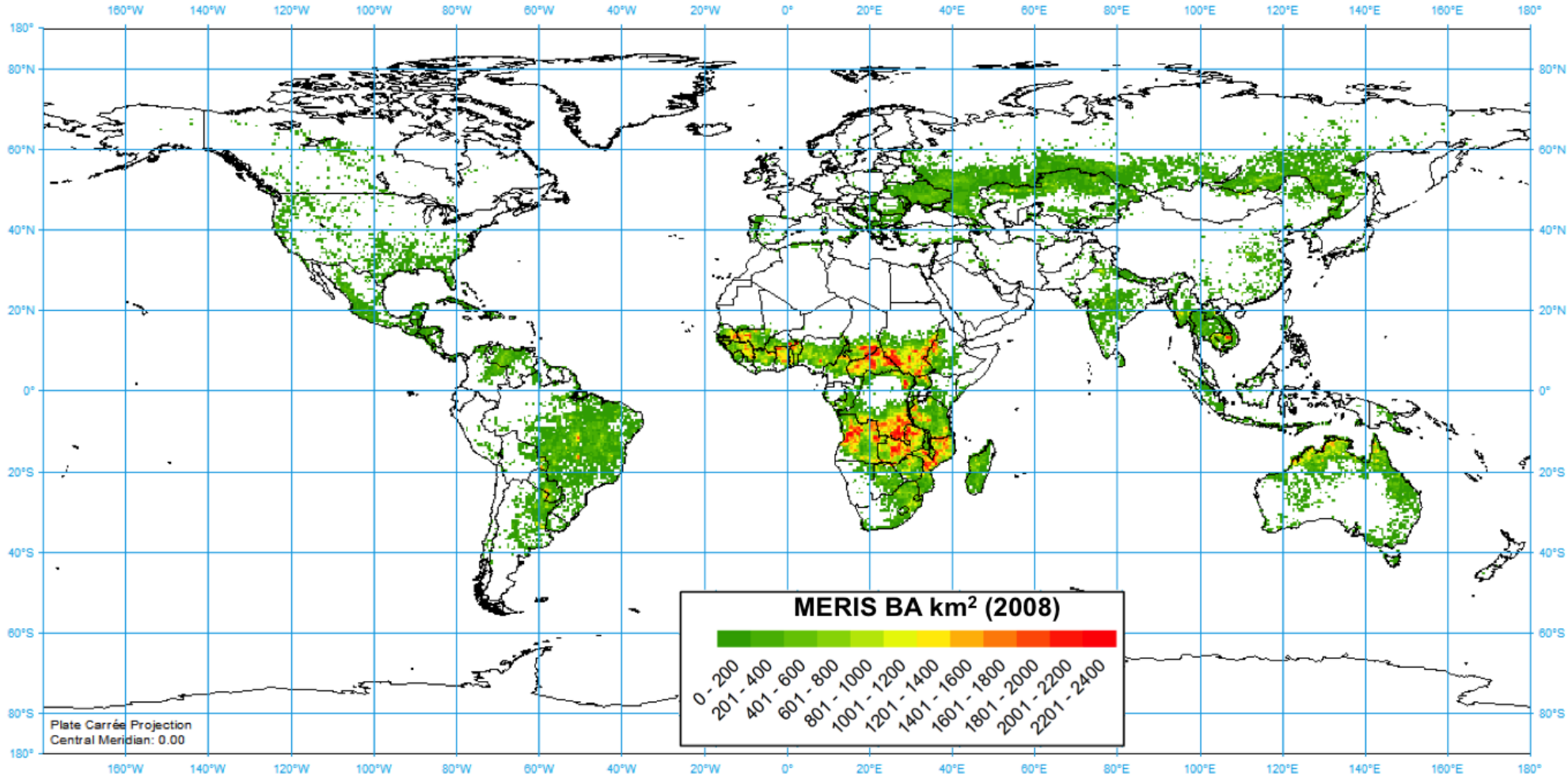

Figure 46 Global BA obtained with the MERIS algorithm for 2008.

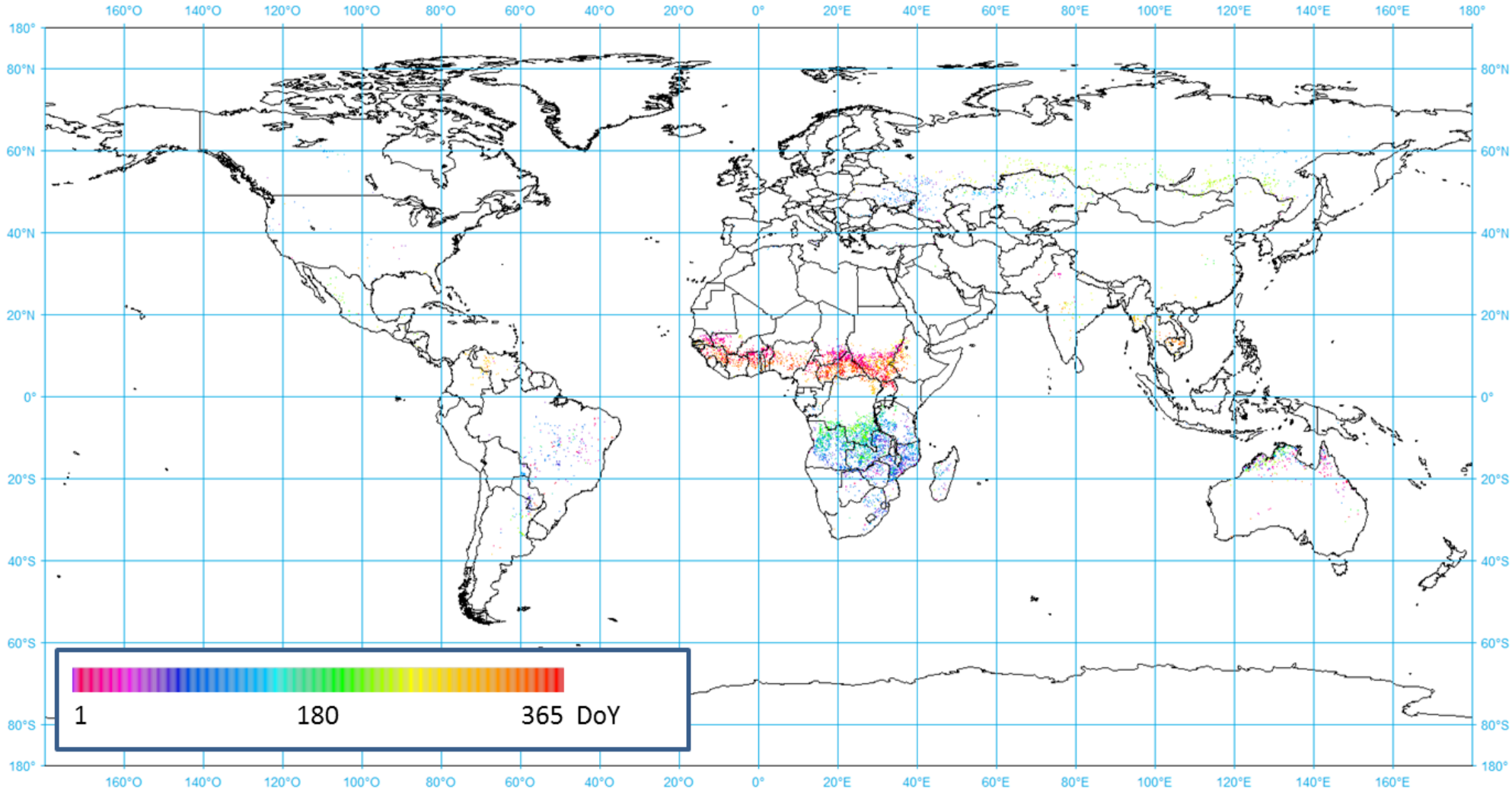

Figure 47. Julian date of burn for 2008.

A detail of these burns is shown in figure 48 for Africa, the continent where more burns occurred (>70% from these results and other sources). Seasonal trends can be clearly identified for this case, with the fire peaks associated to the central months of the dry season, at the beginning of the year for the Northern part, and in the middle of the year for the Southern fires. Most of the burnable areas of the African continent present fire events at a certain point during the year. As illustrated in Figure 49 the extent of these burns is more relevant in the Central African Republic for the Northern part, and in Angola, South of Congo, Zambia and Mozambique for the Southern belt. This behaviour is verified for the three consecutive years, being these areas the ones that burn the most (more than 2400 km^2). These areas are mainly covered by Tropical savannah.

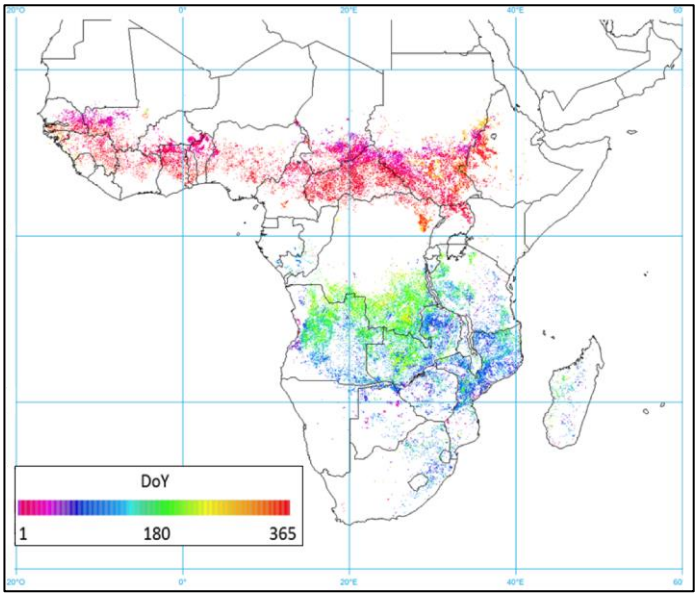

Figure 48. Julian dates of burn for Africa in 2008

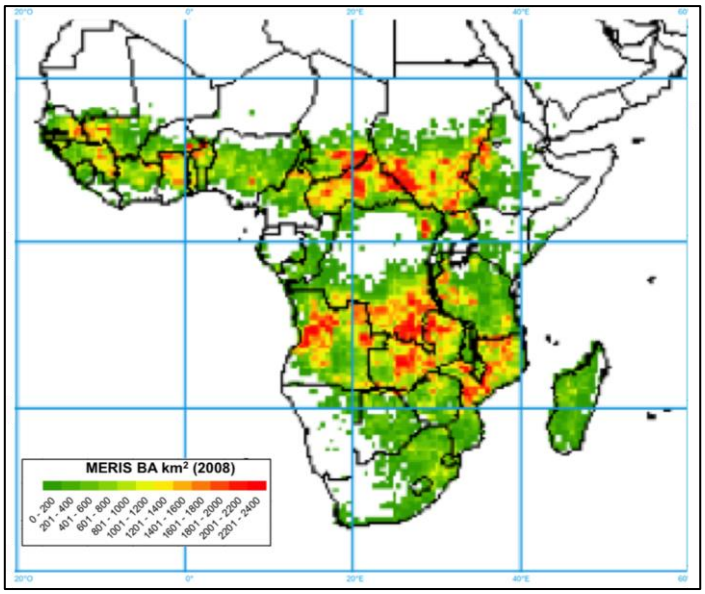

Figure 49. BA in km^2 in Africa for 2008.

4.2. VALIDATION AND PERIMETER ASSESSMENT RESULTS.

In this section, two exercises will be introduced to assess the performance of the BA product obtained. First, the complete validation strategy developed with Landsat perimeters will be presented for 2008. Second, a fire perimeter assessment in four larger areas and for years 2006 to 2008 will be shown. In this case, also fire perimeter size obtained with the MERIS product will be identified.

4.2.1. VALIDATION RESULTS.

Table 14 shows the results of the validation metrics computed from the 105 global validation sites. They were divided in two subsamples, based on the proportion of burned area. The vast majority (100) had less than 10% of burned area, while the rest had more than that threshold. Overall accuracy was high in both cases (>87%). Omission and commission errors were higher for those areas with very low burned area proportion than for those with more fire occurrence. The Dice coefficient (DC) (see Padilla et al., 2015), which combines the omission and commission errors, was also higher for the sites with more BA proportion (0.48). Error balance (over and underestimation) was close to 0 for areas with larger BA, but showed underestimation for the overall sample and for those areas with minor BA. In relative terms (relB) the overall sample showed underestimation by 34%.

Table 14. Estimated accuracy metrics for MERIS BA estimates (courtesy of Padilla, M. personal communication).

OA	DC	Ce	Oe	B	relB	BA proportion
0.9581	0.312	0.597	0.745	-0.0137	-0.3657	<0.1
0.879	0.486	0.517	0.510	0.0018	0.0157	>0.1
0.996	0.290	0.640	0.760	-0.12	-0.34	All

Table 15 shows the MERIS validation metrics, with no distinction of burned area proportion (Padilla et al., 2015). Validation metrics are also shown for other three products evaluated: MODIS MCD45, MCD64 and GEOLAND2. These results were also obtained for 2008.

Comparison with existing BA products showed that MERIS BA and GEOLAND2 results have similar overall accuracy than the two MODIS BA products (MCD45 and MCD64) (OA>0.99). However, MERIS showed significantly higher commission and omission errors (CE=0.64; OE=0.76), than MCD64 (CE=0.42; OE=0.68), and higher commission error than MCD45 (0.46 vs 0.64). The errors found with the MERIS product were significantly lower than the ones from GEOLAND-2, particularly for the OE (Padilla et al. 2015). In terms of error balance, an overall trend towards underestimation was observed. The relative balance of errors of MERIS showed better results than MCD64 and MCD45 with a 34% of underestimation for MERIS, versus 44 % for MCD64 and 48% for MCD45.

Table 15. OA, OE, CE, DC, B and relB of several BA products: MODIS MCD 45 and MCD64, Geoland and MERIS (Padilla et al. 2015).

PRODUCT	OA (%)	CE (%)	OE (%)	DC (%)	B (%)	relB(%)
MCD64	99.6	42	68	42	-0.17	-44
MCD45	99.7	46	72	37	-0.17	-48
GEOLAND-2	99.6	74	91	16	-0.23	-68
MERIS_CCI	99.6	64	76	29	-0.12	-34

4.2.2. FIRE PERIMETERS ASSESSMENT.

Table 16 shows the cross tabulation results between MERIS BA estimations and those derived from external fire perimeters, in four study sites: Australia, Canada, Portugal and California. In this case, errors should be better considered as disagreements between the two sources, since the sample was not derived with the standard CEOS Cal-Val protocol (based on two-date satellite images), but from fire perimeters obtained from national forest services. Nevertheless, those external perimeters have also their own validation and therefore can be considered reliable. In addition, as previously said, they complement the temporal validation, as they cover BA during the whole year. The Australian site had the largest BA for the three years, with a BA proportion between 0.18 and 0.45. Portugal had the lowest fire occurrence (<0.001), while in the Californian

and Canadian sites BA varied from 0.007 to 0.013 and 0.013 to 0.027, respectively. Total burned area in the four sites ranged from 97.410 to 146.894 km^2.

Table 16. Cross tabulation of MERIS results and assessment sites for 2006 to 2008. CE = Commission error, OE = omission error, OA = overall accuracy, BAp = BA Proportion of total site

	2006				2007				2008			
	CE	OE	OA	BAp	CE	OE	OA	BAp	CE	OE	OA	BAp
Australia	0.085	0.425	0.789	0.447	0.111	0.429	0.808	0.250	0.176	0.444	0.850	0.181
Canada	0.306	0.467	0.981	0.027	0.032	0.560	0.993	0.013	0.102	0.753	0.981	0.026
Portugal	0.440	0.236	0.998	0.002	0.655	0.395	0.999	0.001	0.851	0.642	0.999	<0.001
California	0.326	0.341	0.997	0.007	0.354	0.333	0.996	0.010	0.144	0.438	0.996	0.013
TOTAL	0.117	0.424	0.966	0.029	0.125	0.431	0.971	0.025	0.147	0.472	0.975	0.019

Overall agreement was high, above 0.9 for most sites and years, with lower values for the Australian site (close to 0.8). This area showed the lowest commission errors, particularly in 2006, that was the most severely burned. Omission errors were higher than commission errors (>0.4), but still lower than those estimated by the validation sample. The Portuguese study site showed the highest overall accuracy, but also the highest errors of the burned category, particularly commission errors in some years, when the proportion of burned area was very low. The Californian and Canadian sites presented intermediate values, with omission and commission errors in the range of 0.17 to 0.46 for California, and 0.03 to 0.7 in Canada. Overall accuracies in both cases were above 98%. When considering the four areas together, covering around 1.6 million km^2 and the three target years, the overall accuracies were above 96%. Commission was lower than omission, with values ranging from 0.12 to 0.15 for the former and 0.42-0.47 for the latter.

A comparison between the errors obtained with version 1 and version 2 (modifications in the seed and growing phases of the algorithm) is shown in Table 17. According to the fire perimeter assessment, new results show that OE diminishes while there is little increase in the commission errors for the four study sites.

Table 17. Omission and commission errors for version 1 (Chapter 4, Annex 2) and version 2 (Annex 3).

		Version 1	Version 2
Australia	CE	0.18	0.21
	OE	0.44	0.40
Canada	CE	0.10	0.12
	OE	0.75	0.51
Portugal	CE	0.85	0.84
	OE	0.64	0.61
California	CE	0.14	0.15
	OE	0.44	0.33

Significant reduction of the OE is obtained in the regions of Canada and California. Figure 50 illustrates the differences between version 1 and 2 in the number of perimeters detected as well as in the characterization of BA in Canada. Version 2 is the one that will be used to process the full MERIS time series (2002-2012).

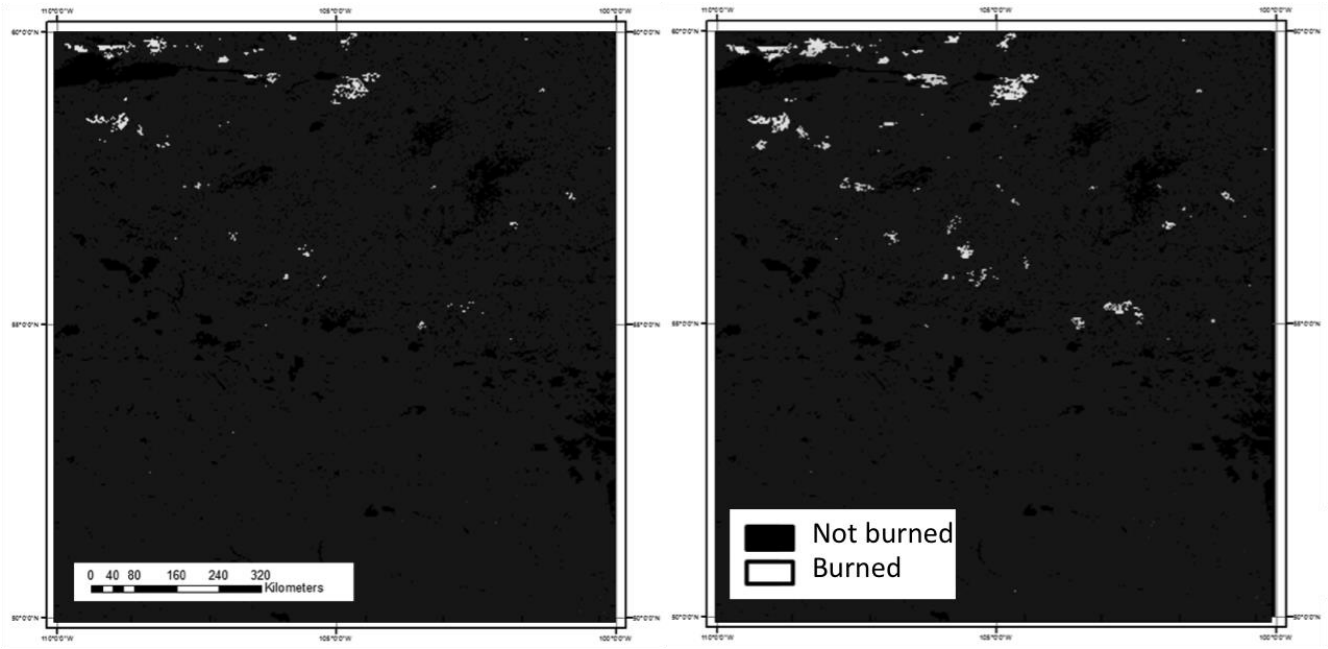

Figure 50. BA detected in Canada with version 1 and version 2 of the algorithm.

In terms of fire size, Table 18 shows the perimeters detected in 2008 with the MERIS BA version 1 of the algorithm, versus the perimeters obtained from the four assessment sites. They are separated by fire size in four categories. Percentage of detected fire perimeters is shown for each case. In the case of fires bigger than 10.000 ha the algorithm detected more than 80 % of the fires (except in the case of Portugal, where no fires of this size exist for 2008), identifying the totality of fires of this type in Australia (which was the area that showed higher BAp). For fires between 1000 and 10.000 ha at least 50% of the fires were detected, increasing this value up to 92% for Australia. In the case of fires between 100 and 1000 ha detection rates were still high for Portugal and Australia (74% and 62% respectively), whereas lower detection rates were obtained for Canada and California (25% and 8% respectively). For fires smaller than 100ha detection rates were below 38%. When considering the total number of perimeters, Portugal is the study site where more fires were detected (53%), followed closely by Australia (46%) and Canada (45%), whereas the number of perimeters identified in California was 15% of the total.

Table 18. Fire perimeters detected in the four assessment sites separated by size.

Study site		**Fire size (ha)**			**ALL**
	<100	<1000	<10000	>10000	46% of total nº of per. det
AUSTRALIA					
Total nº of per.	12174	4652	1373	209	18408
% detected	34%	62%	92%	100%	46%
CANADA					
Total nº of per.	30	20	28	34	112
% detected	0%	25%	54%	88%	45%
PORTUGAL					
Total nº of per.	24	19	4	0	47
% detected	38%	74%	50%	-	53%
CALIFORNIA					
Total nº of per.	98	48	25	5	176
% detected	4%	8%	60%	80%	15%

4.3. INTER-COMPARISON WITH OTHER BA COLLECTIONS.

In order to obtain the inter-comparison, the products were converted into grid format at 0.5 degrees resolution, which is the resolution at which the MERIS grid product was delivered (following product specifications agreed within the project consortium). The products used for the inter-comparison were MDC45, GFED v4 (derived from the MCD64A1 product aggregated at 0.25° spatial resolution) and the GEOLAND2 product, which is part of the Land Copernicus Services component. Table 19 includes total BA estimations from these 3 products and from MERIS, for the three years when global outputs were available.

Table 19. GFED v4, MCD45, MERIS and GEOLAND BA in km^2 for years 2006 to 2008.

	GFED v4	MCD45	MERIS_CCI	GEOLAND2
2006	3.417.863	3.374.125	3.652.355	2.546.002
2007	3.644.122	3.523.728	3.773.855	2.379.485
2008	3.307.377	3.308.200	3.624.146	2.047.937

MERIS BA estimates are 3 to 9% higher than GFED v4, 7-9% higher than MCD45 and 30-43% higher than GEOLAND2. MERIS presents a good agreement with the two MODIS collections, also showing the same increase identified in those products for 2007. GEOLAND2 provides significantly lower estimations than the other BA products.

In terms of BA spatial distribution, Figure 52 illustrates the GFED v4, MCD45, GEOLAND2 and MERIS_CCI BA products in 2008 separated by eco-region (following the geographical eco-regions defined by Giglio et al. (2006b). These ecoregions are illustrated in Figure 51.

Figure 51. Ecoregions as defined by Giglio et al. 2006. AUST: Australia, BOAS: Boreal Asia, BONA: Boreal North America, CEAM: Central America, CEAS: Central Asia, EQAS: Equatorial Asia, EURO Europe, MIDE: Middle East, NHAF: Northern Hemisphere Africa, NHSA: Northern Hemisphere South America, SEAS: Southeast Asia, SHAF: Southern Hemisphere Africa, SHSA: Southern Hemisphere South America, TENA: Temperate North America.

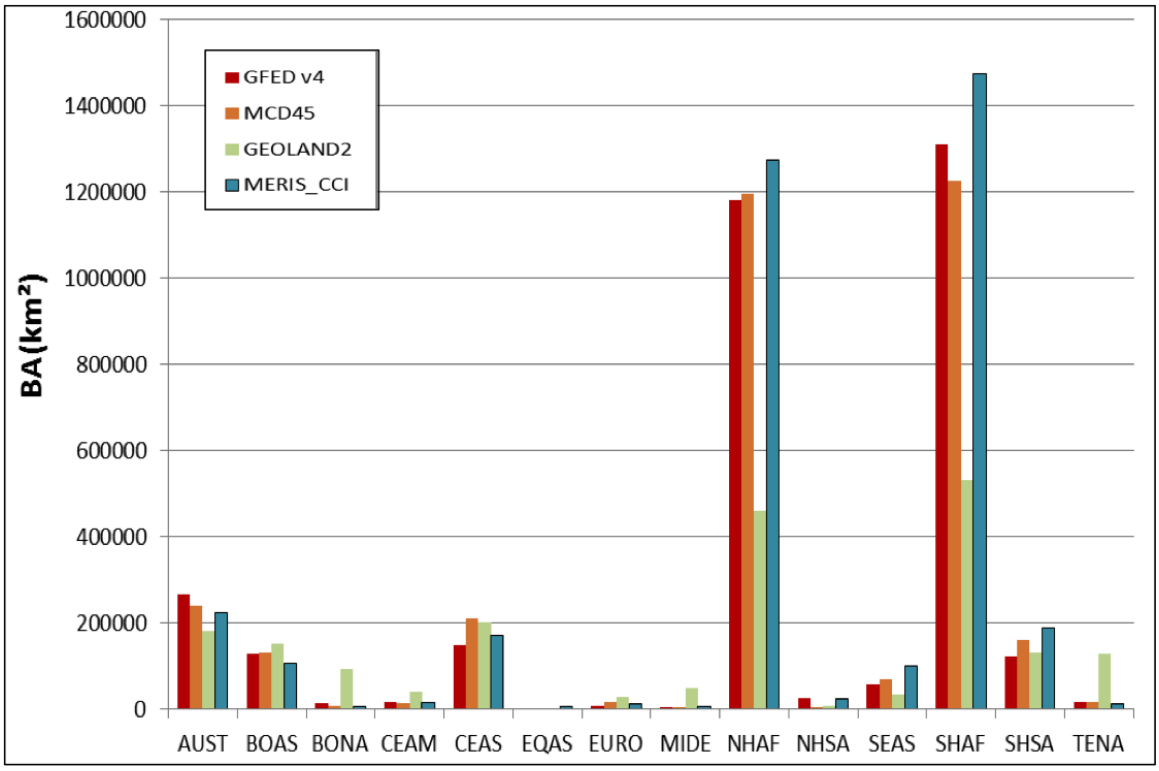

Figure 52. BA 2008 estimations for MCD45, GFED v4, GEOLAND2 and MERIS_CCI for the 14 ecoregions defined in Giglio et al. (2006b)

The four products show that the vast majority of BA occurred in the two African hemispheres (NHAF, SHAF, summing both 70 % of total), followed by Australia, Central Asia, South America and Boreal Asia. For nine regions (CEAM, EQAS, EURO, MIDE,

NHAF, SEAS, SHAF, SHSA, and TENA) MERIS estimates were higher or in the same order as the GFED v4 and MCD45 ones. GEOLAND2 reported higher values in boreal and temperate regions (BOAS, BONA, CEAS and TENA) and significantly lower in tropical areas (NHAF and SHAF). Overall, a high level of agreement was found between MERIS, GFED v4 and MCD45 (r^2>0.99), when total areas of the different eco-regions were compared.

A more in depth comparison with the GFED product follows, as this collection is widely used in the modelling community, and validation results showed its better performance over the other products (Padilla et al., 2015). Mean burned area of the three years of MERIS and GFED products, expressed as fraction of burned area per 0.5 degrees is shown in Figure 53. The agreement between the average values is quite high. In order to better illustrate the differences, the ratio between the two products is shown in Figure 54. The differences when comparing the grid products of MERIS and GFED 4 are lower than +-10% for most areas, except for the regions of Angola, Zambia and Botswana where GFED estimates are higher, and Namibia, where they are lower.

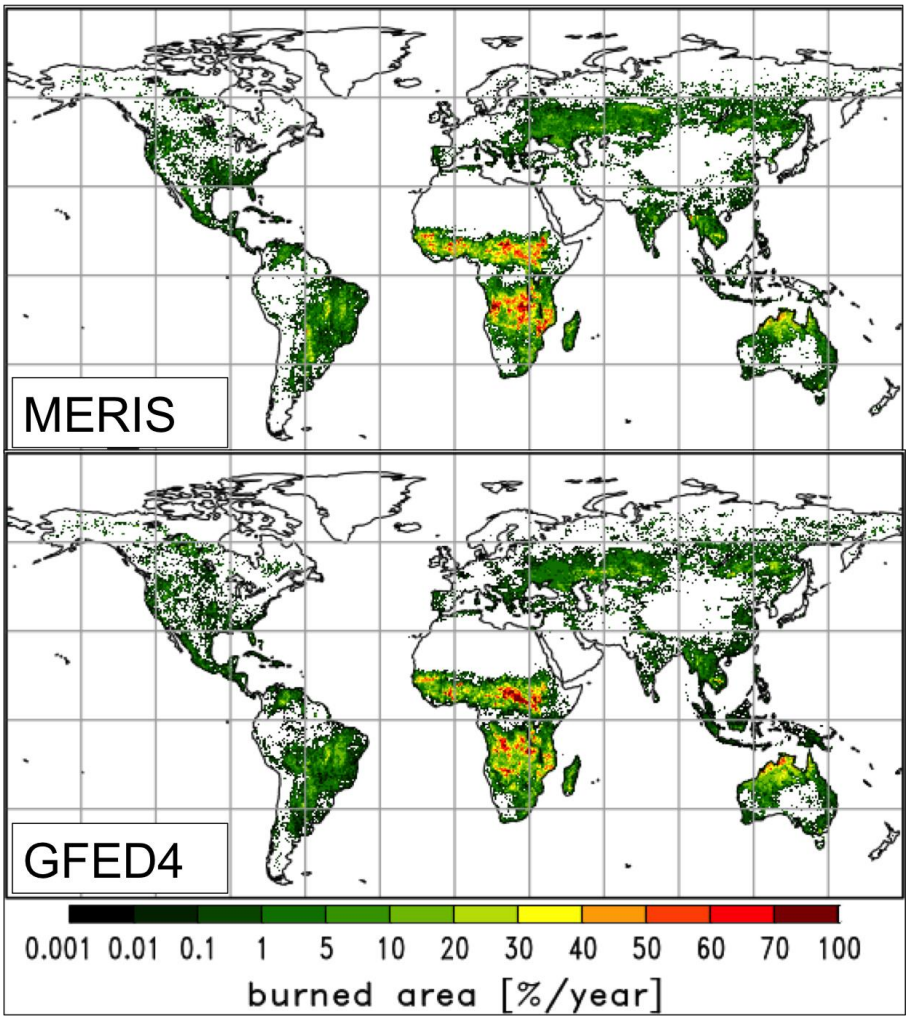

Figure 53. MERIS and GFED mean annual burned area (Ramo et al, 2014).

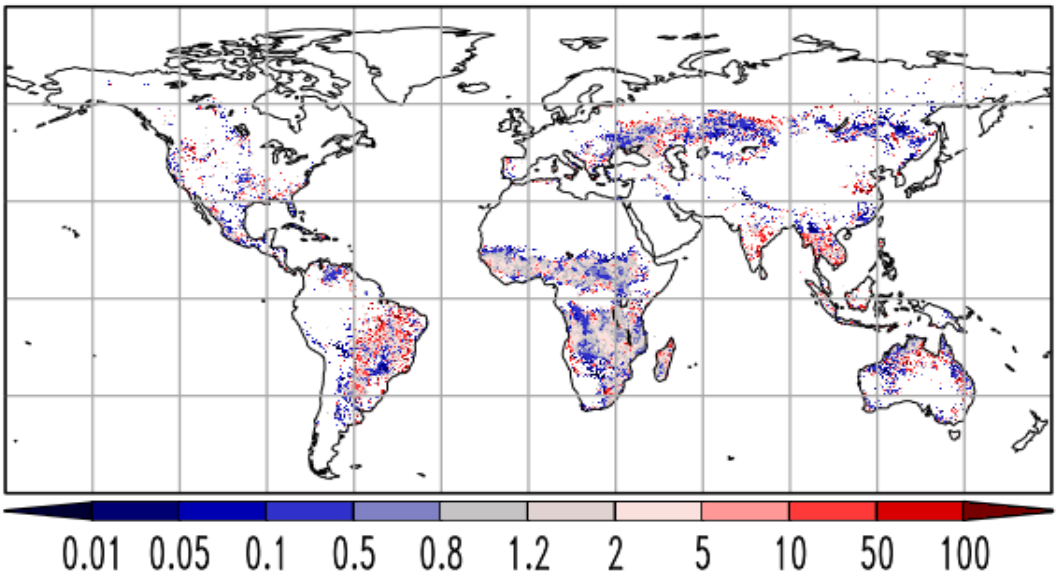

Figure 54. Ratio between MERIS and GFED4 products (Ramo et al, 2014).

Regression lines were computed for the two products separating them by eco-region and year. Results are shown in Figure 55. A high level of agreement between the two products is also found in this case. When comparing the results by eco-region, correlation coefficients between the two products were 0.974, 0.9986 and 0.9969 respectively for years 2006 to 2008.

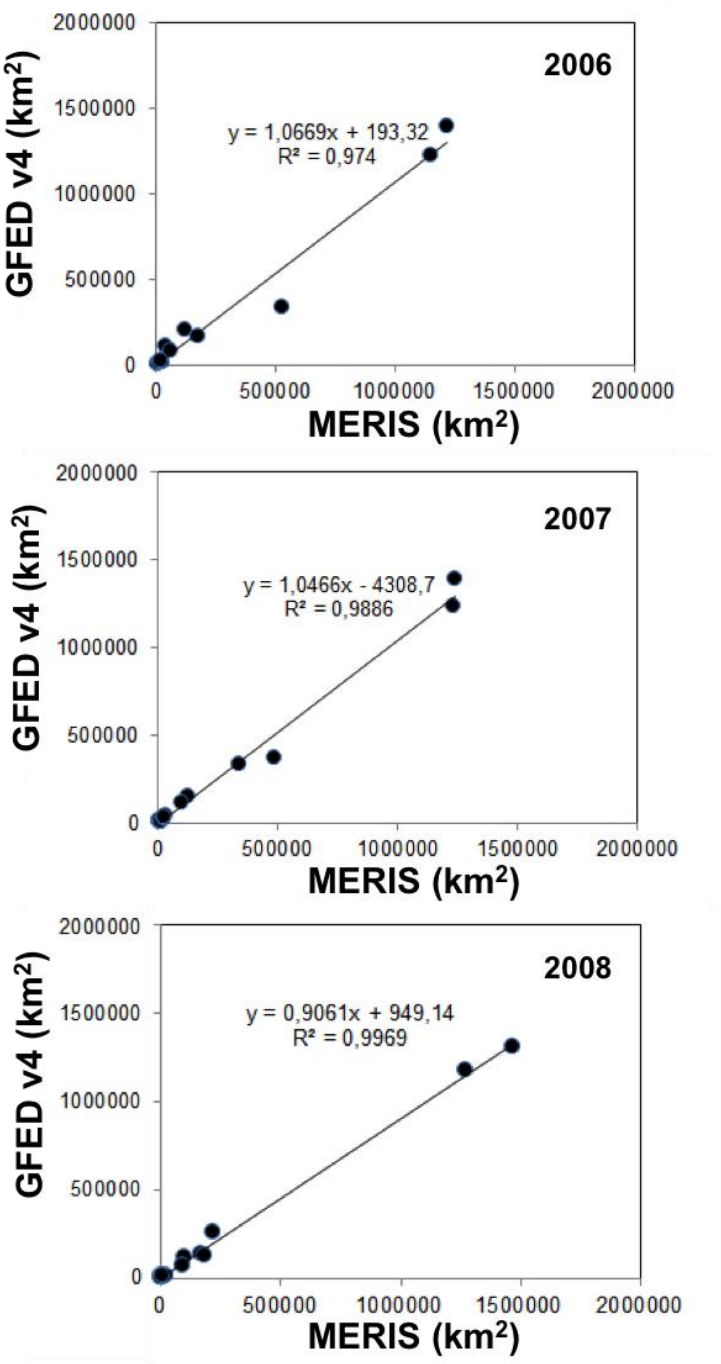

Figure 55. Correlation between MERIS and GFED 4 for 2006 to 2008.

When looking at seasonal trends, a comparison was made between the MERIS BA extent found for each month of the 3 years and the GFED values. A high level of agreement was found between the two time series. Figure 56 includes these global monthly BA estimations by MERIS and GFED v4 from 2006 to 2008. According to the figure, the trend between products was consistent in terms of magnitude through the temporal series. GFED v4 underestimates when compared to MERIS, except for October and November 2006, and August and September 2007 and 2008.

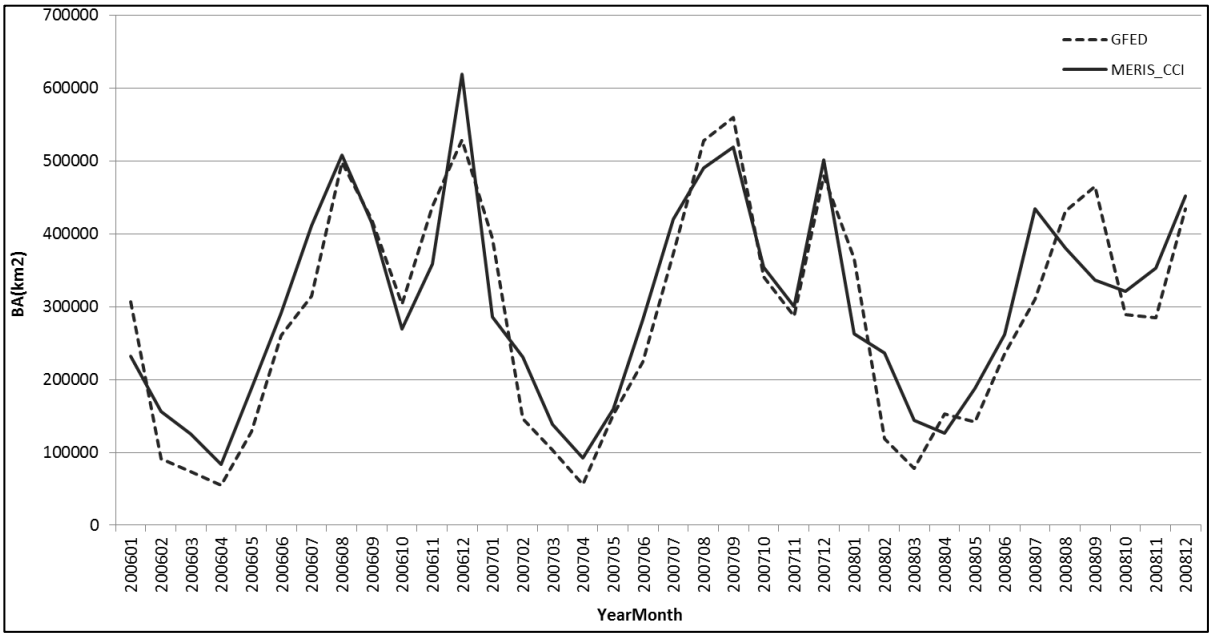

Figure 56. Monthly global BA in 2006 to 2008 for MERIS_CCI and GFED v4.

CHAPTER 5

DISCUSSION

5.1. ON THE ALGORITHM DESIGN

In this research, the analysis of the different steps to obtain a BA algorithm from MERIS data, as well as the analysis and assessment of a three year time series of global BA outputs have been performed. MERIS temporal and spectral characteristics are not optimal for BA detection for mainly two reasons. First, temporal coverage is achieved every three days, which might not provide enough information to detect certain types of fires. Second, the sensor does not include some of the useful bands to detect fires (SWIR and MIR), complicating the detection or possibility to diminish confusion with other surfaces that might behave similarly in certain cases. On the positive side, MERIS presents higher spatial resolution than other sensors used to obtain global BA products, such as MODIS and VEGETATION. Furthermore, it has a high number of bands in the red edge and NIR (Pereira et al. 1999b) space that make it potentially interesting to retrieve BA. The developments performed, which helped enhancing these characteristics and circumvent the sensor's limitations, show that MERIS images complemented with HS information can provide reliable estimations of BA.

5.1.1. INPUT DATA

MERIS input data characteristics and sensor bands have been analysed to obtain a proper algorithm configuration. Pre-processing steps and prior data corrections are important for the retrieval of BA. Several authors have reported the impact pre-processing has in mapping land changes (Jensen 2005; Lu et al. 2004; Scheidt et al. 2008). Other effects such as BRDF have been identified as potential misleading factors, since these effects introduce changes in the temporal series as relevant as the ones caused by a fire (Justice et al. 2006). On the input data side, two processing chains have been analysed. Even though the atmospheric correction of DLR's pre-processing chain gave more accurate results, temporal stability was better achieved with the BC pre-processing chain. Furthermore, the processing times needed to obtain the input data were much lower with the latter. This is an important factor to consider when building a global algorithm, since the actual generation of the global products is very demanding in terms of computing resources. Therefore the BC chain was chosen. The noise present in the time series, as well as the number of MERIS observations, were limiting factors that already pointed the algorithm configuration towards a certain direction. Time

series change strategies, used by several authors to retrieve BA (Roy et al. 2005; Boschetti et al. 2002) were discarded, since not enough information could be extracted from them, and since the unexpected NIR minima values would have led to detection errors if a strategy of that type was chosen. Some treatment could have been performed on the time series to diminish its noise. The low number of observations complicates the inclusion of BRDF correction, which might explain part of the noise (Roy et al. 2005). A smoothing applied to the time series could have been another approach to reduce the noise in the time series, but very little information could have been inferred after that type of treatment, since the smoothing would have obscured the post-fire decrease in NIR reflectance. These limitations already pointed out in the direction of a composite strategy to perform the BA detection.

From what respects the bands analysis, the NIR band has been used in both phases of the MERIS algorithm. This band has been identified by several authors (Fredericksen et al. 1990; López García and Caselles 1991; Pereira and Setzer 1993b; Stroppiana et al. 2003; Tanaka et al. 1983) as the most adequate to retrieve BA. Previous findings from Oliva et al. (2011) on MERIS data showed that regionally the most sensitive bands to detect BA regionally were band 10, and bands 8 and 10 when combined in the GEMI index. This configuration was used to obtain the BA results for years 2006 to 2008. A more in depth study on the sensitivity of the bands was performed latter; to identify the bands sensitivity characteristics on a more generic scale. Simulations using the PROSPECT and GEOSAIL models were performed to obtain pre and post fire scenarios. The aim was to identify the most adequate bands on the MERIS sensor to perform BA discrimination from unburned areas. In fact, the interest in using MERIS, besides the spatial resolution, stands on the semi-hyperspectral characteristics of its bands, as well as on the big number of bands on the VIS-NIR space. Furthermore, the presence of 4 bands in the red-edge makes the sensor potentially interesting for vegetation applications (Clevers et al. 2001) but also for fire applications. The Bhattacharyya distance was used to determine the separability of each band between pre and post fire conditions. This strategy has been used by several authors to identify the most adequate bands in different studies (Chuvieco et al. 2002; Lasaponara 2005; Roy et al. 2002). Findings from this study are still in an early stage, but preliminary results showed that band 13 located in the NIR region, was the one with bigger Bhattacharyya distance,

having therefore more power to differentiate between the burned and unburned classes, followed by bands 10 and 12 located in the red edge. Band 7 was the one that gave better separation in the red region, whereas bands in the blue region had less power to discriminate burned area. A similar procedure will be applied to the OLCI bands in order to identify which ones are more suitable for detecting BA in this new sensor. The results obtained with this study are more generic than the ones obtained with the analysis from Oliva et al. (2011), since they cover a wider range of scenarios.

5.1.2. COMPOSITING STRATEGY

It was decided to perform the detections on composites, since this approach gives higher spatial consistency when little information is available. Composites have been used in several BA mapping studies, as means to group the information (Fernández et al. 1997; Fraser and Li 2002; Kasischke et al. 1995; Kasischke et al. 1993; Chuvieco et al. 2005; Giglio et al. 2009; Souza et al. 2005). Different composites were created using NIR and the GEMI and BAI indices. Results were evaluated in the study sites. Battacharyya distance was used to perform the separability analysis between the pre and post fire cases, in order to discriminate which indices performed better to detect the BA. Monthly and annual configurations were tested, finding that the former provided better results.

Generally, methods to build composites are based on minimum or maximum values found in a time series (Chuvieco et al. 2005; Fernández et al. 1997; Fraser et al. 2000). In this thesis, a new method was developed to build the composite, in order to ensure higher spatial and temporal stability. The method was based on the use of a Thiessen matrix, built with the HS product dates, to help guiding the approximate possible date of burning, and the identification of 3 NIR minima close to this date. This strategy helped minimising the time series instability, while ensuring spatial consistency in the BA. Since the composites were obtained on a monthly basis, but retrieving information in a two-month period, the detection of fires that occurred at the end of the month was also considered. NIR and GEMI were the band and index used to perform the detections, as the separability analysis indicated the adequacy of these bands to retrieve BA, already identified by several authors (Barbosa et al. 1999b; Pereira et al. 1999a; Pereira et al. 1999b; Stroppiana et al. 2003). On the seed phase only the NIR composite was used to

identify the seed pixels. NIR and GEMI monthly and annual composites were used on the growing phase of the algorithm.

5.1.3. ALGORITHM STRUCTURE.

The algorithm proposed was based on a two-step process, since results introduced by other authors showed that this approach could give good performance, obtaining a good balance between omission and commission errors (Barbosa et al. 1999a; Chuvieco et al. 2008b; Pereira et al. 1999a; Vafeidis and Drake 2005).

An hybrid approach combining information from MERIS reflectances and from the MOD14 active fires product was chosen. This approach has been followed by several authors (Fraser and Li 2002; Fraser et al. 2000; Giglio et al. 2009; Gong et al. 2006; Pu et al. 2007; Roy et al. 1999) obtaining good results. Furthermore, a study by Hantson et al. (2013) showed an estimation of omission and commission errors in the HS product. These results can give an idea on the adequacy and limitations of the MOD14 when used as an auxiliary product that would help overcoming some of MERIS limitations.

Different strategies were implemented. Processing time, and spatial and temporal consistency were the main parameters used to define the final configuration. The advantages of using a two-phase algorithm were identified. This is illustrated in Table 20 where OE and CE are shown after the seed and growing phases of the algorithm for the four study sites.

Table 20. OE and CE in the seed and growing phases of the algorithm.

		AUSTRALIA	CANADA	PORTUGAL	CALIFORNIA
C.E.	SEED	0.14	0.1022	0.8475	0.0996
	GROWING	0.1756	0.1036	0.8512	0.1437
O.E.	SEED	0.6745	0.7809	0.7482	0.4479
	GROWING	0.4441	0.7530	0.6429	0.4379

The use of the growing phase reduces OE in the four study sites, particularly in Australia (which is also the area with bigger Burned Area proportion), and Portugal. Commission

errors increase after the growing phase, but in a lower proportion than the decrease in the omission errors, except for California, where the algorithm does not have a good performance on the growing phase. This indicates that California is one of the areas where more commission introduced in the seed phase might exist, since there is little decrease in the OE, while the CE increases significantly. The OE reduction in Canada is small, while the CE remains stable. This indicates that the growing phase is not providing the expected results in this area, either because the conditions might be too restrictive for this region, or because the composite strategy is not appropriate for this area. This behaviour was improved with version 2 of the algorithm, showing a decrease in OE while CE remained similar.

5.1.3.1. SEED PHASE

In this phase the most clearly burned pixels need to be identified. For the MERIS BA algorithm, two procedures were tested, in order to obtain the final seed pixels: tests for threshold identification and tests for seed extension.

Firstly, tests were identified and formulated to obtain the option that would better separate between burned and unburned CDFs. First of all, the strategy to define burned and unburned pixels was determined. The basis was to use criteria that would help maximising the distance between the CDFs of the burned and unburned classes. The unburned CDF was therefore built with values found in areas of 64x64 pixels where no HS were detected. The burned CDF was built with the minimum value of the 9 MERIS pixels covered by one HS detection and where there was a drop in NIR reflectance. Later, the identification of a threshold that would help separating between the two classes was performed. Once these curves were built the threshold was identified by intersecting the curves, choosing the immediate lower decile of the burned curve that would correspond to the first decile of the unburned curve. This criterion implies accepting as much as 10% commission error inherent in the seed phase, while the omission error would be estimated by the selected decile of the burned CDF, being higher when the curves are closer. The aim of this strategy is to be more restrictive when there is a higher confusion between classes, and rather have higher omission than commission errors in that case, since the aim in this phase is to minimise commission errors, while omission errors can be reduced in the growing phase of the algorithm.

Secondly, tests were also performed to extend the seeds. Version 1, defined seeds as the pixels that had 2 HS in a 9x9 matrix around the pixel, with a drop in NIR reflectance and with a NIR value lower than the threshold identified. This method to define the seeds was selected based on the number of perimeters detected in the four study sites where perimeters were available versus commission errors. This seed configuration was used to process the 3 years of MERIS data globally.

Fire perimeter assessment and validation revealed a tendency towards omission and therefore the strategy to detect seeds was revised. The new configuration obtained in version 2, helped detecting more perimeters, and was based on filtering the number of HS with the median NIR values of pre and post fire individual images, combined with a restriction if the ratio between the number of HS and the number of PAFS was bigger than two. This configuration makes profit of the HS but filters them by using a longer period of MERIS data instead of only one pre-fire value, which is less robust considering the noise in the time series. Moreover, this strategy will be less or more restrictive according to the number of HS filtered with the median process, which adapts to the fact that the HS product presents a tendency towards commission in certain regions more than in others.

Version 2 of the algorithm is more robust and at the same time helps detecting more perimeters. In fact, an increase of 12% in the number of perimeters detected is found with this configuration (58% of total number of perimeters detected) in comparison to the 9x9 2HS one (46% of total number of perimeters detected) in the four study sites analysed.

Different techniques can be used to identify the seed pixels, as shown by several authors. For instance, in the ITALSCAR project (Paganini et al. 2003) seed pixels were identified through time series change detection, applying a series of thresholds. Vafeidis et al. (2005) identified seed thresholds from computed for NDVI, VI3 and VI3T based on median and standard deviation values. Chuvieco et al. (2008b) combined static thresholds from BAI and NBR and a multi-temporal approach. Chuvieco et al. (2008a) selected the seed pixels through the definition of temporal thresholds from BAI and GEMI indices. Giglio et al. (2009) based the identification of seeds on a series of training

pixels for the burned and unburned classes. Bastarrika et al. (2011) identified the seeds using the BAI index and statistical thresholds.

The main advantage of the strategy developed for the MERIS BA algorithm stands on the fact that the thresholds to select the seeds are regionally oriented. This is a key concept when developing a global burned area algorithm since conditions are very different worldwide and static conditions that adapt adequately to a certain region might perform poorly in other regions. Instead, the MERIS BA algorithm adapts to the conditions and data available in each area, and for each period of the year. In fact, it has an important statistical component, and therefore does not assume prior values in the distributions; those values are computed on a monthly basis for each tile, tailoring the thresholds by region and period.

Another advantage of this method is that it becomes more or less restrictive according to the confusion that exists between the burned and unburned classes. In fact, the definition of the burned class limits (the threshold) is based on the unburned class limits (decile 1 of the unburned CDF). This implies that commission errors will be limited and criteria will be stricter when more confusion exists between classes, since a lower decile of the burned class will be chosen as threshold limit. Furthermore, in version 2, an estimation of the potential commission errors in the HS is performed for each region and month. The ratio between the HS and the PAFs (obtained after applying the median pre and post fire criteria) is computed, giving an idea of the amount of commission errors in each region. According to this ratio, the conditions to identify the seeds will be more or less restrictive, becoming more robust against the errors inherent to the HS product.

Other criteria still need to be developed to decrease the number of perimeters that remain undetected in the seed phase, since there are no chances of detecting them in the second phase of the algorithm. A possible approach would be to identify, with some of the criteria already defined (NIR threshold, decrease in NIR…), other potential burned areas on the region analysed, or implementing a time series change detection approach if more data become available (for instance with the use of the future OLCI). Another option would be to use other sources of information to help determining which pixels can also be considered seeds. The inclusion of other HS information coming from

geostationary satellites could be considered for this purpose, since the temporal resolution of these sensors is much better than the MODIS ones. Even if the spatial resolution is coarser, these sensors have more chances to detect active fires than the low orbit ones, since the number of images is significantly higher.

A limitation found with the computation of statistics on the 10x10° tiles was that in certain cases (where fire behaviour, number of HS and vegetation conditions might differ between tiles) the thresholds computed and the growing in two neighbouring tiles might vary heavily. This can translate in some cases in discontinuities between the tiles, having fires that cover the intersection between two tiles and where the fire grows more in one tile than in the other one. Results obtained for two adjacent tiles are illustrated in Figures 57 and 58 for two different areas. Figure 57 shows the BA retrieved in the area of Thailand and Myanmar (covered by the tiles v06h27 and v07h27) in 2006. Figure 58 shows BA results for the African region of Mali, Burkina Faso, Cote d'Ivoire and Ghana (covered by tiles v07h17 and v08h17) in 2008. As illustrated in the figures, the problem is partially solved in version 2 since the way the seeds are computed differs from version 1 (median filtering and HS restriction). An extra condition was applied to reinforce this improvement. The statistics in the tiles where fires were not growing adequately were analysed. It was found that the decile used to obtain the NIR threshold in some of these cases was decile 1. This meant that there was a poor separation between classes, and therefore a very restrictive threshold was used to define the seeds. Nevertheless, in practice, the poor growing in these cases illustrated that there was no need to use such a restrictive threshold for certain tiles. It was decided that in cases where decile 1 was identified, the number of HS in that tile would be considered in order to modify this decile. If the number of HS was higher than 500, the decile to obtain the threshold would be increased to decile 3. In cases where the number of HS was below 500, the threshold would still be defined from decile 1. These values were set empirically. As illustrated in Figures 57 and 58, these strategies diminish the discontinuity between tiles, but some edges are still noticeable.

A possible strategy to diminish these discontinuities would be to apply smoothing criteria between the tiles once the BA is computed. In order to further limit these discontinuities, and to tailor in a more specific way the thresholds obtained dynamically, the curves that are generated on a 10°x10° basis could be computed by

type of vegetation. In fact, this could help discriminating better different cases (for instance darker or lighter vegetation). This possibility should be considered carefully, since errors on the type of vegetation would be introduced by the errors inherent to the land cover map. Furthermore, the separation in vegetation types could also lead to other spatial discontinuities (for instance in the limits of different types of vegetation). This option was not included in the algorithm since it was decided that on a first approach it would be more convenient to maintain the development independent from another source of information, since inherent errors to the LC map would have an impact also on the quality of the BA detections.

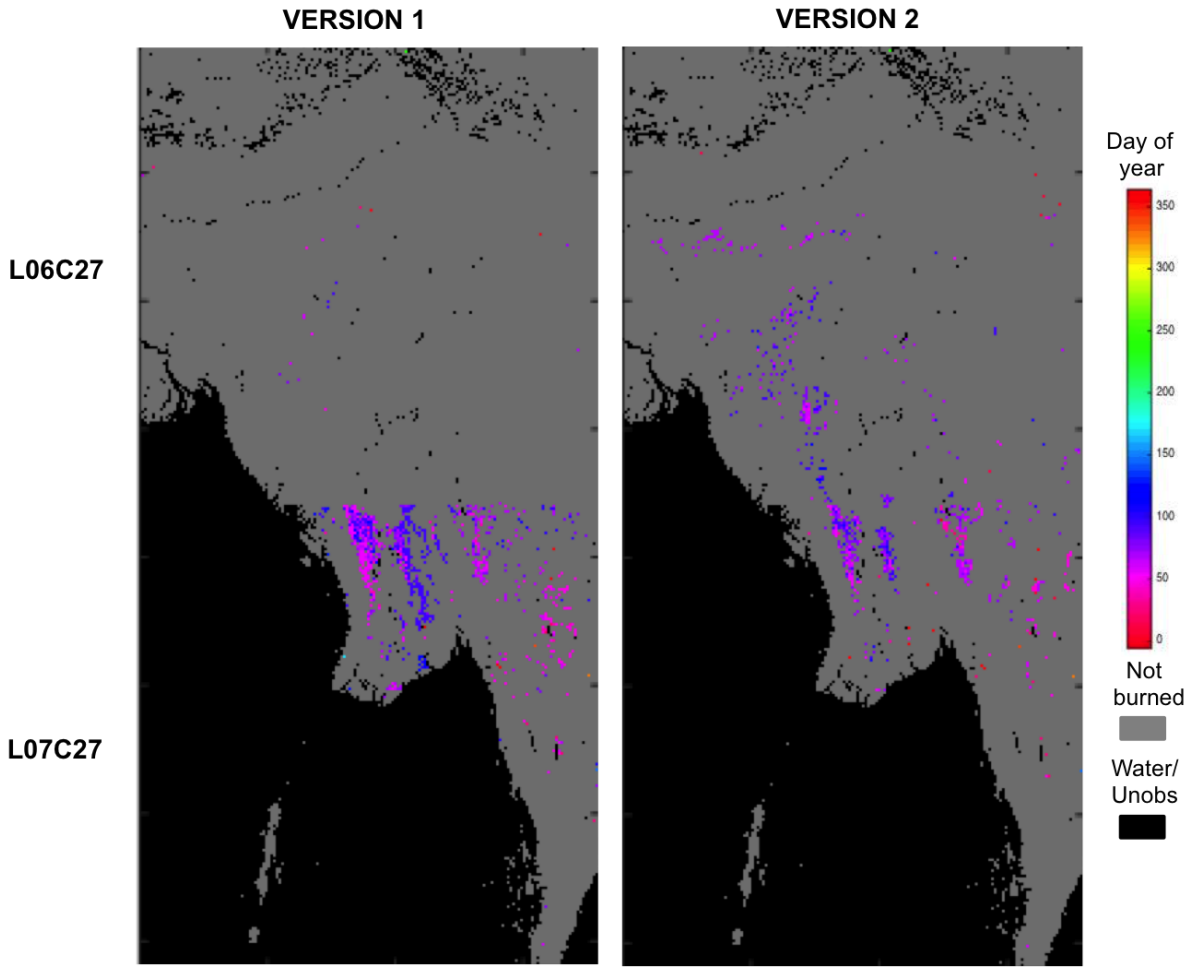

Figure 57. Discontinuities between adjacente tiles (L06C27, L07C27) in version 1 and 2 (with extra condition).

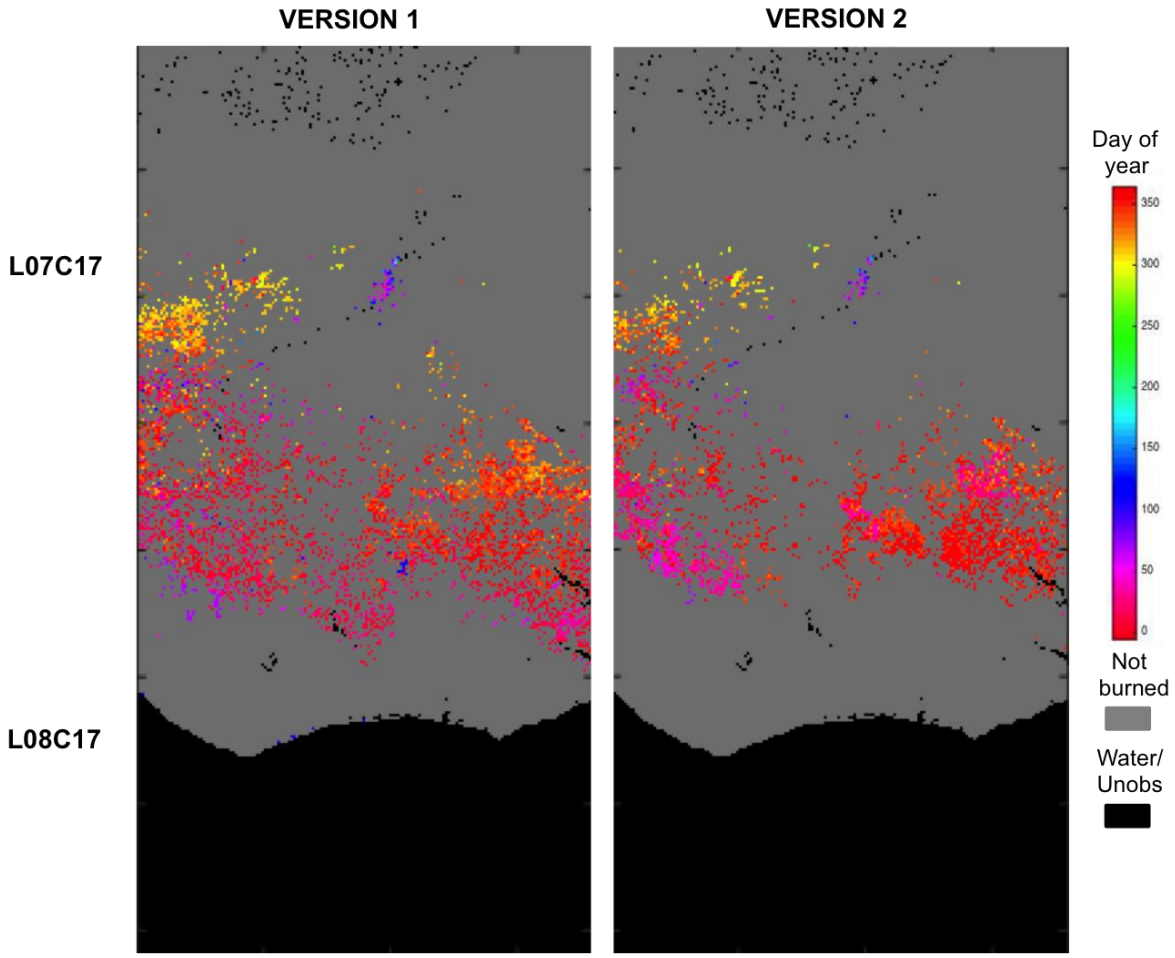

Figure 58. Discontinuities between adjacente tiles (L07C17, L08C17) in version 1 and 2 (with extra condition).

5.1.3.2. GROWING PHASE

On a global scale, algorithms developed to obtain BA are generally based on pixel approaches (Ershov and Novik 2001; Giglio et al. 2009; Roy et al. 2005; Silva et al. 2003; Carmona-Moreno et al. 2005; Eva and Lambin 1998; Grégoire et al. 2003; Piccolini and Arino 2000; Plummer et al. 2007; Tansey et al. 2008).

In this work, different strategies were tested in order to develop the growing phase of the algorithm. The main lines of research were based on retrieving the BA on pixel and object based strategies. Pixel-based approaches are more stable to noise (Kamdi and Krishna 2012) and are more tailored to each pixel. Object based approaches were used in regional studies, showing the potential of this technique to map BA (Dragozi et al. 2014; Gitas et al. 2004; Mitri and Gitas 2002; Polychronaki and Gitas 2010; Quintano et al. 2006; Shimabukuro et al. 2015). Tests performed in different sites, as well as

assessment from the fire perimeters in four areas, showed the better performance of the pixel based strategy. This was therefore the method selected for processing the 3 years of MERIS data. Object based techniques performed well in some cases, but it was found that there was an increased difficulty in defining a set of conditions systematically that would give good results on a global scale.

Other possible implementations such as neural networks or SVMs could also be considered, as well as further implementations based on OBIA techniques. Nevertheless, all these implementations will encounter the same limitations found with the object-based methods tested, i.e. defining the object size and threshold parameters used to determine the burned/unburned, or the training sets that would potentially work on a global scale. Object based approaches might have higher probabilities of leading to larger commission errors in the BA product due to a HS or seed commission error than pixel based approaches. On the pixel based approach, a HS commission error that was not filtered in the seed phase can lead to errors in the growing phase, but the conditions to classify the pixels around this one will be checked again, and need to be fulfilled to classify that pixel as burned. On the object based approaches, if seeds are used to determine objects, commission coming from the seeds will already become a commission error for a complete object, having a higher number of pixels classified as burned, without any other conditions checked. Ideally a fusion of these techniques should be considered. This way combining the advantages of the two techniques should be possible.

Once the 3 year results were analysed with the validation exercise and the perimeters assessment, omission errors were found from poor growing in some regions. This indicated that further developments needed to be performed on this line. It was decided to test the use of individual daily images to perform the growing phase detections. Once the seed phase is performed, individual images can be used again, since the noise in the time series does not affect the threshold and statistics extraction of the growing phase in each individual image. In fact, individual images showed more contrast between burned and unburned areas than the composite built. Therefore the composite was kept for the seed phase, but the growing phase was performed on individual images, improving the detection since the degree of detail and the separability between burned

and unburned was found higher in those cases. The main drawback of this change is that if the image did not cover the full extent of the fire some BA might not be detected, but still having the chance of detecting it in the following days. The use of individual images in the growing phase is implemented in version 2 of the algorithm, to obtain the long term BA time series from MERIS.

The difference between the use of the composite and the individual images for the growing phase is illustrated in Table 21 where OE and CE are shown. In both cases the seeds were obtained with the 9x9 and 2HS strategy.

Table 21. OE and CE when using individual images and composite for the growing phase of the algorithm.

		AUSTRALIA	CANADA	PORTUGAL	CALIFORNIA
C.E.	COMPOSITE	0.1756	0.1022	0.8512	0.1437
	SINGLE IMAGE	0.2066	0.1315	0.9434	0.2372
O.E.	COMPOSITE	0.4441	0.7530	0.6429	0.4379
	SINGLE IMAGE	0.4135	0.5491	0.5483	0.3427

There is a reduction on the OE in the four sites when the growing is performed on the individual images. This decrease in the OE is more relevant in Canada and California, which were the two areas previously identified where the growing in the composite was not performing properly. An important decrease in Portugal exists as well, but with the same proportion of increase in the CE. Nevertheless, the purpose of these results is to show the interest in performing the growing part of the algorithm on the individual images. The use of the seed option based on the median with restrictions will limit the commission errors that appear in this table.

5.2. ON THE GLOBAL OUTPUT.

Three years of MERIS data were processed with the BA algorithm. The BA obtained for the three years varied between 3.6 and 3.8 million km^2. These estimations are in good agreement with findings from other authors (Csiszar et al. 2005; Giglio et al. 2006a; van der Werf et al. 2006), in spatial and temporal terms. When comparing MERIS results with existing BA products, the estimations can be considered very consistent, both in

terms of total BA values, and geographical and temporal distribution, with better estimations (according to validation results) than existing European BA products, particularly in Tropical regions. Further comparison of the MERIS results with GFED v4, one of the most widely used by climate modellers, showed similar spatial and temporal trends for the 3 years processed. Global estimations were 3 to 9% higher than GFED v4 for the three years computed, while geographical and monthly trends showed high correlation values.

The validation results (Padilla et al. 2015) confirmed that MERIS algorithm provided acceptable results. When estimating total BA in the statistically designed validation sample, MERIS provided lower but comparable accuracy metric values to the MODIS-based BA products (MCD45 and MCD64). Overall accuracy was high (OA>0.99) but the BA category of the MERIS product showed higher commission errors (CE=0.64) than MCD64 and MCD45 and similar omission errors (OE=0.76) to the MCD45. The relative balance of errors showed better results than MCD64 and MCD45 with a 34% of underestimation. Errors were lower for the areas with higher proportion of burned area (OE=0.51 and CE=0.52). MERIS BA results showed some detection problems, particularly in temperate regions, where fires are unusual and commission errors were found by misclassification with agricultural areas. In Tropical regions, omissions were higher, which may be caused by the omission errors included in HS detections, becoming more relevant in areas with small fires (Hantson et al. 2013). The use of HS also implies a certain contribution to overall BA error. HS have proven very reliable to detect active fires, with very low commission error, but they are not frequent or sensitive enough to detect all active fires, and therefore omission errors are higher (Csiszar et al. 2005; Giglio et al. 2006a; Hantson et al. 2013). This omission error inherent to HS is also included in other BA products based on HS (such as the GFED-MCD64). Some of the possible improvements to overcome these limitations have been discussed in the previous paragraphs, and some improvements have already been included in version 2 of the algorithm.

Since the MERIS BA algorithm relies on MODIS HS and MERIS reflectance information, the results cannot be considered fully independent from MODIS products, particularly from MCD64, which uses a hybrid approach as well. However, the structure of the

algorithm is quite different from the Giglio et al. (2009) one, and it is built on the particular spectral space detected by the MERIS sensor. Spatial variations between MERIS BA results and GFED v4 for instance, show that HS input does not fully determine the output results.

Estimations of errors obtained with the validation exercise, may be considered pessimistic, as some of these errors are caused by the low temporal frequency of the MERIS sensor, and therefore include both classification and temporal reporting errors. Temporal reporting accuracy of the MERIS product was computed by obtaining the difference between MERIS BA detection dates and HS dates. It was observed that 50% of the MERIS detections occurred with a difference of 4, 22, 12 and 8 days from the HS date for the Australian, Californian, Canadian and Portuguese sites, respectively, whereas 75% occurred within 9, 30, 19 and 15 days for the same sites respectively. The temporal accuracy is therefore lower in these cases than the one obtained globally by Boschetti et al. (2010) for the MCD45 product (50% within one day and 75% within four days). The MERIS reporting accuracy increases the likelihood of reporting omission and commission errors even for correctly detected pixels, particularly when the two Landsat images used to obtain the reference perimeters are close in time (as it is the case of Tropical ecosystems where most validation pairs of images were separated by 32 days or less). According to the fire perimeter assessment, when using a full year of fire perimeters in four very large study sites, the omission error in fact decreased to 0.47 and the commission error to 0.15 in the worst value of the three years. This reduction of detection errors compared to the Landsat validation sample should be related to the longer period included in the assessment sites (which covers the full year), when dating errors are expected to affect marginally the accuracy estimations.

A potential interest in retrieving BA from MERIS relies on its higher spatial resolution compared to existing BA collections and therefore the possibility of detecting smaller perimeters. These fires are especially relevant because some authors estimate that they account for almost 35% of total emissions (Randerson et al. 2012). Consequently, there is an interest in better detecting them from space, since it is one of the difficult tasks to achieve with coarse resolution sensors. Results on the number of perimeters detected

with version 1 (used to obtain the 3 years of BA data), version 2, and with the MCD45 product are available in Table 22.

Table 22. Percentage of perimeters detected by fire size with MERIS version 1 and 2 and MCD45.

Study site		Fire size (ha)		
	<100	<1000	<10000	>10000
AUSTRALIA				
Total nº of per.	12174	4652	1373	209
% detected MERIS v1	34%	62%	92%	100%
%detected MCD45	34%	67%	94%	99%
%detected MERIS v2	46%	78%	95%	100%
CANADA				
Total nº of per.	30	20	28	34
% detected MERIS v1	0%	25%	54%	88%
%detected MCD45	3%	15%	86%	100%
%detected MERIS v2	7%	45%	75%	94%
PORTUGAL				
Total nº of per.	24	19	4	0
% detected MERIS v1	38%	74%	50%	-
%detected MCD45	8%	63%	100%	-
%detected MERIS v2	38%	63%	50%	-
CALIFORNIA				
Total nº of per.	98	48	25	5
% detected MERIS v1	4%	8%	60%	80%
%detected MCD45	2%	23%	24%	100%
%detected MERIS v2	4%	21%	80%	100%

The detection of small perimeters increases significantly with version 2 of the MERIS algorithm. For perimeters smaller than 100ha the detection rate is 46%, 7%, 38% and

4% for the Australian, Canadian, Portuguese and Californian study sites respectively. These detection rates should be considered acceptable in the case of Australia and Portugal, if we consider that one MERIS pixel covers 9ha and one MODIS HS pixel covers 100ha. This explains partially the lower number of detections in the case of small perimeters. Furthermore, small fires are likely to burn for shorter periods of time, therefore it is more probable that the satellite will not be covering the area when those fires are burning. In fact, for fire perimeters of size between 100 and 1000 ha the detection rate increases up to 78%, 45%, 63% and 21% for the four study sites respectively. Results obtained with version 2 show that in Australia and Canada an increase in the number of perimeters detected for all fire sizes is achieved, compared to version 1. In California there is an increase for fires bigger than 100 ha. In Portugal the number of perimeters detected remains the same as in version 1, except for fires of size between 100and 1000ha, where there is a decrease of 11%. This result was expected since this area was identified as one of the regions with higher HS commission errors in the Hantson et al. (2013) study, and therefore, the more restrictive conditions applied in version 2 for those cases was expected to diminish the number of perimeters detected.

When compared to the MCD45 product, version 2 of the algorithm detects the same number (2 cases) or more (9 cases) fire perimeters except for four cases: Canada for fires <10000 and >10000 ha, Portugal for fires between 1000 and 10000ha and California for fires between 100 and 1000ha. These results highlight the interest in obtaining BA collections from different methods and sensors (with better spatial resolution), since the results obtained can be complementary in some cases, enhancing the quality obtained by each product individually.

5.3. ON THE RELEVANCE OF OBTAINING A NEW BA PRODUCT

BA characterization is relevant from a climatic and atmospheric point of view. Currently a number of BA products exist, but at this stage it is relevant to ensure measurements continuity with the use of sensors on operational missions, as well as to fit certain user requirements, such as uncertainty characterization, or higher spatial resolution. Furthermore, the development of different BA collections helps identifying areas where BA is properly characterized, diminishing uncertainty, and also to better understand

where each product is having better performance, identifying strengths and weaknesses of each one of them.

The users of the fire_cci project assessed the MERIS BA product. A complete report is available in the Climate Assessment Report (Yue et al. 2014) and the Product Intercomparison Report (Ramo et al. 2014). A summary of their conclusions is included hereafter.

It was found that MERIS is in good agreement with GFED, in terms of total amount of burned area, spatial and temporal distribution of fires. Some differences were also reported between the products, which highlights the interest in obtaining different BA collections. For example, across Europe, except for the Kazakhstan steppe region, fire_cci estimates are 2 to 5 times higher than those from GFED4. Across agricultural India, fire_cci estimates are typically more than 4 times higher than in GFED4. An example of these differences is shown in Figure . In spring 2006, an important fire event took place in Eastern Europe. The event caused high air pollution in the European Arctic, as documented by Stohl et al. (2007). The predominantly agricultural fires show up as strong increase of MODIS active fire detections between April and May (Figure). While the fires are well reflected in the MERIS BA product, they are largely missed by GFED3 and GFED4. The figure also shows that GFAS, the Global Fire Assimilation System from EC's Operational Copernicus Atmosphere Monitoring Service (CAMS), also recorded this event. This highlights the fact that each fire product has different commission and omission characteristics dependent upon the region and the period selected.

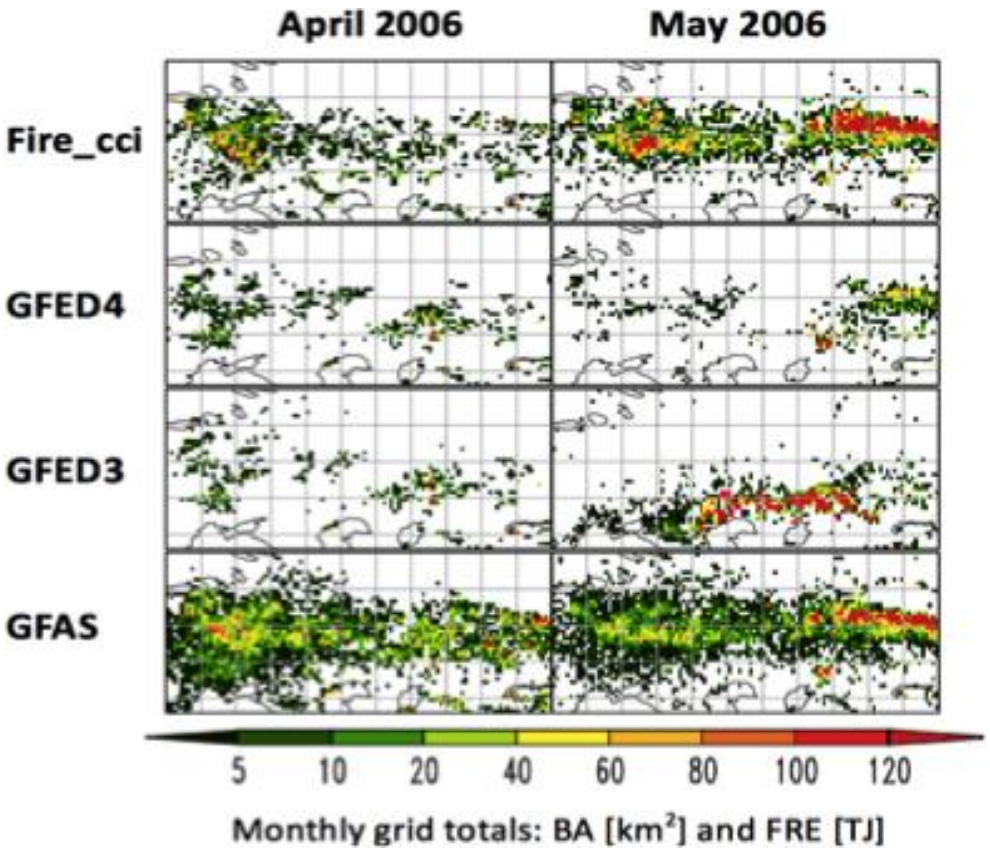

Figure 59. BA from MERIS, GFED and GFAS in April and May 2006 in Eastern Europe (Ramo et al. 2014).

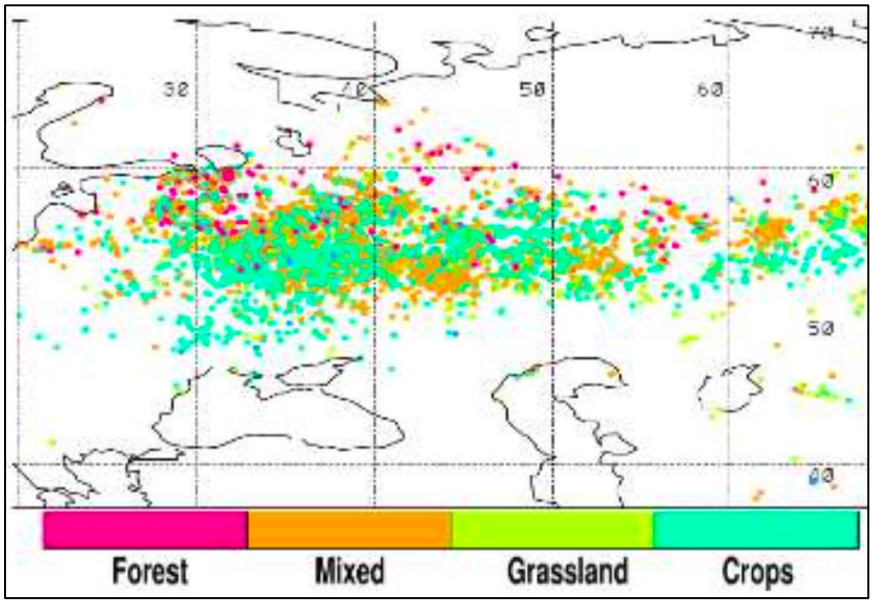

Figure 60. MODIS active fire detections in the period from 21st of April to 5th of May 2006, indicating the type of vegetation for each detection (Ramo et al. 2014).

The users also found that the quality improvement with the MERIS BA data was significant compared to previous European products (Globcarbon, L3JRC, GEOLAND) in terms of correctly capturing the spatial and temporal distribution of fires.

CO2 and CO emission from biomass burning, as derived by the ORCHIDEE model being forced with MERIS BA data yield similar seasonal patterns and magnitudes than GFED v3.1 (Yue et al, 2014). This suggests that MERIS data are well suitable for atmospheric applications related with the trace gas emissions from fires (Chuvieco et al. 2015).

Comparison with national statistics pointed out that there is a generic underestimation of BA from remote sensing collections, mostly of small fires. MERIS version 1 and GFED performed equally in this comparison, showing an accurate inter-annual variability.

The MERIS BA pixel product analysis showed that characterising path structure is feasible from this dataset. The BA information retrieved on the pixel level can be used on a global scale to obtain a comprehensive description of patch complexity, elongation and direction, which are some key variables for global fire spread/intensity modelling.

In general, the user assessment reported on the potential interest of having a longer time series of this product, having obtained promising results with the processing of years 2006 to 2008.

CHAPTER 6

CONCLUSIONS

AND

PERSPECTIVES

The growing interaction between fire and climate highlights the relevance of accessing global burned area (BA) information, particularly for climate and dynamic vegetation models (Mouillot et al. 2014). This need was identified with the ECV fire disturbance and consequently in the ESA's fire_cci project, which aimed at monitoring burned areas on a global scale, in order to study its relation to climate change. The work presented in this thesis has been developed within the framework of the fire_cci and has therefore implicitly the objective of contributing to these international efforts.

The main aim of this work was to develop for the first time a global algorithm to detect burned areas on a global scale from MERIS data. The sensor had some features that made it potentially interesting to map BA. It presented a high number of bands in the red edge and NIR space, and a higher spatial resolution than the sensors used up to date to obtain BA on a global scale. On the other hand, the challenge in mapping BA with MERIS was that temporal coverage was not optimal, and the sensor did not include SWIR and MIR bands, which are useful to detect fires.

Considering these limitations, and after analysing the results of the MERIS BA algorithm, it can be concluded that the aim of the thesis was achieved, as the algorithm developed within this research provided reliable global BA products from MERIS data. The developments discussed in this document, which aimed to benefit from MERIS spatial and spectral bands characteristics, while mitigating its limitations, show that MERIS images, complemented with HS information, provide fair estimations of global BA.

MERIS input data characteristics and sensor bands were analysed. BC pre-processing data chain was selected as input data to ingest into the algorithm. A study on the MERIS most suitable bands to discriminate BA was performed. Simulations using the PROSPECT and GEOSAIL models were performed to obtain pre and post fire scenarios. Results showed that band 13 located in the NIR region, was the one with more power to differentiate between the burned and unburned classes, followed by bands 10 and 12 located in the red edge. Band 7 was the one that gave better separation in the red region, whereas bands in the blue region had less power to discriminate burned area. NIR and GEMI index were selected as the most adequate to identify BA. BA detections

were performed on composites, that helped obtaining higher spatial and temporal consistency.

The algorithm proposed was based on a two-step process, divided in seed and growing phases. On the first phase, cumulative distribution functions were computed to discriminate the most clearly burned pixels, using regionally-oriented NIR thresholds and choosing criteria that would maximise the distance between the CDFs of the burned and unburned classes. Final configuration of version 1, defined the seeds as the pixels that would have 2 HS in a 9x9 matrix around the pixel, with a drop in NIR reflectance and with a NIR value lower than the threshold identified. This seed configuration was used to process 3 years of MERIS data globally. On the second phase, different strategies were tested to obtain the region growing. Main lines of research were based on pixel and object based strategies. Tests performed in different sites, as well as assessment from the fire perimeters showed the better performance of the pixel-based strategy, which was used for version 1 of the algorithm.

Fire perimeter assessment and validation revealed a tendency towards omission. This indicated that further developments were needed. Seed and growing phases strategies were revised. For the seed phase, version 2 was based on filtering the number of HS with the median NIR values of 5 pre and post fire individual images and a ratio restriction based on the relation between HS and PAFs. This configuration was more robust than the previous one, detecting 12% more fire perimeters. In version 2, it was decided to reconsider the use of individual daily images for the growing phase. According to the fire perimeter assessment, the use of daily images instead of monthly composites, diminished omission errors with little increase in the commission errors, for the four study sites. Version 2 of the algorithm will be used to process the full MERIS time series (2003-2012) to obtain a longer BA collection. This will provide a complementary view on the existing knowledge of BA trends.

Three years of MERIS data were processed with version 1 of the BA algorithm. BA found for the three years varied between 3.6 and 3.8km^2. Patterns of fire activity were identified (African Tropical regions, Northern regions of Australia, Central Brazil, Central and South East Asia, Russia, Canada and South East USA) as well as seasonal

trends. MERIS BA estimates showed similar although lower accuracy than existing MODIS BA products, based on a validation dataset produced from multi-temporal Landsat images. Some of the observed errors were related to temporal reporting problems associated to the MERIS coverage frequency. In fact, errors were found much lower when results were compared with external fire perimeters that consider the full fire season. Global estimations were 3 to 9% higher than GFED v4 for the three years computed, while geographical and monthly trends showed high correlation values. Results indicated that there was a significant improvement in BA characterization compared to previous European BA datasets.

Number of perimeters detected by fire size with the MERIS product was computed. In the four assessment sites, BA estimated from version 2 of the algorithm detected 58% of the total number of fire perimeters.

The algorithm developed presents some limitations in terms of dependency from active fire information and temporal reporting accuracy. MERIS BA results showed some detection problems, particularly in temperate regions, where fires are unusual and commission errors were found by misclassification with agricultural areas. In Tropical regions, omissions were higher, which may be caused by the omission errors included in HS detections, becoming more relevant in areas with small fires (Hantson et al. 2013).

Future developments are needed in order to overcome the limitations identified. An improved seed procedure in which very clear fire-related reflectance changes may be included in future versions, ensuring also more independency from the thermal information. Additional research is also needed to build more robust time series from MERIS reflectance data. This could be achieved also from its successor, the OLCI, or by using MODIS data. The seed phase could benefit from the inclusion of information coming from other sources. The use of active fire information from geostationary satellites should also be investigated for this purpose. The growing phase could combine object and pixel based approaches to overcome the limitations of the latter.

The use of land cover maps should be tested in future developments, in order to obtain statistical thresholds more tailored to each type of vegetation, and to overcome the discontinuities found between tiles. Special care would need to be taken with this approach, since inherent errors to the LC map would have an impact also on the quality of the BA detections.

A longer BA time series is needed to obtain information on climate behaviour and interactions between climate and fires, as well as to infer and understand which areas will be more affected by changes in their fire regimes.

The MERIS algorithm could be adapted to the OLCI sensor, on board the future Sentinel-3 (expected launch December 2015). This satellite will also have a thermal sensor (the SLSTR), with active fire detection capabilities. Therefore, the methods developed in this work could be implemented without the need of using data from other satellites. The algorithm developed could also be adapted to other sensors that are constrained to the red-near infrared space, as it is the case of the higher spatial resolution (250 m) bands of MODIS. In fact, the adaptation of the MERIS BA algorithm to MODIS bands 1 and 2 and to OLCI is foreseen for the second phase of the fire_cci project, ensuring continuous monitoring of fire disturbance from space.

CHAPTER 7

REFERENCES

Ackerman, S., Strabala, K., Menzel, P., Frey, R., Moeller, C., & Gumley, L. (1998). Discriminating clear sky from clouds with MODIS. *Journal of Geophysical Research, 103*, 141-157

Achard, F. et al. (2014). Determination of tropical deforestation rates and related carbon losses from 1990 to 2010. *Global Change Biology, 20*

Adams, H.D., Guardiola-Claramonte, M., Barron-Gafford, G.A., Villegas, J.C., Breshears, D.B., Zoue, C.B., Troch, P.A., & Huxman, Y.E. (2009). Temperature sensitivity of drought-induced tree mortality portends increased regional die-off under global-change-type drought. *Proceedings National Academy of Sciences, 106*, 7063–7066

Alexander, L. (1983). SAIL canopy model fortran software. *Lyndon B. Johnoson Space Center. NASA technical report, JSC-18899*

Alonso-Canas, I., & Chuvieco, E. (2015). Global burned area mapping from ENVISAT-MERIS and MODIS active fire data. *Remote Sensing of Environment, 163*, 140-152

Ambrosia, V.G., & Brass, J.A. (1988). Thermal analysis of wildfires and effects on global ecosystem cycling. *Geocarto International, 1*, 29-39

Andreae, M.O., & Merlet, P. (2001). Emission of trace gases and aerosols from biomass burning. *Global Biogeochemical Cycles, 15*, 955-966

Archer, S. (1994). Woody plant encroachment into southwestern grasslands and savannas: rates, pat- terns and proximate causes. . *Ecological implica- tions of livestock herbivory in the West (ed. by M. Vavra, W. Laycock & R. Piepper)Society of Range Management, Denver.*, 13-60

Archibald, S., Roy, D.P., B., V.W., & J., S.R. (2009). What limits fire? An examination of drivers of burnt area in Southern Africa. *Global Change Biology, 15*, 613-630

Arino, O., Gross, D., Ranera, F., Bourg, L., Leroy, M., Bicheron, P., Latham, J., Di Gregorio, A., Brockman, C., & Witt, R. (2007). GlobCover: ESA service for global land cover from MERIS. *IGARSS Symposium* (pp. 23-28). Barcelona

Arino, O., & Melinotte, J.M. (1998). The 1993 Africa Fire Map. *International Journal of Remote Sensing, 19*, 2019 -2023

Arino, O., & Piccolini, I. (2000). Development and testing of algorithms for a global burnt area product from ERS ATSR-2. *Igarss 2000: Ieee 2000 International Geoscience and Remote Sensing Symposium, Vol I - Vi, Proceedings*, 304-306

Arino, O., Simon, M., Piccolini, I., & Rosaz, J.M. (2001). The ERS-2 ATSR-2 World Fire Atlas and the ERS- 2 ATSR-2 World Burnt Surface Atlas projects. *Proceedings of the 8th ISPRS conference on Physical Measurement and Signatures in Remote Sensing*

Arora, V.K., & Boer, G.J. (2005). Fire as an interactive component of dynamic vegetation models. *Journal of Geophysical Research, 110*, G02008

Bachmann, M., E., B., Fichtelmann, B., Gunther, K., Krauss, T., Muller, A., Muller, R., Richter, R., & Wum, M. (2014). Algorithm theoretical Basis Document, Volume I, Pre-processing

Barbosa, P.M., Grégoire, J.M., & Pereira, J.M.C. (1999a). An algorithm for extracting burned areas from time series of AVHRR GAC data applied at a continental scale. *Remote Sensing of Environment, 69*, 253-263

Barbosa, P.M., Stroppiana, D., Gregoire, J.M., & Pereira, J.M.C. (1999b). An assessment of vegetation fire in Africa (1981-1991): Burned areas, burned biomass, and atmospheric emissions. *Global Biogeochemical Cycles, 13*, 933-950

Bastarrika, A., Chuvieco, E., & Martin, M.P. (2011). Automatic Burned Land Mapping From MODIS Time Series Images: Assessment in Mediterranean Ecosystems. *IEEE Transactions on Geoscience and Remote Sensing, 49*, 3401-3413

Benvenuti, M., Chuvieco, E., & Conese, C. (2001). A new double step methodology based on satellite image processing for forest fire mapping on the Italian territory. In E. CHUVIECO, & P. MARTIN (Eds.), *Proceedings of the 3rd International Workshop on Remote Sensing and GIS applications to Forest Fire Management: New Methods and Sensors* (pp. 127-129). Paris: European Association of Remote Sensing Laboratories

Boardman, J.B., Kruse, F.A., & Green, R.O. (1995). Mapping target signatures via partial unmixing of AVIRIS data. In R.O. Green (Ed.), *Fifth Annual JPL Airborne Earth Science Workshop* (pp. 23-26). Pasadena, CA: NASA, Jet Propulsion Laboratory

Bojinski, S., Verstraete, M., Peterson, T.C., Richter, C., Simmons, A., & Zemp, M. (2014). The concept of essential climate variables in support of climate research, applications and policy. *Bulletin of the American Meteorological Society*, 1431-1443

Boschetti, L., Eva, H.D., Brivio, P.A., & Gregoire, J.M. (2004). Lessons to be learned from the comparison of three satellite-derived biomass burning products. *Geophysical Research Letters, 31*, L21501, doi:21510.21029/22004GL021229

Boschetti, L., Flasse, S., Jacques de Dixmude, A., & Trigg, S. (2002). A multitemporal change-detection algorithm for the monitoring of burnt areas with SPOT-Vegetation data, in Analysis of Multi-temporal Remote Sensing Images. *World Scientific Publishing, L. Bruzzone and P. Smith, Editors*, 75-82

Boschetti, L., Roy, D.P., Justice, C.O., & Giglio, L. (2010). Global assessment of the temporal reporting accuracy and precision of the MODIS burned area product. *International Journal of Wildland Fire, 19*, 705-709

Bourg, L. (2011). The AMORGOS MERIS CFI (Accurate MERIS Ortho-Rectified Geo-location Operational Software) processing *Validation report (PO-RP-ACR-GS-0014) ACRI-ST*

Bourg, L., D'Alba, L., Colagrande, P., & Goryl, P. (2008). Technical note – MERIS Smile Effect Characterization and Correction. *ESA*

Bourgeau-Chavez, L., Harrel, P., Kasischke, E., & French, N. (1995). The detection and interpretation of Alaskan fire-disturbed boreal forest ecosystems using ERS-1 SAR imagery. In, *Proceedings IGARSS'95: Quantitative Remote Sensing for Science and Applications* (pp. 1246-1248). Firenze: IEEE Publications

Bowman, D.M.J.S., Balch, J.K., Artaxo, P., Bond, W.J., Carlson, J.M., Cochrane, M.A., D'Antonio, C.M., DeFries, R.S., Doyle, J.C., Harrison, S.P., Johnston, F.H., Keeley, J.E., Krawchuk, M.A., Kull, C.A., Marston, J.B., Moritz, M.A., Prentice, I.C., Roos, C., Scott, A., Swetnam, T., Van der Werf, G., & Pyne, S.J. (2009). Fire in the Earth system. *Science, 324*, 481-484

Brassel, K.E., & Reif, D. (1979). A procedure to generate Thiessen polygons. *Geographical Analysis, 11*, 289-303

Brivio, P.A., Maggi, M., Binaghi, I., Gallo, I., & J-M., G. (2002). Exploiting spatial and temporal information for extracting burned areas from time series of SPOT-VEGETATION data. *Analysis of Multi-temporal Remote Sensing Images, Joint Research Centre*

Caetano, M.S., Mertes, L.A.K., & Pereira, J.M.C. (1994). Using Spectral Mixture Analysis for Fire Severity Mapping. *Proceedigns of 2nd International Conference on Forest Fire Research* (pp. 667-677). Coimbra

Calle, A., Casanova, J.L., & Romo, A. (2006). Fire detection and monitoring using MSG Spinning Enhanced Visible and Infrared Imager (SEVIRI) data. *Journal of Geophysical Research - Biosciences, 111*, doi:10.1029/2005JG000116

Carmona-Moreno, C., Belward, A., Malingreau, J.P., Hartley, A., Garcia-Alegre, M., Antonovskiy, M., Buchshtaber, V., & Pivovarov, V. (2005). Characterizing interannual variations in global fire calendar using data from Earth observing satellites. *Global Change Biology, 11*, 1537-1555

Cisbani, E., Bartoloni, A., Marchese, E., Efisel, G., & Salvati, E. (2002). Early fire detection system based on multi-temporal images of geostationary and polar satellites. *Proceedings IGARSS Symposium, 3*

Clevers, J.G.P.W., De Jong, S.M., Epema, G.F., van der Meerb, F., Bakkerb, W., Skidmoreb, A., & Addink, E.A. (2001). MERIS and the red-edge position. *International Journal of Applied Earth Observation and Geoinformation, 3*

Congalton, R.G., & Green, K. (1999). *Assessing the Accuracy of Remotely Sensed Data: Principles and Applications*. Boca Raton: Lewis Publishers

Cope, M., & Chaloner, W. (1985). Wildfire: an interaction of biological and physical processes. . *Tiffnery BH, Geological factors and the evolution of plants*, 257-277

Costantini, M., Zavagli, M., Cisbani, E., & Greco, B. (2006). A technique for automatic fire detection from geostationary optical sensors and its validation on MSG SEVIR data. . *Proceedings IGARSS Symposium*, 4153-4156

Csiszar, I., Denis, L., Giglio, L., Justice, C.O., & Hewson, J. (2005). Global fire activity from two years of MODIS data. *International Journal of Wildland Fire, 14*, 117-130

Chandler, C., Cheney, P., Thomas, P., Trabaud, L., & Williams, D. (1983). *Fire in Forestry. Forest Fire behavior and effects*. Nueva York: John Wiley and Sons

Chang, D., & Song, Y. (2009). Comparison of L3JRC and MODIS global burned area products from 2000 to 2007. *Journal of Geophysical Research, 114*, 10.1029/2008JD11361

Christian, T.J., Kleiss, B., Yokelson, R.J., Holzinger, R., Crutzen, P.J., Hao, W.M., Saharjo, B.H., & Ward, D.E. (2003). Comprehensive laboratory measurements of biomass-burning emissions: 1. Emissions from Indonesian, African, and other fuels. *Journal Of Geophysical Research-Atmospheres, 108*

Chuvieco, E. (2014). Product Specifications Document. *ESA CCI ECV Fire Disturbance (fire_cci)*

Chuvieco, E., & Congalton, R.G. (1988). Using cluster analysis to improve the selection of training statistics in classifying remotely sensed data. *Photogrammetric Engineering & Remote Sensing, 54*, 1275-1281

Chuvieco, E., & Congalton, R.G. (1989). Application of remote sensing and Geographic Information Systems to Forest fire hazard mapping. *Remote Sensing of Environment, 29*, 147-159

Chuvieco, E., De Santis, A., Riaño, D., & Halligan, K. (2007). Simulation approaches for burn severity estimation using remotely sensed images. *Journal of Fire Ecology, 3*, 129-150

Chuvieco, E., Englefield, P., Trishchenko, A.P., & Luo, Y. (2008a). Generation of long time series of burn area maps of the boreal forest from NOAA–AVHRR composite data. *Remote Sensing of Environment, vol. 112*, 2381-2396

Chuvieco, E., Martín, M.P., & Palacios, A. (2002). Assessment of different spectral indices in the red-near-infrared spectral domain for burned land discrimination. *International Journal of Remote Sensing, 23*, 5103-5110

Chuvieco, E., Opazo, S., Sione, W., Del Valle, H., Anaya, J., Di Bella, C., Cruz, I., Manzo, L., López, G., Mari, N., González-Alonso, F., Morelli, F., Setzer, A., Csiszar, I., Kanpandegi, J.A., Bastarrika, A., & Libonati, R. (2008b). Global Burned Land

Estimation in Latin America using MODIS Composite Data. *Ecological Applications, 18*, 64-79
Chuvieco, E., Riaño, D., Danson, F.M., & Martín, M.P. (2006). Use of a radiative transfer model to simulate the post-fire spectral response to burn severity. *Journal of Geophysical Research - Biosciences, 111*, doi:10.1029/2005JG000143
Chuvieco, E., Ventura, G., Martín, M.P., & Gomez, I. (2005). Assessment of multitemporal compositing techniques of MODIS and AVHRR images for burned land mapping. *Remote Sensing of Environment, 94*, 450 – 462
Chuvieco, E., Y, C., Heil, A., Mouillot, F., Alonso-Canas, I., Padilla, M., Tansey, K., & Pereira, J.O., D (2015). A new global burned area product for climate assessment of fire impacts. *Global Ecology and Biogeography, under review*
Daniau A.L. et al (2012). Predictability of biomass burning in response to climate changes. *Global Biogeochemical Cycles, 26*
Davies, D., Ilavajhala, S., Wong, M., & Justice, C. (2009). Fire information for resource management system: archiving and distributing MODIS active fire data. *Geoscience and Remote Sensing, IEEE Transactions on, 47*, 72-79
Domenikiotis, C., Dalezios, N.R., Loukas, A., & Karteris, M. (2002). Agreement assessment of NOAA/AVHRR NDVI with Landsat TM NDVI for mapping burned forested areas. *International Journal of Remote Sensing, 23*, 4235-4246
Dozier, J. (1981). A method for satellite identification of surface temperature fields of subpixel resolution. *Remote Sensing of Environment, 11*, 221
Dragozi, E., Gitas, I., Stavrakoudis, D., & Theocharis, J. (2014). Burned Area Mapping Using Support Vector Machines and the FuzCoC Feature Selection Method on VHR IKONOS Imagery *Remote Sensing, 6*
Dubovik, O., Holben, B., Eck, T.F., Smirnov, A., Kaufman, Y.J., King, M.D., Tanre, D., & Slutsker, I. (2002). Variability of absorption an
d optical properties of key aerosol types observed in worldwide
locations. *Journal of Atmospheric Science, 59*
Duncan, B.N., Martin, R.V., Staudt, A.C., Yevich, R., & Logan, J.A. (2003). Interannual and seasonal variability of biomass burning emissions constrained by satellite observations. *Journal of Geophysical Research, 108*, doi: 10.1029/2002JD002378
EPA, U. (2008). Wildfire smoke: a guide for public health officials*., US Environmental Protection Agency*
EPA, U. (2009). Integrated science assessment for particulate matter (final report)*, US Environmental Protection Agency.*, EPA/600/R-608/139F
Ershov, D.V., & Novik, V.P. (2001). Mapping burned areas in Russia with SPOT4 VEGETATION (S1 product) imagery,. *Final report, Contract 18176-2001-07-F1EI ISP RU, Eur. Comm. Joint Res. Cent., Brussels.*
ESA (2006). *MERIS Product Handbook, European Space Agency, Issue 2.01,*
Eva, H., & Lambin, E.F. (1998). Burnt area mapping in Central Africa using ATSR data. *International Journal of Remote Sensing, 19*, 3473-3497
Eva, H.D., Belward, A.S., Grégoire, J.M., Moula, M., Brustet, J.M., Janodet, E., & N, V. (1995). The application of Along Track Scanning Radiometer to burnt area mapping in different savannah ecosystems in central Africa. In, *Proceedings of the 1995 Meteorological Satellite Data User's Conference* (pp. 201-208). Winchester
Fernández, A., Illera, P., & Casanova, J.L. (1997). Automatic mapping of surfaces affected by forest fires in Spain using AVHRR NDVI composite image data. *Remote Sensing of Environment, 60*, 153-162
fire_cci (2009). Fire Disturbance Annex K. *http://www.esa-fire-cci.org/*

França, H., & Setzer, A.W. (2001). AVHRR analysis of a savanna site through a fire season in Brazil. *International Journal of Remote Sensing, 22*, 2449-2461

Fraser, R.H., Fernandes, R., & Latifovic, R. (2003). Multi-temporal Mapping of Burned Forest over Canada Using Satellite-based Change Metrics. *Geocarto International, 18*, 37 - 47

Fraser, R.H., Hall, R.J., Landry, R., Lynham, T., Raymond, D., Lee, B., & Li, Z. (2004). Validation and calibration of Canada-wide coarse-resolution satellite burned-area maps. *Photogrammetric Engineering and Remote Sensing, 70*, 451-460

Fraser, R.H., & Li, Z. (2002). Estimating fire-related parameters in boreal forest using SPOT VEGETATION. *Remote Sensing of Environment, 82*, 95-110

Fraser, R.H., Li, Z., & Cihlar, J. (2000). Hotspot and NDVI Differencing Synergy (HANDS): a new technique for burned area mapping over boreal forest. *Remote Sensing of Environment, 74*, 362-376

Fredericksen, P., Langaas, S., & Mbaye, M. (1990). NOAA-AVHRR and GIS-BASED monitoring of fire activity in Senegal- a provisional methodology and potential applications. In J.G. Goldammer (Ed.), *Ecological Studies* (pp. 400-417). Berlin: Springer-Verlag

French, N., Kasischke, E., Bourgeau-Chavez, L.L., harrel, P.A., & Christensen, N.L. (1994). Relating soil water measurements at fire disturbed sites in Alaska to ERS-1 SAR image signature. *Proceedings IGARSS Symposium*, 246-248

Fuller, D.O., & Fulk, M. (2001). Burned area in Kalimantan, Indonesia mapped with NOAA-AVHRR and Landsat TM imagery. *International Journal of Remote Sensing, 22*, 691-697

Gao, B.C. (1996). NDWI. A normalized difference water index for remote sensing of vegetation liquid water from space. *Remote Sensing of Environment, 58*, 257-266

García-Haro, F.J., Gilabert, M.A., & Meliá, J. (2001). Monitoring fire-affected areas using Thematic Mapper data. *International Journal of Remote Sensing, 22*, 533-549

GCOS (2006). Systematic observation requirements for satellite based products for Climate *Supplemental details to the satellite based component of the implementation plan for the Global Observing System for Climate in Support of the UNFCCC. GCOS-1'7 (WMO/TD No.1338)*

George, C., Rowland, C., Gerard, F., & Baltzer, H. (2006). Retrospective mapping of burnt areas in Central Siberia using a modification of the normalised difference water index. *Remote Sensing of Environment, 104*, 346-359

Gerard, F., Plummer, S., Wadsworth, R., Sanfeliu, A.F., & Iliffe, L. (2003). Forest Scar detection in the Boreal Forest with multi-temporal SPOT-VEGETATION data. *IEEE Transac-tions on Geoscience and Remote Sensing, 41*, 2575-2585

Giglio, L. (2005). MODIS Collection 4 Active Fire Product User's Guide. Version 2.2. In. Colle Park: University of Maryland

Giglio, L. (2010). *MODIS Collection 5 Active Fire Product User's Guide, Version 2.4*. http://modis-fire.umd.edu/Documents/MODIS_Fire_Users_Guide_2.4.pdf

Giglio, L., Csiszar, I., & Justice, C.O. (2006a). Global distribution and seasonality of active fires as observed with the Terra and Aqua Moderate Resolution Imaging Spectroradiometer (MODIS) sensors. *Journal of Geophysical Research-Biogeosciences, 111*, doi:10.1029/2005JG000142

Giglio, L., Descloitres, J., Justice, C.O., & Kaufman, Y.J. (2003a). An Enhanced Contextual Fire Detection Algorithm for MODIS. *Remote Sensing of Environment, 87*, 273-282

Giglio, L., Kendall, J.D., & Mack, R. (2003b). A multi-year active fire dataset for the tropics derived from the TRMM VIRS. *International Journal of Remote Sensing, 24*, 4505-4525

Giglio, L., Loboda, T., Roy, D.P., Quayle, B., & Justice, C.O. (2009). An active-fire based burned area mapping algorithm for the MODIS sensor. *Remote Sensing of Environment, 113*, 408-420

Giglio, L., Randerson, J.T., & van der Werf, G. (2013). Analysis of daily, monthly, and annual burned area using the fourth-generation global fire emissions database (GFED4). *Journal of Geophysical Research: biogeosciences, 118*, 317–328

Giglio, L., Randerson, J.T., van der Werf, G.R., Kasibhatla, P.S., Collatz, G.J., Morton, D.C., & DeFries, R.S. (2010). Assessing variability and long-term trends in burned area by merging multiple satellite fire products. *Biogeosciences Discuss., 7*, 1171-1186, doi:1110.5194/bg-1177-1171-2010,

Giglio, L., van der Werf, G.R., Randerson, J.T., Collatz, G.J., & Kasibhatla, P. (2006b). Global estimation of burned area using MODIS active fire observations. *Atmospheric Chemistry and Physics, 6*, 957-974

Gitas, I.Z., Mitri, G.H., & Ventura, G. (2004). Object-based image classification for burned area mapping of Creus Cape, Spain, using NOAA-AVHRR imagery. *Remote Sensing of Environment, 92*, 409-413

Gong, P., Pu, R.L., Li, Z.Q., Scarborough, J., Clinton, N., & Levien, L.M. (2006). An integrated approach to wildland fire mapping of California, USA using NOAA/AVHRR data. *Photogrammetric Engineering and Remote Sensing, 72*, 139-150

Gonzalez-Alonso, F., Merino-De-Miguel, S., Roldan-Zamarron, A., Garcia-Gigorro, S., & Cuevas, J.M. (2007). MERIS Full Resolution data for mapping level-of-damage caused by forest fires: the Valencia de Alcantara event in August 2003. *International Journal of Remote Sensing, 28*, 797-809

González-Alonso, F., Salgado, V., Calle, V., Casanova, J.L., Sanz, J., de la Fuente, D., Goldammer, J.G., Li, Z., Qin, X., Zhang, X., Deng, G., Liu, Q., Li, G., Cai, H., & Huang, Z. (2009). Forest burn in China by means of MERIS and MODIS images. . *Dragon 2 Symposium, June 2009, Barcelona.*

Gower, J.F.R., & Borstad, G.A. (2004). On the potential of MODIS and MERIS for imaging chlorophyll fluorescence from space. *International Journal of Remote Sensing, 25*, 1459-1464

Grégoire, J.M. (1993). Use of AVHRR data for the study of vegetation fires in Africa: Fire management perspectives. In. Ispra, Italy: Commission of the European Communities. Joint Research Centre

Gregoire, J.M., Tansey, K., & Silva, J.M.N. (2003). The GBA2000 initiative: developing a global burnt area database from SPOT-VEGETATION imagery. *International Journal of Remote Sensing, 24*, 1369-1376

Grégoire, J.M., Tansey, K., & Silva, J.M.N. (2003). The GBA2000 initiative: Developing a global burned area database from SPOT-VEGETATION imagery. *International Journal of Remote Sensing, 24*, 1369 - 1376

Hantson, S., Padilla, M., Corti, D., & Chuvieco, E. (2013). Strengths and weaknesses of MODIS hotspots to characterize global fire occurrence. *Remote Sensing of Environment, 131*, 152-159

Hicke, J.A., Allen, C.D., Desai, A.R., Dietze, M.C., Hall, R.J., Kashian, D.M., Moore, D., Raffa, K.F., Sturrock, R.N., & Vogelmann, J. (2012). Effects of biotic disturbances on forest carbon cycling in the United States and Canada. *Global Change Biology, 18*, 7-34

Hoelzemann, J.J., Schultz, M.G., Brasseur, G.P., Granier, C., & Simon, M. (2004). Global Wildland Fire Emission Model (GWEM): Evaluating the use of global area burnt satellite data. *Journal of Geophysical Research, 109*, D14S04, doi:10.1029/2003JD003666

Hollmann, R., Merchant, C.J., Saunders, R.W., Downy, C., Buchwitz, M., Cazenave, A., Chuvieco, E., Defourny, P., Leeuw, G.d., Forsberg, R., Holzer-Popp, T., & Paul, F. (2013). The ESA Climate Change Initiative: satellite data records for essential climate variables. *Bulletin of the American Meteorological Society, doi 10.1175/BAMS-D-11-00254.1*

Huang, S., & Siegert, F. (2004). ENVISAT multisensor data for fire monitoring and impact assessment. *International Journal of Remote Sensing, 25*, 4411-4416

Huemmrich, K.F. (2001). The GeoSail model: a simple addition to the SAIL model to describe discontinuous canopy reflectance. *Remote Sensing of Environment, 75*, 423-431

Huete, A.R. (1988). A soil-adjusted vegetation index (SAVI). *Remote Sensing of Environment, 25*, 295-309

Hunt, E.R., & Rock, B.N. (1989). Detection of changes in leaf water content using near and middle-infrared reflectances. *Remote Sensing of Environment, 30*, 43-54

Ito, A., & Penner, J.E. (2004). Global estimates of biomass burning emissions based on satellite imagery for the year 2000. *Journal Of Geophysical Research-Atmospheres, 109*

Jacquemoud, S. (1990). PROSPECT: a model to leaf optical properties spectra. *Remote Sensing of Environment, 34*, 74-91

Jacquemoud, S., Verhoef, W., Baret, F., Bacour, C., Zarco-Tejada, P., Asner, G., François, C., & Ustin, S. (2009). PROSPECT + SAIL Models: A Review of Use for Vegetation Characterization. *Remote Sensing of Environment, 113, Supplement 1*, S56-S66

Jain, A.K., Tao, Z.N., Yang, X.J., & Gillespie, C. (2006). Estimates of global biomass burning emissions for reactive greenhouse gases (CO, NMHCs, and NOx) and CO2. *Journal of Geophysical Research: atmospheres, 111*

Jasinski, M.F., & Eagleson, P.S. (1990). Estimation of subpixel vegetation cover using red-infrared scattergrams. *IEEE Transactions on Geoscience and Remote Sensing, 28*, 253-267

Jensen, J.R. (2005). Digital change detection. Introductory Digital Image Processing, A Remote Sensing perspective. *Pearson Prentice Hall, New York*, 467–494.

Justice, C., Giglio, L., Boschetti, L., Roy, D., Csiszar, I., Morisette, J., & Kaufman, Y.J. (2006). Algorithm Theoretical Basis Document MODIS FIRE products

Kachmar, M., & Sanchez-Azofeifa, G.A. (2006). Detection of post-fire residuals using high- and medium-resolution satellite imagery. *Forestry Chronicle, 82*, 177-186

Kailath, T. (1967). The Divergence and Bhattacharyya Distance Measures in Signal Selection. *IEEE Trasnactions on Communication Technology, 15*, 52-60

Kamdi, S., & Krishna, R.K. (2012). Image segmentation and region growing algorithm. *International Journal of Computer Technology and Electronics Engineering, 2*

Kasischke, E., & French, N.H. (1995). Locating and estimating the areal extent of wildfires in Alaskan boreal forest using multiple-season AVHRR NDVI composite data. *Remote Sensing of Environment, 51*, 263-275

Kasischke, E.S., Bourgeau-Chavez, L.L., & French, N.H.F. (1994). Observations of variations in ERS-1 SAR image intensity associated with forest fires in Alaska. *IEEE Transactions on Geoscience and Remote Sensing, 32*, 206-210

Kasischke, E.S., Bourgeau-Chavez, L.L., French, N.H.F., Harrel, P., & Christensen, N.L. (1992). Initial observations on using SAR to monitor wildfire scars in boreal forest. *International Journal of Remote Sensing, 13*, 3495-3501

Kasischke, E.S., French, N.H.F., Bourgeauchavez, L.L., & Christensen, N.L. (1995). Estimating Release of Carbon From 1990 and 1991 Forest Fires in Alaska. *Journal Of Geophysical Research-Atmospheres, 100*, 2941-2951

Kasischke, E.S., French, N.H.F., Harrell, P., Christensen, N.L., Ustin, S.L., & Barry, D. (1993). Monitoring of wildfires in Boreal Forests using large area AVHRR NDVI composite image data. *Remote Sensing of Environment, 45*, 61-71

Kaufman, Y.J., & Justice, C.O. (1998). MODIS Fire products. In (p. 77 pp): NASA

Kaufman, Y.J., Martins, J.V., Remer, L.A., Schoebrel, M.R., & Yamasoe, M.A. (2002). Satellite retrieval of aerosol absorption over the sunglint. *Geophysical Research Letters, 29*

Kaufman, Y.J., & Remer, L.A. (1994). Detection of forests using Mid-IR reflectance: an application for aerosol studies. *IEEE Transactions on Geoscience and Remote Sensing, 32*, 672-683

Key, C., & Benson, N. (1999). The Normalized Burned Ratio, a Landsat TM radiometric index of burn severity incorporating multi-temporal differencing. In: U.S. Geological Survey

Kirches, G., Krueger, O., Boettcher, M., Bontemps, S., & Defourny, P. (2013). Algorithm Theoretical Basis Document - Land Cover CCI, Version 2

Kloster, S., Mahowald, N., Randerson, J., & Lawrence, P. (2012). The impacts of climate, land use, and demography on fires during the 21st century simulated by CLM-CN. *Biogeosciences, 9*, 509-525

Kloster, S., Mahowald, N., Randerson, J., Thornton, P.E., Hoffman, F., Levis, S., Lawrence, P., Feddema, J., Oleson, K., & Lawrence, D. (2010). Fire dynamics during the 20th century simulated by the Community Land Model. *Biogeosciences Discuss., 7*, 1877-1902

Kneppeck, I.D., & Ahern, F.J. (1989). Stratification of a regenerating burned forest in Alberta using Thematic Mapper and C-SAR images. *Proceedings IGARSS Symposium*, 1391-1396

Koutsias, N., & Karteris, M. (1998). Logistic regression modelling of multitemporal Thematic Mapper data for burned area mapping. *International Journal of Remote Sensing, 19*, 3499-3514

Koutsias, N., & Karteris, M. (2000). Burned area mapping using logistic regression modeling of a single post-fire Landsat-5 Thematic Mapper image. *International Journal of Remote Sensing, 21*, 673-687

Krawchuk, M.A., Moritz, M.A., Parisien, M.-A., Van Dorn, J., & Hayhoe, K. (2009). Global Pyrogeography: the Current and Future Distribution of Wildfire. *PLoS ONE, 4*, e5102

Kucêra, J., Yasuoka, Y., & Dye, D.G. (2005). Creating a forest fire database for the Far East of Asia using NOAA/AVHRR observation. *International Journal of Remote Sensing, 26*, 2423-2439

Landry, R., Ahern, F., & O'Neil, R. (1995). Forest burn visibility on C-HH radar images. *Canadian Journal of Remote Sensing, 21*, 204-206

Lasaponara, R. (2005). Inter-comparison of AVHRR-based fire susceptibility indicators for the Mediterranean ecosystems of southern Italy. *International Journal of Remote Sensing, 26*, 853-870

Le Page, Y., Pereira, J., Trigo, R., Da Camara, C., Oom, D., & Mota, B. (2007). Global fire activity patterns (1996–2006) and climatic influence: an analysis using the World Fire Atlas. *Atmospheric Chemistry and Physics Discussions, 7*, 17299-17338

Li, Z., Nadon, S., & Cihlar, J. (2000). Satellite-based detection of Canadian boreal forest fires: development and application of the algorithm. *International Journal of Remote Sensing, 21*, 3057-3069

Libonati, R., DaCamara C., Setzera A., Morellia F., de Jesusa S., Candido P., & A., M. (2014). Chapter 6 – Forest Management:Validation of the burned area "(V,W)" Modis algorithm in Brazil". *Advances in forest fire research.*

Lobert, J.M., & Warnatz, J. (1993). Emissions from the combustion process in vegetation. Fire in the Environment: the ecological, Atmospheric and Climate importance of vegetation fires. *Environmental Science Research, 13*, 15-39

Loboda, T., O'Neal,K.J., Csiszar,I. (2007). Regionally adaptable dNBR-based algorithm for burned area mapping from MODIS data. *Remote Sensing of Environment, 109*, 429-442

López-Saldaña, G., Bistinas, I., & Pereira, J. (2015). Global analysis of radiative forcing from fire- induced shortwave albedo change. . *Biogeosciences, 11*, 7775-7796

López García, M.J., & Caselles, V. (1991). Mapping Burns and Natural Reforestation Using Thematic Mapper Data. *Geocarto International, 1*, 31-37

Lu, D., Mausel, P., Brondizio, E., & Moran, E. (2004). Change detection techniques. *International Journal of Remote Sensing, 25*, 2365–2407

Malingreau, J.P., & Belward, A.S. (1989). Vegetation monitoring using AVHRR data at different resolutions. In, *4th NOAA-AVHRR data users meeting* (pp. 141-144)

Malingreau, J.P., & Duchossois, G. (1995). The TREES/ERS-1 SAR'94 Project. *Earth Observation Quartely, 48*, 1-5

Malingreau, J.P., Stevens, G., & Fellows, L. (1985). Remote sensing of forest fires: Kalimantan and North Borneo in 1982-83. *Ambio, 14*, 314-321

Martín, M.P., Ceccato, P., Flasse, S., & Downey, I. (1999). Fire detection and fire growth monitoring using satellite data. In E. Chuvieco (Ed.), *Remote Sensing of Large Wildfires in the European Mediterranean Basin* (pp. 101-122). Berlin: Springer-Verlag

Martín, M.P., & Chuvieco, E. (1993). Mapping and evaluation of burned land from multitemporal analysis of AVHRR NDVI images. In P.J. Kennedy, & M. Karteris (Eds.), *International Workshop: Satellite Technology and GIS for Mediterranean forest mapping and fire management* (pp. 71-83). Thessaloniki, Greece

Martín, M.P., & Chuvieco, E. (1995). Mapping and evaluation of burned land from multitemporal analysis of AVHRR NDVI images. *EARSeL Advances in Remote Sensing, 4 (3)*, 7-13

Martín, M.P., & Chuvieco, E. (2001). Propuesta de un nuevo índice para cartografía de áreas quemadas: aplicación a imágenes NOAA-AVHRR y Landsat-TM. *Revista de Teledetección, 16*, 57-64

Martín, M.P., Domínguez, L., & Chuvieco, E. (1995). Estimating forest fire danger from AVHRR data. In J. Askne (Ed.), *Sensors and Environmental Applications of Remote Sensing* (pp. 371-376). Rotterdam: A.A. Balkema

Martín, M.P., Gómez, I., & Chuvieco, E. (2005). Performance of a burned-area index (BAIM) for mapping Mediterranean burned scars from MODIS data. In J. Riva, F. Pérez-Cabello, & E. Chuvieco (Eds.), *Proceedings of the 5th International Workshop on Remote Sensing and GIS applications to Forest Fire Management: Fire Effects Assessment* (pp. 193-198). Paris: Universidad de Zaragoza, GOFC-GOLD, EARSeL

Matson, M., & Dozier, J. (1981). Identification of subresolution high temperature sources using a thermal IR sensor. *Photogrammetric Engineering and Remote Sensing, 47*, 1311-1318

Mitri, G.H., & Gitas, I. (2002). The development of an object-oriented classification model for operational burned area mapping on the Mediterranean islando of Thasos using Landsat TM images. . *Forest fire research and wildland fire safety, Millpress*, 79

Mota, B., Pereira, J., Oom, D., Vasconcelos, M.J.P., & Schultz, M. (2006). Screening the ESA ATSR-2 World Fire Atlas (1997-2002). *Atmospheric Chemistry and Physics, 6*, 1409-1424

Mouillot, F., & Field, C.B. (2005). Fire history and the global carbon budget: a 1 degrees x 1 degrees fire history reconstruction for the 20th century. *Global Change Biology, 11*, 398-420

Mouillot, F., Schultz, M.G., Yue, C., Cadule, P., Tansey, K., Ciais, P., & Chuvieco, E. (2014). Ten years of global burned area products from spaceborne remote sensing - A review: Analysis of user needs and recommendations for future developments. *International Journal of Applied Earth Observation and Geoinformation, 26*, 64-79

Muller, J.P. et al. (2011), The ESA GlobAlbedo Project for mapping the Earth's land surface albedo for 15 years from European sensors, EGU, *Geophysical Research Abstracts*, Vol.13. EGU2011-10969.

Nielsen, T.T., Mbow, C., & Kane, R. (2002). A statistical methodology for burned area estimation using multitemporal AVHRR data. *International Journal of Remote Sensing, 23*, 1181-1196

Oliva, P., Martin, P., & Chuvieco, E. (2011). Burned area mapping with MERIS post-fire image. *International Journal of Remote Sensing, 32*, 4175-4201

Olson, D.M., E. Dinerstein, E.D. Wikramanayake, N.D. Burgess, G.V.N. Powell, E.C. Underwood, J.A. D'amico, I. Itoua, H.E. Strand, J.C. Morrison, C.J. Loucks, T.F. Allnutt, T.H. Ricketts, Y. Kura, J.F. Lamoreux, W.W.Wettengel, P. Hedao, & K.R. Kassem (2001). Terrestrial Ecoregions of the World: A New Map of Life on Earth. *BioScience, 51*, 933-938

Padilla, M., Stehman, S.V., & Chuvieco, E. (2014). Validation of the 2008 MODIS-MCD45 global burned area product using stratified random sampling. *Remote Sensing of Environment, 144*, 187-196

Padilla, M., V. Stehman S., Hantson S., Oliva P., Alonso-Canas I., Bradley A., Tansey K., Mota B., Pereira JM, & E., C. (2015). Comparing the Accuracy of Global Burned Area Products using Stratified Random Sampling. *Remote Sensing of Environment, 120*, 114-121

Paganini, M., Arino, O., Benvenuti, M., Cristaldi, M., Bordin, M., Coretti, C., & Musone, A. (2003). ITALSCAR, a regional burned forest mapping demonstration project in Italy. *Proceedings IGARSS Symposium, 2*, 1290-1292

Pechony, O., & Shindell, D. (2010). Driving forces of global wildfires over the past millennium and the forthcoming century. *Proceedings of the National Academy of Sciences, 107*, 19167–19170

Pereira, J., Mota, B., Oom, D., Calado, T., Alonso-Canas, I., P., O., & Gonzalez-Alonso, F. (2014). Algorithm Theoretical Basis Document - Volume 2 - BA algorithm development. *Fire_cci_Ph3_ISA_D3_6_2_ATBD_II_v2_2*

Pereira, J.M.C. (1999). A Comparative Evaluation of NOAA/AVHRR Vegetation Indexes for Burned Surface Detection and Mapping. *IEEE Transactions on Geoscience and Remote Sensing, 37*, 217-226

Pereira, J.M.C., Sa, A.C.L., Sousa, A.M.O., Martín, M.P., & Chuvieco, E. (1999a). Regional-scale burnt area mapping in Southern Europe using NOAA-AVHRR 1 km data. In E. Chuvieco (Ed.), *Remote Sensing of Large Wildfires in the European Mediterranean Basin* (pp. 139-155). Berlin: Springer-Verlag

Pereira, J.M.C., Sa, A.C.L., Sousa, A.M.O., Silva, J.M.N., Santos, T.N., & Carreiras, J.M.B. (1999b). Spectral characterisation and discrimination of burnt areas. In E. Chuvieco (Ed.), *Remote Sensing of Large Wildfires in the European Mediterranean Basin* (pp. 123-138). Berlin: Springer-Verlag

Pereira, M.C., & Setzer, A.W. (1993a). Spectral characteristics of deforestation fires in NOAA-AVHRR images. *International Journal of Remote Sensing, 14*, 583-597

Pereira, M.C., & Setzer, A.W. (1993b). Spectral characteristics of fire scars in Landsat-5 TM images of Amazonia. *International Journal of Remote Sensing, 14*, 2061-2078

Piccolini, I., & Arino, O. (2000). Towards a Global Burned Surface World Atlas. *Earth Observation Quartely, 65*, 14-18

Pinty, B., & Verstraete, M.M. (1992). GEMI: a non-linear index to monitor global vegetation from satellites. *Vegetatio, 101*, 15-20

Pleniou, M., & Koutsias, N. (2013). Sensitivity of spectral reflectance values to different burn and vegetation ratios: A multi-scale approach applied in a fire affected area. *ISPRS Journal of Photogrammetry and Remote Sensing, 69*, 199-210

Plummer, S., Arino, O., Ranera, F., Tansey, K., Chen, J., Dedieu, G., Eva, H., Piccolini, I., Leigh, R., & Borstlap, G. (2007). An update on the GlobCarbon initiative: multi-sensor estimation of global biophysical products for global terrestrial carbon studies. In, *Envisat Symposium*. Montreux, Switzerland: ESA SP-636

Polychronaki, A., & Gitas, I. (2010). The development of an operational procedure for burned area mapping using object based classification and ASTER imagery. . *International Journal of Remote Sensing, 31*, 1113-1120

Ponzoni, F.J., Lee, D.C.L., & Filho, P.H. (1986). Assessment of area burnt and vegetation recovery at Brasilia National Park, using Landsat TM data. In, *IV Simpósio Brasileiro de Sensoriamento Remoto,* (pp. 615-621). São José dos Campos: INPE

Price, C. (2009). Will a drier climate result in more lightning? *Atmospheric Research, 91*, 479–484

Prins, E.M., Feltz, J.M., Menzel, W.P., & Ward, D.E. (1998). An overview of GOES-8 diurnal fire and smoke results for SCAR-B and 1995 fire season in South America. *Journal of Geophysical Research, 103*, 31821-31836

Prins, E.M., & Menzel, W.P. (1992). Geostationary satellite detection of biomass burning in South America. *International Journal of Remote Sensing, 13*, 2783-2799

Pu, R., & Gong, P. (2004). Determination of Burnt Scars Using Logistic Regression and Neural Network Techniques from a Single Post-Fire Landsat-7 ETM+ Image. *Photogrammetric Engineering and Remote Sensing, 70*, 841-850

Pu, R.L., Li, Z.Q., Gong, P., Csiszar, I., Fraser, R., Hao , W.-M., Kondragunta, S., & Weng, F. (2007). Development and analysis of a 12-year daily 1-km forest fire North America from NOAA/AVHRR data. *Remote Sensing of Environment, 108*, 198-208

Quintano, C., Fernández-Manso, A., Fernández-Manso, O., & Shimabukuro, Y.E. (2006). Mapping burned areas in Mediterranean countries using spectral mixture analysis from a uni-temporal perspective. *International Journal of Remote Sensing, 27*

Ramo, R., Heil, A., & Chuvieco, E. (2014). Product Intercomparison Report *Fire_cci_Ph3_UAH_D4_1_3_PIR_v1_4*

Randerson, J., T., M., C.J., Werf, V.d.G.R., Rogers, B.M., & Morton, D.C. (2012). Global burned area and biomass burning emissions from small fires. *Journal of Geophysical Research: biogeosciences, 117*

Randerson, J.T., Liu, H., Flanner, M.G., Chambers, S.D., Jin, Y., Hess, P.G., Pfister, G., Mack, M.C., Treseder, K.K., Welp, L.R., Chapin, F.S., Harden, J.W., Goulden, M.L., Lyons, E., Neff, J.C., Schuur, E.A.G., & Zender, C.S. (2006). The impact of boreal forest fire on climate warming. *Science, 314*, 1130-1132

Randerson, J.T., van der Werf, G.R., Collatz, G.J., Giglio, L., Still, C.J., Kasibhatla, P., Miller, J.B., White, J.W.C., DeFries, R.S., & Kasischke, E.S. (2005). Fire emissions from C3 and C 4 vegetation and their influence on interannual variability of atmospheric CO2 and D13 CO2. *Global Biogeochemical Cycles, 19*, doi:10.1029/2004GB002366

Rast, M., Bezy, J.L., & Bruzzi, S. (1999). The ESA Medium Resolution Imaging Spectrometer MERIS - a review of the instrument and its mission. *International Journal of Remote Sensing, 20*, 1681-1702

Razafimpanilo, H., Frouin, R., Iaocobellis, S.F., & Somerville, R.C. (1995). Methodology for estimating burned area from AVHRR reflectance data. *Remote Sensing of Environment, 54*, 273-289

Riaño, D., Ruiz, J.A.M., Isidoro, D., Ustin, S.L., & Riaño, D. (2007). Global spatial patterns and temporal trends of burned area between 1981 and 2000 using NOAA-NASA Pathfinder. *Global Change Biology, 13*, 40-50, doi: 10.1111/j.1365-2486.2006.01268.

Richter, R. (1997). Correction of atmospheric and topographic effects for high spatial resolution satellite imagery. *International Journal of Remote Sensing, 18*, 1099-1111

Riggan, P., Franklin, S., Brass, J., & Brooks, F. (1994). Perspectives on fire management in Mediterranean ecosystems of southern California. In M. JM, & O. WC (Eds.), *The Role of Fire in Mediterranean-Type Ecosystems.* (pp. 140-162). New York: Springer-Verlag

Roberts, G., Wooster, M.J., Perry, G.L.W., Drake, N., Rebelo, L.M., & Dipotso, F. (2005). Retrieval of biomass combustion rates and totals from fire radiative power observations: Application to southern Africa using geostationary SEVIRI imagery. *Journal of Geophysical Research, 110*, D21111, doi:21110.21029/22005JD006018

Robinson, J.M. (1991). Fire from space: global fire evaluation using infrared remote sensing. *International Journal of Remote Sensing, 12*, 3-24

Roldan-Zamarron, A., Merino-De-Miguel, S., Gonzalez-Alonso, F., Garcia-Gigorro, S., & Cuevas, J.M. (2006). Minas de Riotinto (south Spain) forest fire: Burned area assessment and fire severity mapping using Landsat 5-TM, Envisat-MERIS, and Terra-MODIS postfire images. *Journal of Geophysical Research-Biogeosciences, 111*

Rouse, J.W., Haas, R.W., Schell, J.A., Deering, D.H., & Harlan, J.C. (1974). Monitoring the vernal advancement and retrogradation (Greenwave effect) of natural vegetation. In. Greenbelt, MD. USA: NASA/GSFC

Roy, D., Jin, Y., Lewis, P., & Justice, C. (2005). Prototyping a global algorithm for systematic fire-affected area mapping using MODIS time series data. *Remote Sensing of Environment, 97*, 137-162

Roy, D., & Landmann, T. (2005). Characterizing the surface heterogeneity of fire effects using multi-temporal reflective wavelength data. *International Journal of Remote Sensing, 26*, 4197-4218

Roy, D., Lewis, P.E., & Justice, C.O. (2002). Burned area mapping using multi-temporal moderate spatial resolution data—a bi-directional reflectance model-based expectation approach. *Remote Sensing of Environment, 83*, 263-286

Roy, D.P., & Boschetti, L. (2009). Southern Africa Validation of the MODIS, L3JRC and GlobCarbon Burned-Area Products. *IEEE Transactions on Geoscience and Remote Sensing, 47*, DOI 10.1109/TGRS.2008.2009000

Roy, D.P., Boschetti, L., & Justice, C.O. (2008). The collection 5 MODIS burned area product — Global evaluation by comparison with the MODIS active fire product. *Remote Sensing of Environment, 112*, 3690-3707

Roy, D.P., Giglio, L., Kendall, J.D., & Justice, C.O. (1999). Multi-temporal active-fire based burn scar detection algorithm. *International Journal of Remote Sensing, 20*, 1031-1038

Running, S.W. (2006). Is global warming causing more, larger wildfires? *Science, 313*, 927-928

Sapkota, A., Symons, J.M., Kleissl, J., Wang, L., Parlange, M., Ondov, J., Breysse, P., Diette, G., Eggleston, P., & Buckley, T. (2005). Impact of the 2002 Canadian forest fires on particulate matter air quality in Baltimore City. *Environmental Science and Technology, 39*, 24-32

Scott, A.C., & Glasspool, I.J. (2006). The diversification of Paleozoic fire systems and fluctuations in atmospheric oxygen concentration. *Proceedings of the National Academy of Sciences, U.S.A. 103*

Scheidt, S., Ramsey, M., & Lancaster, N. (2008). Radiometric normalization and image mosaic generation of ASTER thermal infrared data: an application to extensive sand sheets and dune fields. *Remote Sensing of Environment, 112*, 920–933

Schroeder, W., P., O., Giglio, L., & Csiszar, I. (2014). The new VIIRS 375m active fire detection data product: algorithm description and initial assessment. *Remote Sensing of Environment, 143*, 85-96

Schultz, M., Mouillot, F., Chao, Y., Cadule, P., & Ciais, P. (2011). User Requirements Document. *ESA CCI ECV Fire Disturbance (fire_cci)*

Seiler, W., & Crutzen, P.J. (1980). Estimates of gross and net fluxes of carbon between the biosphere and the atmosphere from biomass burning. *Climatic Change, 2*, 207-247

Shimabukuro, Y.E., Miettinen, J., Beuchle, R., Grecchi, R.C., Simonetti, D., & Achard, F. (2015). Estimating Burned Area in Mato Grosso, Brazil, Using an Object-Based Classification Method on a Systematic Sample of Medium Resolution Satellite Images *IEEE Journal of selected topics in applied earth observations and remote sensing*

Shrivakshan, G.T. (2012). A Comparison of various Edge Detection Techniques used in Image Processing. *International Journal of Computer Science Issues, 9*

Silva, J., Sá, A., & Pereira, J.M.C. (2005). Comparison of burned area estimation derived from SPOT-VEGETATION and Landsat ETM+ data in Africa: Influencia de spatial pattern and vegetation type. *Remote Sensing of Environment, 96*, 188-201

Silva, J.M.N., Cadima, J.F.C.L., Pereira, J.M.C., & Gregoire, J.M. (2004). Assessing the feasibility of a global model for multi-temporal burned area mapping using SPOT-VEGETATION data. *International Journal of Remote Sensing, 25*, 4889-4913

Silva, J.M.N., Pereira, J.M.C., Cabral, A.I., Sa, A.C.L., Vasconcelos, M.J.P., Mota, B., & Gregoire, J.M. (2003). An estimate of the area burned in southern Africa during the 2000 dry season using SPOT-VEGETATION satellite data. *Journal Of Geophysical Research-Atmospheres, 108*

Silva, J.M.N., Sousa, A.M.O., Pereira, J.M.C., Tansey, K., & J-M., G. (2002). A contribution for a global burned area map. In D.X. Viegas (Ed.), *IV International Conference on Forest Fire Research. 2002 Wildland Fire Safety Summit* (p. 13). Luso, Coimbra, Portugal: Millpress

Simon, M., Plummer, S., Fierens, F., Hoelzemann, J.J., & Arino, O. (2004). Burnt area detection at global scale using ATSR-2: The GLOBSCAR products and their qualification. *Journal of Geophysical Research - Atmospheres, 109, D14S02, doi:10.1029/2002JD003622*, 1-16

Soja, A.J., Sukhinin, A.I., Cahoon, D.R., Shugart, H.H., & Stackhouse, P.W. (2004). AVHRR-derived fire frequency, distribution and area burned in Siberia. *International Journal of Remote Sensing, 25*, 1939-1960

Sousa, A.M.O., Pereira, J.M.C., & Silva, J.M.N. (2003). Evaluating the performance of multitemporal image compositing algorithms for burned area analysis. *International Journal of Remote Sensing, 24*, 1219–1236

Souza, C.M., Roberts, D.A., & Cochrane, M.A. (2005). Combining spectral and spatial information to map canopy damage from selective logging and forest fires. *Remote Sensing of Environment, 98*, 329-343

Stewart, O.C. (1956). Fire as a first great force employed by man. *Thomas WI, 8th edition Man's role in changing the face of the earth*, 115-133

Stohl, A., Berg, T., Burkhart, J.F., Fjaeraa, A.M., Forster, C., Herber, A., Hov, O., Lunder, C., McMillan, W.W., Oltmans, S., Shiobara, M., Simpson, D., Solberg, S., Stebel, K., Strom, J., Torseth, K., Treffeisen, R., Virkkunen, K., Yttri, K.E., & (2007). Arctic smoke - record high pollution levels in the European Arctic due to agriculturar fires in Eastern Europe in spring 2006. *Atmospheric Chemistry and Physics, 7*, 511-534

Stroppiana, D., Grégoire, J.M., & Pereira, J.M.C. (2003). The use of SPOT VEGETATION data in a classification tree approach for burnt area mapping in Australian savanna. *International Journal of Remote Sensing, 24*, 2131-2151

Stroppiana, D., Pinnock, S., Pereira, J.M.C., & Grégorie, J.M. (2002). Radiometric analysis of SPOT-VEGETATION images for burnt area detection in Northern Australia. *Remote Sensing of Environment, 82*, 21-37

Sukhinin, A.I., French, N.H.F., Kasischke, E.S., Hewson, J.H., Soja, A.J., Csiszar, I.A., Hyer, E.J., Loboda, T., Conrad, S.G., Romasko, V.I., Pavlichenko, E.A., Miskiv, S.I., & Slinkina, O.A. (2004). AVHRR-based mapping of fires in Russia: New products for fire management and carbon cycle studies. *Remote Sensing of Environment, 93*, 546-564

Tanaka, S., Kimura, H., & Suga, Y. (1983). Preparation of a 1:25.000 Landsat map for assessment of burnt area on Etajima Island. *International Journal of Remote Sensing, 4*, 17-31

Tanase, M.A., Santoro, M., de la Riva, J., F, P.r.-C., & Le Toan, T. (2010). Sensitivity of X-, C-, and L-band SAR backscatter to burn severity in Mediterranean pine forests. *Geoscience and Remote Sensing, IEEE Transactions on, 48*, 3663-3675

Tansey, K. (2002). Implementation of the regional burnt area algorithms for the GBA-2000 initiative. *European Commission, Brussels Publ EUR 20532 EN*

Tansey, K., Grégoire, J.M., Defourny, P., Leigh, R., Peckel, J.F., Bogaert, E.V., & Bartholome, J.E. (2008). A new, global, multi-annual (2000–2007) burnt area product at 1 km resolution. *Geophysical Research Letters, 35, L01401, doi:10.1029/2007GL03156*

Tansey, K., Grégoire, J.M., Stroppiana, D., Sousa, A., Silva, J., Pereira, J.M., Boschetti, L., Maggi, M., Brivio, P.A., Fraser, R., Flasse, S., Ershov, D., Binaghi, E., Graetz, D., & Peduzzi, P. (2004). Vegetation burning in the year 2000: Global burned area

estimates from SPOT VEGETATION data. *Journal of Geophysical Research - Atmospheres, 109, D14S03, doi:10.1029/2002JD003598*, 2-22

Thonicke, K., Spessa, A., Prentice, I.C., Harrison, S.P., Dong, L., & Carmona-Moreno, C. (2010). The influence of vegetation, fire spread and fire behaviour on biomass burning and trace gas emissions: results from a process-based model. *Biogeosciences, 7*, 1991–2011

Thonicke, K., Venevsky, S., Sitch, S., & Cramer, W. (2001). The role of fire disturbance for global vegetation dynamics: coupling fire into a Dynamic Global Vegetation Model. *Global Ecology and Biogeography, 10*, 661-677

Tosca, M.G., Randerson, J.T., Zender, C.S., Flanner, M.G., & Rasch, P.J. (2010). Do biomass burning aerosols intensify drought in Equatorial Asia during El Nino? *Atmospheric Chemistry and Physics, 10*, 3515– 3528

Trigg, S., & Flasse, S. (2001). An evaluation of different bi-spectral spaces for discriminating burned shrub-savannah. *International Journal of Remote Sensing, 22*, 2641–2647

Vafeidis, T.A., & Drake, N.A. (2005). A two step method for estimating the extent of burnt areas with the use of coarse-resolution data. *International Journal of Remote Sensing, 26*, 2441-2459

van der Werf, G.R., Dempewolf, J., Trigg, S.N., Randerson, J.T., Kasibhatla, P.S., Giglio, L., Murdiyarso, D., Peters, W., Morton, D.C., Collatz, G.J., Dolman, A.J., & Defries, R.S. (2008a). Climate regulation of fire emissions and deforestation in Equatorial Asia. *Proceedings National Academy of Sciences, 105*, 20350–20355

van der Werf, G.R., Randerson, J., T., Collatz, G.J., & Giglio, L. (2003). Carbon emissions from fires in tropical and subtropical ecosystems. *Global Change Biology, 9*, 547-562

van der Werf, G.R., Randerson, J., T., Collatz, G.J., Giglio, L., Kasibhatla, P.S., Arellano, A.F., Olsen, S.C., & Kasischke, E.S. (2004). Continental scale-partitioning of fire emissions during the 1997 to 2001 El Niño/La Niña period. *Science, 303*, 73-76

van der Werf, G.R., Randerson, J.T., Giglio, L., Collatz, G., Mu, M., Kasibhatla, P.S., Morton, D.C., DeFries, R.S., Jin, Y., & van Leeuwen, T.T. (2010). Global fire emissions and the contribution of deforestation, savanna, forest, agricultural, and peat fires (1997-2009). *Atmospheric Chemistry and Physics, 10*, 11707–11735

van der Werf, G.R., Randerson, J.T., Giglio, L., Collatz, G.J., Kasibhatla, P.S., & Arellano, A.F. (2006). Interannual variability in global biomass burning emissions from 1997 to 2004. *Atmospheric Chemistry and Physics, 6*, 3423-3441

van der Werf, G.R., Randerson, J.T., Giglio, L., Gobron, N., & Dolman, A.J. (2008b). Climate controls on the variability of fires in the tropics and subtropics. *Global Biogeochemical Cycles, 22*

Verhoef, W. (1984). Light scattering by leaf layers with application to canopy reflectance modeling: the SAIL model. *Remote Sensing of Environment, 16*, 125-141

Westerling, A.L., Hidalgo, H.G., Cayan, D.R., & Swetnam, T.W. (2006). Warming and earlier spring increase western US forest wildfire activity. *Science, 313*, 940-943

Wooster, M.J., & Xu, W. (2012). SLSTR ATBD fire product. *Sentinel 3 products and algorithm definition, S3-L2-SD-03-T04-KCL-ATBD_FIREPRODUCT*

Yokelson, R.J., Susott, R., Ward, D.E., Reardon, J., & Griffith, D.W.T. (1997). Emissions from smoldering combustion of biomass measured by open-path Fourier transform infrared spectroscopy. *Journal of Geophysical Research, 102*, 18865-18877

Yue, C., Ciais, P., Cadule, P., Thonicke, K., Archibald, S., Poulter, B., Hao, W.M., Hantson, S., Mouillot, F., Friedlingstein, P., Maignan, F., & Viovy, N. (2014). Modelling fires in the terrestrial carbon balance by incorporating SPITFIRE into the global vegetation model ORCHIDEE - Part 1: Simulating historical global burned area and fire regime. *Geosci. Model Dev. Discuss.,, 7*, 2377-2427

Yue, C., Mouillot,F., Heil,A. (2014). ESA CCI ECV Fire Disturbance - Climate assessment report, Fire_cci_Ph3_LSCE_D4_2_CAR_v2_0.pdf, https://www.esa-fire-cci.org

Zhang, Q.F., Pavlic, G., Chen, W.J., Fraser, R., Leblanc, S., & Cihlar, J. (2005). A semi-automatic segmentation procedure for feature extraction in remotely sensed imagery. *Computers & Geosciences, 31*, 289-296

Zhang, X., Friedl, M.A., Schaaf, C.B., Strahler, A.H., Hodges, J.C.F., Gao, F., Reed, B.C., & Huete, A. (2003). Monitoring vegetation phenology using MODIS. *Remote Sensing of Environment, 84*, 471-475

Zhang, Y., Fu, R., Yu, H., Dickinson, R.E., Juarez, R.N., Chin, M., & Wang, H. (2008). A regional climate model study of how biomass burning aerosol impacts land-atmosphere in- teractions over the Amazon. *Journal of Geophysical Research, 113*

ANNEX 1

LIST OF ACRONYMS

AATSR	Advanced Along Track Scanning Radiometer
AMORGOS	Accurate MERIS Ortho Rectified Geo-location Operational Software
ANN	Artificial Neural Network
AQL	Área Quemada En Latinoamérica
ASAR	Advanced Synthetic Aperture Radar
ASTER	Advanced Spaceborne Thermal Emission And Reflection Radiometer
ATCOR	Atmospheric and Topographic Correction
ATSR	Along Track Scanning Radiometer
AVHRR	Advanced Very High Resolution Radiometer
AVIRIS	Airborne Visible/Infrared Imaging Spectrometer
AWiFS	Advanced Wide Field Sensor
BA	Burned Area
BAI	Burned Area Index
BAp	Burned Area proportion
BC	Brockmann Consult
BRDF	Bi-Directional Reflectance Distribution Function
CEOS	Committee of Earth Observation Satellites
CCI	Climate Change Initiative
CDF	Cumulative Distribution Function
CE	Commission Error
CNFDB	Canadian National Fire Database
C3S	Copernicus Climate Change Services
DEM	Digital Elevation Model
DLR	Deutsches Zentrum für Luft- und Raumfahrt
EC	European Commission
ECV	Essential Climate Variable
EFFIS	European Forest Fire Information System
ENVISAT	Environmental Satellite
EOS	Earth Observing System
EPA	Environmental Protection Agency
ERS	European Remote Sensing
ESA	European Space Agency
ETM+	Landsat Enhanced Thematic Mapper
ETRS89	European Terrestrial Reference System 1989
fAPAR	Fraction Of Absorbed Photosynthetically Active Radiation
FDA	Fire Damage Assessment
FIRMS	Fire Information for Resource Management System
FR	Full Resolution
FRAP	Fire and Resource Assessment programme
GBA2000	Global Burnt Area 2000
GCOS	Global Climate Observing System
GEMI	Global Environmental Monitoring Index
GESAVI	Generalized Soil-Adjusted Vegetation Index
GFED	Global Fire Emissions Database
GHG	Green House Gases
GLOBCARBON	Global Land Products For Carbon Model Assimilation
GLOBSCAR	ATSR Global Burned Forest Mapping
GOES	Geostationary Operational Environmental Satellite
GOFC	Global Observation Of Forest Cover
GOFC/GOLD	Global Observations Of Forest And Land Cover Dynamics
HANDS	Hotspot And NDVI Differencing Synergy
HS	HotSpot
ICSU	International Council of Scientific Unions

IGBP	International Geosphere-Biosphere Program
IHDP	International Human Dimensions Programme
IOC	Intergovernmental Oceanographic Commission
IPCC	Intergovernmental Panel on Climate Change
JRC	Joint Research Centre
Landsat	Land Satellite
LAI	Leaf Area Index
LC	Land Cover
MERIS	Medium Resolution Imaging Spectrometer
MIR	Mid-Infrared
MIRBI	Mid-Infrared Burn Index
MLP	Multi-Layer Perceptron
MODIS	Moderate Resolution Imaging Spectroradiometer
MSG	Meteosat Second Generation
NAFI	North Australian Fire Information
NASA	National Aeronautics And Space Administration
NBR	Normalized Burnt Ratio
NDII	Normalized Difference Infrared
NDSWIR	Normalized Difference SWIR
NDVI	Normalized Difference Vegetation Index
NDWI	Normalized Difference Water Index
NIR	Near InfraRed
NOAA	National Oceanic And Atmospheric Administration OPS Optical Sensor
OE	Omission Error
OLCI	Ocean Land Colour Instrument
PAF	Potential Active Fire
PM	Particulate Matter
RDA	Rapid Damage Assessment
RR	Reduced Resolution
SAI	Spectral Angle Images
SAVI	Soil adjusted vegetation index
SLSTR	Sea and Land Surface Temperature Radiometer
SPOT	Système Pour l'Observation De La Terre
SRF	Spectral Response Function
SWIR	Short Wave Infrared
SWVI	Short Wave Vegetation Index
TSA	Thiessen scene areas
TIR	Thermal Infrared
TM	Landsat Thematic Mapper
TRMM	Tropical Rainfall Measurement Mission
UNESCO	United Nations Educational, Scientific and Cultural Organization
UNEP	United Nations Environment Programme
UNFCCC	United Nations Framework Convention on Climate Change
VISSR-VAS	Visible-Infrared Spin-Scan Radiometer Atmospheric Sounder
VIRS	Visible and Infrared Scanner
VGT	Vegetation
WCP	World Climate research Programme
WFA	World Fire Atlas
WGS84	World Geodetic System 1984
WiFS	Wide Field Sensor
WMO	World Meteorological Organization

ANNEX 2

FIRST PUBLICATION

Remote Sensing of Environment 163 (2015) 140–152

Contents lists available at ScienceDirect

Remote Sensing of Environment

journal homepage: www.elsevier.com/locate/rse

Global burned area mapping from ENVISAT-MERIS and MODIS active fire data

Itziar Alonso-Canas *, Emilio Chuvieco

Environmental Remote Sensing Research Group, Dep. of Geology, Geography and the Environment, University of Alcalá, c/Colegios 2, 28801 Alcalá de Henares, Spain

ARTICLE INFO

Article history:
Received 28 July 2014
Received in revised form 13 March 2015
Accepted 14 March 2015
Available online 4 April 2015

Keywords:
Fire
Biomass burning
MERIS
MODIS HS
Burned area

ABSTRACT

We present the development of a global burned area (BA) algorithm based on MERIS imagery along with the assessment of the global BA results for three years (2006–2008). This work was developed within the Fire Disturbance project under the European Space Agency Climate Change Initiative programme, which aimed to generate long-term BA information for climate models. Our algorithm combined temporal series of MERIS reflectances with thermal information from MODIS HS (hotspot) product. The algorithm included two-steps. Firstly, cumulative distribution functions were computed to discriminate the most clearly burned pixels using regionally-oriented near infrared reflectance thresholds. Secondly, a contextual criterion improved the spatial detection of the burned patches from the seed pixels. BA estimates for the three target years range from 3.6 to 3.8 million km^2. Results were validated from a statistically designed sample of fire perimeters generated from Landsat multi-temporal imagery. Intercomparison with existing BA products was also carried out. Results from global validation datasets provided an average overall accuracy higher than 0.95. The accuracy of the BA category was lower than the accuracy of the unburned one. Within the former, average omission and commission errors were lower for areas where the proportion of burned area was higher (for pixel-based error matrices, commission error (CE) was 0.52 and omission error (OE) was 0.51), than for those areas with very low BA proportion (CE = 0.60 and OE = 0.74). In terms of total BA estimation, errors were generally well balanced, with a tendency towards underestimation (34%). Relevant impact of temporal reporting accuracy was found for these validation datasets. Intercomparison with other existing BA datasets pointed out similar spatial and temporal trends, with high correlation with GFED v4 BA estimations for the three years ($r^2 > 0.974$).

1. Introduction

Fire is a key component of the carbon cycle, related to greenhouse gases and aerosol emissions to the atmosphere (Andreae & Merlet, 2001; van der Werf et al., 2010). Biomass burning has a critical relevance for global vegetation dynamics (Kloster, Mahowald, Randerson, & Lawrence, 2012; Thonicke et al., 2010), increasingly affecting human lives and property (Bowman et al., 2009).

Even though the current understanding of climate–fire interactions is limited, there is also increasing evidence on their mutual influence (Kloster et al., 2012; Krawchuk, Moritz, Parisien, Van Dorn, & Hayhoe, 2009; Mouillot & Field, 2005; Pechony & Shindell, 2010; Running, 2006). Expected temperature and rainfall changes are likely to increase wildfire frequency in some regions, while others may experience decrease in fire activity as a result of decreased biomass production (Daniau A.L., Bartlein P.J., Harrison S.P., Prentice I.C., Brewer S., Friedlingstein P., et al., 2012; Krawchuk et al., 2009).

The growing interaction between fire and climate highlights the relevance of accessing global burned area (BA) information, particularly for climate and dynamic vegetation models (Mouillot et al., 2014). The extended use of these models emphasises the need to have long-term and consistent time series of BA information, with proper error and uncertainty characterisation. This is the main goal of the Fire Disturbance (fire_cci) project (http://www.esa-fire-cci.org/ last accessed November 26, 2014). Fire is one of the Essential Climate Variables (ECV) within the European Space Agency Climate Change Initiative (ESA-CCI). The ESA-CCI is part of the European contribution to the Global Climate Observing System (GCOS) programme. Currently, the ESA CCI programme includes 13 ECVs that involve atmospheric (ozone, greenhouse gases, aerosols and clouds), oceanic (ocean colour, sea ice, ocean height and temperature), and terrestrial products (fire, glaciers, ice sheets, soil moisture and land cover) (Hollmann et al., 2013). The objective of the fire_cci project was to improve global mapping of BA and the use of this information in global vegetation and atmospheric models. This project aimed at developing burned area (BA) information from European medium resolution sensors: (A)ATSR (Advanced Along Track Scanning Radiometer) on board ERS (European Remote Sensing) and ENVISAT (Environmental Satellite), VEGETATION (VGT) on board the SPOT (Satellite Pour

* Corresponding author.
E-mail addresses: itziar.alonsoc@uah.es (I. Alonso-Canas), emilio.chuvieco@uah.es (E. Chuvieco).

http://dx.doi.org/10.1016/j.rse.2015.03.011
0034-4257/

l'Observation de la Terre) and MERIS (MEdium Resolution Imaging Spectrometer) on board ENVISAT. Following user recommendations, BA information should be offered at pixel level (monthly products at full resolution: 1000 m for VGT and ATSR and 300 m for MERIS) and grid level (fortnightly products at 0.5° cell resolution) retaining in both cases the date of detection. Both products included a set of auxiliary variables to facilitate their use by the climate modelling community (http://www.esa-fire-cci.org/webfm_send/771 last accessed November 26, 2014).

Monitoring areas affected by biomass burning has been performed over the last decades using a wide variety of sensors, from very high-spatial resolution such as Ikonos for fine scales (Kachmar & Sanchez-Azofeifa, 2006), to medium resolution sensors such as Landsat-TM/ETM + or SPOT-HRV for regional coverages (Bastarrika, Chuvieco, & Martin, 2011b; Pu & Gong, 2004) and to coarse spatial resolution sensors for continental to global studies (Chang & Song, 2009; Chuvieco et al., 2008; Giglio et al., 2010; Roy, Boschetti, & Justice, 2008; Tansey et al., 2008). The latter are the most relevant within the context of climate modelling and they are commonly offered in coarser resolution grids (0.25 to 0.5° cell).

The first attempts to globally map burned areas were based on NOAA (National Oceanic and Atmospheric Administration)-AVHRR (Advanced Very High Resolution Radiometer) data, mostly using multi-temporal changes of vegetation indices (Kasischke et al., 1993), although hybrid algorithms based on thermal and optical channels were also developed (Fraser, Li, & Cihlar, 2000; Roy, Giglio, Kendall, & Justice, 1999). Extensive regions were mapped from AVHRR HRPT (High Resolution Picture Transmission) (1.1 km at nadir) temporal series, especially in the boreal forest of Russia (Sukhinin et al., 2004) and Canada (Fraser et al., 2000). A few studies were also undertaken to map global BA using degraded spatial resolution AVHRR products, such as the 8 km PAL (Pathfinder Land) or LTDR (Long Term Data Record) series (Carmona-Moreno et al., 2005; Riaño, Ruiz, Isidoro, Ustin, & Riaño, 2007).

More recently, other sensors with greater sensitivity for mapping burned patches have been used to create global inventories of BA (Table 1). The GBA2000 was produced from VGT data of the year 2000, using a set of regional algorithms based on multi-temporal changes in daily reflectances or spectral indices (Tansey et al., 2004). This product was later extended to the 2000–2007 series and named L3JRC, still based on VGT data (Tansey et al., 2008). The ESA promoted another global BA product, named GLOBSCAR (Simon, Plummer, Fierens, Hoelzemann, & Arino, 2004), based on day time ATSR-2 images. Later, the approaches of these two European projects were combined within the Globcarbon project, which produced a 1998–2007 BA product based on both ATSR and VGT data (Plummer et al., 2007). More recently, the Copernicus land product services has released the Geoland BA variable, based on SPOT-VGT. In addition to European products, MODIS (MOderate Resolution Imaging Spectroradiometer) data on board the NASA (National Aeronautics and Space Administration) Terra and Aqua satellites have shown great potential for global mapping of BA. Currently, two MODIS global BA products are available. The standard one, named MCD45A1, is based on temporal differences of observed versus predicted reflectance using the inversion of a bidirectional reflectance model (Roy, Jin, Lewis, & Justice, 2005). The second one, the MCD64, is part of the Collection 5.1 Direct Broadcast products, and it is based on a hybrid algorithm combining active fire detections and multi-temporal changes in spectral indices (Giglio, Loboda, Roy, Quayle, & Justice, 2009). This product is the basis for the BA estimation included in the GFED (Global Fire Emissions Database) (Giglio et al., 2010), widely used by climate and carbon modellers.

All these global products have strengths and weaknesses and have been used in a wide range of modelling efforts (Mouillot et al., 2014). A proper validation and inter-comparison of all these products are still to be done, although regional comparisons have already been published (Boschetti, Eva, Brivio, & Gregoire, 2004; Roy & Boschetti, 2009). Recent papers have shown the use of statistical design frameworks for validation of global BA products (Padilla, Stehman, & Chuvieco, 2014; Padilla et al., 2015).

The goal of this paper is to present a global BA algorithm specifically tailored for the ENVISAT MERIS sensor in the context of the fire_cci project. MERIS was mainly designed for ocean colour applications, and provides high spectral resolution (Table 2) in the range of the blue to the near infrared regions (Gower & Borstad, 2004). The spatial resolution is 300 m in the full resolution mode (FRS) and 1200 m in the Reduced Resolution (RR) mode. The total field of view of MERIS is 68.5° around nadir, covering a swath width of 1150 km, and yielding to a 3 day revisit time for equatorial regions. The application of MERIS data to fire applications is scarce: identification of smoke plumes (Huang & Siegert, 2004) and discrimination of burn severity (Chuvieco, De Santis, Riaño, & Halligan, 2007; Roldan-Zamarron, Merino-De-Miguel, Gonzalez-Alonso, Garcia-Gigorro, & Cuevas, 2006). Mapping BA with MERIS was performed only at regional level (Oliva, Martin, & Chuvieco, 2011) using different vegetation indices, while González-Alonso et al. (2009) combined fire hotspots from MODIS and near infrared (NIR) reflectance values from MODIS and MERIS imagery.

MERIS presents some challenges for mapping burned areas. Spectral and temporal resolutions are not ideal for BA discrimination, as the sensor does not include short-wave infrared bands and global coverage of the Earth is obtained every three days. However, the potential of MERIS for improving current information of BA relies on its greater spatial resolution in the FRS mode (used throughout this paper), thus

Table 1
Summary of existing BA products.

	Sensor	Time series	Spatial res	Type of algorithm/detection	Reference
MCD 45	MODIS Aqua Terra	2001–present	500 m	Bi-directional reflectance model-based change detection approach	Roy et al. (2005)
MCD 64	MODIS Aqua Terra	2001–present	500 m	HS and multi temporal spectral indices changes	Giglio et al. (2009)
GBA 2000	SPOT VGT	11/1999–12/2000	1 km	Multi temporal changes in daily reflectances or spectral indices (IFI and UTL algorithms)	Ershov and Novik (2001) Silva et al. (2003) Grégoire, Tansey, and Silva (2003)
GBS	NOAA AVHRR	1982–1999	8 km	Multi temporal change detection	Carmona-Moreno et al. (2005)
GLOB SCAR	ERS2 ATSR2	2000	1 km	K1: contextual algorithm based on geometrical characteristics of burned pixels in the near-infrared (NIR, 0.87 μm)/thermal infrared (TIR, 11 μm). E1: series of fixed thresholds applied to the data from four spectral channels.	Piccolini and Arino (2000) Eva and Lambin (1998)
GLOB CARBON	ERS2 ATSR2 SPOT VGT ENVISAT AATSR	1998–2007	1 km	Based on two GBA2000 algorithms: IFI and UTL and two GLOBSCAR algorithms: K1 and E1.	
L3JRC	SPOT VGT	2000–2007	1 km	Temporal index, based on GBA2000 experience.	Tansey et al. (2008)
GEO LAND2	SPOT VGT	1999–present	1 km	Temporal index and thresholds	(http://www.geoland2.eu/ last accessed November 26, 2014)

Table 2
MERIS bands characteristics.

Band	Band centre (nm)	Bandwidth (nm)
1	412.5	10
2	442.5	10
3	490	10
4	510	10
5	560	10
6	620	10
7	665	10
8	681.25	7.5
9	705	10
10	753.75	7.5
11	760	2.5
12	775	15
13	865	20
14	890	10
15	900	10

potentially providing better detection of small burn patches than coarser resolution sensors. Furthermore, this sensor has a follow up version on the OLCI (Ocean and Land Colour Instrument) sensor, and will be complemented with the SLSTR (Sea and Land Surface Temperature Radiometer), both payloads on board Sentinel 3, scheduled for launch in 2015 within the EC Copernicus programme.

2. Methods

2.1. Framework

The design of a global BA algorithm requires considering the great diversity of biomass burning conditions worldwide. The most extended approaches for mapping BA can be classified in two groups: those that use the thermal contrast of active fires (commonly named hot spots, HSs) from the surrounding background (Giglio et al., 2006b), and those based on reflectance changes caused by burning effects (changing of leaf and soil colour, leaf losses, char background, etc.) (Bastarrika, Chuvieco, & Martin, 2011a; Roy et al., 2005). The former approach is more reliable because thermal radiance (and consequently the signal amplification) increases exponentially with temperature, while fire-related reflectance changes are more subtle. However, thermal signal lasts very shortly (minutes to hours) while the fires are active, whereas post-fire reflectance changes last much longer (days to years). In addition, BA mapping based on active fires only implies a sample of the total area burned (what is actually burning when the satellite observes the area), while reflectance changes are noticeable in the whole area affected by the fire (providing the impact of fire is severe enough).

Several authors have proposed hybrid algorithms to overcome the limitations of each approach. These algorithms commonly use HS information either to guide the characterisation of BA statistics or to confirm potential burned pixels. The use of thermal anomalies helps avoiding commission errors related to reflectance changes caused by non-fire events (such as crop harvest, seasonal flooding, or topographic shades), which are not associated to sharp increases of temperature. This hybrid approach was initially proposed for the AVHRR sensor (Fraser et al., 2000; Roy et al., 1999), with partial success, as the AVHRR thermal channel was not particularly suitable for detecting active fires. More recently, hybrid algorithms have been used to generate the MCD64 product (Giglio et al., 2009).

Considering the spectral and temporal limitations of MERIS, it was decided to develop the BA algorithm from a hybrid approach, using a combination of HS information derived from MODIS data (http://modis-fire.umd.edu/ last accessed January 27, 2015) and temporal trends of MERIS reflectance bands. In order to consider a proper balance between omission and commission errors, the algorithm included two different phases (Chuvieco, Englefield, Trishchenko, & Luo, 2008). First, a seed identification phase, which aimed to minimise commission by applying a series of criteria to determine those pixels that were most likely to be burned. Second, a contextual phase, which applied region growing analysis to improve the delimitation of burned patches. These two phase algorithms have been successfully used in previous BA studies (Bastarrika et al., 2011a; Chuvieco et al., 2008; Martín, Gómez, & Chuvieco, 2005). The algorithm was developed and tested in 10 different study sites, which were selected to take into account the diversity of burning conditions worldwide, including different biomes and fire regimes (Fig. 1).

2.2. Generation of corrected reflectances and spectral indices

Corrected MERIS reflectances were received from Brockmann Consult (http://www.brockmann-consult.de/ last accessed November 26, 2014). The pre-processing chain was based on the one developed for the Landcover CCI project, with modifications to obtain daily reflectances instead of weekly composites (as it was required by that project). Geometric correction was obtained through the AMORGOS software (Accurate MERIS Ortho Rectified Geo-location Operational Software, Bourg, 2011), improving MERIS FR geolocation (RMS < 70 m). Calibration and smile correction were also performed, as well as land water delineation, cloud screening and atmospheric correction (more details of these processes in http://www.esa-landcover-cci.org/?q=webfm_send/75 last accessed November 26, 2014). The surface directional reflectances were delivered as floats between 0 and 1. In addition to corrected reflectances, the images included a standard error associated to each band, as well as the Sun and satellite zenith and azimuth angles. A status layer was provided as well, with values 1 (clear land), 3 (snow/ice), or 0 (i.e. water, cloud, no observation). Output files were gridded into tiles of 10 × 10° (3600 × 3600 pixels at MERIS FRS spatial resolution). These tiles were the input files for all processes of our BA algorithm.

The NIR region was selected as main input for the algorithm, since this spectral band is highly sensitive to recent burns, as both green vegetation and dry vegetation have substantially higher reflectance than recent burns in the NIR (Chuvieco, Englefield, Trishchenko and Luo, 2008; Chuvieco, Martín, & Palacios, 2002; Koutsias & Karteris, 2000; Trigg & Flasse, 2001). In addition to the NIR band, we computed the Global Environmental Monitoring Index (GEMI) (Pinty & Verstraete, 1992), which was proven the best performing index to detect burned areas among the spectral indices based on the red-NIR space (Barbosa, Grégoire, & Pereira, 1999; Chuvieco, Englefield, Trishchenko and Luo, 2008; Chuvieco et al., 2002; Martín et al., 2005; Pereira, 1999). GEMI was computed as follows:

$$\mathrm{GEMI} = \eta(1-0.25\eta) - \frac{(\rho_R - 0.125)}{(1-\rho_R)}$$

$$\eta = \frac{2\left(\rho_{NIR}{}^2 - \rho_R{}^2\right) + 1.5\rho_{NIR} + 0.5\rho_R}{(\rho_R + \rho_{NIR} + 0.5)},$$

where ρ_{NIR} is the reflectance in the NIR (in our case MERIS band 10) and ρ_R is the reflectance in the red (MERIS Band 8). The selection of MERIS bands 8 (673.75 nm to 688.75 nm), and 10 (746.25 nm to 761.25 nm), was based on the results from Oliva et al. (2011), which showed that short NIR bands (bands 9 to 12) had better sensitivity than long NIR bands (bands 13 to 15) to discriminate BA (Table 2).

2.3. Temporal compositing

Temporal resolution of input data is an important aspect to consider when building a global BA algorithm, since the analysis of post-fire reflectance may be easily contaminated by clouds or weaken by quick vegetation recovery. Therefore, the number of observations is a limiting factor for detecting fires, particularly in Tropical regions, where

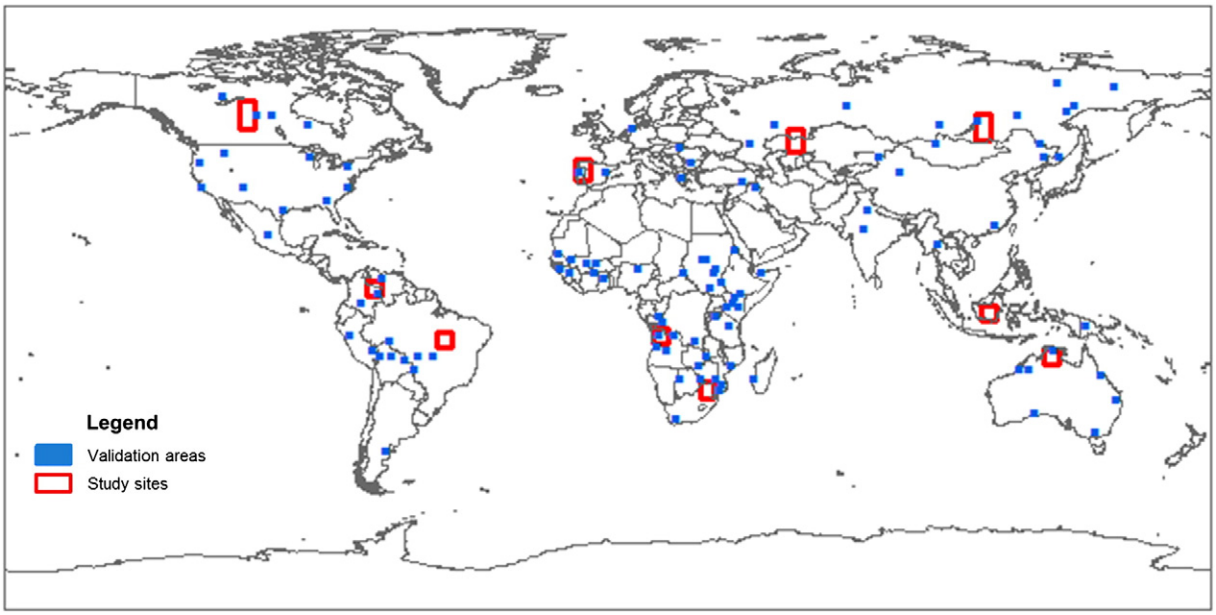

Fig. 1. Study and validation sites.

vegetation recovery is quite quick after fire. The MERIS sensor has a temporal resolution of 3 days at the Equator. In practice, taking into account cloud contamination and potential gaps in data reception, the temporal resolution becomes lower. Fig. 2 shows the maximum number of valid observations per month in 2008 for sample study sites of $10 \times 10°$ in different biomes.

Considering that some areas had little spatial continuity, we generated monthly composites of NIR to fill the potential gaps in day-to-day images, therefore improving the spatial coherence for BA detection. These composites were the basis for the two phases of the algorithm.

Different compositing techniques have been proposed in previous BA studies, most commonly maximising or minimising a certain input band to enhance the burned signal (Chuvieco, Ventura, Martín, & Gomez, 2005; Sousa, Pereira, & Silva, 2003). The criteria for generating the monthly NIR-GEMI composites were chosen as to emphasise the sensitivity of the outputs to the burned signal. Two criteria were used: maximise the proximity to fire dates and minimise the NIR signal. Both criteria aimed to select the most clearly burned pixel in the time series.

Since HS provide a very accurate estimation of burning dates (Boschetti, Roy, Justice, & Giglio, 2010), we first generated an auxiliary file selecting for each location the closest date to the closest HS. For doing so, a Thiessen matrix (Brassel & Reif, 1979) was created for each temporal composite labelling each pixel with the date of the closest HS. The Thiessen matrix was computed considering also those HS located within a buffer of 0.5° outside the edges of each tile. This option mitigated potential continuity problems between tiles, when for instance a fire occurred at the border of two tiles.

The second compositing criterion implied minimising the NIR reflectance values of the temporal series, as reflectance from a BA is expected to have a very low NIR value. However, since low NIR values can also be caused by other factors (cloud or topographic shadows, for instance), instead of selecting the minimum NIR of the period, we chose the first minimum after the date stored in the Thiessen HS file, as this would select a more immediate value to the post-fire burn reflectance. If no minima existed after that date, then the second minimum of the times series was chosen. Once the most suitable date for each pixel of the composite was obtained, two files were created, one with the NIR reflectance and the other one with the GEMI index for that particular date.

Composites were built for each month by selecting images from a bi-monthly time series (Fig. 3) to mitigate the impact of low MERIS temporal resolution, which is especially relevant for cloudy regions and for fires occurring at the end of the monthly period.

In addition to the monthly post-fire composites, an annual reference composite was created for the contextual phase of the algorithm. This annual composite maximised the GEMI value to account for the maximum seasonal greenness of each pixel. We assumed that the change between the annual maximum and the post-fire value (included in the GEMI monthly composite) should be the highest for burned pixels, thus emphasising post-fire spectral changes.

2.4. Seed selection phase

The first part of the seed selection focused on generating statistics of burned and unburned areas for each tile, based on the monthly composite NIR values and on the distribution of HS in the same month. Since burned conditions are very diverse worldwide, we aimed to obtain regional-

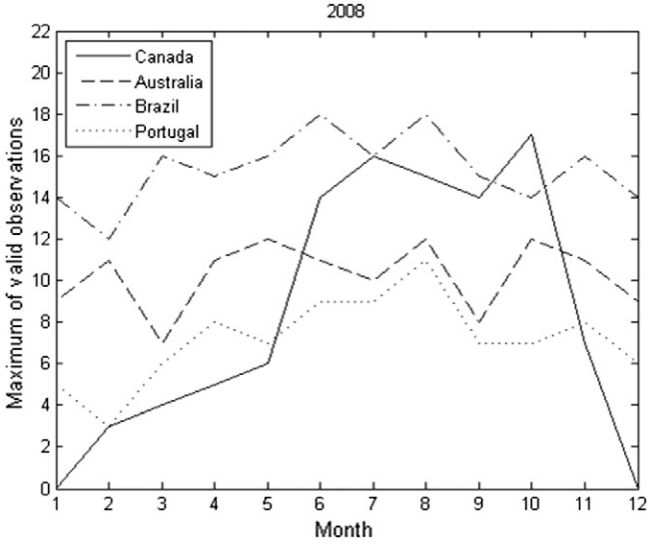

Fig. 2. Maximum number of MERIS valid observations per month in 2008. The areas selected are tiles of $10 \times 10°$ located in Canada (L03C07), Brazil (L09C20), Portugal (L05C17), and Australia (L10C31).

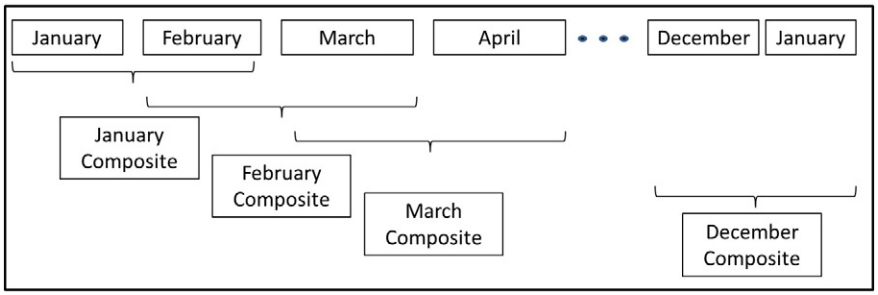

Fig. 3. Monthly composites generation based on MERIS information from two consecutive months.

oriented NIR thresholds, based on the 10 × 10° tiles, which should be adapted to different post-fire reflectance conditions. Cumulative distribution functions (CDFs) were created for each tile to establish regionally-oriented thresholds of NIR values, in order to emphasise discrimination between burned and unburned categories. Thresholds selected changed in each tile and period, and therefore it was expected that they would better tackle the spatial and temporal variations of BA. The 10 × 10 tiles are the direct output from the pre-processing chain. It was decided to keep them as input to obtain the CDFs as this division offered a good balance between considering regional diversity and processing time. Use of land cover maps may have been helpful, but they would have also incorporated the inherent errors to any land cover product. Future versions would consider including this information in the algorithm, based on collaboration with the landcover_cci team.

The burned pixels to obtain the CDF of BA were obtained from the information provided by the MODIS HS. Since HS have an original resolution of 1000 × 1000 m, instead of assuming that all nine MERIS pixels covered by the HS pixel were active fires, we considered that the potential active fire (PAF) was more likely located at the minimum NIR value of the 3 × 3 window covered by the HS. To avoid commission errors, we introduced an additional temporal change constraint, and accepted as PAF only pixels that showed a NIR reflectance decrease in time t from the previous period (t − 1). The CDF of the unburned category was generated from the values of those pixels that did not have any HS in a 64 × 64 pixel matrix and that were not detected by the BA algorithm in the previous months.

The NIR threshold value of the burned category (TB) was defined by selecting the immediately lower decile of the burned pixels' CDF that intersected the first decile of the unburned pixels' CDF. This criterion implies in fact that we accepted to have as much as 10% commission error. The omission error would be estimated by the selected decile of the burned CDF. This omission was expected to be higher as the burned and unburned CDFs were closer, but it should be reduced in phase 2 (contextual analysis) of the algorithm.

Fig. 4 shows two examples of the CDFs to illustrate the computation of TB. In Fig. 4a) the CDFs of the burned and unburned classes are closer (implying poorer separation between both categories), while in Fig. 4b) the CDFs have better discriminability. In both cases, the criterion to select the TB was the same, but the actual TB value changed following the CDFs. In the former case, the TB was 0.108, corresponding to the NIR value of the fourth decile of the burned CDF, which was the lower close to the first decile of the unburned CDF. In the latter case, the TB value was 0.115, corresponding to the eight decile of the burned CDF. Therefore, the probability of omission would be lower than in the first case. This illustrates that the more separated the CDFs between burned and unburned categories were, the less chances of confusion. On the opposite, the closer the CDFs the more pixel values were shared by the burned and unburned distributions, and therefore more omission errors should be expected. For this reason, the decile used to define the TB was taken into account for phase 2 of the algorithm.

Once the TB was defined, pixels were considered BA seeds and therefore used for the contextual phase of the algorithm when three criteria were met:

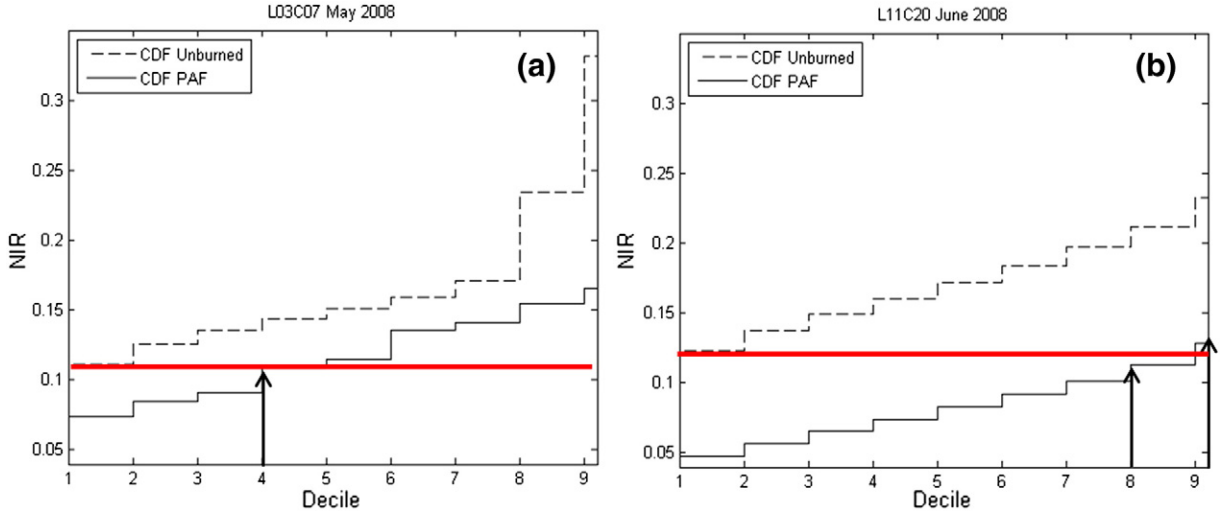

Fig. 4. Threshold based on decile 10 of the unburned CDF for cases with worse (a) and better (b) discrimination between classes, correspondent to May 2008 in tile L03C07 (Canada) and June 2008 in L11C20 (South Africa) respectively. In a) TB for seed and growing phases remains the same (single arrow). In b) TB for the seed phase corresponds to decile 8 (left arrow) and TB for the growing phase corresponds to decile 9 (right arrow).

a) The NIR value was lower than the computed TB of that tile and period.
b) At least one PAF should be found in a neighbour 9 × 9 matrix;
c) The NIR value for month t should be lower than the NIR value of month t − 1.

Fig. 5 includes a diagram that illustrates the main steps of seed and growing phases.

2.5. Region growing phase

Contextual algorithms have been previously used for BA mapping (Bastarrika et al., 2011b; Pu et al., 2007). The goal of these algorithms is to reduce omission errors that may result from the seed phase, while avoiding the increase of commission errors. One of the critical issues to obtain a good performance of these algorithms for BA mapping relies on obtaining a sound method to stop the region growing process (Zhang et al., 2005). Otherwise the iterative process may create severe overestimation.

For the MERIS BA algorithm only pixels surrounding the BA seeds were analysed for contextual analysis. This second phase of the BA algorithm included three growing conditions, which accounted for a proper balance between reducing omission errors (by extending the incomplete burned patches around seed pixels), while avoiding commission errors. Pixels around each seed were analysed recursively until they did not meet the growing conditions, which implied the end of the process (Fig. 5). If the criteria were met, the pixel was considered as a new seed and also its surrounding pixels were analysed.

The first condition implied that NIR values should be below TB, but the TB was less strict than in phase 1 if the CDFs of burned and unburned pixels were well separated. The criterion to increase or not the TB of the seed phase was based on which decile was used to establish the TB. When this value came from decile seventh or higher, the new TB was increased to the ninth decile of the burned CDF (Fig. 4b). Otherwise it was kept to the TB of the seed phase (Fig. 4a).

The second condition aimed to assure that the decrease in the NIR values (DNIR) between t and t − 1 for each candidate BA pixel was higher than the decrease observed for unburned areas. With this criterion, we tried to avoid neighbour areas to the seeds that might have fire-unrelated changes.

Finally, the third condition was based on detecting the vegetation loss as a result of fire, based on the differences in GEMI values between the target monthly composite and the annual GEMI composites. This criterion was defined as 0.9 times the difference found in the GEMI value between the target pixel and those labelled as burned (either original or new seeds).

A final test was applied to avoid large commission errors in a few areas with dark covers, where the region growing process did not perform properly (specific regions of Australia, China and India, for instance). In this case, we filtered out large polygons when the number of burned pixels largely exceeded the number of hotspots. We established an empirical value of 30 times (MERIS BA pixels/HS), based on previous findings from Hantson, Padilla, Corti, and Chuvieco (2013), who compared the distribution of HS and Landsat-derived burned patches in the same study sites used to develop this algorithm (Fig. 1).

2.6. Product assessment

Two assessments were performed with the MERIS BA results. The first one was based on a set of global validation sites, and the second one was an intercomparison with existing BA products. The methodology for the two approaches is introduced hereafter.

A complete global and temporal validation strategy has been developed within the Fire-CCI project (http://www.esa-fire-cci.org/webfm_send/779 last accessed November 26, 2014). The validation of the different BA products was performed using a statistically selected global sample of reference BA sites. The year 2008 was selected as the reference for validation following a CCI programmatic decision. Stratified random sampling was used to select 105 non-overlapping Thiessen scene areas (TSA), considering both ecosystem variation and historical fire occurrence (Padilla et al., 2014). Reference fire perimeters were generated by a semi-automatic BA algorithm developed by Bastarrika et al. (2011b, 2014) applied to two multi-temporal Landsat TM/ETM+ images for each sampled TSA. The reference files followed the standard protocol defined by the CEOS Cal-Val (http://lpvs.gsfc.nasa.gov/fire_home.html, last accessed November 26, 2014). Whenever the input images were ETM+, only the central strip of the images was processed, to avoid the impacts of the SLC-off gaps.

The validation metrics were derived from fuzzy error matrices to account for the different pixel size of TM/ETM and MERIS sensors. Six

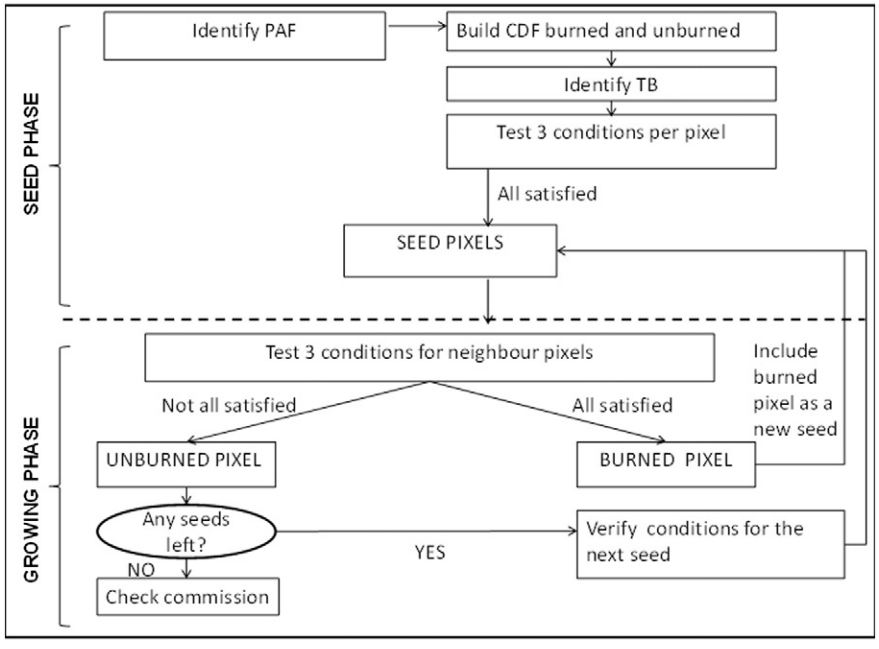

Fig. 5. Main steps of the algorithm: seed and growing phases.

accuracy measures were computed (overall accuracy, omission error, commission error, Dice coefficient, bias and relative bias) to satisfy criteria specified by end-users of burned area products. More details on the validation strategy can be found in Padilla et al. (2014) and Padilla et al. (2015).

The second assessment was based on intercomparison of spatial and temporal trends of our results with existing global BA products available for the same time series (2006–2008): GEOLAND-2, MCD45A1, and GFED v4. GEOLAND-2 was selected as representative of BA products based on European sensors, since the precursors (L3JRC and GlobCarbon) were not available for 2008, the key year for global validation. The two MODIS-based BA products (MCD45 and GFED v4) are currently the most broadly used in modelling studies (Mouillot et al., 2014).

2.7. Uncertainty

Uncertainty characterisation of the fire_cci products was based on a sample of study sites from 2006 to 2008 not used in the validation. A total of 23 pairs of Landsat TM/ETM + images were processed to generate these reference fire perimeters. For the MERIS pixel product (300 m), uncertainty was estimated in probabilistic terms (% confidence), based on regression analysis using as inputs the confidence level of the classification, the number of neighbour burned pixels, and the land cover. For the grid product, similar models were used, and the output was expressed as a standard error of the total burned area for each grid cell, following approaches of existing products (Giglio et al., 2010). Further details of the procedure can be found in the fire_cci project documentation (https://www.esa-fire-cci.org/webfm_send/791 last accessed November 26, 2014)

3. Results

3.1. Spatial and temporal trends

Three years of MERIS data (2006 to 2008) were processed with our algorithm. Total BA obtained with the MERIS algorithm ranges from 3.6 to 3.8 million km^2. In terms of spatial variability, Fig. 6 shows the gridded burned area obtained for 2008. The most extensive burnings occurred in the Tropical regions, particularly in the African continent, followed by the Northern regions of Australia, Central Brazil, Venezuelan and Colombian Llanos, and SE Asia. A second belt of burned regions is noticeable in the temperate grasslands and croplands of central Asia, and SE USA. The boreal forests of Russia and Canada have also a substantial role in global biomass burnings. Similar trends were obtained for 2006 and 2007.

The basic information used to compute BA was the date of detection, which showed seasonal trends of fire activity, with predominant January–March fires in the Northern Tropical belt, July–September in the Southern Tropical fringe, Northern Boreal and Temperate Regions of America and Eurasia. Fig. 7 includes the Julian dates of burn in Africa for 2008. The seasonal trends can be clearly identified for this case, with the fire peaks associated to the central months of the dry season.

Fig. 8 shows the estimation of uncertainty values for the same area, with a spatial variation associated mainly to the omission error, related to the availability of input images, with lower values for cloudy regions.

3.2. Validation

Table 3 shows the results of the validation metrics computed from the 105 global validation sites. They were divided in two subsamples, based on the proportion of burned area. The vast majority (100) had less than 10% of burned area, while only a few had more than that threshold. Overall accuracy was high in both cases (>87%), but BA accuracy was lower. Omission and commission errors were higher for those areas with very low burned area proportion than for those with more fire occurrence. The Dice coefficient (DC), which combines the omission and commission errors, was also higher for the sites with more BA proportion (0.48). Error balance (over and underestimation) was close to 0 for areas with larger BA, but showed underestimation for the overall sample and those areas with minor BA. In relative terms (relB) the overall sample showed BA underestimation by 34%.

Comparison with existing BA products showed that MERIS BA results have similar overall accuracy than the two MODIS BA products (MCD45 and MCD64) (OA > 0.99), but it showed significantly higher commission and omission errors than MCD64 (CE = 0.42; OE = 0.68), and higher commission error than MCD45 (CE = 0.46; OE = 0.72) (Padilla et al., 2015). The errors found with the MERIS product were significantly lower than the ones from existing European BA products. In terms of error balance, the estimations showed different trends for areas with very small BA and for those with higher BA proportion, but an overall trend towards underestimation was observed. The relative balance of errors showed better results than MCD64 and MCD45 with a 34% of underestimation for MERIS, versus 44% for MCD64 and 48% for MCD45 (Padilla et al., 2015).

3.3. Intercomparison with existing products

Table 4 includes total BA estimations from the MERIS BA product and from the MODIS-based (MCD45 and MCD64) products for the three years when global outputs were available. GFED v4 is derived from the MCD64A1 product aggregated to 0.25° spatial resolution for the period 2000–present. Prior to 2000, GFED BA estimates are obtained by calibrating active fire data from the Tropical Rainfall Measuring Mission (TRMM), Visible and Infrared Scanner (VIRS) and Along-Track Scanning Radiometer (ATSR) with the MCD64A1. MERIS BA estimates are 3 to 9% higher than GFED v4 and 7–9% higher than MCD45.

In terms of spatial distribution of BA Fig. 9 illustrates the GFED v4, MCD45, GEOLAND2 and MERIS_CCI BA products in 2008 separated by ecoregion (following the geographical ecoregions defined by Giglio, van der Werf, Randerson, Collatz, & Kasibhatla, 2006). The vast majority of BA occurred in the two African hemispheres (NHAF, SHAF, summing both 70% of total), followed by far by Australia, Central Asia, South America and Boreal Asia. For nine regions (CEAM, EQAS, EURO, MIDE, NHAF, SEAS, SHAF, SHSA, and TENA) MERIS estimates were higher or in the same order as the GFED v4 and MCD45 ones. GEOLAND2 reported higher values in boreal and temperate regions (BOAS, BONA, CEAS and TENA) and significantly lower in Tropical areas (NHAF and SHAF). Overall, a high level of agreement was found between MERIS, GFED v4 and MCD45 ($r^2 > 0.99$).

When looking at seasonal trends, a high level of agreement was also found between MERIS and existing BA products. Fig. 10 includes monthly estimations by MERIS and GFED v4 of global BA from 2006 to 2008. According to the figure, the trend between products was consistent in terms of magnitude through the temporal series. GFED v4 underestimates when compared to MERIS, except for October, November 2006 and July and August 2007 and 2008.

4. Discussion

This paper presents the first global algorithm to detect burned areas from MERIS ENVISAT imagery. Even though the sensor's temporal and spectral characteristics are not optimal for BA detection, we have shown that MERIS images complemented with HS information can provide reliable estimations of BA. Certainly, MERIS is no longer available (as ENVISAT mission ended in 2012). However, a long time series (2003 to 2012) could be computed from this algorithm, thus providing a complementary view on the existing knowledge of BA trends. In addition, the future ESA Sentinel-3 satellite (to be launched in 2015) will include a similar sensor (OLCI), which could benefit from our algorithm to build a semi-operational BA product. As this satellite will also incorporate a thermal sensor (the SLSTR), with active fire detection capabilities, the

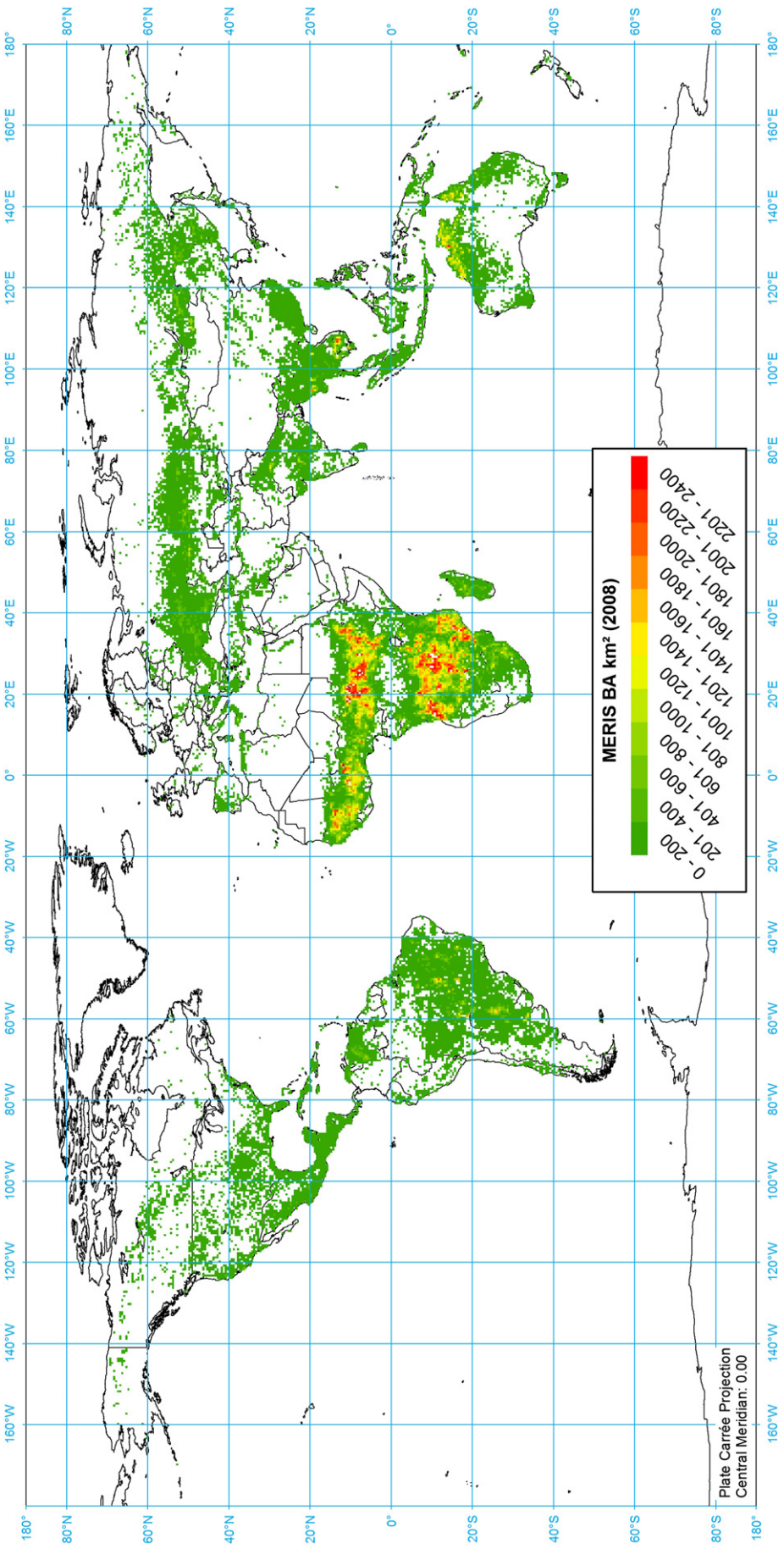

Fig. 6. MERIS global BA for 2008.

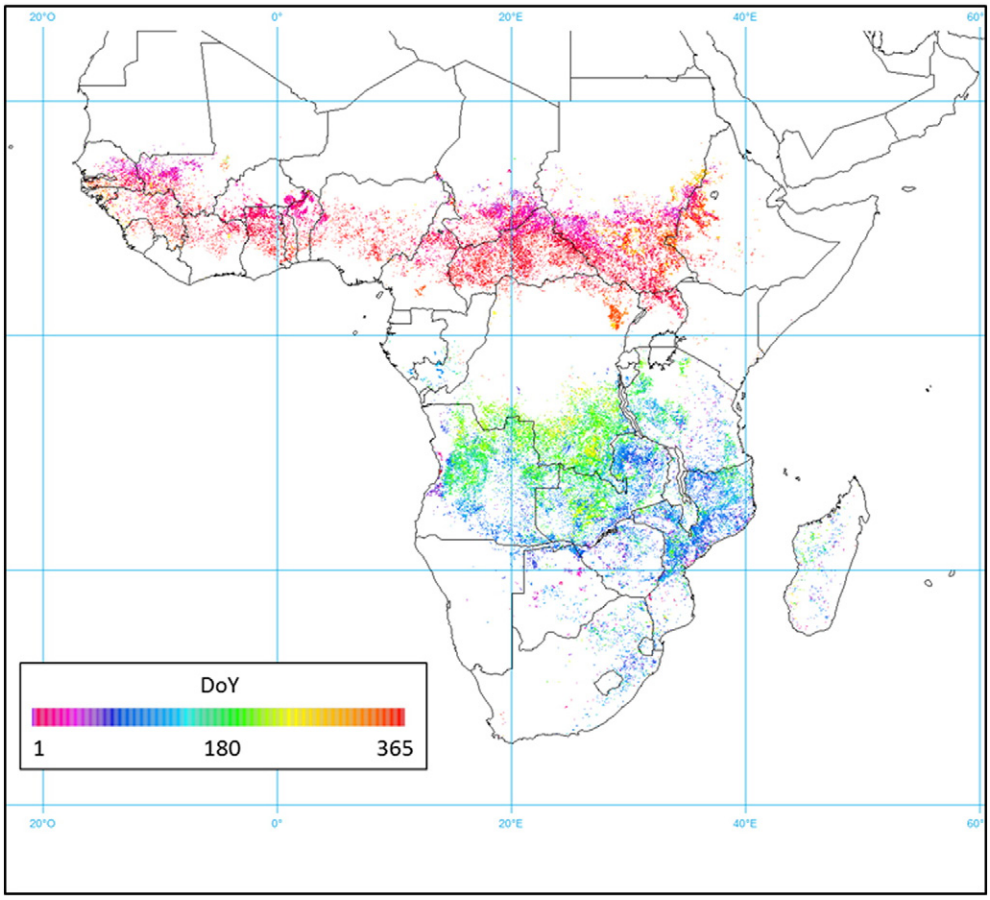

Fig. 7. MERIS burn detection dates for Africa in 2008.

methods presented in this paper could be implemented without the need of using data from other satellites. On the other hand, our hybrid approach can also be useful for other sensors that are constrained to the red-near infrared space, as it is the case of the higher spatial resolution (250 m) bands of MODIS.

Since our algorithm relies on MODIS HS and MERIS reflectance information, the results cannot be considered fully independent from MODIS products, particularly from MCD64, which uses a hybrid approach as well. However, the structure of the algorithm is quite different from Giglio et al. (2009), and it is built on the particular spectral space detected by the MERIS sensor. Spatial variations between our results and GFED v4 for instance, show that HS input does not fully determine the output results.

Our hybrid approach takes advantage from both the more sensitive thermal characterisation of active fires and the more permanent reflectance changes of burned patches. HS information helped establishing regional thresholds for BA discrimination, while mitigating potential commission errors. However, the use of HS also implies a certain contribution to overall BA error (not yet fully assessed in our results). HSs have proven very reliable to detect active fires, with very low commission error, but they are not frequent or sensitive enough to detect all active fires, and therefore omission errors are higher (Csiszar, Denis, Giglio, Justice, & Hewson, 2005; Giglio, Csiszar, & Justice, 2006; Hantson et al., 2013). Alternative criteria based on change detection techniques to complement HS information were considered in our project, particularly in those regions where omissions are more relevant, but could not finally be implemented due to the low temporal frequency of MERIS acquisitions (Fig. 2). This omission error inherent to HS is also included in other BA products based on HS (such as the GFED-MCD64). An improved seed procedure with very clear fire-related reflectance changes may be included in future versions, ensuring also more independency from the thermal information. However, additional research is needed to build more robust time series from MERIS reflectance data. This could be achieved also from its successor, the OLCI on board Sentinel 3, since temporal coverage will improve (revisit time will be 2.2 days with one satellite and 1.1 day when both satellites are launched).

The two assessment exercises presented in this paper confirmed that MERIS algorithm provided acceptable results. When estimating total BA in the statistically designed validation sample, MERIS provided lower but comparable accuracy metric values to the MODIS-based BA products (MCD45 and MCD64). Overall accuracy showed very high values (OA > 0.95), but the product showed higher commission errors (CE = 0.64) than MCD64 and MCD45 and similar omission errors (OE = 0.76) to the MCD45. The relative balance of errors showed better results than MCD64 and MCD45 with a 34% of underestimation. Errors were lower for the areas with higher proportion of burned area (OE = 0.51 and CE = 0.52; Table 3). MERIS errors were significantly lower than the ones obtained with other European BA products (Padilla et al., 2015).

These estimations of errors may be considered pessimistic, as some of these errors are in fact caused by the low temporal frequency of the MERIS sensor. We computed the temporal reporting accuracy of our results by obtaining the difference between MERIS BA detection dates and HS dates. We observed that 50% of the MERIS detections occurred with a difference of 4 to 22 days from the HS in four test sites (>250,000 km^2) located in Tropical (Australia), Temperate (California and the Iberian Peninsula) and Boreal (Canada) ecosystems, reaching up to 9–30 days when the threshold was increased to 75%. The temporal accuracy was therefore lower than the values obtained globally by Boschetti et al. (2010) for the MCD45 product (50% within one day and 75% within four days). The low MERIS reporting accuracy increases the likelihood of omission and commission errors, particularly when the two Landsat

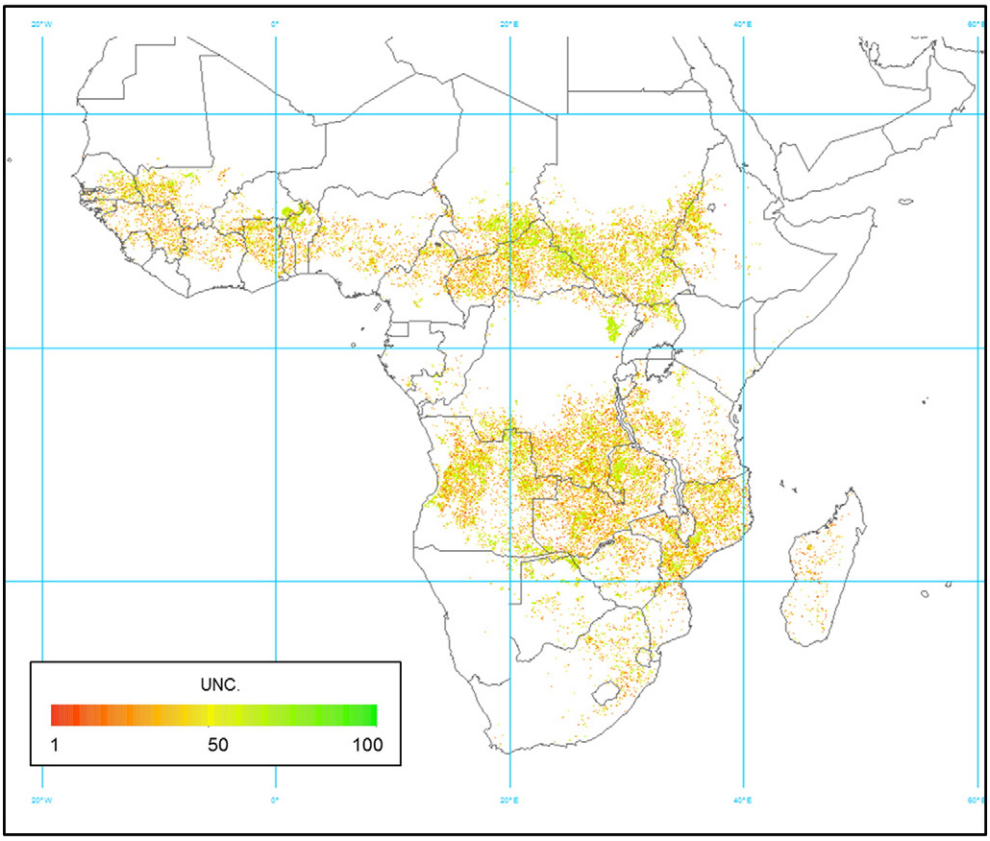

Fig. 8. Uncertainty relative to MERIS BA estimates for Africa in 2008.

images used to obtain the reference perimeters were close in time (as it was the case of Tropical ecosystems where most validation pairs of images were separated by 32 days or less). In fact, when comparing our results for 2008 with existing fire perimeters in the four test sites where temporal accuracy was tested (Australia, California, Iberian Peninsula and Canada), we found that both commission and omission errors decreased to 0.47 and 0.15 respectively. This reduction of detection errors compared to the Landsat validation sample should be related to the longer period included in the test sites (which covers the full year), when dating errors are expected to affect marginally the accuracy estimations.

Our results showed similar estimations to existing BA products, both in terms of total BA values, and geographical distribution, with better estimations (according to validation results) than existing European BA products, particularly in Tropical regions. Further comparison of the MERIS results with GFED v4, one of the most widely used by climate modellers, showed similar temporal trends for the 3 years processed. Global estimations were 3 to 9% higher than GFED v4 for the three years computed, while geographical and monthly trends showed high correlation values.

However, our MERIS results still show some detection problems, particularly in temperate regions, where fires are unusual and commission errors were found by misclassification with agricultural areas. In Tropical regions, omissions were higher, which may be caused by the errors associated to the HS detections, becoming more relevant in areas with small fires (Hantson et al., 2013). In addition, the conditions for contextual analysis should be reviewed for future versions of the algorithm, particularly in relation to fragmentation of fires and in cloudy areas that caused temporal gaps in the MERIS time series.

5. Conclusions

A hybrid algorithm to estimate burned areas on a global scale from MERIS reflectance and MODIS HS time series was developed within the framework of the Climate Change Initiative of the European Space Agency. This algorithm makes use of thermal, NIR and visible information to detect burned pixels. It is based on a two-step process: seed and growing phases. Results were obtained for three years of data, estimating a total BA from 3.6 to 3.8 million km^2. Patterns of fire activity were also identified (African Tropical regions, Northern regions of Australia, Central Brazil, Central and South East Asia, Russia, Canada and South East USA) as well as seasonal trends. MERIS BA estimates showed similar although lower accuracy than existing MODIS BA products, based on a validation dataset produced from multitemporal Landsat images. Some of the observed errors were related

Table 3
Estimated accuracy metrics for MERIS BA.

OA	DC	Ce	Oe	B	relB	Burned area proportion
0.9581	0.312	0.597	0.745	−0.0137	−0.3657	<0.1
0.879	0.486	0.517	0.510	0.0018	0.0157	>0.1
0.996	0.290	0.640	0.760	−0.12	−0.34	All

Table 4
GFED v4, MCD45 and MERIS BA in km^2 for years 2006 to 2008.

	GFED v4	MCD45	MERIS_CCI
2006	3,417,863	3,374,125	3,652,355
2007	3,644,122	3,523,728	3,773,855
2008	3,307,377	3,308,200	3,624,146

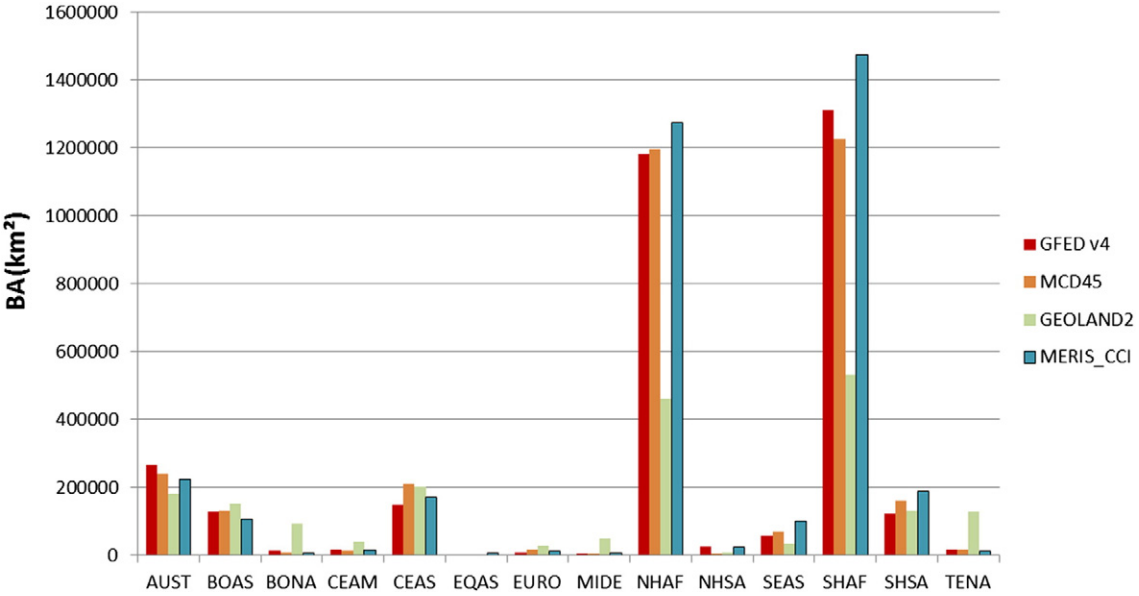

Fig. 9. BA 2008 estimations for MCD45, GFED v4, GEOLAND2 and MERIS_CCI for the 14 ecoregions defined in Giglio, van der Werf, Randerson, Collatz and Kasibhatla (2006) (BONA = Boreal North America, TENA = Temperate North America, CEAM = Central America, NHSA = Northern Hemisphere South America, SHSA Southern Hemisphere South America, EURO = Europe, MIDE = Middle East Africa, NHAF = Northern Hemisphere Africa, SHAF = Southern Hemisphere Africa, BOAS = Boreal Asia, CEAS = Central Asia, SEAS = Southeast Asia, EQAS = Equatorial Asia, AUST = Australia).

to temporal reporting problems associated to the MERIS coverage frequency.

This algorithm will be the basis for computing a full BA time series for the second phase of the fire_cci project (2003 to 2012), while preparing the upcoming generations of the European Space Agency burned area products, particularly those based on Sentinel-3 OLCI-SLSTR sensors. The availability of alternative BA time series would complement existing BA products, providing more robust estimations and improvements in the uncertainty characterisation of BA inputs for climate models (Mouillot et al., 2014). On the other hand, different BA products can provide diverse regional accuracies and therefore, merging outputs from global synthesis may greatly improve how BA trends are currently characterised.

Acknowledgements

This work was developed within the Fire-CCI project, in the framework of the European Space Agency Climate Change Initiative programme. Early developments of the MERIS algorithm were produced by Teresa Calado, Patricia Oliva and Federico González, all part of the fire_cci project consortium. The validation dataset was generated by Marc Padilla, Stijn Hantson, Dante Corti, and Ruben Ramo. Validation metrics were developed by Marc Padilla. Intercomparison analysis with existing BA products was partially computed by Ruben Ramo.

The final MERIS BA product can be freely downloaded from the web page of the fire_cci project: http://www.esa-fire-cci.org/ (last accessed November 26, 2014).

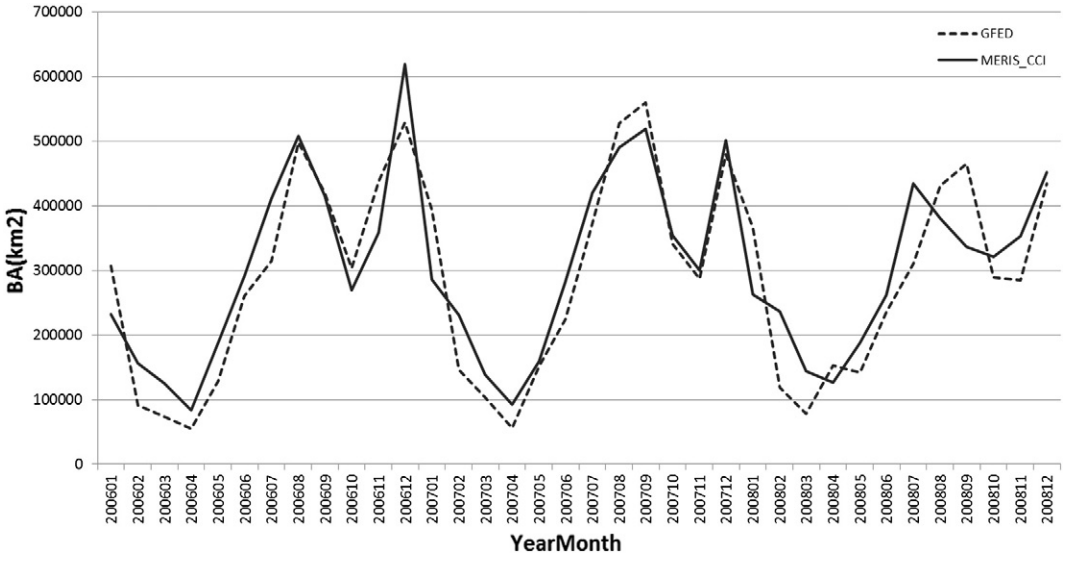

Fig. 10. Monthly global BA in 2006 to 2008 for MERIS_CCI and GFED v4.

References

Andreae, M. O., & Merlet, P. (2001). Emission of trace gases and aerosols from biomass burning. *Global Biogeochemical Cycles*, *15*, 955–966.

Barbosa, P. M., Grégoire, J. M., & Pereira, J. M. C. (1999). An algorithm for extracting burned areas from time series of AVHRR GAC data applied at a continental scale. *Remote Sensing of Environment*, *69*, 253–263.

Bastarrika, A., Alvarado, M., Artano, K., Martinez, M., Mesanza, A., Torre, L., et al. (2014). BAMS: A tool for supervised burned area mapping using Landsat data. *Remote Sensing*, *6*, 12360–12380.

Bastarrika, A., Chuvieco, E., & Martin, M. P. (2011a). Automatic burned land mapping from MODIS time series images: Assessment in Mediterranean ecosystems. *IEEE Transactions on Geoscience and Remote Sensing*, *49*, 3401–3413.

Bastarrika, A., Chuvieco, E., & Martin, M. P. (2011b). Mapping burned areas from Landsat TM/ETM+ data with a two-phase algorithm: Balancing omission and commission errors. *Remote Sensing of Environment*, *115*, 1003–1012.

Boschetti, L., Eva, H. D., Brivio, P. A., & Gregoire, J. M. (2004). Lessons to be learned from the comparison of three satellite-derived biomass burning products. *Geophysical Research Letters*, *31*, L21501 (21510.21029/22004GL021229).

Boschetti, L., Roy, D. P., Justice, C. O., & Giglio, L. (2010). Global assessment of the temporal reporting accuracy and precision of the MODIS burned area product. *International Journal of Wildland Fire*, *19*, 705–709.

Bourg, L. (2011). *The AMORGOS MERIS CFI (Accurate MERIS Ortho-Rectified Geo-location Operational Software) processing.* Validation report (PO-RP-ACR-GS-0014) ACRI-ST.

Bowman, D. M. J. S., Balch, J. K., Artaxo, P., Bond, W. J., Carlson, J. M., Cochrane, M. A., et al. (2009). Fire in the Earth system. *Science*, *324*, 481–484.

Brassel, K. E., & Reif, D. (1979). A procedure to generate Thiessen polygons. *Geographical Analysis*, *11*, 289–303.

Carmona-Moreno, C., Belward, A., Malingreau, J. P., Hartley, A., Garcia-Alegre, M., Antonovskiy, M., et al. (2005). Characterizing interannual variations in global fire calendar using data from Earth observing satellites. *Global Change Biology*, *11*, 1537–1555.

Chang, D., & Song, Y. (2009). Comparison of L3JRC and MODIS global burned area products from 2000 to 2007. *Journal of Geophysical Research*, *114*. http://dx.doi.org/10.1029/2008JD11361.

Chuvieco, E., De Santis, A., Riaño, D., & Halligan, K. (2007). Simulation approaches for burn severity estimation using remotely sensed images. *Journal of Fire Ecology*, *3*, 129–150.

Chuvieco, E., Englefield, P., Trishchenko, A. P., & Luo, Y. (2008a). Generation of long time series of burn area maps of the boreal forest from NOAA–AVHRR composite data. *Remote Sensing of Environment*, *112*, 2381–2396.

Chuvieco, E., Martín, M. P., & Palacios, A. (2002). Assessment of different spectral indices in the red-near-infrared spectral domain for burned land discrimination. *International Journal of Remote Sensing*, *23*, 5103–5110.

Chuvieco, E., Opazo, S., Sione, W., Del Valle, H., Anaya, J., Di Bella, C., et al. (2008b). Global burned land estimation in Latin America using MODIS composite data. *Ecological Applications*, *18*, 64–79.

Chuvieco, E., Ventura, G., Martín, M. P., & Gomez, I. (2005). Assessment of multitemporal compositing techniques of MODIS and AVHRR images for burned land mapping. *Remote Sensing of Environment*, *94*, 450–462.

Csiszar, I., Denis, L., Giglio, L., Justice, C. O., & Hewson, J. (2005). Global fire activity from two years of MODIS data. *International Journal of Wildland Fire*, *14*, 117–130.

Daniau, A. L., Bartlein, P. J., Harrison, S. P., Prentice, I. C., Brewer, S., Friedlingstein, P., et al. (2012). Predictability of biomass burning in response to climate changes. *Global Biogeochemical Cycles*, *26*.

Ershov, D. V., & Novik, V. P. (2001). Mapping burned areas in Russia with spot4 vegetation (S1 product) imagery. *Final report, Contract 18176-2001-07-F1EI ISP RU, Eur. Comm. Joint Res. Cent., Brussels*.

Eva, H., & Lambin, E. F. (1998). Burnt area mapping in Central Africa using ATSR data. *International Journal of Remote Sensing*, *19*, 3473–3497.

Fraser, R. H., Li, Z., & Cihlar, J. (2000). Hotspot and NDVI differencing synergy (HANDS): A new technique for burned area mapping over boreal forest. *Remote Sensing of Environment*, *74*, 362–376.

Giglio, L., Csiszar, I., & Justice, C. O. (2006a). Global distribution and seasonality of active fires as observed with the Terra and Aqua Moderate Resolution Imaging Spectroradiometer (MODIS) sensors. *Journal of Geophysical Research-Biogeosciences*, *111*. http://dx.doi.org/10.1029/2005JG000142.

Giglio, L., van der Werf, G. R., Randerson, J. T., Collatz, G. J., & Kasibhatla, P. (2006b). Global estimation of burned area using MODIS active fire observations. *Atmospheric Chemistry and Physics*, *6*, 957–974.

Giglio, L., Loboda, T., Roy, D. P., Quayle, B., & Justice, C. O. (2009). An active-fire based burned area mapping algorithm for the MODIS sensor. *Remote Sensing of Environment*, *113*, 408–420.

Giglio, L., Randerson, J. T., van der Werf, G. R., Kasibhatla, P. S., Collatz, G. J., Morton, D. C., et al. (2010). Assessing variability and long-term trends in burned area by merging multiple satellite fire products. *Biogeosciences Discuss*, *7*, 1171–1186 (1110.5194/bg-1177-1171-2010).

González-Alonso, F., Salgado, V., Calle, V., Casanova, J. L., Sanz, J., de la Fuente, D., et al. (2009). Forest burn in China by means of MERIS and MODIS images. *Dragon 2 Symposium, June 2009, Barcelona*.

Gower, J. F. R., & Borstad, G. A. (2004). On the potential of MODIS and MERIS for imaging chlorophyll fluorescence from space. *International Journal of Remote Sensing*, *25*, 1459–1464.

Grégoire, J. M., Tansey, K., & Silva, J. M. N. (2003). The GBA2000 initiative: Developing a global burned area database from SPOT-VEGETATION imagery. *International Journal of Remote Sensing*, *24*, 1369–1376.

Hantson, S., Padilla, M., Corti, D., & Chuvieco, E. (2013). Strengths and weaknesses of MODIS hotspots to characterize global fire occurrence. *Remote Sensing of Environment*, *131*, 152–159.

Hollmann, R., Merchant, C. J., Saunders, R. W., Downy, C., Buchwitz, M., Cazenave, A., et al. (2013). The ESA climate change initiative: Satellite data records for essential climate variables. *Bulletin of the American Meteorological Society*. http://dx.doi.org/10.1175/BAMS-D-11-00254.1.

Huang, S., & Siegert, F. (2004). ENVISAT multisensor data for fire monitoring and impact assessment. *International Journal of Remote Sensing*, *25*, 4411–4416.

Kachmar, M., & Sanchez-Azofeifa, G. A. (2006). Detection of post-fire residuals using high- and medium-resolution satellite imagery. *Forestry Chronicle*, *82*, 177–186.

Kasischke, E. S., French, N. H. F., Harrell, P., Christensen, N. L., Ustin, S. L., & Barry, D. (1993). Monitoring of wildfires in boreal forests using large area AVHRR NDVI composite image data. *Remote Sensing of Environment*, *45*, 61–71.

Kloster, S., Mahowald, N., Randerson, J., & Lawrence, P. (2012). The impacts of climate, land use, and demography on fires during the 21st century simulated by CLM-CN. *Biogeosciences*, *9*, 509–525.

Koutsias, N., & Karteris, M. (2000). Burned area mapping using logistic regression modeling of a single post-fire Landsat-5 Thematic Mapper image. *International Journal of Remote Sensing*, *21*, 673–687.

Krawchuk, M. A., Moritz, M. A., Parisien, M. -A., Van Dorn, J., & Hayhoe, K. (2009). Global pyrogeography: The current and future distribution of wildfire. *PLoS One*, *4*, e5102.

Martín, M.P., Gómez, I., & Chuvieco, E. (2005). Performance of a burned-area index (BAIM) for mapping Mediterranean burned scars from MODIS data. In J. Riva, F. Pérez-Cabello, & E. Chuvieco (Eds.), *Proceedings of the 5th International Workshop on Remote Sensing and GIS applications to Forest Fire Management: Fire Effects Assessment* (pp. 193–198). Paris: Universidad de Zaragoza, GOFC-GOLD, EARSeL.

Mouillot, F., & Field, C. B. (2005). Fire history and the global carbon budget: a 1 degrees × 1 degrees fire history reconstruction for the 20th century. *Global Change Biology*, *11*, 398–420.

Mouillot, F., Schultz, M. G., Yue, C., Cadule, P., Tansey, K., Ciais, P., et al. (2014). Ten years of global burned area products from spaceborne remote sensing — A review: Analysis of user needs and recommendations for future developments. *International Journal of Applied Earth Observation and Geoinformation*, *26*, 64–79.

Oliva, P., Martin, P., & Chuvieco, E. (2011). Burned area mapping with MERIS post-fire image. *International Journal of Remote Sensing*, *32*, 4175–4201.

Padilla, M., Stehman, S. V., & Chuvieco, E. (2014). Validation of the 2008 MODIS-MCD45 global burned area product using stratified random sampling. *Remote Sensing of Environment*, *144*, 187–196.

Padilla, M., Stehman, S. V., Ramo, R., Corti, D., Hantson, S., Oliva, P., et al. (2015). Comparing the accuracies of remote sensing global burned area products using stratified random sampling and estimation. *Remote Sensing of Environment*, *160*, 114–121.

Pechony, O., & Shindell, D. (2010). Driving forces of global wildfires over the past millennium and the forthcoming century. *Proceedings of the National Academy of Sciences*, *107*, 19167–19170.

Pereira, J. M. C. (1999). A comparative evaluation of NOAA/AVHRR vegetation indexes for burned surface detection and mapping. *IEEE Transactions on Geoscience and Remote Sensing*, *37*, 217–226.

Piccolini, I., & Arino, O. (2000). Towards a global burned surface world atlas. *Earth Observation Quarterly*, *65*, 14–18.

Pinty, B., & Verstraete, M.M. (1992). GEMI: A non-linear index to monitor global vegetation from satellites. *Vegetatio*, *101*, 15–20.

Plummer, S., Arino, O., Ranera, F., Tansey, K., Chen, J., Dedieu, G., et al. (2007). An update on the GlobCarbon initiative: Multi-sensor estimation of global biophysical products for global terrestrial carbon studies. *Envisat Symposium. Montreux, Switzerland: ESA SP-636*.

Pu, R., & Gong, P. (2004). Determination of burnt scars using logistic regression and neural network techniques from a single post-fire Landsat-7 ETM+ image. *Photogrammetric Engineering and Remote Sensing*, *70*, 841–850.

Pu, R. L., Li, Z. Q., Gong, P., Csiszar, I., Fraser, R., Hao, W. -M., et al. (2007). Development and analysis of a 12-year daily 1-km forest fire North America from NOAA/AVHRR data. *Remote Sensing of Environment*, *108*, 198–208.

Riaño, D., Ruiz, J. A. M., Isidoro, D., Ustin, S. L., & Riaño, D. (2007). Global spatial patterns and temporal trends of burned area between 1981 and 2000 using NOAA-NASA Pathfinder. *Global Change Biology*, *13*, 40–50. http://dx.doi.org/10.1111/j.1365-2486.2006.01268.

Roldan-Zamarron, A., Merino-De-Miguel, S., Gonzalez-Alonso, F., Garcia-Gigorro, S., & Cuevas, J. M. (2006). Minas de Riotinto (south Spain) forest fire: Burned area assessment and fire severity mapping using Landsat 5-TM, Envisat-MERIS, and Terra-MODIS postfire images. *Journal of Geophysical Research-Biogeosciences*, *111*.

Roy, D. P., & Boschetti, L. (2009). Southern Africa validation of the MODIS, L3JRC and GlobCarbon burned-area products. *IEEE Transactions on Geoscience and Remote Sensing*, *47*. http://dx.doi.org/10.1109/TGRS.2008.2009000.

Roy, D. P., Boschetti, L., & Justice, C. O. (2008). The collection 5 MODIS burned area product — Global evaluation by comparison with the MODIS active fire product. *Remote Sensing of Environment*, *112*, 3690–3707.

Roy, D. P., Giglio, L., Kendall, J. D., & Justice, C. O. (1999). Multi-temporal active-fire based burn scar detection algorithm. *International Journal of Remote Sensing*, *20*, 1031–1038.

Roy, D., Jin, Y., Lewis, P., & Justice, C. (2005). Prototyping a global algorithm for systematic fire-affected area mapping using MODIS time series data. *Remote Sensing of Environment*, *97*, 137–162.

Running, S. W. (2006). Is global warming causing more, larger wildfires? *Science*, *313*, 927–928.

Silva, J. M. N., Pereira, J. M. C., Cabral, A. I., Sa, A. C. L., Vasconcelos, M. J. P., Mota, B., et al. (2003). An estimate of the area burned in southern Africa during the 2000 dry season using SPOT-VEGETATION satellite data. *Journal of Geophysical Research-Atmospheres*, *108*.

Simon, M., Plummer, S., Fierens, F., Hoelzemann, J. J., & Arino, O. (2004). Burnt area detection at global scale using ATSR-2: The GLOBSCAR products and their qualification. *Journal of Geophysical Research-Atmospheres*, *109*, D14S02. http://dx.doi.org/10.1029/2002JD003622 (1-16).

Sousa, A. M. O., Pereira, J. M. C., & Silva, J. M. N. (2003). Evaluating the performance of multitemporal image compositing algorithms for burned area analysis. *International Journal of Remote Sensing*, *24*, 1219–1236.

Sukhinin, A. I., French, N. H. F., Kasischke, E. S., Hewson, J. H., Soja, A. J., Csiszar, I. A., et al. (2004). AVHRR-based mapping of fires in Russia: New products for fire management and carbon cycle studies. *Remote Sensing of Environment*, *93*, 546–564.

Tansey, K., Grégoire, J.M., Defourny, P., Leigh, R., Peckel, J. F., Bogaert, E. V., et al. (2008). A new, global, multi-annual (2000–2007) burnt area product at 1 km resolution. *Geophysical Research Letters*, *35*, L01401. http://dx.doi.org/10.1029/2007GL03156.

Tansey, K., Grégoire, J. M., Stroppiana, D., Sousa, A., Silva, J., Pereira, J. M., et al. (2004). Vegetation burning in the year 2000: Global burned area estimates from SPOT VEGETATION data. *Journal of Geophysical Research-Atmospheres*, *109*, D14S03. http://dx.doi.org/10.1029/2002JD003598 (2–22).

Thonicke, K., Spessa, A., Prentice, I. C., Harrison, S. P., Dong, L., & Carmona-Moreno, C. (2010). The influence of vegetation, fire spread and fire behaviour on biomass burning and trace gas emissions: Results from a process-based model. *Biogeosciences*, *7*, 1991–2011.

Trigg, S., & Flasse, S. (2001). An evaluation of different bi-spectral spaces for discriminating burned shrub-savannah. *International Journal of Remote Sensing*, *22*, 2641–2647.

van der Werf, G. R., Randerson, J. T., Giglio, L., Collatz, G., Mu, M., Kasibhatla, P. S., et al. (2010). Global fire emissions and the contribution of deforestation, savanna, forest, agricultural, and peat fires (1997–2009). *Atmospheric Chemistry and Physics*, *10*, 11707–11735.

Zhang, Q. F., Pavlic, G., Chen, W. J., Fraser, R., Leblanc, S., & Cihlar, J. (2005). A semi-automatic segmentation procedure for feature extraction in remotely sensed imagery. *Computers & Geosciences*, *31*, 289–296.

ANNEX 3

SECOND

PUBLICATION

Desarrollo de un algoritmo global de área quemada para imágenes del sensor ENVISAT-MERIS[1]

Itziar Alonso-Canas* and Emilio Chuvieco

Environmental Remote Sensing Research Group, Dep. of Geology, Geography and the Environment, University of Alcalá, c/ Colegios 2, 28801 Alcalá de Henares, Spain.

E-mail addresses: itziar.alonsoc@uah.es (I. Alonso-Canas), emilio.chuvieco@uah.es (E.Chuvieco)

*Corresponding author
Keywords: Fire, biomass burning, MERIS, MODIS HS, burned area.

RESUMEN

En este artículo se presentan los avances recientes en el desarrollo de un algoritmo para cartografiar área quemada a partir de imágenes MERIS. El trabajo se ha desarrollado en el ámbito del programa de cambio climático de la ESA. El análisis de resultados de la primera versión del algoritmo condujo a implementar una serie de tests para mejorar la configuración. Se probaron estos tests en 4 zonas: Australia, Canadá, California y Península Ibérica, cubriendo un área total de 2.500.000 km^2. Los resultados obtenidos para los distintos tests se compararon con los perímetros de área quemada generados por los gestores de incendios en cada zona, identificando mejoras sustanciales respecto a la primera versión del algoritmo. Para el año 2008, se obtuvo una fiabilidad global de 0,982 (frente al 0,975 de la versión anterior). Esta nueva versión del algoritmo se utilizará para procesar la serie completa de datos MERIS (2002-2012).

[1] Alonso-Canas, I. y Chuvieco, E. (2015): "Desarrollo de un algoritmo de área quemada para imágenes del sensor ENVISAT-MERIS", Geofocus (Artículos), en revisión.

Palabras clave: área quemada, MERIS, incendios, quemada de biomasa.

DEVELOPMENT OF A GLOBAL BURNED AREA ALGORITHM FROM ENVISAT-MERIS IMAGERY

ABSTRACT

In this paper we present the recent developments of an algorithm to detect burned areas from MERIS imagery. This work has been developed in the framework of ESA's climate change initiative. The analysis of the results obtained in the first phase led to the implementation of a series of tests to improve the algorithm configuration. The tests were applied to 4 areas: Australia, Canada, California and Iberian Peninsula, covering an area of 2.500.000 km^2. The results obtained for the different tests were compared to burned area perimeters generated by fire managers in each area. Improvements compared to the first version of the algorithm were identified. For 2008, an overall accuracy of 0.982 was obtained (compared to the 0.975 from the previous version). This new version of the algorithm will be used to process the complete MERIS archive (2002-2012).

Keywords: burned area, MERIS, fires, biomass burning.

1. Introducción.

1.1. Contexto.

La necesidad de conocer los efectos que los incendios tienen tanto a nivel regional como global, así como a las pérdidas económicas y el riesgo de pérdida de vidas humanas que conlleva, supone que este fenómeno sea objeto de un creciente interés por parte de la comunidad científica (Bowman et al 2009). Por otro lado, se observa que la interacción entre clima e incendios es cada vez mayor (Kloster et al 2012). Los cambios en el clima tienen el potencial de influir en los regímenes de incendios, principalmente a través de los cambios en el régimen térmico y en las precipitaciones, que afectan no solo a la extensión de la estación de incendios, sino que también aumentan su severidad y extensión (Daniau et al 2012, Krawchuck et al 2009). Por otro lado, a su vez estos

incendios contribuirán a un mayor calentamiento global, debido a la emisión de gases de efecto invernadero (Van der Werf et al 2010), así como a la modificación de uso de suelo que puede darse a raíz de estos eventos. A su vez, los aerosoles emitidos pueden contribuir de forma negativa en el balance radiativo.

Para poder evaluar estos efectos es necesaria una adecuada caracterización de los incendios así como de la superficie quemada (Mouillot et al 2014). La obtención de registros de área quemada (AQ) a escala global mediante sensores de baja resolución para largos períodos de tiempo es el objetivo principal del proyecto fire_cci que se engloba dentro de la Iniciativa de Cambio Climático (Climate Change Initiative - CCI) de la Agencia Espacial Europea. El objetivo de esta iniciativa es responder a una serie de requisitos expresados por GCOS (Global Climate Observing System), que identifica algunas variables como climáticas esenciales (ECV). De las que lista GCOS, la ESA (European Space Agency) ha seleccionado para este programa 13 variables, afectando al océano, la atmósfera y las tierras emergidas (Hollman et al 2013). Cada una de esas variables, se aborda por un proyecto en el que participan expertos en observación de la Tierra, junto a modeladores del clima.

En este contexto, el proyecto fire_cci se orienta a cartografiar área quemada a escala global para una serie larga de años. También se incluye el pre-proceso de los datos, la validación de los resultados y la integración de los mismos en modelos de emisiones y dinámica global de la vegetación. En el marco del proyecto fire_cci, nuestro grupo ha desarrollado el algoritmo para la detección de AQ a partir de imágenes del sensor ENVISAT-MERIS, que es el objeto principal de este artículo.

1.2. Productos de área quemada.

La obtención de productos de área quemada se realiza desde principios de los años 90, utilizando para ello imágenes del sensor AVHRR a bordo de uno de los satélites NOAA (Kasischke et al 1993). Para realizar la detección se empleaban principalmente cambios multi-temporales de índices espectrales. También en este periodo se desarrollaron algoritmos que utilizaban la información de los canales térmico y óptico (Fraser et al 2000, Roy et al 1999).

Actualmente existen varias iniciativas que buscan obtener productos de este tipo, tanto a escala global como regional. Por lo que respecta a la escala global, cabe destacar los productos MCD45 (Roy et al 2005a) y MCD64 (Giglio et al 2009), que utilizan datos provenientes del sensor MODIS. El producto MCD45 se basa en la detección de diferencias temporales observadas respecto a las predichas mediante un modelo de reflectancia bidireccional. El MCD64 se basa en un algoritmo que combina las detecciones de incendios activos con cambios multi-temporales en índices espectrales. Además de estos dos productos de área quemada, se han elaborado otros proyectos en la misma línea, como los generados a partir del sensor SPOT-VGT. El primero se denominó GBA2000 (Tansey et al 2004), que estimaba el AQ mediante una serie de algoritmos regionales basados en cambios multi-temporales en la reflectividad o en índices espectrales. Como continuación de este producto se generó el L3JRC (Tansey et al 2008) que extendió la serie temporal para los años 2000 a 2007. Además, dentro de un proyecto ESA, se creó el producto GLOBSCAR (Eva y Lambin 1998, Piccolini y Arino 2000) basándose en los datos del sensor ATSR-2. Posteriormente, el proyecto GlobCarbon (Plummer et al 2007), también de la ESA, combinó los algoritmos desarrollados para VGT y ATSR para crear un producto de AQ que cubriese el periodo 1998 a 2007 basado en datos de VGT y ATSR-2.

El producto fire_cci continúa esta línea de la ESA, pero en este caso los datos de partida se adquirieron por el sensor MERIS (Medium Resolution Imaging Spectrometer), a bordo del satélite ENVISAT (Environmental Satellite), con mejor resolución espacial (300 m) que los anteriores productos de la ESA. El presente trabajo se basa en los datos de este sensor.

1.3. Técnicas para detección de área quemada.

De forma general la detección de AQ puede realizarse basándose en dos medidas: en la primera se tiene en cuenta el contraste térmico producido por los incendios activos, mientras que en la segunda se consideran los cambios en la reflectividad producidos por el fuego. Estas técnicas se pueden combinar dando lugar a los algoritmos híbridos que permiten aunar las ventajas de estas dos técnicas, es decir un

mayor cambio detectable en el térmico y una permanencia en el tiempo detectable en la reflectividad, además de la posibilidad de obtener superficies quemadas completas, mientras que con el contraste térmico solo se conoce la situación del fuego en el momento en que se adquiere la imagen.

Una metodología bastante habitual a la hora de crear algoritmos de AQ se basa en la combinación de dos fases: semillado y crecimiento (Bastarrika et al 2011, Chuvieco et al 2008). El objetivo de estas dos fases es en primer lugar obtener píxeles semilla en los que la probabilidad de quemado es muy alta y después crecer alrededor de estos píxeles semilla. Posteriormente, se aplica un crecimiento alrededor de estos píxeles semilla, verificando las condiciones de los píxeles vecinos. Otras formas de detección de AQ pueden basarse en detección de objetos y segmentación, redes neuronales o SVM (Support Vector Machine).

1.4. Algoritmos de área quemada para el sensor MERIS.

MERIS es un espectrómetro programable con 15 bandas que cubren el rango de los 390 a los 1040 nm. Se instaló a bordo del satélite ENVISAT de la ESA, lanzado en 2002 y operativo hasta 2012. Se trata de un equipo de exploración por empuje (push-broom), que observa la superficie terrestre con un ángulo de visión de ±34.2 grados alrededor de nadir, cubriendo una franja de 1150 km y con una resolución espacial de 300m en el nadir en el modo de resolución completa (FR - full resolution) y de 1200 metros en el modo de resolución reducida (RR - reduced resolution).

El sensor MERIS se había empleado para algunos estudios de área quemada, pero únicamente a escala regional utilizando distintos índices de vegetación (Oliva et al 2011), o mediante la combinación del producto HotSpot (HS) de MODIS con imágenes MERIS y MODIS (González-Alonso et al 2009b). Para todo el planeta, el primer producto generado es el que formó parte del proyecto fire_cci (Alonso-Canas y Chuvieco 2015). Este algoritmo puede clasificarse dentro de la categoría de algoritmo híbrido, ya que combina la información obtenida del contraste térmico (proporcionada por el producto MODIS HS) y de los cambios temporales en las reflectividades de los datos MERIS. Para mejorar la estabilidad temporal y espacial de los datos se decidió crear compuestos

mensuales de infrarrojo cercano (NIR) y GEMI (Pinty y Verstraete 1992). Estos compuestos se basaron en una matriz de Thiessen (Brassel y Reif 1979) en la que cada píxel se etiquetó con la fecha del HS más cercano. El algoritmo consta de dos fases: semillado y crecimiento. En la primera fase, se identificaron los píxeles semilla, es decir los puntos más claramente clasificables como quemados. Para ello se obtuvieron curvas de quemado y no quemado, mediante estadísticas locales (basadas en regiones de 10x10 grados) obtenidas de forma mensual. Estas curvas permitieron definir un umbral de quemado, en el que los píxeles con NIR inferior a este umbral se consideraron posibles semillas. Además de presentar un NIR por debajo del valor umbral, los píxeles analizados debían mostrar una caída en el NIR respecto al mes anterior y tener al menos un HS a una distancia menor de 5 píxeles para ser clasificados como semillas. Si los píxeles cumplían los 3 criterios se clasificaban como semilla. A partir de ellos se realizó el crecimiento de regiones, analizando los píxeles vecinos a estas semillas de forma recursiva. En esta segunda fase se aplicaron de nuevo 3 condiciones. En primer lugar el NIR del píxel examinado debía ser menor que un umbral (más relajado que el de la primera fase). En segundo lugar debía existir una caída respecto al mes anterior. En tercer lugar, tras obtener la diferencia entre el GEMI mensual y la referencia de GEMI del máximo anual, se examinó si esta diferencia era de al menos 0.9 veces la diferencia encontrada en el píxel semilla. Los píxeles que cumplieron estas tres condiciones se clasificaron como quemados, y se comprobó de nuevo si los píxeles inmediatamente vecinos a estos cumplían los criterios a su vez. La descripción completa de estos pasos puede verse en Alonso-Canas y Chuvieco (2015).

El algoritmo descrito se utilizó para generar un producto global de área quemada para el periodo 2006 a 2008. Se obtuvieron estimaciones de área quemada que varían entre 3.6 y 3.8 millones de km^2. Los patrones espaciales y de estacionalidad son consistentes entre estos 3 años y con otros productos de área quemada. La comparación con los tres años de datos derivados de GFED mostró una gran correlación entre este producto y el obtenido mediante el algoritmo MERIS. Los resultados de validación, obtenidos a partir de más de 100 pares de imágenes Landsat (Padilla et al 2015) indicaron una fiabilidad global mayor de 0.95. Los errores de omisión y comisión (OE,CE) fueron menores para las zonas con mayor proporción de área quemada (OE = 0.51, CE = 0.52) siendo algo mayores en zonas con muy baja proporción de área

quemada (OE=0.74, CE = 0.60). Agrupando estos dos resultados se obtuvo una fiabilidad del 0.996, un error de comisión de 0.64 y un error de omisión de 0.76.

Una de las limitaciones principales del sensor MERIS para este tipo de estudios es su resolución temporal, particularmente cuando se trabaja con la versión alta resolución. A modo de ejemplo en la figura 1 se muestran las observaciones válidas anuales que se obtienen para las 4 zonas de interés. Se puede observar que en latitudes altas el número de observaciones puede no sobrepasar las 30 imágenes por año. También el número de observaciones válidas será menor en zonas con alta cobertura nubosa.

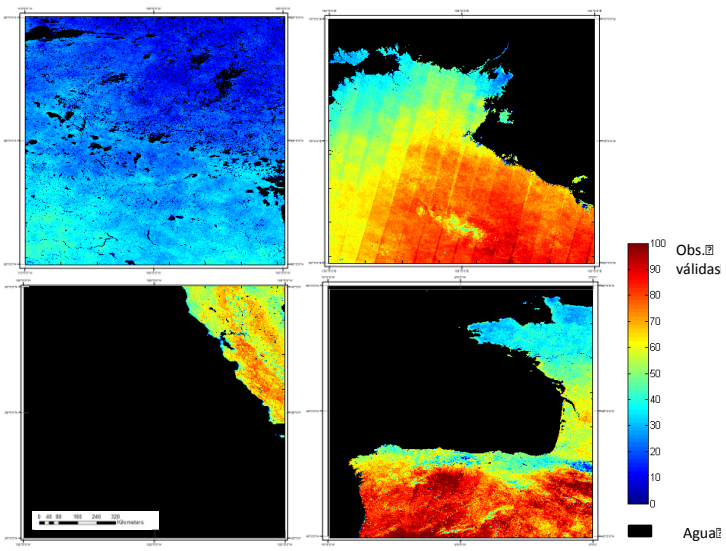

Figura 1. Número de imágenes válidas en el 2008 para 4 zonas de interés: Canadá, Australia, California y Península Ibérica.

MERIS presenta una serie de bandas estrechas en el NIR, útiles para la detección de áreas quemadas. Sin embargo, otras bandas útiles como puede ser el SWIR el TIR no están presentes en este sensor, lo que puede dificultar la capacidad de detección en determinadas regiones.

Además, las series temporales presentaban una variabilidad. Esto puede dar lugar a errores de comisión u omisión. Un ejemplo de la variabilidad de estas series se puede ver en la figura 2. En ella vemos las bandas 10 y 8 de MERIS para un píxel de Angola en el año 2008. Se resalta también la fecha de posible quemado indicada por el HS en rojo.

Se puede ver como en el primer caso el ruido no afecta a la detección mientras que en el segundo estaríamos frente a un posible error de omisión, además de presentar una caída en el NIR en el día 90 mucho mayor que la presentada en la fecha del posible incendio.

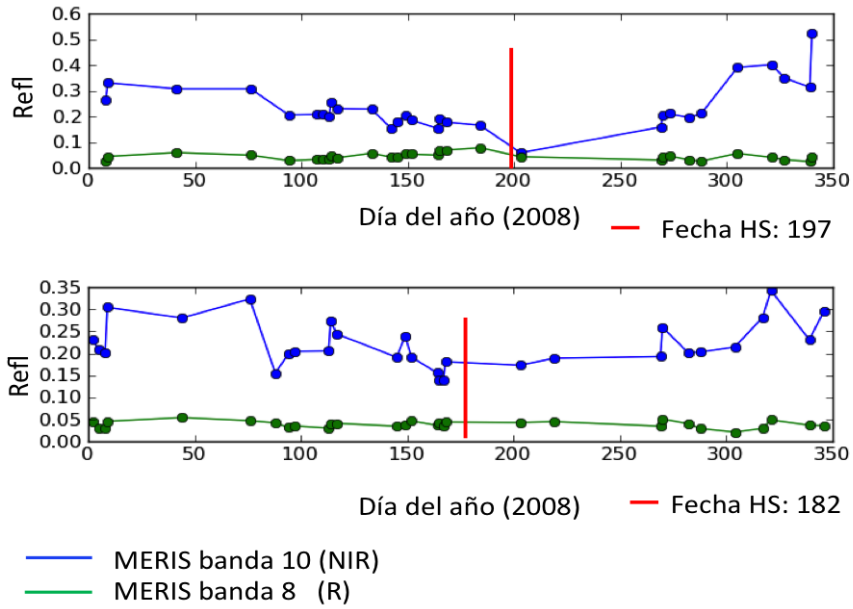

Figura 2. Evolución temporal de la reflectividad para las Bandas 8 y 10 del MERIS en dos píxeles quemados en Angola (datos de 2008)

.

El algoritmo fue diseñado para minimizar estos efectos, así como posibles confusiones con sombras de nubes, con regiones con suelos oscuros o que pudiesen sufrir inundaciones.

2. Objetivos.

En el estudio presentado en este artículo se buscó analizar en detalle a que se debían los errores de omisión y comisión en relación con las fases de la primera versión global del algoritmo de áreas quemadas para datos MERIS, así como mejorar estos resultados incluyendo modificaciones en ambas fases, dando lugar a la segunda versión del algoritmo. Se pretendía reducir los errores de omisión y comisión encontrados en los resultados de la primera versión. Para ello, se analizaron las dos fases del algoritmo teniendo en cuenta las técnicas utilizadas (formación del compuesto, condiciones en las

semillas, condiciones de crecimiento). De cara a abordar este problema, se realizó una comparación en áreas más extensas que las utilizadas en la validación en las que se pretendía comparar los resultados de MERIS de forma anual. Este ejercicio buscaba complementar la validación realizada con las imágenes Landsat ya que los perímetros derivados de estas imágenes solo permitían obtener resultados para las fechas de estas imágenes, pudiendo inducir a errores de omisión y comisión que en realidad estaban relacionados con el fechado, y no con la detección en si. Por esta razón, se seleccionaron cuatro zonas de comparación: Australia, Canadá, California y Península Ibérica (figura 3), donde existían perímetros de áreas quemadas obtenidos por autoridades locales.

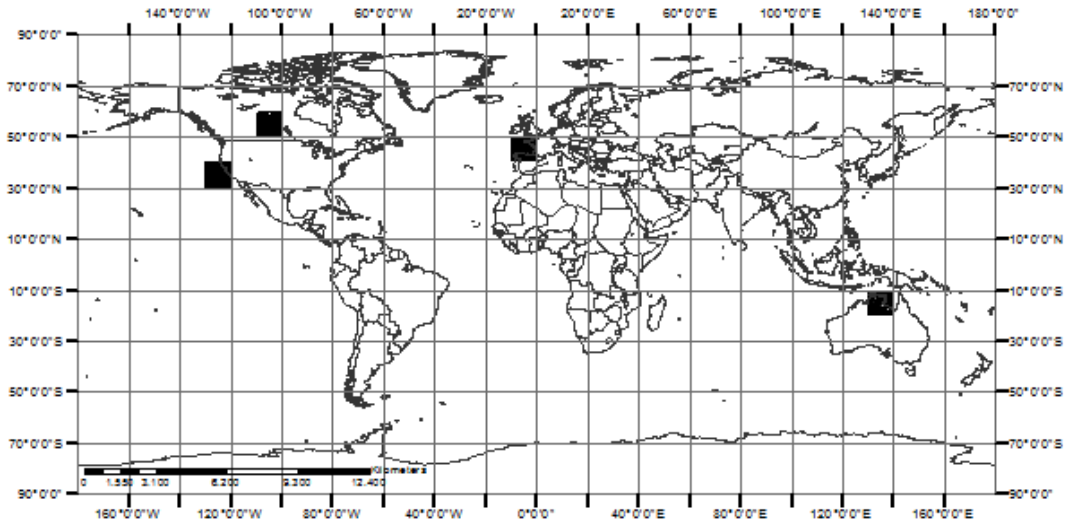

Figura 3. Localización de las 4 zonas seleccionadas para la comparación del producto MERIS con perímetros de incendios.

3. Metodología.

3.1. Problemas detectados en la primera versión del algoritmo MERIS.

En relación con los resultados obtenidos mediante la validación (Padilla et al 2015) se observó como la versión 1 del algoritmo de MERIS tenía tendencia a la subestimación de las áreas quemadas. También a partir de la comparación de perímetros (tabla 1 en la sección de resultados) se pudo ver que para los tres años de datos analizados, en tres de las cuatro zonas de interés los errores de omisión superaban a los de comisión. Esto se debe principalmente a dos motivos: por un lado un número de incendios no estaba siendo detectado en la fase de semillado y por otro lado

las condiciones de crecimiento eran demasiado estrictas no llegando a identificar la totalidad de la mancha de quemado y dando lugar a incendios fragmentados. Un ejemplo de fragmentación de incendio en California se puede ver en la figura 4.

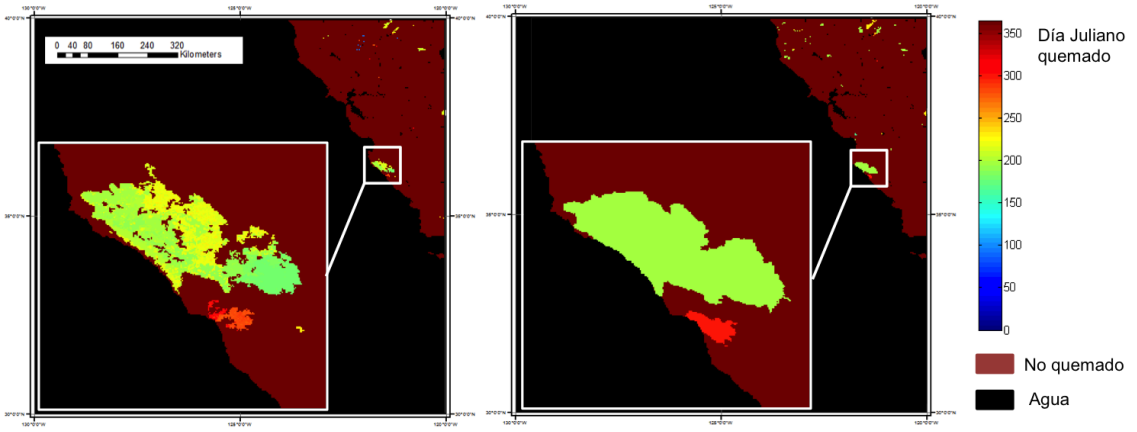

Figura 4. Fragmentación de incendio en la zona de estudio de California. A la izquierda el producto de AQ de MERIS para el año 2008, con una ampliación del incendio principal. A la derecha los perímetros de CALFIRE con una ampliación del mismo incendio.

Además, el crecimiento se veía dificultado por la presencia de estructuras geométricas en el compuesto, derivadas de la matriz de Thiessen y de la agrupación de las distintas imágenes en la formación del compuesto. Un ejemplo de estas estructuras geométricas puede verse en la figura 5.

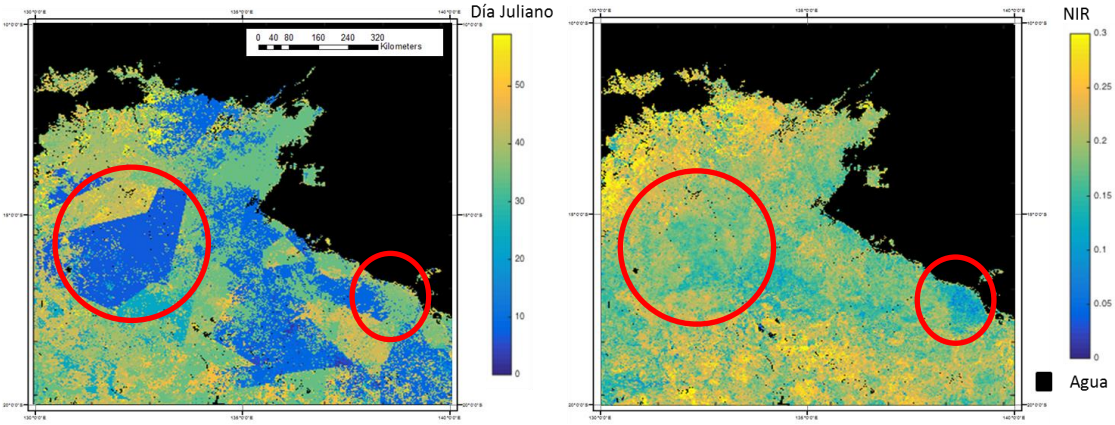

Figura 5. A la izquierda matriz de fechado (día Juliano) para Australia en enero de 2008. Esta matriz se obtiene mediante las imágenes MERIS, y se basa en la matriz de Thiessen obtenida mediante los HS. A la derecha compuesto NIR asociado a la matriz de fechado. En rojo se resalta la presencia de estructuras geométricas en ambos compuestos.

Para mejorar los resultados obtenidos con la primera versión del algoritmo se buscaba aumentar la detección de píxeles quemados, tanto en la fase de semillado como en la de crecimiento. Para ello, se realizaron modificaciones sobre las condiciones generales en la forma de generar las semillas y el crecimiento, estudiando el impacto de estas variaciones sobre la detección.

3.2. Áreas de validación preliminar.

Las distintas pruebas realizadas sobre el algoritmo MERIS se aplicaron a cuatro zonas de estudio en las que se realizó una comparación frente a una serie de perímetros de referencia disponibles, y que además cubrían distintos tipos de ecosistemas (boreal, templado y tropical) (figura 3). Se consideraron zonas mucho más amplias (> 2.500.000 km^2 frente a los < 34.000 km^2 de las escenas Landsat), lo que permitió realizar un mejor análisis de las zonas en las que el área quemada era grande. Además en este caso se compararon los productos de AQ para todo el año, pudiendo así hacer frente a algunos problemas derivados de las zonas Landsat de validación, que únicamente tienen en cuenta períodos cortos de tiempo. Las fuentes de las que se obtuvieron los perímetros de área quemada se detallan a continuación:

- Canadá: Los perímetros se obtuvieron del sistema de Incendios Canadiense. Este sistema incluye los incendios de la base de datos de incendios nacionales canadienses (Canadian National Fire Database (CNFDB)). Es una colección que agrupa datos provenientes de distintas agencias de gestión de incendios Canadienses (provincias, territorios y Parks Canada). De esta base de datos se seleccionó una región de 1.150.000 km^2 cubriendo los bosques boreales de Alberta y Saskatchewan.

- Australia: se seleccionó una región situada al norte de Australia para realizar la comparación de perímetros. Estos se descargaron de la base de datos de incendios del Norte de Australia (North Australian Fire Information database (NAFI)). La zona seleccionada cubre 750,000 km^2 y está cubierta principalmente por sabana y bosque tropical. Los perímetros de AQ de NAFI fueron procesados por el Centro de investigación de la Universidad Charles Darwin. Estos

perímetros se obtuvieron mediante comparación multi-temporal de imágenes MODIS a 250m, utilizando segmentación e interpretación visual.

- California: los perímetros para esta región se obtuvieron del Fire and Resource Assessment programme (FRAP). La región de validación es de 150.000 km^2 incluyendo California y los estados vecinos.

- Península Ibérica: los perímetros se obtuvieron del sistema europeo de información de incendios forestales (European Forest Fire Information System (EFFIS)). EFFIS utiliza también imágenes MODIS para obtener los perímetros de AQ. La región utilizada incluye parte de la península ibérica, cubriendo un área de 500,000 $km^{2.}$

Estas zonas pueden considerarse idóneas para una primera evaluación de la calidad de la detección del área quemada, al cubrir un periodo anual completo, de zonas bastante grandes, y en cuatro ecosistemas bastante impactados por el fuego. No obstante, la comparación de nuestros resultados con esta información de referencia no puede considerarse como una validación estricta, ya que se trata de una muestra seleccionada sin criterios estadísticos, y los perímetros proceden de distintas metodologías. En cualquier caso, puede considerarse como una comparación preliminar, en la línea del análisis de otros autores trabajando con algoritmos globales (Chang y Song 2009, González-Alonso y Merino-de-Miguel 2009a, Pu et al 2007, Giglio et al 2003, Roy y Boschetti 2009). Los datos facilitados por estas cuatro bases de datos fueron proyectados a coordenadas geográficas, para así poder compararlos con los datos de AQ del producto MERIS.

3.3. Mejoras propuestas a raíz del análisis de resultados.

3.3.1. Mejoras en el semillado.

Se consideró que una buena forma de abordar el problema consistía en aumentar el número de perímetros detectados en esta fase sin que esto modificase de forma sustancial los errores de comisión al aplicar las condiciones de crecimiento de regiones.

Para evaluar como afectaban las modificaciones introducidas al rendimiento del algoritmo se decidió evaluar cuantos perímetros se detectaban en cada uno de los casos evaluados. Para ello se realizó una clasificación de los incendios en función del tamaño (<100ha, entre 100 y 1000ha, entre 1000 y 10000 ha y mayor que 10000ha). Esto permitió también hacernos una idea del tipo de incendios que se estaban omitiendo, pudiendo ver que parte era inherente a las características del sensor y que parte estaba relacionada con el algoritmo. Se obtuvieron los resultados para la versión 1 separando entre incendios detectados y no detectados. Se probaron distintas modificaciones en la fase de semillado para ver como afectaban al número de perímetros detectados. Las pruebas realizadas son las siguientes:

- Test 1: en esta prueba se mantuvieron las condiciones de la primera fase pero extendiendo la distancia a la que podría encontrarse un HS, es decir pasando de una matriz de 9x9 píxeles a una matriz de 16x16. Esta opción permitiría aumentar el número de píxeles semilla que se encuentran cercanos a un HS. El uso de una matriz de 16x16 cubriría una zona alrededor del HS relativamente cercana al incendio, considerando así que los píxeles a esta distancia que cumpliesen el resto de condiciones serían también semillas de ese mismo incendio. Esto permitiría analizar en la fase de semillado píxeles algo más alejados del HS y que podrían haberse quemado, pero que podrían no haberse detectado como HS al no tratarse de incendios activos en ese momento, o haber sido omitidos por el sensor. Esta condición no permitiría detectar un mayor número de incendios, pero sí tener un muestreo mayor de los incendios ya detectados, lo que ayudaría a mejorar la detección final una vez aplicado el crecimiento, disminuyendo la fragmentación.

- Test 2: en esta prueba se mantuvieron las condiciones de la primera fase pero se eliminó la restricción de tener para cada píxel una caída en el valor del NIR respecto al mes anterior. Esta opción se probó para analizar como afectaba el ruido de las series temporales de MERIS a la fase de semillado. Es decir, podría darse el caso de que la serie temporal de MERIS afectada por el ruido (figura 2), no permitiese ver la caída en un píxel que realmente se hubiera quemado. Es una prueba intermedia al filtrado posterior que se aplica mediante las medianas (tests 4 y 5). Al ser menos restrictivos con esta

condición el número de perímetros detectados podría aumentar, así como el número de píxeles semilla dentro de cada incendio.

- Test 3: este test es una modificación del test 2. Dado que no se estaba exigiendo que existiera una caída en el NIR para clasificar un píxel como semilla, se estaba siendo menos restrictivo con las condiciones de semillado y eso podría dar lugar a errores de comisión no deseables. Para contrarrestar esto, se buscó que en la matriz de 9x9 alrededor del píxel analizado existieran dos HS en lugar de uno solo como se hacía en la primera versión del algoritmo. Esto permitiría evitar en parte los errores de comisión debidos a los HS, ya que tendría que existir más de una detección de incendio activo en las inmediaciones del píxel para que éste fuese clasificado como semilla. Por lo tanto con esta condición se buscó ampliar el número de incendios detectados, así como el número de semillas por incendio, ya que no se aplicó la restricción de que existiera una caída en el NIR, pero siendo algo más restrictivos que en el caso anterior (test 2), limitando así en mayor medida los errores de comisión. Como contrapunto esta restricción podría limitar el número de incendios detectados en las regiones en que la densidad de HS fuera menor.

- Test 4: para esta prueba se eliminó también la condición de que existiese una caída del valor del NIR entre el mes analizado y el mes anterior. En su lugar se probó a buscar esta tendencia de caída en el NIR en la serie de datos, es decir en una ventana temporal más amplia. Para ello se comprobó si la mediana de los valores del NIR de los 3 meses anteriores a la posible fecha de quemado era mayor que la mediana de los valores del NIR posteriores a la fecha de quemado, en cuyo caso el píxel podría ser clasificado como semilla si cumplía el resto de condiciones de la versión 1. Por lo tanto con esta modificación se buscaba hacer frente a los posibles errores de comisión de los HS, analizando el comportamiento temporal de los datos MERIS en una ventana mayor a la utilizada previamente, pudiendo así disminuir un filtrado erróneo de los HS debido al ruido inherente a los datos MERIS. Esto permitiría ampliar el número de incendios detectados, así como el número de semillas por incendio.

- Test 5: en este caso al igual que en el anterior (Test 4) se buscaba hallar una tendencia temporal en los valores del NIR pero en períodos de tiempo más cortos. El

objetivo era por tanto realizar un filtrado de los HS para evitar errores de comisión. Para ello se calculó la mediana pre y post incendio con los valores obtenidos a partir de las imágenes individuales, no de los compuestos. En lugar de utilizar únicamente 3 valores como en el caso anterior se extendió hasta 5 valores pre y post incendio, ya que al tratarse de imágenes individuales y no de compuestos la permanencia del incendio debería mantenerse para este período de tiempo. Esta nueva medida era, respecto a la anterior, más sensible a la detección de incendios en los que la señal de quemado post incendio no permaneciese mucho en el tiempo (zonas tropicales). Respecto a la versión 1 permitía obtener un filtrado más robusto, pudiendo aumentar el número de incendios detectados y el número de semillas por incendio.

3.3.2. Mejoras en la fase de crecimiento.

También se probaron distintas opciones para el crecimiento. Los errores de la fase de crecimiento de la primera versión del algoritmo estaban relacionados con la forma en la que se generaba el compuesto mensual (creando algunas estructuras geométricas derivadas de la matriz de Thiessen - figura 5) y también con las condiciones demasiado restrictivas de crecimiento para algunos incendios. Las pruebas realizadas se diseñaron para poder modificar estas dos características y así reducir la omisión relacionada con el crecimiento. Se detallan a continuación las pruebas realizadas para las 4 zonas de interés:

- Test 6: se utilizaron las mismas condiciones de crecimiento de la versión 1 pero aplicadas a las imágenes individuales del sensor MERIS en lugar de al compuesto obtenido en la primera fase del algoritmo. En este caso, se buscó para cada semilla la primera imagen disponible de ese mismo día, o la primera inmediatamente posterior y se aplicó el crecimiento sobre esta imagen. El objetivo de esta prueba era analizar el funcionamiento de las condiciones de crecimiento en las imágenes individuales, en las que el incendio podía ser más fácilmente identificable al existir un mayor contraste entre el quemado y el no quemado respecto al compuesto. Además, se asumía que las imágenes individuales estarían libres de las estructuras geométricas derivadas de la matriz de Thiessen utilizada para crear el compuesto.

- Test 7: en el caso de las imágenes individuales, éstas pueden no cubrir de forma completa el incendio. Además, al no realizarse ningún tipo de agrupación, podrían existir muy pocos datos válidos en la imagen en el caso de que hubiese nubes en el momento de paso del sensor. Para hacer frente a esto, se obtuvo un nuevo compuesto, que cubría un período temporal menor que el utilizado en la versión 1, con lo que la permanencia de la señal de quemado sería más fácilmente identificable, y libre de estructuras geométricas. Este compuesto se obtuvo con el mínimo de NIR cada diez días y agrupando las semillas de 10 en 10 días. Se aplicó el crecimiento sobre este nuevo compuesto.

- Test 8: se observó en determinadas regiones que los compuestos de diez días podrían seguir teniendo pocos datos (debido a una mayor persistencia de nubes o peor cobertura del sensor), por lo que en esta prueba se agruparon imágenes en períodos de 20 días para generar el compuesto, buscando las mismas ventajas que en el test 7.

- Test 9: el objetivo de esta prueba era testar el funcionamiento de otras condiciones de crecimiento distintas a las utilizadas en la versión 1. Se buscó un método en el que el crecimiento estuviese adaptado a cada incendio, en lugar de utilizar las estadísticas generales para la zona de 10x10 grados halladas en la versión 1, que se adaptaban en menor medida a cada incendio dentro de esta zona de 10x10 grados. Para esta prueba se aplicó la condición de que el píxel se considerase quemado si su NIR era menor que la mediana + la desviación estándar de los píxeles vecinos quemados. Las estadísticas se calcularon para los píxeles quemados en la matriz de 5x5 alrededor del píxel analizado y únicamente en el caso de que hubiese al menos 3 píxeles ya clasificados como quemados dentro de esta matriz.

- Test 10: se aplicaron las condiciones del test 9 de crecimiento a las imágenes diarias, buscando por lo tanto el mayor contraste existente en las imágenes individuales, así como evitar las estructuras geométricas del compuesto.

4. Resultados.

4.1. Comparación con los perímetros para las 4 zonas analizadas.

En la tabla 1 se muestra la comparación entre los perímetros de nuestras cuatro zonas de referencia y los resultados de la versión 1 del algoritmo (Alonso-Canas y Chuvieco 2015), del que partimos para elaborar este artículo. Se puede ver como los valores de omisión y comisión son más bajos que los obtenidos por Padilla et al (2015) mediante un muestreo estadístico global basado en datos Landsat. En nuestra opinión, esta divergencia puede explicarse porque nuestros datos están menos afectados por la fiabilidad en la detección temporal, que afecta más cuando los periodos de referencia que se comparan son más cortos (pocas semanas en el caso de las imágenes Landsat, frente a todo el año en este caso), y una superficie más grande (frente a la zona abarcada por los pares de imágenes Landsat).

Se observa que la zona de Australia es la que más se quema para los 3 años, con una proporción de área quemada (BAp) que varía entre 0.18 y 0.45. La Península Ibérica tiene la menor ocurrencia de incendios (<0.001), mientras que las zonas de California y Canadá varían entre 0.007 - 0.013 y 0.013-0.027, respectivamente.

Tabla 1. Tabulación cruzada del producto de área quemada de MERIS con perímetros de incendios para 4 regiones en los años 2006 a 2008. CE = error de comisión, OE = error de omisión, OA = fiabilidad global, BAp = proporción de área quemada.

	2006				2007				2008			
	CE	OE	OA	BAp	CE	OE	OA	BAp	CE	OE	OA	BAp
Australia	0.085	0.425	0.789	0.447	0.111	0.429	0.808	0.250	0.176	0.444	0.850	0.181
California	0.326	0.341	0.997	0.007	0.354	0.333	0.996	0.010	0.144	0.438	0.996	0.013
Canadá	0.306	0.467	0.981	0.027	0.032	0.560	0.993	0.013	0.102	0.753	0.981	0.026
Península Ibérica	0.440	0.236	0.998	0.002	0.655	0.395	0.999	0.001	0.851	0.643	0.999	<0.001
TOTAL	0.117	0.424	0.966	0.029	0.125	0.431	0.971	0.025	0.147	0.472	0.975	0.019

4.2. Resultados semillado.

Se detallan los resultados de las pruebas realizadas en la tabla 2. Se muestra el porcentaje de perímetros detectados con cada Test en función del tamaño del incendio.

Tabla 2. Número total de perímetros y porcentaje de perímetros detectados para las 4 zonas de interés en la versión 1 y con las distintas modificaciones (tests 1 a 5) realizadas en la fase de semillado, para el año 2008.

	Zona de estudio	**Tamaño del incendio (has)**			
	AUSTRALIA	<100	<1000	<10000	>10000
Perímetros detectados	Nº total de perímetros	12174	4652	1373	209
	v1	21%	52%	90%	99%
	Test 1	46%	80%	96%	100%
	Test 2	74%	99%	100%	100%
	Test 3	25%	59%	93%	100%
	Test 4	22%	57%	92%	100%
	Test 5	37%	73%	94%	100%
	CANADÁ	<100	<1000	<10000	>10000
	Nº total de perímetros	30	20	28	34
	v1	0%	25%	54%	88%
	Test 1	0%	35%	57%	88%
	Test 2	17%	95%	100%	100%
	Test 3	3%	50%	82%	100%
	Test 4	3%	50%	68%	94%
	Test 5	3%	45%	75%	94%
	PENINSULA IBÉRICA	<100	<1000	<10000	>10000
	Nº total de perímetros	24	19	4	0
	v1	33%	68%	50%	0%

	Test 1	50%	79%	50%	0%
	Test 2	100%	100%	100%	0%
	Test 3	42%	68%	50%	0%
	Test 4	33%	68%	50%	0%
	Test 5	54%	79%	50%	0%
	CALIFORNIA	<100	<1000	<10000	>10000
	Nº total de perímetros	98	48	25	5
	v1	4%	8%	60%	80%
	Test 1	5%	29%	88%	100%
	Test 2	7%	46%	92%	100%
	Test 3	5%	27%	88%	100%
	Test 4	4%	8%	60%	80%
	Test 5	6%	29%	80%	100%

Analizando los resultados de la tabla 2 se puede ver como cualquiera de las pruebas realizadas en este trabajo aumenta el número de incendios detectados respecto a la versión 1 del algoritmo. Aun así es importante remarcar que conviene no elegir la opción que más incendios detecta, si no aquella que combina un aumento en la detección limitando a la vez los posibles errores de comisión. Teniendo en cuenta los resultados obtenidos aplicando el crecimiento de regiones a las distintas opciones, las características de los datos MERIS y el número de perímetros detectados se decidió elegir como nueva condición de semillado la mediana diaria con 5 imágenes pre y post (test 5). Esta configuración es más robusta al ruido de los datos que la que se había elegido en la versión 1 del algoritmo, permitiendo detectar un mayor número de incendios sin aumentar la comisión de forma excesiva.

4.3. Resultados crecimiento.

Los resultados de estas pruebas se detallan en la tabla 3. Se analizan los errores de omisión y comisión para cada uno de estos casos para las 4 zonas de interés en el año 2008.

Tabla 3. Errores de comisión y omisión del área quemada obtenidos para las 4 zonas de estudio en el año 2008 con las distintas versiones de crecimiento.

		Australia	Canadá	Portugal	California
Versión 1	Comisión	0,1756	0,1022	0,8512	0,1437
	Omisión	0,4441	0,7529	0,6429	0.4379
Test 6	Comisión	0.2243	0.1833	0.9708	0.2804
	Omisión	0.3881	0.5107	0.5370	0.3187
Test 7	Comisión	0.1820	0.1556	0.9866	0.3872
	Omisión	0.5192	0.4563	0.5050	0.3067
Test 8	Comisión	0.2720	0.1540	0.9880	0.4174
	Omisión	0.3570	0.4450	0.5021	0.3022
Test 9	Comisión	0.4715	0.2718	0.9935	0.6194
	Omisión	0.1102	0.3524	0.4910	0.1695
Test 10	Comisión	0.3757	0.1955	0.9912	0.4400
	Omisión	0.2607	0.3825	0.5163	0.2698

Se puede ver como en todos los casos los errores de omisión disminuyen y los de comisión aumentan respecto a la versión 1. El crecimiento sobre imágenes individuales (test 6) permite reducir en gran medida los errores de omisión para las regiones de Australia, Canadá y California. Las técnicas de compuesto a 10 y 20 días (Test 7 y 8 respectivamente) obtienen resultados similares para las regiones de Australia y Canadá, pero aumenta mucho la comisión para la región de California. El nuevo crecimiento (Test 9 y 10), utilizando la técnica de la media y desviación estándar, disminuye los errores de omisión de forma sustancial pero aumenta en la misma proporción los errores de comisión.

A través del análisis de estos resultados se concluyó que el crecimiento sobre imágenes individuales (test 6) aplicando el mismo tipo de crecimiento desarrollado en la primera fase sería elegido para la versión 2 del algoritmo. Un ejemplo del impacto de

estos cambios en las detecciones se puede ver en la figura 6. En ella se presentan para la zona de estudio de Canadá en 2008, los resultados de la versión 1 respecto a los de la versión 2. Se puede observar como el número de incendios detectados es mayor y también como la detección de cada mancha mejora ya que éstas se detectan de forma más compacta, teniendo menos fragmentación en cada incendio.

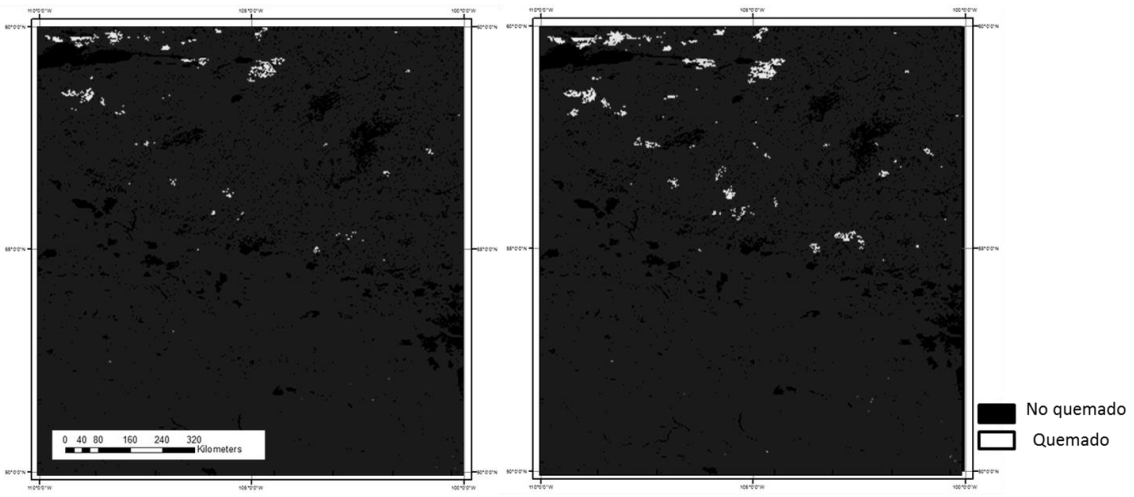

Figura 6. AQ con las versiones 1 (izquierda) y 2 (derecha) del algoritmo MERIS para Canadá 2008.

5. Discusión.

Mediante las pruebas realizadas se ha buscado mejorar los errores de omisión del algoritmo AQ MERIS, evitando aumentar los errores de comisión. Es importante destacar que algunas de las posibles limitaciones a la hora de mejorar estos resultados están relacionadas con las características del propio sensor. La baja frecuencia temporal no permite una implementación de técnicas de series temporales y las bandas presentes en este sensor aún siendo adecuadas presentan una serie de limitaciones. En efecto la región espectral del NIR es aquella en la que la señal de incendios recientes es más clara. Aún así la utilización de otras bandas ha demostrado ser útil especialmente en algunos casos. Por ejemplo el SWIR puede utilizarse en combinación con el NIR por medio de índices que permiten discernir mejor las superficies quemadas que los obtenidos mediante la combinación de VIS/NIR (Roy y Landmann 2005b). Los resultados aquí presentados buscan mejorar los ya obtenidos en la primera fase,

teniendo en cuenta las limitaciones inherentes al sensor MERIS, que no dispone de bandas en el SWIR.

La nueva técnica de semillado identificada (test 5) permite aumentar la detección de perímetros en las regiones de interés en un 16% para las regiones de Australia y Península Ibérica, un 11% en California y un 12% en Canadá. Esta nueva implementación es más robusta que la utilizada previamente ya que al obtener una mediana de los 5 valores pre y post incendio, estamos haciendo frente al ruido presente en los datos. La comprobación de una caída en el NIR en la fecha de quemado respecto al día anterior es menos robusta frente a este ruido, ya que podría darse el caso de que este valor no fuese mayor debido al ruido de la serie, aun tratándose de un píxel quemado, mientras que mediante el cálculo de la mediana el impacto de este efecto quedaría mitigado. Cabe destacar también que el semillado estará influenciado por los errores de omisión y comisión del producto HS. En efecto, podemos comprobar que la región de la Península Ibérica presenta unos errores de comisión mayores que las otras 3 zonas estudiadas. Estos resultados concuerdan con el análisis realizado por Hantson et al (2013), en el que se identifica la región de Portugal como una de las regiones en las que los errores de comisión de los HS son más elevados (no hay que olvidar que nuestro algoritmo se apoya sustancialmente en la detección de puntos de calor que hace el producto MODIS). Se espera obtener resultados similares en regiones como África del Sur o Brasil, ya que estas también presentaron unos mayores errores de comisión en este estudio.

En cuanto a las opciones de crecimiento probadas se ha decidido elegir el crecimiento de la versión 1 aplicado sobre las imágenes diarias (test 6) como la configuración a utilizar en la segunda versión del algoritmo. Se considera que esta es la mejor opción como compromiso entre los errores de omisión y comisión obtenidos y en comparación con las otras opciones testadas. Esta configuración ofrece la posibilidad de ser más exacta en la detección de incendios que la utilizada en la primera fase, ya que las imágenes individuales presentan unas características más claras para la identificación de los incendios. Además no presentarán las estructuras geométricas derivadas de la matriz de Thiessen y de la agrupación de las distintas imágenes en la formación del compuesto (figura 5), que dificultaban la detección sobre el compuesto

mensual obtenido en la primera versión del algoritmo. Como contrapunto es necesario señalar que una importante limitación de esta configuración está relacionada con la imagen a analizar en cada caso. En los casos en los que las imágenes adquiridas no cubran toda la zona de interés del incendio, o en el caso de que la cobertura nubosa sea muy elevada, la detección de incendios sobre imágenes individuales empeorará la realizada a partir de compuestos, ya que no se buscará la continuación de ese incendio en las imágenes sucesivas (salvo que existiesen nuevos HS en los días posteriores). Las pruebas realizadas agrupando los HS de 10 en 10 días y obteniendo compuestos de mínimo NIR de 10 o 20 días (tests 7 y 8) se consideraron como una posible alternativa de mejora a estas limitaciones, pero los errores de omisión obtenidos en el primer caso, y de comisión obtenidos en el segundo, indicaron que no era la opción más adecuada. Estos cambios se deben en parte a que el compuesto creado no es suficientemente estable debido al ruido de las imágenes MERIS y a que la agrupación de semillas puede dar lugar a crecimientos en regiones en las que el incendio ya no puede ser detectado, obteniendo como resultado importantes errores de comisión. Se probó también una nueva técnica de crecimiento, modificando el presentado por Libonati et al (2014). Esta implementación (Tests 9 y 10) que calculaba la mediana y desviación estándar de cada incendio se consideró potencialmente interesante ya que permitía por medio de estos estadísticos adecuarse de forma más concreta a las condiciones particulares de cada evento, en lugar de utilizar las estadísticas obtenidas para las regiones de 10x10 grados. Mientras los errores de omisión disminuyen de la forma esperada, los resultados obtenidos mostraron unos errores de comisión elevados respecto a las otras pruebas realizadas.

Además de los resultados presentados en la sección anterior, fueron probadas otras opciones de crecimiento, como los filtros de bordes y segmentación, tanto sobre compuestos NIR como utilizando también las bandas 5 y 8 de MERIS. Los resultados de estas pruebas no permitieron mejorar los ya obtenidos con la versión 1 del algoritmo por lo que estas posibles implementaciones fueron descartadas. El motivo por el que se considera que estas opciones de crecimiento no fueron satisfactorias está relacionado con el número de imágenes disponibles y con las variaciones que éstas sufren en el tiempo, así como por la imposibilidad de hallar condiciones que funcionasen adecuadamente para estas implementaciones a nivel global. El uso de las mismas

condiciones aplicadas a nivel global disminuye la posibilidad de obtener resultados exactos en todas las regiones, ya que los ecosistemas y dinámicas son muy distintos a nivel global. Para obtener sucesivas mejoras en la detección de incendios se necesitarán series de datos más completas y también tratar el ruido inherente a estas series mediante mecanismos de filtrado o suavizado.

El algoritmo MERIS ha sido desarrollado buscando sacar provecho de la mayor resolución proporcionada por este sensor, respecto a otros productos de área quemada actualmente existentes. Se ha visto como mediante este producto de área quemada es posible realizar la detección de incendios más pequeños, siendo esto de gran relevancia (Randerson et al 2012). Además, el instrumento OLCI a bordo del satélite Sentinel 3, presenta características similares a las de MERIS, pero con una resolución temporal mayor, por lo que los desarrollos que estamos realizando para MERIS podrían ser de gran interés para el programa Sentinel-3, que tiene vocación de servir como una misión operativa y, por tanto, tiene garantizada una mayor continuidad.

6. Conclusiones.

En este artículo se han mostrado los avances para una nueva versión de un algoritmo global para la detección de áreas quemadas con datos MERIS. Se han presentado los resultados de validación, así como la comparación con otros productos y con perímetros en 4 zonas de estudio. El análisis de estos resultados permitió identificar los puntos en los que se podía mejorar este algoritmo. Mediante un nuevo estudio de estos errores y de las condiciones tanto en las fases de semillado como de crecimiento, se realizaron una serie de modificaciones que permitieron obtener nuevos mapas de área quemada y caracterizar los errores con cada una de las opciones probadas. Se identificaron las nuevas condiciones que permitían mejorar los resultados obtenidos hasta la fecha, disminuyendo los errores de omisión en un 5.6%, 24%, 11% y 12% para las zonas analizadas de Australia, Canadá, Península Ibérica y California respectivamente. Estos avances formarán parte de la segunda versión del algoritmo MERIS. Esta nueva versión se utilizará para procesar la serie completa de 10 años de MERIS (2002-2012) al inicio de la segunda fase del proyecto fire_cci.

Referencias bibliográficas.

Alonso-Canas I. y Chuvieco E. (2015): "Global burned area mapping from ENVISAT-MERIS and MODIS active fire data", *Remote Sensing of Environment*,163, 140-152.

Bastarrika, A., Chuvieco, E., y Martín, M.P. (2011): "Mapping burned areas from Landsat TM/ETM+ data with a two-phase algorithm: balancing omission and commission errors", *Remote Sensing of Environment*, 115, 1003-1012.

Bowman, D.M.J.S., Balch, J.K., Artaxo, P., Bond, W.J., Carlson, J.M., Cochrane, M.A., D'Antonio, C.M., DeFries, R.S., Doyle, J.C., Harrison, S.P., Johnston, F.H., Keeley, J.E., Krawchuk, M.A., Kull, C.A., Marston, J.B., Moritz, M.A., Prentice, I.C., Roos, C., Scott, A., Swetnam, T., Van der Werf, G., y Pyne, S.J. (2009): "Fire in the Earth system", *Science*, 324, 481-484.

Brassel, K.E., y Reif, D. (1979): "A procedure to generate Thiessen polygons", *Geographical Analysis*, 11, 289-303.

Canadian National Fire Database (CNFDB) (2008): cwfis.cfs.nrcan.gc.ca/ha/nfdb/ (consultado 02-07-2015).

Chuvieco, E., Opazo, S., Sione, W., Del Valle, H., Anaya, J., Di Bella, C., Cruz, I., Manzo, L., López, G., Mari, N., González-Alonso, F., Morelli, F., Setzer, A., Csiszar, I., Kanpandegi, J.A., Bastarrika, A., y Libonati, R. (2008): "Global Burned Land Estimation in Latin America using MODIS Composite Data", *Ecological Applications*, 18, 64-79.

Chang, D., y Song, Y. (2009): "Comparison of L3JRC and MODIS global burned area products from 2000 to 2007", *Journal of Geophysical Research*, 114, 10.1029/2008JD11361.

Daniau A.L. et al (2012): "Predictability of biomass burning in response to climate changes", *Global Biogeochemical Cycles*, 26.

Eva, H., y Lambin, E.F. (1998): "Burnt area mapping in Central Africa using ATSR data", *International Journal of Remote Sensing*, 19, 3473-3497.

European Forest Fire Information System (EFFIS) (2008): http://forest.jrc.ec.europa.eu/effis/ (consultado 02-07-2015).

Fire and Resource Assessment programme (FRAP) (2008): frap.fire.ca.gov (consultado 02-07-2015).

Fraser, R.H., Li, Z., y Cihlar, J. (2000): "Hotspot and NDVI Differencing Synergy (HANDS): a new technique for burned area mapping over boreal forest", *Remote Sensing of Environment*, 74, 362-376.

Giglio, L., Loboda, T., Roy, D.P., Quayle, B., y Justice, C.O. (2009): "An active-fire based burned area mapping algorithm for the MODIS sensor", *Remote Sensing of Environment*, 113, 408-420.

Giglio, L., J. Descloitres, C. O. Justice y Y. J. Kaufman (2003): "An enhanced contextual fire detection algorithm for MODIS", *Remote Sensing of Environment* 87: 273-282.

González-Alonso, F., y Merino-de-Miguel, S. (2009a): "Integration of AWiFS and MODIS active fire data for burn mapping at regional level using the Burned Area Synergic Algorithm (BASA)", *International Journal of Wildland Fire*, 18, 404-414.

González-Alonso, F., Salgado, V., Calle, V., Casanova, J.L., Sanz, J., de la Fuente, D., Goldammer, J.G., Li, Z., Qin, X., Zhang, X., Deng, G., Liu, Q., Li, G., Cai, H., y Huang, Z. (2009b): "Forest burn in China by means of MERIS and MODIS images", *Dragon 2 Symposium,* June 2009, Barcelona.

Hantson, S., Padilla, M., Corti, D., y Chuvieco, E. (2013): "Strengths and weaknesses of MODIS hotspots to characterize global fire occurrence", *Remote Sensing of Environment*, 131, 152-159.

Hollmann, R., Merchant, C.J., Saunders, R.W., Downy, C., Buchwitz, M., Cazenave, A., Chuvieco, E., Defourny, P., Leeuw, G.d., Forsberg, R., Holzer-Popp, T., y Paul, F. (2013): "The ESA Climate Change Initiative: satellite data records for essential climate variables", *Bulletin of the American Meteorological Society*, doi 10.1175/BAMS-D-11-00254.1

Kasischke, E.S., French, N.H.F., Harrell, P., Christensen, N.L., Ustin, S.L., y Barry, D. (1993): "Monitoring of wildfires in Boreal Forests using large area AVHRR NDVI composite image data", *Remote Sensing of Environment*, 45, 61-71.

Kloster, S., Mahowald, N., Randerson, J., y Lawrence, P. (2012): "The impacts of climate, land use, and demography on fires during the 21st century simulated by CLM-CN", *Biogeosciences*, 9, 509-525.

Krawchuk, M.A., Moritz, M.A., Parisien, M.-A., Van Dorn, J., y Hayhoe, K. (2009): "Global Pyrogeography: the Current and Future Distribution of Wildfire", *PLoS ONE*, 4, e5102.

Libonati R, DaCamara C., Setzera A., Morellia F., de Jesusa S., Candido P., Melchiori A. (2014): " Chapter 6 – Forest Management:Validation of the burned area "(V,W)" Modis algorithm in Brazil", *Advances in forest fire research*.

Mouillot, F., Schultz, M.G., Yue, C., Cadule, P., Tansey, K., Ciais, P., y Chuvieco, E. (2014): "Ten years of global burned area products from spaceborne remote sensing - A review: Analysis of user needs and recommendations for future developments", *International Journal of Applied Earth Observation and Geoinformation*, 26, 64-79.

North Australian Fire Information database (NAFI) (2008): www.firenorth.org.au/nafi2/ (consultado 02-07-2015).

Oliva, P., Martin, P., y Chuvieco, E. (2011): "Burned area mapping with MERIS post-fire image", *International Journal of Remote Sensing*, 32, 4175-4201.

Padilla, M., V. Stehman, S.V., Hantson, S., Oliva, P., Alonso-Canas, I., Bradley, A., Tansey, K., Mota, B., Pereira, J.M., Chuvieco, E. (2015): "Comparing the Accuracies of Remote Sensing Global Burned Area Products using Stratified Random Sampling and Estimation", *Remote Sensing of Environment*, 160, 114-121.

Piccolini, I., y Arino, O. (2000): "Towards a Global Burned Surface World Atlas", *Earth Observation Quartely*, 65, 14-18.

Pinty, B., y Verstraete, M.M. (1992): "GEMI: a non-linear index to monitor global vegetation from satellites", *Vegetatio*, 101, 15-20.

Plummer, S., Arino, O., Ranera, F., Tansey, K., Chen, J., Dedieu, G., Eva, H., Piccolini, I., Leigh, R., y Borstlap, G. (2007): "An update on the GlobCarbon initiative: multi-sensor estimation of global biophysical products for global terrestrial carbon studies", *Envisat Symposium*. Montreux, Switzerland: ESA SP-636.

Pu, R.L., Li, Z.Q., Gong, P., Csiszar, I., Fraser, R., Hao , W.-M., Kondragunta, S., y Weng, F. (2007): "Development and analysis of a 12-year daily 1-km forest fire North America from NOAA/AVHRR data", *Remote Sensing of Environment*, 108, 198-208.

Randerson, J.T., Chen, Y., Werf, G., Rogers, B., y Morton, D. (2012): "Global burned area and biomass burning emissions from small fires", *Journal of Geophysical Research-Biogeosciences*, 117, G04012, doi:10.1029/2012JG002128.

Roy, D.P., Giglio, L., Kendall, J.D., y Justice, C.O. (1999): "Multi-temporal active-fire based burn scar detection algorithm", *International Journal of Remote Sensing*, 20, 1031-1038.

Roy, D., Jin, Y., Lewis, P., y Justice, C. (2005a): "Prototyping a global algorithm for systematic fire-affected area mapping using MODIS time series data", *Remote Sensing of Environment*, 97, 137-162.

Roy, D. P., y Landmann, T. (2005b): "Characterizing the surface heterogeneity of fire effects using multi-temporal reflective wavelength data", *International Journal of Remote Sensing*, 26, 4197–4218.

Roy, D. y L. Boschetti (2009): "Southern Africa validation of the MODIS, L3JRC and Globcarbon burned-area products", *IEEE Transactions on Geoscience and Remote Sensing* 47(4): 1032-1044.

Tansey, K., Grégoire, J.M., Stroppiana, D., Sousa, A., Silva, J., Pereira, J.M., Boschetti, L., Maggi, M., Brivio, P.A., Fraser, R., Flasse, S., Ershov, D., Binaghi, E., Graetz, D., y Peduzzi, P. (2004): "Vegetation burning in the year 2000: Global burned area estimates from SPOT VEGETATION data", *Journal of Geophysical Research - Atmospheres*, 109, D14S03, doi:10.1029/2002JD003598, 2-22

Tansey, K., Grégoire, J.M., Defourny, P., Leigh, R., Peckel, J.F., Bogaert, E.V., y Bartholome, J.E. (2008): "A new, global, multi-annual (2000–2007) burnt area product at 1 km resolution", *Geophysical Research Letters*, 35, L01401, doi:10.1029/2007GL03156

Van der Werf, G.R., Randerson, J.T., Giglio, L., Collatz, G., Mu, M., Kasibhatla, P.S., Morton, D.C., DeFries, R.S., Jin, Y., y van Leeuwen, T.T. (2010): "Global fire emissions and the contribution of deforestation, savanna, forest, agricultural, and peat fires (1997-2009)", *Atmospheric Chemistry and Physics*, 10, 11707–11735.